

HIGH TEMPERATURE CRACKING IN THE WELD HEAT AFFECTED

ZONE OF HIGH STRENGTH FERRITIC STEELS

by

R.H. Phillips, B.Sc.

28 nov 73 167479

A thesis submitted for the degree
of Doctor of Philosophy of the
University of Aston in Birmingham

THESIS

621.791

PHI

October 1973

SYNOPSIS

A study has been made of the effects of steel composition and welding parameters on hot cracking in the heat affected zone of high strength ferritic steels. In addition, the hot ductility test has been studied to determine whether it is capable of distinguishing unambiguously between crack sensitive and crack resistant steels. This has involved parallel weld cracking and hot ductility tests on low alloy steels to specifications SAE 4130, EN 24 and ASTM A387B.

Both composition and welding parameters were shown to have a marked influence on cracking severity. Consideration of composition confirmed the detrimental effects of carbon, sulphur and phosphorus. High levels ($>0.030\%$ wt) of either sulphur or phosphorus could cause significant cracking; phosphorus being the more detrimental. For a constant steel composition, cracking was found to increase with (i) Increasing Heat Input/unit length; (ii) Increasing depth of finger penetration; (iii) Application of external restraint; (iv) Increasing distance along the weld bead.

Metallographic and fractographic examination of welded specimens has shown that cracking occurs only within a discrete zone in the high temperature region of the H.A.Z., and is associated with the modification of MnS type inclusions. Furthermore, in the high sulphur steels, this crack susceptible zone is brittle at ambient temperatures due to extensive sulphide films at the grain boundaries.

It was found that the H.A.Z. hot cracking severity of a steel could be related quantitatively to the zero ductility range, measured during the cooling portion of a simulated weld thermal cycle, providing the peak temperature was equivalent to the nil-strength temperature or above. The greatest sensitivity was achieved with a peak temperature of 12°C below the bulk melting temperature.

CONTENTS

	<u>Page</u>
1. <u>Introduction</u>	1
2. <u>Literature Review</u>	5
2.1. Introduction	5
2.2. Description of H.A.Z. Hot Cracking	7
2.3. Theoretical Treatment of Hot Cracking	9
2.3.1. Introduction	9
2.3.2. Theories of Weld Metal Hot Cracking	9
2.3.2.1. Shrinkage-Brittleness Theory	10
2.3.2.2. Strain Theory	10
2.3.2.3. Generalized Theory of Super Solidus Cracking	11
2.3.2.4. Polygonisation Theory	12
2.3.3. Theories of H.A.Z. Hot Cracking	13
2.3.3.1. Preferential Grain Boundary Melting	13
2.3.3.2. Adsorption from the Molten Weld Pool	13
2.3.3.3. Low Melting Point Segregates	14
2.4. Factors Influencing Cracking	15
2.4.1. Composition Effects	15
2.4.2. Segregation and Inclusions	21
2.4.3. Microstructure	25
2.4.4. The Fusion Boundary	26
2.4.5. Welding Process Effects	27
2.4.5.1. Thermal Cycle	27
2.4.5.2. Strain	27
2.5. Techniques Used in the Investigation of H.A.Z. Hot Cracking	30

	<u>Page</u>
2.5.1. Weld Cracking Tests	30
2.5.2. Hot Ductility Studies	31
2.5.2.1. Introduction	31
2.5.2.2. Description of Equipment	32
2.5.2.3. Development of the Hot Ductility Test	34
2.5.2.4. Temperature Measurement	40
2.5.2.5. Summary	41
2.5.2.6. Future Work	42
2.6. Summary	43
3. <u>Experimental Investigation</u>	46
3.1. Introduction	46
3.2. Selection of Materials	46
3.3. Weld Cracking Program	48
3.3.1. Effect of Welding Procedural Variables	48
3.3.1.1. Selection of Significant Variables	48
3.3.1.2. Experimental Procedure and Design	49
3.3.1.3. Analysis of Variance Results	51
3.3.1.4. Detailed Metallographic Examination	51
3.3.2. Effect of Distance Along Weld Bead upon Cracking Propensity	53
3.3.3. Effect of Steel Composition and Restraint on Cracking Propensity	54
3.3.3.1. Testing Procedure	54
3.3.3.2. Results - Effect of External Restraint	55
3.3.3.3. Results - Effect of Composition	55
3.3.3.4. Regression Analysis	58
3.3.4. Fractographic Examination	58
3.4. Hot Ductility Testing Program	62

	<u>Page</u>
3.4.1. Description of Equipment and Testing Procedure	62
3.4.2. Calibration Work on the Mechanical 'Gleeble' Weld Simulator	66
3.4.2.1. Determination of Specimen Dimensions	66
3.4.2.2. Temperature Reproducibility	68
3.4.2.3. Thermocouple Calibration	69
3.4.2.4. Temperature Distribution	72
3.4.2.5. Summary of Calibration Studies	73
3.4.3. Hot Ductility Testing	75
3.4.3.1. Effect of Peak Temperature	75
3.4.3.2. Effect of Thermal Cycle	76
3.4.3.3. Effect of Composition	76
3.4.4. Correlation of Hot Deformation Behaviour with Cracking Propensity	79
3.4.4.1. The Rate of Recovery of On-Cooling Ductility	79
3.4.4.2. The Zero Ductility Range	80
3.4.4.3. Recovery to Specific Ductility Levels	81
3.4.4.4. Recovery Rate of Strength	81
3.4.5. Impact Testing	81
3.4.6. Metallography of Hot Ductility Specimens	82
3.4.6.1. Metallography	82
3.4.6.2. Fractography	83
4. <u>Discussion</u>	88
4.1. The Crack Susceptible Zone	88
4.2. Correlation Between Hot Ductility and Weld Cracking Test Results	89

	<u>Page</u>
4.2.1. Comparison of Metallurgical Features	89
4.2.2. Correlation Between Actual Cracking Behaviour and Hot Ductility Test Results	95
4.3. Effect of Welding Parameters	97
4.4. Effect of Composition	100
4.5. Implications of Results in the Context of Weldment Failure	104
5. <u>Conclusions</u>	106
6. <u>Recommendations for Further Work</u>	107
7. <u>Acknowledgements</u>	109
8. <u>Appendix - Publication:</u> Temperature Measurement and Distribution in Weld Thermal Simulation	110
9. <u>References</u>	121
<u>Tables</u> 1 - 13	
<u>Figures</u> 1 - 83	

1. INTRODUCTION

The past two decades have seen considerable development in the production of high strength steels with ultimate tensile strengths in excess of 1.6 KN/mm^2 (100 T.S.I.). This group includes: conventional and modified quenched and tempered steels, secondary hardening steels and maraging steels. A critical review of their development, applications and limitations has been made by Ineson.⁽¹⁾ The main impetus to the development of these steels has been given by the aerospace industry and the Armed Services who particularly require components of high strength to weight ratios. These steels also have advantages in that new design considerations can be applied to the fabrication of smaller and lighter components, ensuring reliable operation under severe service conditions.

Applications of these steels in the aerospace industry include rocket motor casings and aircraft undercarriage equipment. In ordnance, where one of the prime requirements of armaments is lightness combined with high fire power, applications include mortar and rifle tubing and breach blocks. Other applications include submarine and torpedo hulls, automobile main shafts, axle shafts, high duty engine connecting rods, spindle and power transmission gears and pressure vessels.

Important steels within the conventional quenched and tempered group are the $1\frac{1}{2}\%$ Ni-Cr-Mo, and the 1% Cr-Mo types. Examples within this group are EN24, SAE4130 and ASTM387B. The first two are of particular interest in the aerospace industry. They develop their strength and toughness through a tempered martensitic structure. The latter is primarily an elevated temperature, pressure vessel steel.

Despite the obvious attractions of these steels, their use in industry is not as widespread as might be expected. One of the main reasons for this is the problem of fabricating components into finished

products. Essentially this means welding, as this form of fabrication is by far the most widely used, due to the economies and the flexibility of design which it affords. Indeed for the majority of constructions, welding is the only fabrication process which is a realistic proposition today.

In common with other welded steel structures, failure in high strength steels, when it occurs, usually initiates from defects associated with the welded joint. Indeed, as the strength of the steel increases, so the associated welding problems escalate.

One of the serious problems in the welding of high strength steels is high temperature cracking in the weld metal and the heat-affected zone (H.A.Z.). A considerable amount of work has been carried out on this problem over the past fifteen years. However, the problem is still troublesome in industry and the need for further work has been confirmed by Baker.⁽²⁾

High temperature cracking (hot cracking) in the H.A.Z. takes the form of small (microscopic) intergranular separations adjacent to the fusion boundary. They are usually associated with segregated non-metallic films which decorate the prior austenite grain boundaries. Despite the minute size of these cracks, they may lead to subsequent service failure due to the cracks acting as initiating sites for hydrogen induced cold cracking, post-weld heat treatment cracks, brittle failure and fatigue failure; or because cracking is so extensive with respect to the load carrying area, that failure occurs through over-loading. These cracks are of particular significance in high strength steels because the critical crack length for fast fracture is so small. Randall, Monroe and Rieppel⁽³⁾ quoted an average value of 1.9 mm. in their study of AISI 4340 type steel, and reported that cracks of 0.25 mm. can promote failure. The problem of hot cracking is compounded by the fact that the minute size of the defects prevents, or makes very

difficult, detection by normal non-destructive testing techniques (viz. radiography, ultrasonics and dye penetrants). Hence, they may pass unnoticed into service where subsequent failure may occur.

In broad terms, the problem of hot cracking in ferritic steels has been identified and the main factors responsible for it have been defined. Hot cracking in the weld metal and H.A.Z. occur by similar mechanisms, viz. separation along planes of weakness under the action of tensile strains produced by the welding thermal cycle. These planes of weakness are usually associated with a second phase of low ductility. It has been shown that the incidence of cracking is particularly dependent on the levels of C, S and P although other alloy additions are also believed to affect cracking susceptibility. Unfortunately, in the case of the H.A.Z., quantitative relationships between composition and cracking are lacking.

Welding process parameters appear to have an effect but unfortunately conflicting results have left the picture somewhat obscure. In addition there has so far been no attempt to study the interaction between welding parameters and steel composition. Lack of information in this area prevents a systematic approach to the fabrication of materials under the various welding procedures and leads to a costly 'trial and error' approach.

Clearly it would be very desirable to have a laboratory test capable of distinguishing between crack sensitive and crack resistant materials. Since the occurrence of cracking must be associated with reduced ductility, at some intermediate temperature range during cooling, a great deal of attention has been focussed on hot ductility testing carried out under simulated welding conditions as a quantitative test for distinguishing between crack sensitive and crack resistant materials. However, although the concept would appear to have great potential,

quantitative correlation between hot ductility data and the crack susceptibility of materials has yet to be achieved. The test itself is in fact in need of rigorous examination to determine its suitability as a measure of crack susceptibility.

The two aspects of the problem of H.A.Z. hot cracking that are in need of investigation appear to be the quantitative relationship of composition and process parameters to cracking, and the establishment of laboratory testing procedures.⁽²⁾ The present investigation was intended to meet these two requirements and two parallel approaches were adopted. These were:

(i) Quantitative study of the combined effects of composition and welding procedural effects upon crack propensity using weld cracking tests.

(ii) Rigorous examination of the hot ductility test as a means of predicting cracking susceptibility by studying the behaviour of test materials known to be crack sensitive and crack resistant.

Most work was concentrated on SAE 4130 (composition in wt% is: C = 0.30, Cr = 1.00, Mo = 0.20) because of its interest in aerospace applications; however, EN 24 (composition in wt% is: C = 0.40, Ni = 1.40, Cr = 1.10, Mo = 0.26) and ASTM 387B (composition in wt% is: C = 0.12, Cr = 0.90, Mo = 0.36) were also used to permit variations of carbon content and other alloying elements.

2. LITERATURE REVIEW

2.1. Introduction

High temperature cracking, commonly abbreviated to the simpler term of hot cracking, is not restricted to weldments in ferritic steels, but can occur in the weldments of a large range of metal alloys; these include Al-base alloys, Ni-base alloys, as well as austenitic steels. The high temperature can approximately be defined as being $0.5 T_m$, where T_m is the melting point or solidus in $^{\circ}\text{K}$.⁽⁴⁾ Cracks can occur in the weld metal and/or the heat-affected zone (H.A.Z.) immediately adjacent to the fusion boundary. It is generally accepted that cracks are due to intergranular separations, which propagate with low overall ductility when the weld metal is subjected to the tensile shrinkage strains that result from the weld thermal cycle.

An attempt to classify the various types of hot cracking has been made by Hemsworth et al⁽⁴⁾ on the basis of their microstructural characteristics. (Fig. 1) They list two types, Type 1 - separations along boundaries decorated by films of second phases resulting from microsegregation; Type 2 - cracking of migrated grain boundaries free from films but associated with a 'ductility dip' in the material. These two types of cracking can occur in the H.A.Z., weld metal, and weld metal reheated by subsequent passes. In ferritic materials, Type 1 cracking is by far the most common.

The problem of hot cracking in high strength steel weldments became apparent in the 1930's, when it was reported that cracking was largely dependent on carbon, sulphur and phosphorus levels.^(5,6) Though cracking occurred in both weld metal and H.A.Z., no differentiation between them was made. Since that time many investigators have confirmed the detrimental effect of high sulphur, phosphorus and carbon levels.⁽⁷⁻¹³⁾

In addition, the effects of many alloying elements have also been covered. Most of this work relates to weld metals, where several hot cracking susceptibility formulae have been produced. (9-13) The limited work on the H.A.Z. confirms the effects of the major elements, namely carbon, sulphur, possibly phosphorus and also manganese. (14,15) However, quantitative formulae relating chemical composition to cracking susceptibility of the H.A.Z. have yet to be produced.

Segregation is a necessary condition for the occurrence of hot cracking. In ferritic materials, it has been shown that the primary crack inducing elements, sulphur and phosphorus, cause damage by combining with other elements to form low melting point liquid films around the grain boundaries. (15,16)

Only a limited amount of work has been conducted on the influence of welding procedural variables. Unfortunately the results of this work have so far proved inconclusive. It has been claimed that arc energy input (17,18) and the specific welding process (14) significantly influence cracking behaviour. Other evidence, however, indicates that this is not the case. (19)

The theoretical treatment of hot cracking, which has its origins in the study of hot shortness in aluminium alloys, (20,21) has mainly been developed for the case of weld metals. These theories are usually then extended to include the specific case of H.A.Z. hot cracking. Most theories propose the critical stage in the cracking process is reached when a liquid film covers nearly all the grain face. Cracking occurs when the solid metal bridges connecting the grains cannot accommodate the strains caused by the welding thermal cycle. On the other hand, some workers favour a solid state mechanism. (22)

The important factors influencing H.A.Z. hot cracking then are: composition, segregation and probably welding variables. The existing knowledge of these findings, particularly in relation to low alloy

quenched and tempered steels, is discussed critically in the literature review. The final section deals with the two general techniques which have been used in the investigation of H.A.Z. cracking. They are:

(i) 'In-situ' studies, where various welded test pieces are examined metallographically, for cracks and their associated segregated material.

(ii) Hot ductility studies, in which measurements are made of the ductility and breaking stress of a steel specimen when subject to a simulated welding thermal cycle. This is based on the premise that it should be possible to correlate the high temperature deformation behaviour of a material, subject to the weld thermal cycle experienced in the H.A.Z., with its hot cracking susceptibility.

2.2. Description of H.A.Z. Hot Cracking

Hot cracking in the H.A.Z. is always intergranular in appearance, following either the grain boundaries or 'ghost' boundaries. It usually occurs when the steel is in the austenitic condition. Cracking is mainly restricted to the coarse grained (high temperature) region of the H.A.Z., although it may continue across the fusion boundary into the weld metal.

It has also been observed that both weld metal and H.A.Z. cracks often occur in close proximity to each other near the fusion boundary. H.A.Z. hot cracking has been observed in a wide range of ferritic steels. These include: plain carbon steels, carbon-manganese steels, and low alloy quenched and tempered steels. In HY 80 it has been observed that the partially melted region of the H.A.Z. was the most crack sensitive area.⁽²³⁾ A similar observation has been made for Ni based alloys.⁽²⁴⁾

Cracking is often perpendicular to the fusion boundary,⁽¹⁴⁾ but cracks running parallel to the fusion boundary have also been noted. The direction of cracking appears to be dictated by the nature of the

stress field. It has been observed that cracks often initiate from triple points. (19,25)

Reports indicate that crack size can vary considerably. Meitzner and Stout (14) report average crack lengths of 0.05 mm to 0.08 mm in low alloy quenched and tempered steels. Jordan, (25) investigating similar steels, measured sizes from 0.01 mm to 0.40 mm. Boniszewski and Baker, (16) investigating a carbon-manganese steel, report variations from short microcracks confined to part of a grain boundary to large ones several grain diameters long. So far, measurements of crack length have only been made from polished and etched metallographic surfaces, usually taken normal to the welding direction. No measurements have yet been published on area of crack surfaces. Such a parameter would be essential when accurately assessing the risks of hot crack defects initiating fast fracture.

It has recently been established (4) that there are two distinct types of hot cracks, namely,

(a) Liquefaction cracking along grain or 'ghost' boundaries. This cracking is associated with liquid films which result from micro-segregation. In the case of low alloy steels, these films have been identified as predominantly manganese sulphide. (16,26,27) One of the striking characteristics of liquefaction cracking is its jagged edges and variable openings, which may indicate locally enhanced pockets of liquefaction. Electron fractography of crack and grain boundary surfaces provides clear indication of film formation.

(b) 'Ductility-dip' cracking. This cracking occurs at boundaries which are free from films, and it is suggested (4) that this form of cracking is accompanied by a ductility trough (Fig. 2) when the metal is tested on cooling following simulated H.A.Z. heating. These cracks are clearly defined, smooth, and have no films at the crack surface or grain boundary.

Observations of this type of cracking have mainly been confined to austenitic steels and Ni-based alloys. This mode of cracking has not yet been identified in ferritic materials.

2.3. Theoretical Treatment of Hot Cracking

2.3.1. Introduction

Most theoretical research into the fracture of metals at high temperatures has been directed at creep failure. Much less has been directed at hot cracking. Though both cracks are intergranular, they have different characteristics and form under different conditions. The temperature range in which creep failure is investigated is usually well below the solidus temperature and liquation is not a necessary condition of creep failure, while hot cracking occurs only in regions melted or heated close to the solidus. The strain rate in hot cracking is much faster than creep which probably precludes void formation and grain boundary sliding, the major mechanisms responsible for creep failure, from being significant cracking mechanisms.

2.3.2. Theories of Weld Metal Hot Cracking

To date, most theoretical models of hot cracking have been developed from the case of weld metals. These theories are usually then extended to include the specific case of H.A.Z. hot cracking.

The theories on weld metal hot cracking can be divided into the following two groups, based upon the temperature of crack formation:

- (a) The 'liquation' theories, which propose that cracks are initiated above the solidification temperature of the lowest melting phase present. These theories include: the shrinkage-brittleness theory, the strain theory, and the so called 'generalised theory'.
- (b) The 'solid-state' theories, which propose that cracking is initiated in the solid state below the solidus of the lowest melting phase. The polygonisation theory is the only member of this group which has been

developed in detail.

2.3.2.1. Shrinkage - Brittleness Theory

This theory resulted from the studies of hot shortness in aluminium alloy castings by Lee, Singer, Cottrell, Pumphrey and Jennings. (20,21,28,29) The theory was then extended to the hot cracking of aluminium alloy welds and later to the hot cracking of non-ferrous and ferrous welds. From these studies, it was proposed that during solidification, primary dendrites form, come into contact and interlock, thereby forming a semi-rigid network of dendrites. As cooling continues, contraction strains develop and so cracking may occur. These cracks will persist if insufficient liquid remains to 'heal' them. Once the temperature is below the solidus, cracks are unlikely to form as the solid metal is more ductile at these temperatures. Thus cracks are only likely to occur between the solidus and the temperature at which the primary dendrites interlock. This is termed the 'brittle' range. Pumphrey and Jennings (21) state that cracking tendency is directly proportional to the 'brittle' range, and to the contraction due to cooling through that range. Where this range is narrow, cracking susceptibility is low; where it is wide, cracking susceptibility is high. These ideas have been extended by Medovar (30) for alloys with elements forming continuous solid solutions. In this case, hot cracking tendency is determined by the length of the freezing range. In general, if the freezing range is short, hot cracking should not occur.

2.3.2.2. Strain Theory

Similar to the Shrinkage-brittleness theory is the Strain theory by Pellini et al. (31,32,33) They postulate that during solidification, an essentially continuous network of thin liquid films exists between masses of solid grains. These films, which have only low strength and ductility, may then part under the action of tensile strains caused by

the thermal gradients associated with solidification. This differs slightly from the previous theory, in that it is argued that hot cracking cannot occur during the mushy stage of solidification since the shrinkage strains are uniformly distributed. Cracks only occur when the film stage is reached and the localised strains are very high. Low melting point segregate films are the most dangerous of all, as they are molten below the equilibrium solidus where strains are increasing.

2.3.2.3. Generalised Theory of Super-Solidus Cracking

Borland ⁽³⁴⁾ has attempted to rationalise the previous two theories into his generalised theory. His theory considers the four stages of the solidification process as outlined by Portevin and Dannenmüller:- ⁽³⁵⁾

- (a) Primary dendrite formation,
- (b) Dendrite interlocking,
- (c) Grain boundary development (critical solidification range),
- (d) Solidification.

The beginning of stage (b) corresponds to the start of the brittle range of the Shrinkage-brittleness theory. (Fig. 3) Borland proposes stage (c) to be the significant stage in cracking (critical solidification range). In this stage the flow of liquid is restricted, and healing cannot occur. However, straining without cracking can occur up to a certain limit. This process is termed 'accommodation'. Thus cracks will form if the accommodation is insufficient for the shrinkage strains. Borland disagrees with the idea that a wide freezing range alone is sufficient for cracking to occur. He proposes that, in addition, the alloy must pass through a stage in which high localized stresses are built up between grains. This condition is achieved when a liquid phase occupies almost all of the grain faces, but leaves solid narrow bridges between the grains where high stresses can be built up.

On the other hand, if the liquid covers only grain edges and corners, then the relatively extensive solid-solid interfaces prevent high stresses from being built up along grain boundaries and so there is much less tendency to crack.

The angle of contact (Θ) of the liquid phase with the solid (viz. the angle of 'wetting') is determined by the relative free energies of the grain boundaries and the interphase boundaries. When Θ is 0° , the liquid completely 'wets' the grain faces. When it is slightly above 0° , almost complete wetting occurs. This is believed to be the most crack susceptible condition. As Θ increases, progressively less of the faces are covered, until at $\Theta = 60^\circ$, liquid can only exist as a network along the grain edges.

2.3.2.4. Polygonisation Theory

This solid-state mechanism for hot cracking has been developed by Movchan.⁽²²⁾ It applies only to alloys which solidify as a single phase solid solution with a face centred cubic structure, e.g. plain carbon steel above 0.22% C, low alloy steels and austenitic steels. Cracks initiate behind the crystallization front, at the intersections of the polygonisation boundaries and the regions of segregation, e.g. grain boundaries. The polygonisation boundaries are formed by the grouping of dislocations and vacancies. The cracks propagate under the influence of weld solidification strains.

The polygonisation theory has not found much favour to date, as it has been widely held that cracking is most likely to initiate in the liquid-film stage. However, it has been recognised recently⁽⁴⁾ that hot cracking need not necessarily be associated with liquid film formation. This second type of cracking is termed 'ductility-dip' cracking. Clearly a different mechanism applies to this type of cracking as opposed to liquation cracking. Thus the solid state Polygonisation

theory may well apply to this case.

2.3.3. Theories of H.A.Z. Hot Cracking

The theories of H.A.Z. liquation cracking are derived from the case of weld metal cracking as it is proposed that, in those parts of the H.A.Z. close to the fusion face, the grains are surrounded by liquid films. The mechanisms proposed for producing the films are:

- (i) Preferential grain boundary melting.
- (ii) Adsorption from the molten weld pool.
- (iii) Low melting point grain boundary segregates.

2.3.3.1. Preferential Grain Boundary Melting

Preferential melting of large angle boundaries can occur just below the equilibrium melting point. The rate of melting increases with increasing applied stress, heating rate and impurity content. However, as such films must be very small in extent, this mechanism is probably of little importance.

2.3.3.2. Adsorption from the Molten Weld Pool

This mechanism, sometimes called the Rehbinder-Medovar effect, (36) proposes that certain solute atoms may be adsorbed from the molten weld pool into the grain boundaries of the H.A.Z. It has been shown (37) that solidification of weld metal begins by epitaxial growth from the solid grains at the fusion boundary, and that grain boundaries are continuous across the fusion face. Thus grain boundary diffusion of solute may readily occur from the solute rich regions of the weld metal, into the H.A.Z., particularly as the diffusion rate at grain boundaries may be up to a million times as fast as in the bulk solid. This process could thus contribute to considerable solute enrichment of H.A.Z. grain boundaries.

This mechanism would explain base-metal cracks which develop in a segregate-free base material. On the other hand, it would not explain

how additions of low impurity, crack resistant filler metals have failed to stop H.A.Z. cracking in certain materials. (23)

2.3.3.3. Low Melting-Point Segregates

The presence of segregates at grain boundaries with considerably lower melting points than the surrounding matrix, is the most widely proposed mechanism for producing liquid films along grain boundaries. There is considerable speculation on how solute atoms become concentrated at grain boundaries during the short time available in the normal weld thermal cycle. It has been hypothesized (37) that the grain boundaries accumulate solute (particularly those adjacent to the fusion face) by their motion during extensive grain growth. However, this has been refuted by other workers (38) who claim that there is a decrease in the solute concentration of grain boundaries which migrate. At a critical velocity, the migrating boundary breaks away from the excess atoms.

A more attractive mechanism is that of constitutional liquation, proposed by Pepe and Savage. (39) They explain that this phenomenon can occur in any material consisting of a high melting point inter-metallic or non-metallic compound distributed as a second phase in a solid matrix. The phenomenon can be explained by considering the heating of such an alloy at various rates. With slow rates of heating the second phase dissociates and diffuses into the adjacent material to form a high alloy content solid solution, which then diffuses into the matrix to produce a single phase homogeneous solid solution. Melting does not occur until the solidus temperature is reached. With rapid heating, however, the high alloy content envelope formed around the second phase may not have time to diffuse away before the temperature reaches its melting point. Thus a liquid film forms around the remaining second phase particle at a temperature below the bulk solidus of the alloy. As the grain boundaries migrate, due to the rapid grain

growth in the high temperature region of the H.A.Z., they intersect these liquid phases and are 'wetted' by them, thus forming a grain boundary film. The hypothesis of constitutional liquation was in fact confirmed experimentally by Pepe and Savage in the H.A.Z. of maraging steels.⁽³⁹⁾ The liquation of non-metallic inclusions 'in-situ' has also been noted in the H.A.Z. of ferritic steels.^(15,18)

A specific model relating the presence of liquid films, the thermally induced stresses of welding, and the type of H.A.Z. cracking has been proposed by Puzak et al ⁽³³⁾ and is shown in Fig. 4. On welding, the base metal adjacent to the fusion boundary is stressed initially in compression. Melting of grain boundary segregates occurs to a distance determined by the nature of the segregates and by the thermal cycle perpendicular to the weld in the heat affected zone. As the welding arc moves on, the H.A.Z. becomes stressed in tension as a result of cooling and subsequent contraction. The tensile stresses result in separation of regions containing a liquid film. The position and relative extent of the resulting cracking are dependent upon the amount of liquid film present, the unit strain rate developed, and the film life.

H.A.Z. 'ductility-dip' cracking on the other hand has only recently been recognised. This form of cracking is characterised by the complete absence of liquid films at grain boundaries and resembles the wedge cracking of creep rupture. It has so far only been observed in austenitic materials. The actual mechanism of crack formation is not clear, though it would appear that solid solution segregation of solute atoms to grain boundaries is involved.

2.4. Factors Influencing Cracking

2.4.1. Composition Effects

As early as the 1930's ^(5,6) carbon and the impurities, sulphur

and phosphorus, were recognised as major elements causing hot cracking in high strength ferritic steel weldments. It was found that the concentration of sulphur and phosphorus together, which could be tolerated, decreased with increasing carbon content. In the early investigations of weld metal and H.A.Z. cracking in 1% Cr-Mo aircraft steels, ⁽⁵⁾ it was recommended that sulphur and phosphorus combined should not exceed 0.040% for a 0.20% carbon steel. When the carbon level was raised to 0.30%, then the combined sulphur and phosphorus had to be below 0.020%. Since this time, most investigations of compositional effects have been restricted to the weld metal; few have been specifically conducted on the H.A.Z.

The high potency of sulphur and phosphorus in weld metals has been noted by several workers. ^(7,8,40) Investigations by Wilkinson, Cottrell and Huxley ^(9,10) of both the weld metal and H.A.Z. of 1% Cr-Mo aircraft steels again confirmed the overwhelming potency of sulphur and phosphorus. This was further developed by Huxley ⁽¹¹⁾ who showed that for weld metals, whilst sulphur was constant in its effect, the influence of phosphorus could vary widely, depending upon steel composition. While the precise effect of phosphorus upon H.A.Z. hot cracking is not known, it has been suggested ⁽⁴¹⁾ that phosphorus cannot induce hot cracking without the presence of sulphur, as it cannot segregate in the absence of phases which are already liquid.

Brockhurst and Muir ⁽⁴²⁾ in their weld metal studies found that increasing carbon raised the ability of sulphur to induce cracking. Similar results have been obtained for the H.A.Z. Boniszewski and Watkinson ⁽¹⁵⁾ have shown for a plain carbon steel containing 0.01% S and no manganese, that hot cracking depends on carbon content, and begins above 0.25% C. Baker and Tremlett ⁽⁴³⁾ have noted that in certain low alloy steels, hot cracking can occur at carbon levels

considerably below 0.27%. Meitzner and Stout ⁽¹⁴⁾ have observed that for a given Mn:S ratio, cracking density increases with increasing carbon content. This adverse effect of carbon is explained by Boniszewski and Watkinson ⁽¹⁵⁾ in terms of an apparent incompatibility of carbon and sulphur in iron. The higher the carbon content, the more sulphur will tend to be rejected from solid solution and precipitate at grain boundaries, thereby increasing cracking susceptibility.

Considerable importance has been attached to the Mn:S ratio. Jones, ⁽⁴⁴⁾ investigating hot cracking in low alloy steel weld metal, found that increasing the Mn:S ratio up to about 50, substantially reduced cracking. As the carbon level increased, then the Mn:S ratio also had to be increased to avoid cracking, e.g. for C = .11%, Mn:S for crack-free conditions was 22; for C increased to 0.155%, Mn:S had to be increased to 59. Borland ⁽⁴⁵⁾ in his work on thin sheet low alloy steel weld metal, claims that the Mn:S ratio is significant in effecting cracking only at ratios less than 50-80. Bonomo ⁽¹²⁾ also finds Mn:S ratio has a definite influence on cracking, though the range of Mn:S values was very small (9.1 to 10.5). Meitzner and Stout, ⁽¹³⁾ investigating H.A.Z. cracking in a wide range of quenched and tempered steels, also conclude that the Mn:S ratio was very important. Low Mn:S ratios (<50) favoured cracking whereas no cracking was observed in steels with a high Mn:S ratio (130-175). However, as the sulphur levels were not constant the results could equally be interpreted as being due to straight sulphur effects.

It has been noted that rare earth additions are beneficial in reducing hot cracking, both in the weld metal ^(8,44,46) and the H.A.Z., ⁽¹⁴⁾ of ferritic steels. This is thought ⁽¹⁴⁾ to be due to desulphurization. Small additions of uranium have also been shown to substantially reduce hot cracking in ferritic weld metals. ⁽⁴⁷⁾

Recent work has shown that oxygen has a powerful inhibiting effect upon cracking in 1% Cr-Mo weld metal.^(13,48) Not only did increasing the base metal oxygen content markedly reduce weld metal cracking during autogenous T.I.G. welding, but addition of oxygen to the argon shielding gas also resulted in a large reduction in cracking in crack sensitive steels.

The effect of many other elements upon hot cracking susceptibility has also been investigated. It has been suggested⁽⁴⁹⁾ that they act by either enhancing or retarding the segregation of sulphur and phosphorus to grain boundaries. Elements favouring initial solidification as austenite are thought to be crack promoters, as sulphur and phosphorus have a lower solubility in this phase; examples being, silicon and nickel. On the other hand, elements favouring initial solidification as ferrite, such as Cr, Mo and V, are beneficial. Paradoxically, the presence of manganese, an austenitizer, decreases cracking susceptibility. This is explained by Marshall⁽⁴⁹⁾ in terms of the affinity of manganese for sulphur, with the subsequent formation of globular grain boundary inclusions which do not 'wet' the grain boundaries. This interpretation is supported by most of the empirical formulae which have been used to predict cracking sensitivity. However, it has recently been observed that increasing the chromium content from 1.2% to 6.3% in high strength Cr-Mo-V alloy sheet steel significantly increased the amount of weld metal cracking.⁽⁴⁷⁾

Quite expectedly, there have been numerous attempts to devise empirical formulae based on chemical composition that would quantitatively predict cracking susceptibility. Almost entirely these formulae were determined for weld metals. In the few cases where the H.A.Z. is considered, it is treated jointly with the weld metal. This approach was rationalised by noting that the two types of cracks are almost

identical morphologically and frequently occur in close proximity. In one such case, Wilkinson and Cottrell ⁽¹⁰⁾ working on 1% Cr-Mo aircraft steels, and considering only the principle crack inducing elements C, P & S, produced the following relationship for freedom from cracking:

$$S + P < .007/C$$

Later a more extensive formula for low alloy steel sheet ⁽⁹⁾ which included the effects of alloying elements was proposed:

$$\text{H.C.S.} = \frac{C(S + P + \frac{Si}{25} + \frac{Ni}{100}) \times 10^3}{3 \text{ Mn} + \text{Cr} + \text{Mo} + \text{V}}$$

The H.C.S. is termed the hot cracking susceptibility and is used to predict the susceptibility of steels to hot cracking. In this case it was found that steels with an H.C.S. value of less than 4 showed good cracking resistance.

Similar in form, though slightly different in detail, is the following H.C.S. formula produced by Bonomo ⁽¹²⁾ after his investigations on high S (~0.1%) weld metal:

$$\text{H.C.S.} = \frac{C(S + P + \frac{Si}{25} + \frac{Ni}{40}) \times 10^3}{3 \text{ Mn} + \text{Cr} + 2 (\text{Mo} + \text{V})}$$

The effect of phosphorus has been shown to be quite variable. Huxley ⁽¹¹⁾ has quantified its effect for constant S (.01%) thus:

$$\text{crack susceptibility} \propto P \left(C + \frac{Ni}{30} - \frac{Mo}{10} - \frac{Cr}{100} - \frac{V}{100} \right)$$

Recently, test data obtained by Bristol Aerojet Limited, using the Huxley Test, on some 80 sheet aircraft steels has been examined

statistically by Morgan-Warren.⁽¹³⁾ Using the analysis of regression of crack susceptibility factor (C.S.F.) on single chemical elements, he proposed the following simple linear formulae:

$$\begin{aligned} \text{C.S.F.} = & 36(\text{C}) + 12(\text{Mn}) + 8(\text{Si}) + 540(\text{S}) + 812(\text{P}) \\ & + 5(\text{Ni}) + 3.5(\text{Co}) - 20(\text{V}) - 13 \end{aligned}$$

Subsequent work on a further 25 steels, but this time including the oxygen content of the steel, lead to the following revised expression:

$$\text{C.S.F.} = 42(\text{C}) + 847(\text{S}) + 265(\text{P}) - 10(\text{Mo}) - 3042(\text{O}) + 19$$

This expression predicts a very powerful crack-inhibiting effect of oxygen.

Other formulae, different from those listed, have also been proposed for weld metal hot cracking. The various H.C.S. formulae for weld metal seem to hold quite well over the limited ranges of composition and testing procedures for which they were determined. However, it appears inadvisable to use them to quantitatively predict the cracking behaviour of steel compositions outside the range tested.

The value of these formulae in predicting H.A.Z. cracking is of course highly debatable. Though the formulae of Wilkinson et al⁽⁹⁻¹¹⁾ purport to apply equally to weld metal and H.A.Z. on the grounds that the cracks are morphologically similar and frequently occur close together, there is a distinct lack of evidence to support this contention. However, in the absence of detailed correlation between weld metal and H.A.Z. cracking with respect to composition, the formulae listed above might, at best, be considered to give a guide line for susceptibility to H.A.Z. hot cracking.

From this survey, it can be seen that the quantitative effect of composition on H.A.Z. cracking is by no means clear. Sulphur is

definitely a major element, and increasing carbon, increases its potency. Increasing manganese on the other hand decreases the potency of sulphur. Phosphorus is also regarded as potent, though mainly on the basis of weld metal studies. The effect of other elements on H.A.Z. cracking has not been conclusively shown, though from weld metal studies it appears likely that Mo and V are beneficial, and Ni and Si detrimental. In any case their effects are quite secondary to those of S, P and C. The powerful inhibiting effect of oxygen has so far only been investigated for the weld metal case. It is most important that its effect should also be investigated in the H.A.Z.

2.4.2. Segregation and Inclusions

The process of segregation in the H.A.Z. is a necessary condition for the occurrence of H.A.Z. hot cracking; without it cracking could not occur. Significant segregation is only found in the grain coarsened region, adjacent to the fusion face.⁽³⁷⁾ This region is seldom more than a few grains wide. Investigation of the role of segregation and inclusions appear to be limited to the liquation type of crack.

In ferritic materials, as shown in the previous section, the primary crack inducing elements are sulphur and phosphorus. These elements induce damage by combining with other elements to form low melting point liquid films around grain boundaries. The existence of these grain boundary films has been demonstrated by several workers using electron microscopy^(15,16,26,41) and scanning electron microscopy⁽⁵⁰⁾ on both actual^(15,16,41) and simulated^(26,50) H.A.Z.'s.

An insight into film formation was initially gained from investigations of overheating and burning in low alloy steels.⁽⁵¹⁻⁵³⁾ It was found⁽⁵³⁾ that a molten sulphide layer, predominantly MnS, was formed at the γ grain boundaries on heating to temperatures approaching the solidus. The molten sulphide then precipitates out at the

grain boundaries in the form of dendrites. In this condition the steel is said to be 'burned' and its former properties cannot be recovered by subsequent heat treatment. It is now believed that the process of burning in steel is analogous to the process of liquation in the H.A.Z., although the latter involves relatively fast heating and cooling rates and short times at peak temperatures.

These observations were largely confirmed by Boniszewski et al^(15,16) during investigations of the H.A.Z. of a high S (0.056% S) C-Mn steel. They examined carbon extraction replicas of fracture faces taken through the H.A.Z., by electron microscopy and electron diffraction and found inclusions of α -MnS associated with dendritic films. These dendritic films are indicative of prior liquation. They also observed that the inclusions of α -MnS present in the steel could be considerably affected by the high temperatures experienced in the H.A.Z. near the fusion boundary. In some cases voids were formed indicating rapid dissolution of MnS in the austenite. In other cases there was evidence of MnS inclusions melting 'in-situ'. This led them to propose that in some cases 'wetting' of grain boundaries may be due to rapidly migrating grain boundaries impinging on molten inclusions. They also noted, like Jordan⁽²⁵⁾, that hot cracking was often associated with the presence of these modified inclusions.

Extensive dendritic films, identified as α -MnS, were also identified by Vinckier^(26,27) on the fracture faces of low alloy steel specimens, containing 0.020% S, subjected to simulated H.A.Z. thermal cycles. These films were only observed when peak temperatures in excess of 1380°C were used. From his observations, Vinckier⁽²⁷⁾ postulated that once a sulphide particle, located on an austenite grain boundary, becomes molten, it spreads as an almost continuous film along the neighbouring grain boundaries. This is probably intensified by the slight compressive

forces caused by thermal expansion during the heating cycle. He also calculated that 0.02 wt % sulphur will give rise to 0.1 vol % of sulphide film. Assuming a uniform grain size of 0.1 mm and a film thickness of 0.1μ , then there should be sufficient sulphide to completely wet all the grain boundaries present. On the other hand, Widgery,⁽⁴¹⁾ examining the H.A.Z. of the C-Mn steels, observed that the liquated film of MnS was not continuous around the grain boundaries. This can be explained⁽⁵⁴⁾ by the relatively high interfacial energy between MnS and the matrix, preventing complete 'wetting' of the grain boundaries. When a very low Mn (<0.1% Mn) steel was used, an almost continuous grain boundary film of FeS was found. This continuous film was thought to be due to the lower interfacial energy between this compound and the matrix.

Considerably less information is available on the presence and effect of phosphorus in these liquid films. Brammer,⁽⁵³⁾ in experiments on the burning of low alloy steel, found that under very high cooling rates, (brine quenching), phosphorus would precipitate as an Fe - Fe P eutectic. Moreover, it was associated with the molten sulphide and found to be the last constituent to solidify. This last observation may explain why some investigators have found phosphorus to be so potent in inducing weld metal cracking. At slower cooling rates, it was noted that phosphorus would not precipitate, but instead would redissolve in the matrix. These observations have been confirmed by Widgery⁽⁴¹⁾ who has identified phosphide lamellar eutectics of 10.5% P (the Fe - Fe P eutectic composition). He also observed that phosphorus rich inclusions are found only where signs of liquation are present. This suggests that there is no driving force to cause P, which is considerably more soluble in the matrix than S, to segregate to the grain boundaries unless these contain a liquid phase in which phosphorus is still more soluble. From these considerations he proposed that for

H.A.Z. cracking, the effect of phosphorus should remain secondary to that of sulphur.

The proposal that phosphorus will not segregate unless a liquid phase is present is now in dispute following recent work by Revière (55) on overheating and burning in low alloy steels. He demonstrated that phosphorus would segregate to a free surface (low energy site) in increasing concentrations from about 900°C. Sufficient phosphorus was present at 1400°C to produce a liquid phase. In addition there was an interaction between sulphur and phosphorus that caused additional phosphorus to be thrown out of solution when the sulphur content was high. The relevance of these results for the H.A.Z. is uncertain as chemical analysis was made from a free surface, not grain boundary; after thirty minutes at peak temperature, rather than a few seconds as occurs during a welding thermal cycle. None the less, it has now been shown that phosphorus will segregate to low energy sites, without the presence of a liquid phase.

It is not immediately clear why liquated manganese sulphide films should be present during the weld thermal cycle. The melting point of pure MnS is about 1610°C and normal welding conditions will not liquate it in the H.A.Z. However, it is well known from the shape of the most common form of manganese sulphide inclusions in ferritic steel (Type 1) that they were still liquid when the steel was solid. Boniszewski (18) has discussed this point and has shown that additions of Fe S to MnS lower the melting point considerably. The binary Fe S - MnS diagram indicates a solidus of 1180°C at 72-75% FeS; melting points of 1400°C are achieved at much lower FeS contents. Manganese sulphide type inclusions in a carbon-manganese steel (Mn = 1.10%) have been examined by Salmon Cox and Charles, (56) at room temperature, using microprobe X-ray analysis. They found the concentration of FeS dissolved in the

MnS inclusions could range from 3% to 25% FeS. The proportion of dissolved FeS is known to increase as the Mn:S ratio decreases, so a higher proportion of FeS would be expected in the manganese sulphide inclusions of low alloy steels like A.S.T.M. 387B (Mn = 0.50%). Furthermore, the solubility of FeS in MnS increases with increasing temperature, and it has been shown by Chao et al (57) that MnS can dissolve 72% FeS at 1180°C. Apart from iron, other alloying elements added to steel will also affect the composition, and hence the physical properties of the sulphides. Small additions of deoxidisers, such as aluminium and zirconium, may also concentrate in the sulphides. It should be remembered that not only may the melting temperature alter, but also the wetting angle of any subsequent film may be lowered, producing a more extensive grain boundary film.

2.4.3. Microstructure

It has been suggested (58) that increased grain size increases the hot cracking susceptibility of steels. As grain size increases, the grain boundary surface area per unit volume decreases. For a given volume of grain boundary impurities, the concentration of impurities at the grain boundaries increases as the total grain boundary area decreases. So far, however, there has been no direct experimental evidence for this contention as it is difficult to separate the effects due to an increase in grain size and those due to other causes, e.g. diffusion and liquation, that occur concurrently with changes in the thermal cycle.

The microstructure of low alloy steels at ambient temperatures has not been observed to influence their hot cracking susceptibility, as cracking initiates in the austenite region before the $\gamma \rightarrow \alpha$ transformation. An exception to this general statement are reports that hot cracking can be associated with pronounced banding. (27,46)

There have been suggestions that the temperature at which the

δ - ferrite \rightarrow austenite transformation occurs could be very important. (27,49) Alloying steel with elements that widen the δ - ferrite region towards lower temperatures are thought to reduce cracking susceptibility as it is believed that δ - ferrite grain boundaries reject wetting by liquid sulphides, and that phosphorus is very soluble in ferrite.

2.4.4. The Fusion Boundary

The actual position of, and the metallurgical processes which occur at, the weld metal - H.A.Z. boundary have received a certain amount of attention. This work arose from observations by some workers that hot cracking was most severe in this region and that H.A.Z. hot cracking could still be a problem, even when low impurity filler metals had eliminated weld metal cracking. (23,37) It has also been noted that weld metal and H.A.Z. cracks frequently occur in close proximity.

Savage and Szekeres, (23) using a special etching technique, revealed a solidification substructure, in HY 80, within what appeared to be the H.A.Z., as etched using a conventional etchant. This they claimed was an unmixed weld metal region where the base metal had melted and resolidified again without becoming alloyed with the weld metal.

The concept of an 'unmixed' molten zone within the H.A.Z. is disputed by Duvall and Owczarski (59) who investigated the fusion boundary region of nickel alloys using microprobe analysis. They found a filler metal depleted area 0.08 mm to 0.15 mm wide in the weld metal adjacent to the fusion boundary. A composition gradient extended across this region from the base metal composition at the fusion boundary out to the average weld metal composition. From this work they deduced that this filler metal depleted area of the weld metal could be a site for hot cracking even when crack insensitive additions are used.

2.4.5. Welding Process Effects

The effect of process variables upon hot cracking propensity has received less attention than has the effect of metallurgical variables. Basically the process variables may affect cracking propensity by their influence on the thermal cycle and/or the strain situation in the H.A.Z.

2.4.5.1. Thermal Cycle

It has been reported by Widgery and Boniszewski ⁽¹⁷⁾ that the welding process can influence the degree of hot cracking. They observed extensive hot cracking when a C-Mn steel was welded using the oxyacetylene process, but no cracking was observed when they used the metal arc process. This, they deduced, was due to the longer times spent at high temperatures by the H.A.Z., which characterises the oxyacetylene process. In a later paper, Boniszewski ⁽¹⁸⁾ observed that for C-Mn steels, hot cracking is not a problem where the H.A.Z. is narrow (low heat input/unit length - e.g. electric arc at low current and fast travel), whereas extensive hot cracking could occur where the H.A.Z. is wide (high heat input/unit length - e.g. oxyacetylene process at low travel speed, or sub arc and electroslog at high currents). Meitzner and Stout ⁽¹⁴⁾ also observed an apparent increase in cracking propensity with increasing heat input/unit length in the range 0.87 - 5.55 kJ /mm (22 - 142 kJ /in), though there was no direct relationship.

In contrast, however, Masubuchi and Martin ⁽¹⁹⁾ report no difference in the cracking propensity of HY 80 in the heat input range 0.67 - 1.57 kJ/mm (17 - 40 kJ/in). Boniszewski and Watkinson ⁽¹⁵⁾ also report no difference in cracking behaviour of a C-Mn steel for heat inputs in the range 0.55 - 2.75 kJ/mm (14 - 70 Kj /in).

2.4.5.2. Strain

It has been shown ⁽¹⁵⁾ that H.A.Z. hot cracking will only occur in C-Mn materials when weld metals with a freezing temperature greater

than 1285°C are used. This indicates that a constraint must be imposed on the H.A.Z. in the austenitic temperature range, when liquid second phase films might exist at prior austenitic grain boundaries. The importance of imposing strain on the H.A.Z. in a critical temperature range has also been confirmed in work on austenitic steel (60), where it was found that cracking could be prevented by using a low solidus weld metal, even though it had a comparatively high hot strength.

Important work by Meitzner and Stout (14) indicates that cracking propensity can be directly related to the weld bead profile, and that cracking is confined to the area under the shoulder of the weld (Fig. 5). In particular they related crack density with a parameter, D, which was proportional to finger penetration (Fig. 6). An increase in crack density with the D parameter was obtained for all energy inputs used. This, they claimed, showed that bead contour is influential in determining the local stress pattern in the H.A.Z. immediately after welding, and hence the likelihood of cracking. This work clearly infers that the occurrence of cracking will be affected by welding process, and that pronounced finger penetration should give greatest susceptibility to cracking, e.g. M.I.G. welded. In fact Meitzner and Stout showed that the M.I.G. process produced more cracking in HY 80 than did the shielded arc or the submerged arc processes.

On the other hand, investigations by Jordan (25) on HY 80 showed more cracking when welded using submerged arc than when welded by the M.I.G. process at a similar energy input, although finger penetration was more pronounced in the latter case. Masubuchi and Martin (19) report no differences in the cracking propensity of HY 80 when welded using the T.I.G. and metal-arc processes, though in this case, no comparisons of weld bead profile were made.

Disagreement exists also on the effect of joint detail. Laboratory

cracking tests by Masubuchi and Martin ⁽¹⁹⁾ on several joint details showed little difference in cracking behaviour. From these results, Boniszewski and Watkinson ⁽¹⁵⁾ argue that the long range stress-strain system dependent on joint geometry does not have time to develop within the critical temperature range for crack formation. However, Meitzner and Stout ⁽¹⁴⁾ point out that joint geometry may be important through its effect on the contour of the solidifying bead. They speculate that in crack sensitive materials, a butt weld or outer bead of multipass joints may solidify in such a way to cause H.A.Z. hot cracking, whereas single welds deposited in fillets or U grooves would tend to solidify with a more rounded contour and might contain very little cracking.

From a theoretical viewpoint it has been pointed out ⁽⁴⁾ that strain may be needed to be included as a variable of prime importance when considering the likelihood of cracking for a given welding procedure. Unfortunately, determination of specific values of strain, which depends on a complex interplay of plastic and elastic strains, solid state transformations, and transient heat flow, does not usually appear a feasible proposition. Apart from the factors already mentioned, the amount of strain in the H.A.Z. of any particular weldment will be determined by a number of factors. These include: plate thickness, bead size, joint geometry, welding sequence and weld metal strength. A schematic representation of the effect of bead size, plate thickness and joint geometry, on strain and restraint is shown in Fig. 7. In addition, the presence of any notches acting as stress concentrations may also cause severe local straining and thus increase the likelihood of cracking.

Measurements of strain have been made by Cargill, ⁽⁶²⁾ who reports tensile strains in the H.A.Z. of a Tee joint of up to 2%. However, even this work is of limited value as the measurements were made after

the weldment had cooled to ambient temperature.

2.5. Techniques Used in the Investigations of H.A.Z. Hot Cracking

2.5.1. Weld Cracking Tests

The most commonly used testing procedure for examining actual H.A.Z.'s is the bead-on-plate test.^(14,15,16,25,43) This is regarded by Boniszewski and Watkinson⁽¹⁵⁾ as sufficient for the assessment of hot tearing regardless of any eventual joint geometry applied in practice, as evidence from Masubuchi and Martin⁽¹⁹⁾ indicates that joint geometry has no effect on hot tearing. In the work of Boniszewski et al,^(15,16,43) weld beads were deposited normal to the rolling direction. Under such conditions the fusion boundary is normal to the fibre (segregated impurity regions elongated by mechanical working) direction, and they observed that hot cracking was usually parallel with the fibre. They also regard the taper section with its enlarged view of the H.A.Z. as essential. Meitzner and Stout⁽¹⁴⁾ and Jordan,⁽²⁵⁾ on the other hand, deposited weld beads parallel to the rolling direction. Both dispute the necessity of taper sections, relying instead on multiple transverse sections. Boniszewski et al also maintain that weld metal of matching composition or mild steel is necessary to reveal cracking, since it is absent with a lower yield point or lower melting point weld metal.

Since the microcracks are very small, careful metallographic techniques are needed to reveal them and the modified inclusions associated with them. Meitzner and Stout recommend a polish-etch-polish-etch procedure for specimen preparation.

Little progress has been made in quantifying the severity of cracking, most workers being content to use the qualifying adjectives 'few' and 'many' cracks. Meitzner and Stout have quantified this approach by counting the number of cracks per cross-section. Jordan carries this further by giving the length distribution as well. Being

so small there is often difficulty in deciding which are cracks. It has been noted (15,16) that lines of modified inclusions along grain boundaries drop out during polishing, indicating no cohesion with the matrix. It is thus reasoned that these are, to all intents, cracks.

2.5.2. Hot Ductility Studies

2.5.2.1. Introduction

It is generally accepted that hot cracking in the H.A.Z. occurs when the tensile strains in the weldment induced by the welding thermal cycle are sufficient to open up cracks along prior planes of weakness. These planes of weakness exhibit low ductility and/or strength and open up during the cooling cycle when the weldment strains are tensile. Thus it should be possible to correlate the high temperature deformation behaviour of a material subject to the weld thermal cycle experienced in the H.A.Z., with the hot cracking susceptibility of that material. This is the rationale behind the hot ductility test initially developed by Nippes et al (63) and subsequently used by a large number of other workers (63-80) in their investigations on hot cracking susceptibility.

Basically, the object of hot ductility testing is to devise a procedure which will clearly differentiate between 'crack sensitive' and 'crack resistant' materials. The test also has the ability to take account of welding process parameters, such as thermal cycle and strain. The great advantage of this test is that it should be possible to classify materials in degrees of crack sensitivity. 'In-situ' welding tests show only 'crack' - 'no crack' situations under specific conditions. A material in which cracking is incipient cannot be distinguished from a very crack resistant material.

The testing sequence is carried out in a thermo-mechanical weld simulator (termed 'Gleeble' by the Rensselaer Polytechnic Institute).

A review of these weld simulators, describing their principal features and applications has recently been made by Widgery. (64) The equipment reproduces in a cylindrical test bar, the time-temperature cycle which a desired portion of the H.A.Z. experiences during welding. At any selected instant during this simulated thermal cycle, the specimen may be pulled to failure by the application of a tensile load. During the test, a record is made of the thermal cycle, the ultimate tensile load required for failure, and the elongation. Subsequently, the reduction in area is measured.

Initially, the recovery of ductility on cooling from the 'nil-ductility' temperature, as measured by the reduction in area, was used to predict the cracking susceptibility of materials. However, discrepancies in the predicted behaviour of some materials has lead to proposals that other parameters may also have to be considered.

2.5.2.2. Description of Equipment

Most developments in thermo-mechanical weld simulation testing equipment to date have come from the United States, particularly by Nippes et al (63,65) at the Rensselaer Polytechnic. However, this type of equipment has also been developed in Russia. (66)

The very fast rates of specimen heating necessary to simulate actual welding thermal cycles are produced by the resistance of the specimen to the passage of electric current. Specimens are generally held in water-cooled copper grips and are supplied with power from a welding transformer. The power supplied to the specimen is controlled by an electronic current contactor by regulating the current to the primary of the heating transformer.

Control of the desired thermal cycle is achieved by electronically comparing the output of the control thermocouple, spot welded to the specimen surface, with that of the reference generator, (viz. the

computed thermal cycle). The difference in signal at any instant, controls the power applied to the specimen. If the output of the control thermocouple is below that of the reference generator, then current of the appropriate magnitude is immediately passed through the specimen to bring it up to the correct temperature. If the temperature of the control thermocouple is above that of the reference generator, the heating current is automatically stopped until the specimen reaches the proper temperature. A wide variety of reference generators have been used in this type of apparatus. These include: potentiometers (65) and electrolytic rheostats (66) operated by interchangeable metal cams giving a continuously varying cycle; also plug-in resistor networks (67) or potentiometer arrays, (68) giving a stepped cycle which approximates to a continuous cycle at very short step times.

The tensile testing system is usually capable of very high strain rates and allows determination of the ultimate load to failure at any selected point in the thermal cycle. The load can be applied by hydraulic (67), air/hydraulic (63,65,69), or electromagnetic systems. (66) Loading has also been applied using an Instron mechanical testing machine. (68) In the original 'Gleeble' apparatus, (65) crosshead speeds varying from 5.08×10^{-5} m/s to 1.14×10^{-1} m/s could be attained. In later versions of this apparatus, crosshead speeds of 5 m/s were reached. Russian equipment (66) is also capable of very high, though uncontrolled, strain rates. There is a limited amount of evidence (69) to suggest that the hot ductility behaviour of metals is invariant with increases in crosshead speed (in the range 3.80×10^{-3} to 1.08×10^{-1} m/s). In any case a short time to failure is desirable, particularly at fast cooling rates, as this enables the testing temperature to be defined more precisely.

2.5.2.3. Development of the Hot Ductility Test

The concept that the hot ductility behaviour of metals should correlate with their hot cracking susceptibility was first introduced by Nippes et al ⁽⁶³⁾ in 1955. It was initially received with considerable enthusiasm, and a number of other investigations quickly followed. ⁽⁶⁹⁻⁷¹⁾

In these early experiments ^(63,70,71) no means were available for measuring the ultimate tensile load to failure. The hot ductility, measured by the reduction in area, was used as the basis for assessing different materials. It was quickly established ⁽⁶³⁾ that the recovery of ductility during the cooling cycle (subsequently referred to as recovery of 'on-cooling' ductility) was markedly dependent upon the peak temperature (test maxima) used. For peak temperatures up to a certain value, the 'on-heating' ductility curve was identical to the 'on-cooling' ductility curve. When peak temperatures above this were used, considerable damage could result in the 'on-cooling' behaviour. It was soon realised that this critical temperature region corresponded to where the reduction in area on heating fell to zero (the 'nil-ductility' temperature), and by 1957 ⁽⁷²⁾ it became an established principle to use the 'nil-ductility' temperature as the test maxima.

Parallel to the establishment of the 'nil-ductility' temperature as the peak temperature, was the realization of the significance of the recovery of 'on-cooling' ductility. Heuschkel, ⁽⁷⁰⁾ testing a type 347 stainless steel forging with a poor weldability history, found that it exhibited a poor recovery in its 'on-cooling' ductility from a peak temperature near the 'nil-ductility' temperature.

More significant results were produced by Soldan and Mayne ⁽⁷¹⁾ who found considerable differences in the recovery of 'on-cooling' ductility between a group of austenitic steels. Moreover they were able to correlate these results with service behaviour. Steels with

a good service record were those which recovered ductility rapidly. On the other hand, steels with a poor recovery of ductility turned out to be crack susceptible in service.

The scope of this work was enlarged when Nippes, Savage and Grotke ⁽⁷²⁾ made a detailed study of the hot ductility characteristics of thirty-four materials of seventeen types of austenitic steels and Ni-based alloys. They were able to classify the hot ductility behaviour of these materials into five groups as shown in Fig. 8. Of these groups, two were for 'on-heating' behaviour only. Materials exhibiting H2 behaviour, viz. gradual reduction of ductility with increasing temperature, were believed to be crack susceptible. For those materials exhibiting H1 behaviour, additional 'on-cooling' tests were necessary to determine cracking susceptibility. Thus materials in class C1 were believed to be crack resistant, whilst those in class C3 (viz. poor recovery of ductility on cooling) were thought to be crack susceptible. Unfortunately of the thirty-four materials tested, there was service data for only seven. Indeed, it appears that the service data from at least several of these seven steels originated from Soldan and Mayne. ⁽⁷¹⁾ Though the service experience of these seven materials correlated well with the proposed classification, the limited service data included in this report makes it much less useful than if more such data had been available.

The measurement of ultimate tensile load to failure during hot ductility tests were being made by 1957, ⁽⁷²⁾ but no attempts were made to use these measurements until Kreisler ⁽⁷³⁾ and Williams ⁽⁶⁷⁾ suggested that hot strength measurements were an important part of testing for hot cracking susceptibility.

With the increasing popularity of hot ductility testing, the hot ductility behaviour of materials was used to predict the effect of various element additions ^(3,8) and of energy input ⁽⁷⁴⁾ upon their

cracking susceptibility. Unfortunately these experiments were not correlated with actual welding tests so again are of limited value.

An early indication that the interpretation of hot ductility behaviour might not be as straightforward as it first seemed, appeared with Moore's ⁽⁷⁵⁾ investigations on hot cracking in austenitic weld metal reheated by subsequent weld runs. He found that although two of the compositions showed a very poor recovery of ductility on cooling (C3 in the classification of Nippes) they could be welded satisfactorily.

Further discrepancies were noted by Kreisler ⁽⁷³⁾ although unfortunately little indication is given as to the proportion of materials whose service behaviour show discrepancies with respect to the Nippes classification. Three cases of materials which show poor ductility recovery yet are crack resistant in tests, and one case which shows good ductility recovery yet is crack sensitive, are quoted. This latter case is disputed by Soldan and Schnabel ⁽⁷⁶⁾ who claim that the material in question shows poor recovery of ductility.

In explaining these discrepancies, Kreisler proposed that the recovery of tensile strength on cooling could be equally important as ductility recovery, in predicting crack susceptibility. According to Kreisler, materials with a high yield strength, which at the temperatures involved is almost equal to the tensile strength, should be able to absorb much of the welding thermal strains elastically; whereas materials of lower yield strength would have to undergo correspondingly larger amounts of plastic strain with the attendant risk of hot cracking. Thus alloys having a high tensile strength at elevated temperature may be resistant to cracking though having poor ductility. Conversely, alloys having moderate ductility and poor strength may be crack susceptible. This work, however, was not continued to consider what combination of strength and ductility was needed to prevent cracking. Moore, ⁽⁷⁶⁾

reconsidering the apparent discrepant results of the two crack resistant weld metals, found that whilst ductility recovered slowly, the strength recovered well, thus supporting Kreisler's proposition.

This role of the recovery of strength has been disputed by Yeniscavich.⁽⁶⁹⁾ He pointed out that if two materials differ in strength at some specific temperature by, say, 68.94 N/mm^2 (10,000 psi) then assuming an elastic modulus of 206.7 GN/m^2 (30×10^6 psi), the extra strain which can be accommodated by the stronger material is only 0.03%. If it is assumed that the strain imposed on the H.A.Z. during its zero ductility range is much greater than this, the recovery of strength is of little importance. Though not stated, there always remains the possibility that a stronger zone in the weld may cause the overall strain to be concentrated in a region better able to accommodate it.

In addition to the recovery of 'on-cooling' strength criteria, Kreisler also proposed that other factors, albeit of secondary importance, might need to be considered when interpreting hot ductility data. These were:

- (a) Properties 'on-cooling' from both 'nil-ductility' and 'nil-strength' peak temperatures.
- (b) Temperature difference between 'nil-ductility' and 'nil-strength' temperatures.
- (c) Temperature range between 'nil-strength' values for weld metal and parent plate.

By assessing all these factors, particularly that of strength recovery, Kreisler was able to show a much improved correlation of hot ductility data of the nickel-based alloys with service performance.

Further attention was focussed on developing the hot ductility test and interpreting the resulting data by Williams⁽⁶⁷⁾ and

Yeniscavich.⁽⁶⁹⁾ Williams showed that damage to 'on-cooling' ductility in austenitic materials could be substantially increased by increasing the peak temperature above the 'nil-ductility' temperature. Moreover it was found that whilst the increase in damage to materials with low crack susceptibility was small, it was greatly increased with materials of high crack susceptibility. This lead Williams to use the 'nil-strength' temperature, rather than the 'nil-ductility' temperature as had been done previously. As the index of crack susceptibility he chose the temperature interval between the 'nil-strength' temperature and the point where ductility begins to recover on cooling (the 'zero ductility range'). This index of crack susceptibility appeared to correlate well with the service data of the materials, where available. Materials with a wide 'zero ductility range' were found to be crack sensitive whereas those with a narrow range were crack resistant. Unfortunately, of the four austenitic and five ferritic steels used, service data was only available for the former. It was observed by Williams that some ferritic materials, HY 80 in particular, displayed an intermediate region of considerably reduced ductility at about 1000°C - 1100°C. Similar ductility dip regions have been noted by other workers^(19,25) and it has been proposed⁽⁴⁾ that this phenomenon is responsible for 'ductility-dip' type cracking. This is partly based on the observation that these cracks appear to form in the region of the H.A.Z. which does not experience the very high temperatures associated with liquation cracking. However, it must be remembered that the 'ductility-dip' region, though associated with intermediate temperatures, only occurs after a peak temperature near the solidus has been reached.

Yeniscavich⁽⁶⁹⁾ also used a test maxima higher than the 'nil-ductility' temperature. He chose the solidus temperature, and like Williams, chose the 'zero ductility range' as the index for crack

susceptibility. This was found to correlate with the observed cracking behaviour of the five heats of Ni-based material examined. In a later paper, Yeniscavich ⁽⁷⁷⁾ reaffirms his confidence in the zero ductility range as the main criterion relating to cracking susceptibility, and that a mid-range ductility dip to zero ductility can be expected to cause severe cracking. He also proposes cracking will occur where a zero ductility plateau intersects the yield strength line. In recent work, again on austenitic steels, Gooch et al ⁽⁷⁸⁾ also showed that the zero ductility range correlated well with service behaviour.

An attempt to arrive at a clearer understanding of the two main criteria for cracking susceptibility, namely, the recovery of ductility and the zero ductility range, has been made by Duval and Owczarski. ⁽⁷⁹⁾ From their data on four Ni-based alloys, they produced three dimensional diagrams showing the zero-ductility at any instant and the recovery of ductility from the 'nil-strength' temperature, as a function of time after passage of the arc, and distance from the fusion line. Their results, which were correlated with service behaviour, showed that the recovery of ductility was by far the most important factor, and that the size of the zero-ductility range was not discriminatory. This they claimed, implied that H.A.Z. cracking occurs after solidification.

Somewhat outside the classical hot ductility tests, are the reports of Shreitz ⁽⁸⁰⁾ and Savage and Krantz. ⁽³⁶⁾ Shreitz examined the cracking susceptibility of HY 80 subject to a similar longitudinal restraint to that experienced in the H.A.Z. during welding. He found that cracks, which were detected ultrasonically, occurred only on cooling, between 1100°C and 1300°C. Savage and Krantz subjected composite specimens of plate materials containing a longitudinal bead-on-plate weld to a set amount of strain at a given temperature during the simulated welding thermal cycle. The strain needed for

incipient cracking was taken as the index for crack susceptibility.

A possible basic weakness in hot ductility testing has been discussed by Heuschkel.⁽⁷⁰⁾ He suggests that the heavy current flowing through the hot ductility specimen during heating will promote localised overheating, and subsequent liquation of non-metallic segregation, due to their higher resistance, at temperatures below those occurring in an actual H.A.Z. Thus it may be necessary to modify the interpretation of hot ductility behaviour and the metallography of hot ductility specimens. To date this suggestion does not appear to have been investigated by other workers.

2.5.2.4. Temperature Measurement

One of the prime requirements in hot ductility studies is that the temperature measurements are accurate and reproducible. This is particularly important where peak temperatures close to the solidus of the material are used, as small differences in these peaks may have a dramatic effect on subsequent behaviour. In addition, it is necessary for the interpretation of fracture faces and microstructure and when comparing data obtained by other workers in the field. Recently considerable confusion has arisen over the accuracy of temperatures measured by the standard technique of bare wire thermocouples, percussion welded to the specimen surface. While some investigators appear to assume implicitly that the recorded surface temperature was identical to the actual specimen temperature, other investigators report discrepancies. In thermal simulation work on ferritic steels, Vinckier⁽²⁶⁾ suggests that 'real temperatures might be higher than recorded temperatures', while Smith et al⁽⁸¹⁾ measured a 30°C difference between surface and centre of the specimen. Dolby and Widgery⁽⁸²⁾ in work with specimens obtained a similar difference which they attributed to the cross sectional temperature gradient and the technique of thermocouple

attachment; attached beads giving lower apparent temperatures than individually attached wires. Indicated surface temperatures over 100°C below the internal values were reported at temperatures of 1200°C by Coleman, ⁽⁸³⁾ who included a third factor, namely that of thermocouple 'heat-sink' effect which had been deduced theoretically by Baker et al. ⁽⁸⁴⁾ Keane, Bower and Hammond ⁽⁸⁵⁾ quote differences of 50°C in the signal from poorly attached thermocouples, compared to well attached thermocouples. Furthermore they report severe transverse and longitudinal temperature gradients in the thermally cycled specimens. At a centre temperature of 1000°C , their results show an immediate drop of 100°C in the first 10 mm along the specimen, with no evidence of a temperature plateau.

Clearly a great deal of confusion exists about the problem of temperature measurement and distribution in hot ductility specimens. This is obviously a deplorable state of affairs, and a systematic investigation to rectify the situation is necessary before embarking on further hot ductility studies.

2.5.2.5. Summary

To date, despite the large volume of work on the subject, there seems no clearly defined interpretation of hot ductility results which will unambiguously predict cracking susceptibility of a given material. It is interesting to observe that had an equivalent amount of effort been concentrated on concrete correlations with actual welding behaviour, instead of 'stamp collecting' hot ductility diagrams and speculating upon their implications, a solution would be much closer to hand. Contributing to the demise is the fact that many investigations are limited in scope, often considering only four or five materials, which are usually within a limited compositional range. Thus there is some uncertainty in confidently applying results, obtained from one material,

to another material. It is also interesting to note that of all the alloys investigated, most emphasis has been placed upon austenitic materials. Only a small number of ferritic alloys have so far been investigated.

Despite this somewhat disappointing progress, the following important points emerge from the developments in hot ductility testing to date:

(a) The rationale for correlating the hot ductility behaviour of alloys with their susceptibility to hot cracking, seems well based.

(b) Raising the test temperature maxima from the 'nil-ductility' temperature to the 'nil-strength' temperature or above, is now the generally accepted criterion for testing, as this usually causes more damage to 'on-cooling' ductility.

(c) At present the two main criteria for assessing crack susceptibility from the hot ductility tests are: the rate of recovery of ductility 'on-cooling' from the test maxima, and the 'zero ductility range'. In borderline cases it has been proposed that other secondary factors may be of significance, such as recovery of tensile strength. Both these main criteria are claimed by their supporters to give qualitative correlation with available service behaviour, in the majority of cases. The degree of quantitative correlation is not clear.

2.5.2.6. Future Work

In order that hot ductility testing may become established as a standard procedural test for determining hot cracking susceptibility, it is now necessary to:-

(a) Establish the parameters obtained from the hot ductility curve, which correlate with the incidence of cracking, under given welding conditions, and to assess their significance.

(b) These parameters would then be expressed as a quantitative

cracking index which can be correlated directly with the incidence of weldment cracking. This cracking index would be a purely material characteristic.

(c) A more sophisticated development would later include the effect of welding conditions, (i.e. thermal cycle, strain cycle, weld metal strength). This would then enable the crack susceptibility of any given material, under any given welding conditions, to be calculated.

2.6. Summary

Composition aspects have so far received most attention in the study of H.A.Z. hot cracking in ferritic steels. Sulphur is clearly one of the most potent elements if not the most potent. Phosphorus is also regarded by some investigators as highly potent, though mainly on the basis of weld metal studies. However, another school of thought suggests its effect is quite secondary to that of sulphur. It is the segregation of sulphur and phosphorus to the grain boundaries to form low melting point films, which can subsequently be pulled apart by tensile welding thermal strains, which is responsible for the occurrence of hot cracking in ferritic steels. Increasing carbon content is known to aggravate the problem, whereas manganese up to certain amounts is beneficial. Typical levels of sulphur, phosphorus and carbon to give a crack susceptible quenched and tempered steel would be: C = 0.20%, S \geq .020%, P \geq .020%. The effect of other elements on H.A.Z. cracking has not been conclusively shown, though from weld metal studies it appears likely that Mo and V are beneficial and Ni and Si detrimental. In any case their effects are quite secondary to those of S, P and C.

Though attempts have been made to quantify the effect of composition on hot cracking for weld metals, no attempts have been made to do this for the H.A.Z. alone. This still remains an important area for investigation.

It is known that adequate strain is necessary for the occurrence of cracking. However, difficulties in quantifying this have prevented the quantitative assessment of its effect, and its importance in relation to composition variables.

The effect of welding process variables has so far received little systematic investigation. Moreover, the evidence from these investigations on the effects of such parameters as heat input/unit length, joint geometry, and external restraint, tends to be conflicting. This is obviously a deplorable gap as it leaves the selection of welding process parameters on an ad hoc basis. Also there has been no work relating the influence of material and welding parameters upon hot cracking. Until this is done systematically, the solution of hot cracking problems in service will remain on a costly 'trial and error' basis.

The lack of quantitative H.A.Z. crack susceptibility formulae, such as have been produced for the weld metal is no doubt due to the time-consuming nature of assessing crack propensity from the standard bead-on-plate test. However, it is now of considerable importance to quantitatively assess the effect of material parameters on cracking as it has been shown that H.A.Z. cracking can still persist even when crack resistant filler wires have eliminated weld metal cracking.

Considerable attention has been placed upon the hot ductility test as a means of determining the hot cracking susceptibility of materials. Unfortunately much confusion over the test has arisen because different testing methods and criteria for evaluation have been used by different investigators. The limited correlation of hot ductility data with 'in-situ' tests and service performance has further delayed acceptance of the hot ductility test as a standard procedure. Thus a rigorous examination of the hot ductility test is still required in order to assess its

capability for differentiating between 'crack sensitive' and 'crack resistant' materials. This would have to include precise definition of the experimental parameters and the significant features of the resulting data in terms of susceptibility to cracking.

3.

EXPERIMENTAL INVESTIGATION

3.1 Introduction

From the review of literature on H.A.Z. hot cracking it can be seen that there are several areas which still require detailed investigation. The most important of these are:-

- (i) An increased knowledge of the influence of material composition and welding procedural variables upon H.A.Z. hot cracking.
- (ii) The establishing of a procedure of hot ductility testing, and interpretation of subsequent results, which will distinguish unambiguously between 'crack sensitive' and 'crack resistant' steels.

It was the object of the project to investigate these problems in low alloy hardenable steels of the $1\frac{1}{2}\%$ Ni-Cr-Mo and 1% Cr-Mo type. This was achieved by parallel weld cracking and hot ductility tests on selected steels. The investigation is concluded by metallographic and fractographic examinations of the specific features associated with hot cracking in both hot ductility specimens and the crack susceptible zone of the H.A.Z.

3.2. Selection of Materials

The choice of steels for the investigation was influenced primarily by two factors:

(i) The need to vary the composition to obtain steels with a wide range of cracking sensitivities. Carbon, sulphur and phosphorus were considered most important in this respect. Carbon levels ranged from 0.11 wt % to 0.46 wt %; sulphur and phosphorus from 0.001 wt % to 0.040 wt %.

(ii) That the steels should be of considerable commercial and technological interest. Two of the steels, SAE 4130 and EN 24, were chosen specifically for their interest in the aerospace industry.

A series of steels to the SAE 4130 specification, for various

combinations of high and low sulphur and phosphorus levels (high being nominally >0.030 wt % and low being nominally <0.010 wt %), were obtained by specially prepared casts, melted by G.L. Willon and Son. To obtain a range of carbon contents, steels to the EN 24 and ASTM A387B specifications at high and low sulphur and phosphorus levels were likewise obtained from Willon and Son. Two commercial casts, one of SAE 4130 and the other of EN 24, donated by Redheugh Iron and Steel Co. Ltd., were also used in the investigation. All steels were hot rolled to a plate thickness of 12.5 mm ($\frac{1}{2}$ in.).

Three additional special steels of SAE 4130, incorporating ultra low sulphur and phosphorus levels (0.001 wt %) were vacuum melted and cast by B.I.S.R.A. These steels were again hot rolled to 12.5 mm ($\frac{1}{2}$ in.) thick plate. The three combinations obtained were: ultra low sulphur, ultra low phosphorus; ultra low sulphur, high phosphorus; high sulphur, ultra low phosphorus. The ultra low sulphur and phosphorus combination was used as a reference material for both hot ductility and weld cracking tests. The latter two combinations were used to study the individual effects of sulphur and phosphorus in the hot ductility and weld cracking tests.

Sulphur and phosphorus levels of 0.001 wt % are impossible to obtain commercially. Electric arc steel making processes can achieve impurity levels down to about 0.010 wt % ea of sulphur and phosphorus. The ultra low levels of sulphur and phosphorus obtained in the present investigation were achieved by using carbonyl iron powder as the starting material. This powder was compacted, hydrogen reduced and sintered prior to being used as the feedstock material in the vacuum melting process.

Table 1 shows the proposed levels of carbon, sulphur and phosphorus which were desired for the investigational work. Chemical analysis figures for the actual steels, which were obtained by Quantivac analysis

and checked by conventional chemistry, are given in Table 2. It can be seen that the materials were generally within specification although they were somewhat less than ideal owing to difficulties in obtaining closely controlled compositions for substantial weights of material. It should be noted that in steel, S.D., extra manganese appears to have been substituted for silicon; and steel, E.C., has a high S, low P, combination instead of the desired high S, high P combination. It was particularly gratifying that the ultra low targets for sulphur and phosphorus were obtained.

For the M.I.G. welding tests, 1.58 mm (1/16 in.) diameter wires of two specifications were chosen; one being mild steel and the other, a 1% Cr-Mo wire for matching weld metal strength. Compositions are shown in Table 3.

3.3 Weld Cracking Program

3.3.1 Effect of Welding Procedural Variables

3.3.1.1 Selection of Significant Variables

The effect of welding procedural variables has so far remained a backwater for systematic study. Due to the conflicting results from the work so far conducted, it still is not immediately apparent which variables significantly influence cracking and why. Clearly there is a need to isolate the variables of primary importance, to compare their influence with that of composition and to determine how they exert their effect.

In the welding of ferritic steels, many process variables can be altered. These include: heat input, weld bead profile, weld metal composition, external restraint, plate thickness, joint detail, welding process, shielding gas, welding speed and so on.

For this investigation four variables were chosen as the most likely to influence cracking, namely weld bead profile, heat input/unit length, restraint and weld metal composition. These were investigated by a 4^2

factorial design experiment, and the results treated by analysis of variance.

3.3.1.2 Experimental Procedure and Design

Experiments were conducted on a crack sensitive SAE 4130 steel, code S.C., using the bead-on-plate technique described previously by Meitzner and Stout.⁽¹⁴⁾ Weld beads were deposited on a 12.5 mm ($\frac{1}{2}$ in.) thick plate, dimensions 0.23 m (9 in.) long, 0.10 m (4 in.) wide, along the rolling direction (Fig. 9a) using the metal inert gas (M.I.G.) process with argon 2% oxygen as shielding gas. Specifically, the weld beads were deposited using a BOC Universal welding head positioned over a traverse table. Gas flow rate was set at 1.27 m³/hr (45 cu. ft./hr). Recordings of travel speed, arc voltage and current were made for all welding runs. All test plates were surface ground free of scale and degreased prior to welding. They were also preheated to 200°C prior to welding to avoid formation of hydrogen induced cold cracking on cooling. These cold cracks, which are formed by a completely different mechanism, might otherwise be confused with hot cracks during metallographic examination.

After welding, transverse sections, 60 mm from the weld bead finish, were taken through the weld bead for metallographic examination and carefully mechanically polished. Since a small amount of disturbed metal on the polished surface could obscure the fine microcracks, the final polishing stages consisted of a polish-etch, polish-etch technique to eliminate the disturbed metal flow. The final etch was just deep enough to delineate the fusion boundary at magnifications of x100 and x500. The number of cracks, the combined crack length and the crack size distribution was then recorded. The combined crack length (c.c.l.) per section, which is the summation of all the crack lengths, was taken as the index of crack propensity, as it gives a better indication of the severity of cracking than does the number of cracks per section.

The investigation takes the form of a 4^2 factorial design experiment, incorporating each of the four variables at 2 levels, i.e. 2 energy inputs, 2 weld bead profiles, 2 restraint conditions and 2 welding wires. This makes a total of $2 \times 2 \times 2 \times 2 = 16$ tests in all. The technique of factorial design is described by Brownlee ⁽⁸⁶⁾ and was used to obtain maximum information from the experimental work.

Welding conditions were chosen to give deep and shallow finger penetration profiles at 1.2 and 3.0 kJ/mm (32 and 75 kJ/mm). Heat input, Q, was calculated from the theoretical heat input formula:

$$\text{Heat input/sec} = Q = \eta V I$$

where η is arc efficiency (taken as 75% for M.I.G. welding)⁽⁸⁷⁾

I is arc current

V is arc voltage

The extent of finger penetration was measured by the finger depth, C, (in terms of Fig. 5); the D parameter is also included. Deep finger penetrations were achieved using high current (500 amps) medium voltage settings, whereas shallow finger penetrations were achieved using low current (330 amps) high voltage (38 volts) settings. Full details of welding conditions and weld bead profile parameters are given in Table 4.

The two welding wires used in this investigation were 1.58 mm diameter, mild steel wire and 1% Cr-Mo wire for matching weld metal strength. Compositions are shown in Table 3.

For the unrestrained tests, weld beads were deposited on the standard test plates, as described previously and shown in Fig. 9a. In the restrained tests, the standard test plate was anchored to a mild steel base plate of dimensions: 0.3 m long, 0.2 m wide and 12.5 mm thick, with 0.95 mm fillet welds along all sides, see Fig. 9b. The test weld bead was then deposited on the standard test plate as before. Strain was thus imposed on the test H.A.Z., both by the constrained top plate and the superimposed welding

residual stresses.

3.3.1.3 Analysis of Variance Results

A full analysis of the cracking behaviour of each specimen, showing the number of cracks, combined crack length, crack length distribution and certain other parameters, per weld section, is given in Table 5. Using the combined crack length as the index of crack propensity, the results were examined by the analysis of variance technique with the aid of the University of Aston ICL 1905 computer statistics package. The analysis of variance as output by the computer is given in Table 6a and the significance tests in Table 6b. The results show that increasing both the heat input/unit length and the depth of finger penetration significantly increases the cracking severity. The types of weld metal used in this investigation did not significantly affect the test results, but there were indications that external restraint did increase cracking severity. In this latter case results were significant at the 10% level.

3.3.1.4 Detailed Metallographic Examination

A detailed metallographic examination of all specimens was made to determine the general nature and location of cracking and its relation to inclusions. In addition it was desired to gain a better understanding of the manner in which heat input/unit length and finger penetration affect cracking behaviour.

H.A.Z. hot cracks were intergranular, following the prior austenite grain boundaries. They occurred only in the coarse grained region of the H.A.Z., immediately adjacent to the fusion boundary, where the temperature had been sufficiently high to substantially modify the Type I Mn S inclusions. This zone is referred to subsequently as the 'modified inclusion zone' or M.I.Z. Micrographs of typical cracks are shown in Figs. 10 and 11.

Cracks varied in length from 0.01 mm to 0.28 mm and were often

associated with pockets of liquation material, indicating that cracking was of the liquation type. This was confirmed by examining crack surfaces using scanning electron microscopy (Figs. 18 to 25). These micrographs clearly show the smooth intergranular surfaces and the associated surface dendritic ferns. These ferns are indicative of prior liquation, and form when the liquid films solidify.

The identification of the modified inclusion zone was considered significant as it was observed that cracking only occurred within this zone. Type I Mn S inclusions were the predominant form of inclusions in the test plates. These inclusions were elongated and were strongly oriented in the rolling direction by the hot rolling process.

The inclusions maintained their morphology in the fine grained and part of the coarse grained region of the H.A.Z. However, in the high temperature coarse grained region immediately adjacent to the fusion boundary, considerable modification to inclusions were noted. Generally, inclusions had broken up into more or less globular particles and had lost their former orientation. In many cases they appeared to have melted in situ, leaving voids. Frequently arrays of these particles decorated the prior austenite grain boundaries, Figs. 12 and 13. In this respect Fig. 13 is particularly interesting as small intergranular cracks appear to originate from inclusions at the grain boundary. In other cases the modified inclusions formed clusters within grains, Fig. 14. In this case the sulphides probably had insufficient time to reach the grain boundaries.

The width of the modified inclusion zone appeared to be dependent upon the temperature isotherms around the weld bead perimeter. It can be seen from Table 5 that the maximum width of the modified inclusion zone is far greater for high heat input welds (0.65 mm) than for low heat input welds (0.30 mm). This in turn dictates the maximum distance

from the fusion boundary to which cracking can occur. The width of the modified inclusion zone could also vary considerably around the weld bead perimeter. This was especially true of the deep penetration welds. As expected the zone was widest at the weld shoulder where most of the heat was concentrated, and the temperature isotherms were widest apart. It was narrowest at the base of the weld finger where the temperature isotherms were closest together.

The H.A.Z. hot cracks were not distributed uniformly around the weld bead perimeter but were concentrated mainly at the weld shoulder. This was especially the case in the deep penetration welds. Cracks were usually perpendicular to the fusion boundary; only a few were parallel to the fibre direction. Weld metal cracks tended to be close to the fusion boundary and also concentrated at the weld shoulder. They were also usually perpendicular to the fusion boundary and in some cases extended across the fusion boundary into the H.A.Z. This preferential location and direction of both H.A.Z. and weld metal cracks indicates a concentration of strain at the weld shoulder.

3.3.2 Effect of Distance Along Weld Bead upon Cracking Propensity

This work was conducted as part of the program to determine the maximum crack inducing conditions. From a laboratory testing viewpoint it is of considerable importance to exaggerate crack inducing conditions so that the relative crack susceptibilities of materials can be assessed with greatest accuracy. It is also of advantage when laboratory welding tests are used as part of materials selection procedure to have a built-in safety factor. Finally, it is desirable to be able to specify all parameters which influence hot cracking severity, so that data obtained by other workers in the field can be analysed on a systematic basis.

Weld bead, S.C.1, (high heat input, deep finger penetration and external restraint), was chosen for this study because of its high

cracking level. Apart from the weld section taken previously at 60 mm from the weld bead finish, three more sections were taken at 20 mm, 50 mm and 120 mm from the weld bead finish and examined for H.A.Z. hot cracks as before. The results, which are set out in Table 7, show a five-fold increase in the combined crack length from near start to near finish of the weld bead. This big increase in the combined crack length along the weld bead is accompanied by an equivalent increase in the number of long cracks. For example, the section at 120 mm has 2 cracks greater than 0.06 mm whereas the 20 mm section has 16 cracks greater than 0.06 mm.

This increase in cracking along the weld bead is probably due to the increased distortional forces that arise as the weld bead progresses. In long butt welds, for instance, it is well known that the butting edges tend to separate as the welding arc progresses along the work piece.

3.3.3 Effect of Steel Composition and Restraint on Cracking Propensity

3.3.3.1 Testing Procedure

All steels to the SAE 4130, EN 24 and ASTM A387B specifications, as listed in Table 2, were used in this test sequence. Tests were undertaken to observe the effect of impurity level and steel type (which in this context essentially means the carbon level) upon cracking severity, and also to educe the relative crack sensitivities of the materials for correlation with the subsequent hot ductility data. In addition, more information was required on external restraint as the previous factorial design experiment, whilst indicating that restraint probably was significant, had not shown it conclusively.

Weld test beads were deposited on both standard and restrained test plates as previously described in section 3.3.1.2. The welding conditions were chosen to replicate the deep finger penetration, high heat input/unit length welds as used previously; they were chosen to maximise crack

inducing conditions. Again arc current was set at 500 amps, arc voltage at 34 volts and travel speed at 4.2 mm/sec. In the restrained test plates, transverse sections were taken at 20 mm and 60 mm from the weld bead finish. In the unrestrained plates they were taken 60 mm from the weld bead finish. The results, which include: number of cracks, combined crack length (crack index), crack length distribution and maximum width of the modified inclusion zone are recorded in Table 8.

3.3.3.2 Results - Effect of External Restraint

Examination of Table 8 shows that the order of the cracking severity of the respective steels (i.e. the order from most to least crack sensitive) observed in the restrained test plates, is similar to that observed in the non-restrained test plates. However, the range of crack severities was considerably amplified in the restrained plates, probably due to the more severe test conditions.

To ensure that this apparent observed effect was in fact significant as it appeared at first sight, the results were statistically analysed using the Paired Comparison method as set out by Duckworth.⁽⁸⁸⁾ The comparison of the crack indices for restrained versus non-restrained test plates, for specimens taken 60 mm from the weld bead finish, is set out in Table 9. From this analysis it can be seen that restraint is in fact highly significant. The significance level being better than 0.5%.

3.3.3.3 Results - Effect of Composition

For ease of interpretation of the composition effects, a schematic graph of crack index, obtained by taking the mean of the combined crack lengths (i.e. at 20 mm and 60 mm from the weld bead finish) in the restrained tests versus impurity level and steel specification, is shown in Fig. 15. The results clearly show that cracking is markedly dependent on the level of both sulphur and phosphorus. Cracking in ASTM A387B

and SAE 4130 was completely eliminated by reducing the impurity content to a sufficiently low level. Tests on the special SAE 4130 steels with ultra low sulphur or phosphorus showed that either element by itself at the high level could induce significant cracking, but phosphorus appeared to be the more deleterious. This deleterious effect of phosphorus is consistent with the observation that the low S, high P combination in SAE 4130 is considerably more crack sensitive than the high S, low P combination.

For a given impurity level, cracking increased from ASTM A387B through SAE 4130 to EN 24, indicating that carbon is also a crack promoter. From a practical viewpoint it is disturbing to note that H.A.Z. hot cracking occurred at the low S, low P level in both SAE 4130 and EN 24. In the latter case cracking was quite pronounced.

The results also suggest that nickel might be a crack promoter as there is a substantial increase in cracking level from SB to EB (low S, low P combination) and from SE to EA (high S, low P combination). Reference to the carbon content indicates insufficient difference to account for the increase in cracking (0.35 wt % C to 0.37 wt % C in the first case and 0.39 wt % C to 0.38 wt % C in the second). The major difference between the two steels is the nickel content.

Examination of the base metal oxygen content did not indicate that it had a first order influence upon cracking. However, as the experimental design did not include a comparison of similar steels at high and low oxygen contents, its role in H.A.Z. cracking must remain, for the moment, a matter of conjecture.

As stated previously, the combined crack length was taken as the index of crack severity. Close examination of the distribution of crack lengths and the distance cracks extend from the fusion boundary indicates this was a reasonable criterion for assessing crack sensitivity. Reference

to Table 8 shows that steels with the highest crack index also have the longest cracks and more cracks greater than a certain size, say 0.06 mm, than steels with lower crack indices. Moreover, cracks generally extend further from the fusion boundary in the steels with the highest crack indices and least in the steels with the lowest crack indices, e.g. 0.50 mm for SC (high S, high P) and 0.15 mm for SB (low S, low P).

As in Section 3.3.1.4 H.A.Z. hot cracking was only observed within the modified inclusion zone for all steels, except SG (ultra low sulphur, high phosphorus). In this latter case the inclusions were so few and small that it was not possible to determine the extent of this zone. Cracking extended up to 0.40 mm from the fusion boundary in SG so in fact it was probably within the M.I.Z. as typical maximum values for the M.I.Z. for the SAE 4130 steels ranged between 0.55 mm and 0.68 mm.

The width of the modified inclusion zone, where this could be measured, appeared to be fairly constant for SAE 4130 and EN 24 steels. Typical values for the maximum width of this zone, as measured at the weld shoulder were between 0.55 mm to 0.68 mm. For steel SB (low S, low P) this fell to 0.50 mm. It was not possible to measure the width of the modified inclusion zone in SY, SG and AA because of the small number of inclusions and their minute size. However, in the ASTM A387B steel AB (high S, high P) the modified inclusion zone appeared significantly narrower, the maximum width being between 0.40 mm and 0.45 mm.

A general examination of crack location in the steels, again showed cracking to be concentrated at the weld shoulder, and the direction of cracking tended to be perpendicular to the fusion boundary. Again weld metal cracks were frequently in close proximity to the fusion boundary and sometimes continued across the fusion boundary into the H.A.Z.

Cracking was not uniformly distributed across the modified inclusion zone but was greatest near the fusion boundary and least near the unmodified H.A.Z. This suggests that cracking severity increases as the peak temperature of the thermal cycle increases.

3.3.3.4 Regression Analysis

To round off the work on composition, a quantitative expression relating the crack index to composition would clearly be desirable. This was done by means of a multiple regression analysis of crack sensitivity on composition using the ICL 1905 computer statistics programme package. All chemical elements were considered singly and the computer was programmed to perform two analyses of regression using first the elements significant at the 99% level, i.e. all elements, then those significant at the 5% level. The analysis obtained at the 5% level is shown in Table 10. The analysis of regression of crack index on single elements significant at the 5% level yields the following equation:

$$\text{Crack Index} = 4.8 C + 26.8 S + 52.5 P \pm 1.04$$

where the elements are represented as wt %. The equation gives calculated values of crack index which show a correlation of 0.92 with observed values and a residual error of 0.50. The residual error is the standard deviation of the distribution of the observations about the regression. For this analysis there were 21 degrees of freedom, thus for 95% confidence the 't' parameter has the value of 2.08. Hence the 95% confidence limits for the prediction of the crack index value is $\pm 0.50 \times 2.08$, i.e. ± 1.04 . Thus the regression confirms the significance of the major crack promoting elements of carbon, sulphur and phosphorus.

3.3.4. Fractographic Examination

A detailed fractographic study was carried out on the heat affected zone cracking encountered in test welds, made with the experimental

steels, in order to gain a deeper insight into the nature and metallurgical features of the crack susceptible zone. This involved the examination of fracture faces, produced by breaking the specimens at room temperature, using scanning electron microscopy. The results from these investigations were also used for comparison with the fracture faces of hot ductility specimens.

Examination of the weldment fracture faces of the steels of medium to high crack sensitivity revealed an intergranular zone immediately adjacent to the fusion boundary in the H.A.Z. In the crack resistant steels no intergranular zone was noted. This intergranular zone was of equivalent width to the modified inclusion zone observed in the polished and etched metallographic sections. Further into the H.A.Z., the expected transgranular failure was observed. A composite micrograph showing the three zones of the weldment, namely the weld metal, intergranular H.A.Z. and transgranular H.A.Z. regions, is shown in Fig. 16. Detail of the weld metal-H.A.Z. boundary is shown in Fig. 17 and of the intergranular-transgranular H.A.Z. boundary in Fig. 18.

The intergranular zone is itself composed of three distinct types of area, see Fig. 19. These are:

- (a) free surfaces
- (b) fern inclusions covering completely or partially the grain faces
- (c) ductile dimpling.

The free surfaces clearly correspond to the liquation crack surfaces produced during welding. This can be seen by the strikingly smooth topography of the free grain surfaces and their association with the surface dendritic ferns. Indeed the association of these ferns with liquation cracking has been noted by other workers.^(4,16) Another striking feature is the grain boundary grooving. Further evidence that

these surfaces were formed at the high temperatures associated with liquation, comes from a comparison of the fracture faces of hot ductility specimens. This is discussed more fully in section 3.4.6 where it will be shown that free surfaces, with virtually identical features, exist on the fracture faces of hot ductility specimens broken 'on-heating' at temperatures of the Nil Ductility Temperature and above; also specimens which break on cooling with zero ductility. Specimens broken 'on-heating' below the Nil Ductility Temperature have an entirely different failure mode.

Examination of substructure on the free surfaces shows they are covered with surface striations which appear to be oriented in crystallographic directions. These striations, of which a detailed scanning micrograph is shown in Fig. 20, appear to be due to surface shear transformation products of martensite and bainite formed during the decomposition of austenite. The morphology and general dimensions of these striations is consistent with that reported by Christian ⁽⁸⁹⁾ in the studies on surface martensite transformations. The thermal faceting observed by Hemsworth et al, ⁽⁴⁾ on some H.A.Z. hot crack surfaces, and which has a thumbprint morphology of a much finer scale was not observed in these investigations. This could be due to the lack of resolution of the microscope or the fine features of faceting being obliterated by the subsequent surface transformations.

There was general similarity in grain shape and development between the various weldment fracture faces. However, some variation, though for the most part not large, was noted. Grain shape varied from a moderately rounded grain edge type (Fig. 19) to a more angular form (Fig. 21), characteristic of a more fully developed grain. Variations were also noted across the intergranular H.A.Z., being more rounded near the fusion boundary, and sharper near the transgranular region.

In general, grain size increased across the intergranular zone, being smallest near the fusion boundary and largest near the transgranular zone. In many cases branch cracking, normal to the fracture surface, was noted, Fig. 22. Holes in the grain faces were a particularly common feature in the intergranular region, Fig. 23. Holes were also frequently located at the centre of the fern dendrites, Fig. 25.

The fern dendrite areas varied in size from covering a small fraction of the grain surface to a virtually continuous grain boundary network. These dendritic areas stand proud of the surface when associated with the liquation crack surfaces, Figs. 19 and 24. Detailed examination of these areas, Fig. 25, indicate they consist of arrays of rod or globular particles separated by the white shear lips of the bulk material. These shear lips were formed during the room temperature fracture and indicate that the fern areas were not free surfaces but solid, albeit brittle, bridges between the grains.

The composition of the rod-like inclusions within the fern dendrites of steel SC (high S, high P) was qualitatively assessed using a Tracor energy dispersive analysis attachment to the scanning electron microscope. The resultant energy spectra for a rod-like inclusion, and also for a region of liquated crack surface without fern dendrites, taken for comparison, are shown in Fig. 26 and Fig. 27. In Fig. 26 (spectrum for rod inclusion) the energy peaks from left to right are sulphur (labelled by the 'bug' or tag), chromium, manganese, iron K_{α} and iron K_{β} . In Fig. 27 (spectrum for crack surface) the only peaks of significance are iron K_{α} and iron K_{β} ; again the 'bug' is on the sulphur position. These figures show a concentration of sulphur, manganese, and to a lesser extent chromium, in the rod inclusion and so is consistent with an Mn S type inclusion. The relative concentration of iron in the inclusion could not be properly assessed due to its overwhelming background swamping effect. It is note-

worthy that phosphorus is absent from the inclusion, probably because it redissolved in the matrix during cooling. No significant concentration of manganese, chromium or sulphur was noted on the actual hot crack surface. Analysis of rod inclusions in the high sulphur, nickel bearing steel, EC, again showed a significant concentration of sulphur, chromium and manganese but only a faint suggestion of nickel.

When the high sulphur steels were broken in regions with no liquation cracks, the intergranular zone was still readily apparent. In these cases the grain faces were covered with fern dendrites, and ductile dimpling, see Fig. 28.

Measurements of the surface area of liquation cracks indicated they may be more extensive than hitherto recognised. In some crack sensitive steels crack surfaces parallel to the welding direction were observed to be ≤ 0.6 mm wide and over 5 mm long. Indeed cracks may have been much longer than this as the specimen lengths examined were only about 5 mm long, i.e. the crack ran the whole length of the specimen. In addition it was noted that these H.A.Z. cracks were sometimes continuous with weld metal cracks to give combined widths of about 2.0 mm. It is interesting to note that the liquation cracks, which are usually referred to in the literature as small microcracks, could in many instances actually be observed by the naked eye in the polished specimens.

3.4 Hot Ductility Testing Program

3.4.1 Description of Equipment and Testing Procedure

Hot ductility tests were conducted using a Duffers Model 510 'Gleeble', which is a commercially available version of the hot ductility testing apparatus described by Nippes et al.⁽⁶³⁾ The hot ductility test consists of performing tensile tests on cylindrical steel specimens heated through simulated welding thermal cycles. Tests are made during both heating and cooling portions of the curve, at preselected temperatures. During the test, the thermal cycle, the ultimate load required for fracture

and the elongation are recorded. Subsequently, the reduction in area is measured.

A general view of the 'Gleeble' is shown in Fig. 29. On the right is the high speed tensile testing device, and on the left is the control console with the reference generator, and control and recording equipment. The load in the tensile testing device is applied using an air/hydraulic system capable of providing a maximum load of 44,822 N (10,000 lb) at any desired strain rate from 0.050 mm/sec to 38 mm/sec. For the present investigation, the highest strain rate of 38 mm/sec was used as this enabled the testing temperature to be defined more precisely. A close-up of the tensile testing system is given in Fig. 30 and this shows, from left to right, the load cell, movable crosshead with cylindrical ways, and the controlled atmosphere chamber completely enclosing the specimen. All tests were conducted in the controlled atmosphere chamber in an argon atmosphere, under slightly reduced pressure to prevent leakage of air back into the box. This prevented the oxidation of specimen fracture faces.

The cylindrical specimen is held in water cooled copper grips and heated with power supplied from the 50 kv-a transformer in the base of the tensile testing device. The water cooled copper grips, apart from serving as grips for tensile testing, provide a means for introducing current through the specimen, and ensure a rapid rate of cooling when the flow of current is stopped. The heating current is controlled electronically throughout the desired thermal cycle by comparing the e.m.f. output of the control thermocouple, welded to the specimen surface, with that of the reference generator (viz. the computed thermal cycle) and the flow of current is increased, decreased, or interrupted as required.

The thermal cycles to be simulated are programmed on the reference

generator program board. The instantaneous reference millivoltage which in turn controls the specimen temperature is taken from the program board by a rotating drum. The speed at which this drum rotates determines the time base of the program and hence the heating and cooling rates of the specimen. The speed at which the drum rotates can be varied by preset control switches to give the desired thermal cycle. A general view of the rotating drum, drive speed controls and reference generator board with typical thermal cycle programmed for simulation, is shown in Fig. 31.

The ends of the cylindrical hot ductility specimens are threaded and fitted with nuts to prevent slipping of the smooth water cooled copper grips during tensile testing. The specimen cross section was uniform, and dependence was placed upon the 'thermal notch' effect to break the specimen at its centre point. This proved effective in all cases.

All hot ductility specimens were machined from plate, or rod (in the case of SG, SH and SY), with their longitudinal axis parallel to the hot deformation direction, i.e. parallel to the 'fibre' direction.

Thermal cycles simulating H.A.Z. locations were determined using a computer program prepared by Coleman ⁽⁸³⁾, based upon Rosenthal's 2-dimensional heat flow equation. ⁽⁹⁰⁾

Rosenthal's heat flow equation states:

$$T - T_o = \frac{Q_o}{2K} \cdot e^{-\lambda v \epsilon} \cdot K_o(\lambda v R)$$

where T = temperature of point of interest in the plate

T_o = initial plate temperature

Q_o = heat input per unit time per unit plate thickness

K = thermal conductivity

$\frac{1}{2\lambda}$ = thermal diffusivity

V = welding speed

-ε = distance of point behind the heat source

$K_0(x)$ = Bessel function (second kind zero order) of the quantity x

$$R = (\epsilon^2 + y^2)^{\frac{1}{2}}$$

The relationship between temperature, welding parameters and co-ordinates is shown in Fig. 32. This expression applies to the welding situation where a full penetration weld is achieved in one pass. The evaluation of this equation in the form of a computer program, prepared specifically for the University of Aston ICL 1905 computer, is described fully by Coleman.⁽⁸³⁾ Typical weld H.A.Z. thermal cycles corresponding to a near solidus peak temperature of 1450°C, for heat inputs/unit length covering the range which might be encountered in practice in the M.I.G. welding of steel (1.0, 2.0 and 4.0 kJ/mm on 12.5 mm thick plate) are shown in Fig. 33.

The 2-dimensional situation was chosen because it most closely represented the welding of thin sheet as used in the aerospace industry. However, in the present investigation direct comparison with the thermal cycles in the actual weld beads was not to be expected because:

- (i) The weld beads were not quite full penetration.
- (ii) The deep finger penetration welds produced a variation in the temperature distribution around the weld bead perimeter and consequently a range of different thermal cycles would be expected.

Comparison of the computed 2-dimensional thermal cycles with data obtained by Shultz and Jackson⁽⁹¹⁾, who determined experimentally a thermal cycle for a 1.9 kJ/mm weld on 12.5 mm plate, showed that whilst the computed curve was generally slower than the experimental curve, they were of the same order of magnitude. In any case, as pointed out previously, there was no unique thermal cycle for the welds investigated in this project.

In fact absolute agreement between the thermal cycles for the hot ductility tests and weld bead-on-plate tests was not mandatory for this project since the former were primarily to be used to investigate the comparative effects of composition on hot deformation behaviour. Moreover, it was found that increasing the simulated heat input/ unit length from 2kJ/mm to 4 kJ/mm, on 12.5 mm thick plate, (curves 2 and 3 in Fig. 33) as shown in section 3.4.3.2, did not significantly affect the recovery rate of ductility or strength.

In view of these considerations the computed thermal cycle corresponding to the lower heat input/unit length of 2 kJ/mm on 12.5 mm thick plate (curve 2, Fig. 33) was used as the standard thermal cycle for examining the effect of steel composition on hot deformation behaviour. Subsequent comparisons of simulated and real H.A.Z. microstructures and fracture faces demonstrated that the particular simulated thermal cycle selected was an acceptable approximation.

3.4.2. Calibration Work on the Mechanical 'Gleeble' Weld Simulator

An essential requirement in hot ductility testing is that a sample of sufficient size for accurate determination of mechanical properties should be cycled accurately through a predetermined thermal program. The requirements which have to be met include selection of a suitable specimen size, accurate reproduction of the required thermal cycles, and detailed knowledge of the temperature distribution in the specimen during testing.

3.4.2.1. Determination of Specimen Dimensions

From the known performance of the 'Gleeble' ⁽⁶⁵⁾, attainment of the range of heating rates to simulate those found in practice, for the specimen dimensions to be considered, presented no difficulty. The major problem in simulating weld thermal cycles is in attaining fast enough cooling rates, and hence the choice of specimen dimensions was mainly based upon this consideration.

Cooling of the hot ductility specimen is achieved by conduction of heat away from the specimen by the massive water cooled copper grips. Controlled cooling rates are attained by balancing resistance heating, and conduction cooling, to give the programmed cooling cycle. It therefore follows that for accurate thermal cycle simulation, the natural cooling rate must be greater than the programmed cooling rate.

For a given peak temperature, specimen cooling rate will depend on:

- (i) specimen cross sectional area
- (ii) specimen gauge length.

A series of experiments were thus conducted to determine the combined effects of these two variables for gauge lengths of 12.5 mm, 25 mm and 57 mm and diameters of 6.2 mm and 10 mm. From the results shown in Fig. 34, it can be seen the gauge length is the main factor affecting the cooling rate, and that diameter is of secondary importance. Consequently the larger specimen diameter of 10 mm was chosen, as this would enable the most accurate determination of load. This latter point is particularly important at high temperatures, near the solidus, where the tensile load to failure becomes very small. The larger diameter specimen also gives a larger area for subsequent metallographic examination.

The choice of specimen gauge length was based on two opposing considerations:

- (i) That it had a natural cooling rate which was faster than the programmed cooling curve.
- (ii) That within the restrictions placed by (i) it should be as long as possible, in order to decrease the longitudinal temperature gradient (section 3.4.2.4.) and to facilitate a more accurate reproduction of the programmed thermal cycle.

These requirements were fulfilled for the standard thermal cycle of 2.0 kJ/mm by using a gauge length of 25 mm, see Fig. 34.

3.4.2.2. Temperature Reproducibility

The accuracy and reproducibility of temperature measurement and control *are* of critical importance in hot ductility testing, where the peak temperatures used are close to the solidus of the material and small differences in these peaks can have dramatic effects on subsequent hot deformation behaviour.

The temperature of a specimen heated in the 'Gleeble', is measured and controlled by a thermocouple welded to the specimen surface. It was envisaged that for any specimen material the reproducibility of the signal from a surface thermocouple would be affected by the type of thermocouple and the method of attachment. Accordingly, experiments were conducted with 0.25 mm diameter bare wire couples in Chromel/Alumel and Pt/Pt 13% Rh. The former couple has an emf output four times that of the second for a given temperature, but is restricted in application by its melting temperature of 1400°C. The methods of attachment involved beads and individual wires using percussion (capacitor discharge) and resistance spot welding.

The specimen set-up used to determine the reproducibility is shown in Fig. 35. A is the bare wire surface thermocouple and B is a sheathed thermocouple inserted into a close fitting blind hole drilled to the specimen centre. For each temperature determination the surface thermocouple was taken to a constant emf value and the corresponding internal temperature read directly from a potentiometer. The range of temperatures recorded by the sheathed thermocouple was taken as a direct assessment of the surface thermocouple reproducibility. After each determination the surface thermocouple was removed, the specimen surface cleaned, and a new couple set in place. A total of 10 measurements were made for each system and the results are shown in Table 11.

From the experiments with the percussion welded Chromel/Alumel couples it is clear that the reproducibility is much better with separately

attached wires than with the beads. At an indicated surface temperature of 1115°C the internal temperature varied by $\pm 7^{\circ}\text{C}$ for the former to $\pm 33^{\circ}\text{C}$ for the latter. In the case of the Pt/Pt 13% Rh at the higher indicated surface temperature of 1285°C , poor reproducibility ($\pm 38^{\circ}\text{C}$) was obtained with percussion welded separate wires but good reproducibility ($\pm 7^{\circ}\text{C}$) could be recovered by substitution of resistance spot welding as the technique of attachment. In all subsequent hot ductility experiments, the control Pt/Pt 13% Rh thermocouples were spot welded to the specimen surface as separate wires. These results show that surface attached thermocouples can give reproducible behaviour but that they are very sensitive to the technique of attachment. Furthermore a technique which is suitable for one thermocouple-material combination may be unsuitable for another combination. Presumably the latter must be explained in terms of the soundness of the metallurgical bond produced by each technique for the materials covered.

The ability to reproduce the programmed thermal cycle in the specimen using the 'Gleeble' controls, which was the other main factor affecting temperature reproducibility, was also investigated. From the u.v. chart records, it was found that temperatures were reproduced within $\pm 7^{\circ}\text{C}$. Somewhat better reproducibility was achieved during the cooling portion of the curve. When the odd test run did not fall within $\pm 7^{\circ}\text{C}$ of the objective peak temperature, the subsequent results were discarded.

3.4.2.3. Thermocouple Calibration

The experimental work on the reproducibility of thermocouples attached to the specimen surface had shown that the indicated surface temperature was in fact considerably lower than the temperature at the specimen centre. With Chromel/Alumel couples, about 50°C at 1167°C and with Pt/Pt 13% Rh about 110°C at 1285°C , see Table 11. For couples attached as separate wires to the surface these effects

could be due to the cross sectional temperature gradient and the thermocouple 'heat-sink' effect. Examination of the temperature distribution in the specimen which is described later showed that the cross sectional temperature gradient at about 1180°C was $\leq 10^{\circ}\text{C}$. In the light of this fact it appeared that the major effect was due to the surface thermocouple heat-sink effect and that calibration to take care of this could be carried out by comparison with the temperature at the specimen centre.

Measurement of the internal temperature obviously involves the introduction of thermocouples into the specimen interior. It was recognised that this involved disturbing both the heat flow and heating current flow in the specimen. Furthermore the internal couple itself would be subject to a 'heat-sink' effect. Both factors could affect the validity of the thermocouple calibration. In order to assess this problem, four different thermocouple assemblies were used which involved both radial and axial insertion:

- A. A 0.50 mm diameter sheathed Chromel/Alumel couple inserted radially into a close fitting blind hole located at the specimen centre.
- B. As for A, but using a 1.56 mm diameter sheathed Pt/Pt 10% Rh thermocouple.
- C. A 0.25 mm diameter bare wire Pt/Pt 13% Rh thermocouple, insulated using twin hole ceramic insulators, inserted axially along a 2.5 mm diameter blind hole drilled to the specimen centre. The thermocouple was percussion welded to the inside surface.
- D. As for C, but the internal couple, though still at centre, not welded to the inside surface.

In each experiment the temperature of the surface was measured

and controlled using a 0.25 mm diameter bare wire Pt/Pt 13% Rh thermocouple spot welded as separate wires. The specimen temperature was raised in step sequence; being held constant at each step whilst simultaneous potentiometric determinations of surface and internal thermocouple emf were made. Full details of the results are shown in Fig. 36 as a graph of surface emf V^S internal temperature and in Fig. 37 as Temperature difference (internal-surface) versus Internal temperature. It is apparent from both graphs that there is considerable variation between the four calibrations. Two factors could be responsible for this variation.

- (i) Radial thermocouples cutting across the lines of current flow may give rise to localised heating at the tip of the sheathed thermocouple due to the reduction in cross sectional area. This would give a high reading.
- (ii) All internal couples may be subject to 'heat-sink' effects which would result in a low reading.

To investigate the former effect, the bare wire surface thermocouple and the sheathed 0.5 mm diameter Chromel V^S Alumel thermocouple, were differentially connected to measure the temperature difference (ΔT) between the surface and interior. The two resulting emf outputs were fed into the two channels of a multi-channel u.v. recorder. The specimen was then taken up to a temperature plateau and the heating current switched off, and on again, to determine its effect. From the resulting Temperature V^S Time, and ΔT V^S Time curves shown in Fig. 38, it can be seen that there is no localised heating of the sheathed thermocouple due to the passage of heating current. In fact there actually appears to be a small cooling effect of about 2°C.

Unfortunately it was not possible to repeat this experiment with

the larger diameter (1.56 mm) Pt V^S Pt 10% Rh internal couple because the small ΔT emf output was swamped by background interference. However, from Fig. 37., it can be seen that the recorded temperature difference between the centre and surface is much larger than for the Chromel-Alumel sheathed couple. This probably indicates that considerable localised heating is occurring in this case.

Both axial thermocouples (C and D) give lower temperatures than the Chromel-Alumel radial couple, indicating they may suffer from 'heat-sink' effects. This seems certainly the case in assembly D, where there is considerable resistance to the transfer of heat from the specimen to the thermocouple junction across the air gap.

An approximate assessment of the validity of these calibrations can be made by considering the melting point of SAE 4130. This is given as 1535°C by the Aerospace Structural Metals Handbook.⁽⁹²⁾ In hot ductility tests it was found that all heats of SAE 4130 melted at a surface indicated emf between 16.45 mV and 16.7 mV. The corresponding temperatures obtained by extrapolating the four calibrations to the melting points are listed in Table 12. From this table it can be seen that calibration A gives best correspondence with the published melting temperature. This is in agreement with the tentative conclusions reached previously. Thus calibration A was used to compute the temperature values in all subsequent hot ductility work.

3.4.2.4. Temperature Distribution

A knowledge of the temperature distribution existing in the thermally cycled specimens is necessary for accurate interpretation of fracture surfaces and of microstructures. It is also important to know how much of the specimen is experiencing the desired thermal cycle.

In establishing the temperature distribution of the thermally cycled cylindrical specimen, measurements were made of both the longitudinal and

cross sectional temperature gradients at a selected peak temperature and over the full thermal cycle. Longitudinal temperature distributions were determined for gauge lengths of 12.5 mm and 25 mm, using thermocouples spot welded along the top surface at various distances from the specimen centre.

The resulting values were converted to internal temperatures using calibration curve A in Fig. 36 and are plotted in Fig. 39. As expected, the shorter gauge length has a much steeper gradient overall. However, in both cases, there is a central plateau of 5 mm, over which the temperature drops by only 10°C .

The cross sectional gradient was measured at the centre section by inserting a 0.5 mm diameter sheathed Chromel V^S Alumel thermocouple into a close fitting diametral hole drilled through the specimen. The first measurement was taken at the surface opposite the point of thermocouple entry; in subsequent measurements it was progressively drawn back through the hole by measured distances. The results, shown in Fig. 40, indicate an asymmetrical temperature distribution about the centre. This is due to the thermocouple heat-sink effect at the smaller immersion depths. Taking this into account, there is a gradient, from surface to centre, of 10°C at an internal temperature of 1200°C . Temperature measurements over the full thermal cycle were made, where it was found that positions experiencing the same peak temperature, also experienced the same thermal cycle.

3.4.2.5. Summary of Calibration Studies

The results obtained with the different thermocouples and methods of attachment have confirmed that wide differences can occur between the indicated surface temperature and the internal temperature of resistance heated ferritic steel specimens. This is made up of a lack of reproducibility in thermocouple behaviour arising from variations in the

bonding to the surface and a reduced signal due mainly to the thermocouple 'heat sink' effect. However, by appropriate choice of attachment technique and careful calibration against the internal temperature, it has proved possible to obtain signals from surface attached thermocouples with a reproducibility of $\pm 7^{\circ}\text{C}$ up to peak temperatures of about 1400°C . This was considered satisfactory for the hot ductility testing program.

It is apparent that the reproducibility of signals from surface thermocouples is strongly influenced by the technique of attachment so that in the present work the scatter varied from $\pm 38^{\circ}\text{C}$ to $\pm 7^{\circ}\text{C}$. From the work with the Chromel/Alumel couples it is clear that attachment of separate wires is superior to fused beads. Furthermore, in the case of the Pt/Pt 13% Rh thermocouples it was necessary to use resistance spot welding instead of the more usual practice of percussion welding, in order to obtain comparable reproducibility to that obtained in Chromel/Alumel couples. Clearly the optimum method of attachment can depend upon the thermocouple-material combination being used. It would therefore appear to be essential to confirm experimentally that the optimum thermocouple technique has been established before embarking upon thermal simulation work.

The recorded surface temperatures were consistently lower than the internal temperatures of the cylindrical steel specimens; being about 35°C at 1000°C and about 60°C at 1400°C . Since the cross sectional temperature gradient was $\leq 10^{\circ}\text{C}$ the major part of this difference was due to the thermocouple 'heat sink' effect. Once reproducible behaviour has been obtained, the surface thermocouple can be calibrated against the internal temperature using small diameter thermocouples inserted radially from the surface.

It is apparent that the temperature distribution in the central

region of the 10 mm diameter rods was very uniform for both the 12.5 and 25.0 mm gauge lengths. In particular the cross sectional temperature gradients were $\leq 10^{\circ}\text{C}$ at an internal temperature of 1200°C , Fig. 40, and there was a temperature plateau of 5 mm showing less than a 10°C drop for an internal temperature of about 1400°C , Fig. 39. Thus a region of appreciable size in the centre of the specimen receives a uniform reproduction of the thermal cycle to the selected peak temperature. This meets the requirements for the determination of ductility and strength during the thermal cycle which is required for the study of high temperature liquation cracking. In addition it yields specimens of suitable size for study of the room temperature microstructure and properties of heat-affected zones.

3.4.3. Hot Ductility Testing

3.4.3.1. Effect of Peak Temperature

In this first phase of the hot ductility program, the effect of three peak temperatures on the recovery of on-cooling ductility and strength, using the standard thermal cycle of 2kJ/mm (curve 2, Fig. 33) was investigated. These peak temperatures were: the nil ductility temperature (N.D.T.), the nil strength temperature (N.S.T.) and 12°C below the bulk melting temperature. This latter temperature was chosen to simulate the thermal cycle experienced by those regions of the H.A.Z. which are very close to the fusion boundary. The melting temperature was taken as that temperature where melting was sufficiently extensive to cause the specimen to sag visibly under its own weight. The crack sensitive steel, SC, was used in this investigation to ensure maximum damage to the on-cooling deformation properties at a given peak temperature.

The results of this investigation, in the form of hot ductility and hot strength curves, are set out in Figs. 41a and 41b, and show a marked

increase in damage to on-cooling ductility and strength as the peak temperature is increased. Little damage to the recovery of 'on-cooling' ductility and strength was observed when the nil ductility temperature was used as the test maxima. In this respect it will be noticed that the zero ductility range at this peak temperature is very narrow indeed. In view of the small amount of damage caused by using a peak temperature of the N.D.T., all subsequent work was concentrated on using the N.S.T. and 12°C below the melting temperature as test maxima.

3.4.3.2. Effect of Thermal Cycle

This program was conducted, using crack sensitive steel, SA, to determine the effect of thermal cycle, corresponding to different weld heat inputs, upon the rate of recovery of 'on-cooling' ductility and strength. Two computed thermal cycles corresponding to weld heat inputs of 2 kJ/mm and 4 kJ/mm on 12.5 mm thick plate (curves 2 and 3 in Fig. 33) were used. Specimens were broken on cooling from the nil strength temperature (1480°C), and the resultant ductility and strength curves shown in Figs. 42a and 42b. From these curves it can be seen that there is no significant effect of thermal cycle, in the range investigated, on the rate of recovery of on-cooling ductility and strength.

3.4.3.3. Effect of Composition

Hot ductility tests were conducted on all steels used in the weld cracking program, with the exception of steel EA. All specimens were subjected to the standard thermal cycle of 2 kJ/mm (curve 2, Fig. 33) and were broken on-heating and on-cooling from two peak temperatures, namely the nil strength temperature and 12°C below the bulk melting temperature of the particular steel. The hot ductility and hot strength curves obtained from this investigation are shown in Figs. 41a and b through to Fig. 52a and b. The nil-ductility temperature, nil strength temperature and melting temperature for each steel are listed in Table 13.

From an examination of these curves, the following generalised points are apparent:

(i) All steels broken on-heating show a slow increase in ductility from the lowest test temperature of about 700°C to over 1350°C . In this range ductility increases from about 80% reduction in area (R.A.) to 99% R.A. It should be noted that there is very little effect of steel type and impurity content in this range although the low sulphur steels show slightly higher ductility values at the lower test temperatures.

(ii) All steels broken on-cooling from both peak temperatures exhibit a zero ductility range (Z.D.R.) before ductility begins to recover.

(iii) For the steels tested, a considerable range of recovery rates of ductility and strength was noted; also there was a considerable variation in the width of the zero ductility range.

In general, crack resistant steels with low impurity contents like SY and AC showed a good recovery of ductility and strength, whereas crack sensitive steels with high impurity contents like SA and SC showed poor recovery of ductility and strength. A detailed analysis of the relation between the cracking sensitivities of the respective steels with their hot deformation behaviour will be considered in the next section (3.4.4.).

(iv) Using the higher test maxima, (12°C below melting), always resulted in more damage to the recovery at on-cooling ductility and strength and an increase in the width of the zero ductility range. The increase in damage to the low impurity, crack insensitive steels was small, whereas in the high impurity, crack sensitive steels the damage was far greater.

(v) For the steels tested there appeared to be a relation between the width of the zero ductility range and the rate of recovery of strength.

Thus, steels which displayed a narrow %D.R. (e.g. SY and AC) also displayed a good rate of recovery of strength. Conversely, steels which showed a wide %D.R., showed a much poorer recovery of strength (e.g. SC and SD).

(vi) Most steels displayed a ductility dip region, similar to that reported by other investigators, between 900°C and 1100°C (67). In this region, the ductility fell to values ranging from 15% R.A. to 55% R.A., depending upon steel type and peak temperature. The ductility dip region was not accompanied by a corresponding 'strength dip' region. It will be noted that the ultra low impurity steel SY, did not display a ductility dip region.

(vii) Reference to Table 13 indicates that the nil ductility temperature, nil strength temperature and melting temperature are dependent on the overall steel composition, and to a lesser extent on the impurity content. The size of the temperature interval between the melting temperature and the N.D.T. is of considerable interest as it is probably related to the width of the crack susceptible zone. It is a well established principle of hot ductility testing that damage to on-cooling ductility and strength only occurs when the particular material experiences peak temperatures of the nil ductility temperature or above. The temperature interval between the N.D.T. and the melting temperature is relatively constant for the EN24 and SAE 4130 steels (being about 75°C), with the exception of the ultra low sulphur, ultra low phosphorus steel, SY, where it falls to 53°C.

Both SG (ultra low S, high P) and SH (high S, ultra low P) display the higher temperature interval of 74°C. The ASTM A387B steels, AA and AB, also have a lower temperature interval, being 52°C and 57°C respectively.

3.4.4. Correlation of Hot Deformation Behaviour with Cracking Propensity

One of the important aims of the work was to establish a procedure of hot ductility testing and interpretation of subsequent results which will distinguish between crack sensitive and crack resistant steels. Thus it is now necessary to examine more closely the hot deformation behaviour of the materials in order to determine which parameter(s) give best correlation with the observed cracking behaviour. A review of the literature has indicated several parameters which might be important in this respect.

- (i) The rate of recovery of on-cooling ductility as proposed by Nippes et al.⁽⁷²⁾
- (ii) The Zero Ductility Range on-cooling proposed by Yeniscavich.⁽⁶⁹⁾
- (iii) The temperature range on-cooling for recovery to a specific ductility level. (Thus would essentially be a combination of (i) and (ii)).
- (iv) The rate of recovery of ultimate tensile strength as proposed by Kreisler.⁽⁷³⁾

The results will now be assessed in the context of these parameters.

3.4.4.1. The Rate of Recovery of On-Cooling Ductility

This criterion proposes that materials showing a good rate of on-cooling ductility should be crack resistant whereas those showing a poor rate of ductility recovery should be crack sensitive. Previous investigators who have used this criterion to assess their results, have considered good and poor recovery on a fairly qualitative basis. For the purposes of this discussion, the recovery rate criterion will be treated in a similar qualitative manner as it was evident that, although there was a general tendency for the rate of ductility recovery to reflect the cracking sensitivity of the material, several discrepancies were immediately apparent. These discrepancies were of a

sufficiently serious nature to indicate that the recovery rate criterion could not be used to distinguish unambiguously between crack sensitive and crack resistant materials. The most serious discrepancies concerned EC (Fig. 52a) which was highly crack sensitive and EB (Fig. 51a) which was moderately crack sensitive. Both these materials showed a relatively fast rate of ductility recovery when tested from the nil strength temperature and would be considered crack resistant using a recovery rate of ductility criterion. Furthermore, AB (Fig. 50a) showed the poorest rate of recovery yet was in fact only moderately crack sensitive whereas SD (Fig. 44a) which was highly crack sensitive showed an intermediate rate of ductility recovery.

3.4.4.2. The Zero Ductility Range

When cooling from a peak temperature above the N.D.T. the ductility remains at zero for a certain temperature range before recovering. The width of this zero ductility range (Z.D.R.) measured from the particular peak testing temperature has been suggested ⁽⁶⁹⁾ as a parameter which can distinguish between crack sensitive and crack resistant materials. Materials with a wide Z.D.R. would be crack sensitive whereas those with a narrow Z.D.R. would be crack resistant. The applicability of this criteria was tested by plotting the crack index for each steel, obtained from the weld cracking tests, against the zero ductility range for each of the 2 peak temperatures used in the hot ductility investigation, see Fig. 53. It can be seen that there is a good correlation between the actual cracking propensity of the steel and the width of zero ductility range obtained using either the nil strength temperature, or 12°C below melting as the peak test temperature. In this respect, the higher peak temperature appeared the more discriminatory as it amplifies the range of Z.D.R.'s between crack sensitive and crack resistant steels. Thus for the nil strength temperature, values ranged from 30°C for the most crack resistant steel to 81°C for the most crack sensitive,

whereas for the higher peak temperature they ranged from 62°C to 178°C.

3.4.4.3. Recovery to Specific Ductility Levels

This is essentially a combination of the Z.D.R. criterion and the recovery rate of ductility criterion. In a similar manner to the previous section, plots were made of crack index V^S the temperature interval between the peak temperature and recovery to various levels of ductility, e.g. 5% R.A. and 25% R.A.

The degree of quantitative correlation with actual cracking behaviour markedly deteriorates as the level of ductility increases, even at the 5% R.A. level the degree of quantitative correlation is poor (Fig. 54). These results indicate that this type of parameter does not discriminate accurately between different levels of cracking sensitivities.

3.4.4.4. Recovery Rate of Strength

As mentioned previously, examination of the hot deformation behaviour of the steels used in this investigation indicated that there was a relation between the width of the zero ductility range and the initial recovery rate of strength up to the point where it recovered to the on-heating values. It was thus not surprising to find that the temperature interval between the peak test temperature and recovery to specific strength levels could also discriminate between the relative cracking tendencies of the various steels. Quantitative correlations were observed up to about 30 MN/m² (which is about 75% of the knee value of the on-heating strength curve) and was best at 20 MN/m², (Fig. 55).

3.4.5. Impact Testing

In order to examine the properties and behaviour of the high temperature region of the weld H.A.Z. more closely, specimens of SAE 4130 were thermally cycled, at the standard cycle corresponding to 2.0 kJ/mm,

to a series of peak temperatures both below and above the nil ductility temperature. The specimens were subsequently impact tested at 100°C. This temperature was chosen to promote a ductile failure mode. These impact specimens were non standard, being the ordinary hot ductility cylindrical specimens of 10 mm diameter, and containing a slit 2 mm deep produced by an abrasive wheel instead of a machined notch. Three impurity levels were investigated, namely; high S, high P (SA); low S, low P (SB); ultra low S, ultra low P (SY). The results, set out in Fig. 56, show that with increasing peak temperatures below the bulk melting temperature, the toughness falls to very low values. When a melted specimen was tested the toughness rose significantly. Considerable damage to the toughness properties at high temperatures was evident even in the ultra-low impurity steel, but the damage markedly increased with increasing impurity content. For the high impurity steel specimens, the nil ductility temperature seems to coincide with the sharp drop in toughness values.

3.4.6. Metallography of Hot Ductility Specimens

Fractographic and conventional metallographic examinations were made on the hot ductility specimens, both for comparison with the studies on the actual H.A.Z., and for interpretation of the hot ductility curves. Most work was centered on the crack sensitive steel, SC, but other steels were also examined to confirm specific features.

3.4.6.1. Metallography

In the metallographic examination, hot ductility specimens were sectioned along the longitudinal axis and polished and etched in the conventional manner. Both nital (2%) and S.A.S.P.A. - teepol were used as etching agents to reveal specific features.

Examination of the polished and etched surfaces of the hot ductility specimens revealed many of the features found in the actual H.A.Z.

Specifically, intergranular cracking and modification to the MnS type inclusions were only observed in specimens experiencing peak temperatures of the nil ductility temperature, and above, e.g. for steel, SC, this was 1440°C, i.e. intergranular cracking was only observed in the high temperature region within the modified inclusion zone.

Furthermore, these inclusions modifications were very similar to those observed in the modified inclusion zone of the actual H.A.Z. Again the formerly MnS stringer type inclusions broke up into more or less spherical particles and lost their former orientations. Examples of modified inclusions decorating prior austenite grain boundaries and of modified inclusion clusters are shown in Figs. 57 and 58. These can be compared with similar formations within the actual H.A.Z., (Figs. 12, 13 and 14). Again many holes were noted at grain boundaries and within grains. Variations in grain size in the longitudinal direction of specimens experiencing peak temperatures close to the melting temperature were also noted. Grain size was smallest in the highest temperature region near the fracture face and increased to a maximum just beyond the modified inclusion zone.

3.4.6.2. Fractography

The fracture faces of hot ductility specimens broken, at specific temperatures, on-heating, on-cooling from the nil strength temperature and on-cooling from 12°C below the melting temperature were examined using scanning electron microscopy. The fracture faces of the impact specimens, thermally cycled to various peak temperatures, were also examined by this method.

(i) Specimens Broken On-heating

The 'on-heating' curve can conveniently be considered in 3 stages, proceeding from lowest to highest testing temperature. This may be observed in any of the actual on-heating curves, Figs. 41 to 52.

Stage I: Slow increase in ductility from the lowest test temperature of 600°C to about 1350°C . In this range ductility increases from about 80% reduction in area (R.A.) to 99% R.A.

Stage II: Sudden decrease in ductility to zero over a very narrow temperature range.

Stage III: Ductility continues at zero until bulk melting occurs.

Specimens broken on-heating during Stage I exhibit an entirely ductile failure mode, Fig. 59. This ductile failure mode continues into the first part of Stage II down to about 50% R.A. Below this, the mode changes to a mixed intergranular/ductile failure; the intergranular mode quickly becomes more dominant with decreasing ductility. By 35% R.A. a few small holes can be seen at the grain faces in the intergranular regions. Specimens broken at the nil ductility temperature exhibit a completely intergranular fracture mode, Fig. 60. At this stage the grain outline is very sharp. Note also the numerous holes at the grain faces. The fracture faces of low sulphur steels, broken at the N.D.T. show far fewer and smaller holes. Examination of the substructure of these 'clean' grain surfaces showed they were covered with striations virtually identical with those observed in the intergranular region of the actual welded specimens. These striations were observed on the surfaces of 'clean' grains broken both on heating and cooling. These striations are particularly well illustrated in Figs. 65 and 67, though they can be readily observed on all specimens broken with zero ductility. For comparison with the actual H.A.Z. see Fig. 20.

As the peak testing temperature increases to just below the nil strength temperature, rounding of grain edges and corners is observed, probably due to preferential melting of these regions; also the holes at the grain faces become larger, see Fig. 61. The rounding process

extends to the grain face in specimens heated above the nil-strength temperature, Fig. 62. The holes at the grain faces become smaller and shallower, presumably due to the progressive melting of the grain surface. Finally, in the specimens heated to within 6°C of the bulk melting temperature, see Fig. 63, extensive melting has obviously occurred. Many of the grains have broken up into small clusters and very few holes can be seen at this stage.

(ii) Specimens Broken On-cooling from the Nil Strength
Temperature

Specimens broken within the zero ductility range (Z.D.R.) exhibit a completely intergranular fracture mode. As ductility begins to recover the failure mode changes to mixed intergranular/ductile, and finally becomes predominantly ductile. Within the Z.D.R. there is a certain amount of variation in the granular appearance and the surface features. Specimens broken at high temperatures, where the loads to failure are low, have a rounded granular appearance with completely free grain surfaces. Examples are shown in Figs. 64 and 65 (detail) where the crack sensitive steel, SC, was broken at 1463°C . As the breaking temperature is lowered, and the loads to failure become higher, the grain outline becomes sharper; branch cracking is also noticeable. Examples are shown in Figs. 66 and 67 (detail) where the specimen was broken at 1432°C . As the breaking temperature is lowered still further to the point where ductility begins to recover, the grain outline becomes sharper, reaching a maximum sharpness plateau, as it were, at the temperature where ductility begins to recover (below this temperature, the grain outline, where this is visible, retains its sharp appearance). As the recovery temperature is approached, small areas of 'fern dendrites' and ductile dimpling begin to appear on the grain faces.

The point where ductility starts to recover, marks a sharp change in fracture appearance, and is readily apparent even in the early stages of recovery where the ductility is still quite low. This is well illustrated in Figs. 68 and 69 (detail) where the SC hot ductility specimen was broken at 1376°C with 6% R.A. A high proportion of ductile dimpling at the grain faces is readily apparent; some fern dendrites were also observed.

Free surface areas, indicative of pockets of liquation, still exist on parts of some grain faces, but signs of distortion are evident. The proportion of these free areas quickly diminishes with increasing ductility and the failure mode was almost completely ductile for the specimen of SC broken at 1240°C , with 32% R.A., Fig. 70. (For the crack insensitive steels, like SY, this stage is reached at the much higher breaking temperature of 1432°C). At the lower breaking temperature of 930°C , which is within the ductility dip region, there were indications of a partial return to intergranular failure, see Fig. 71. No free surfaces were observed on the grain faces which were covered with ductile dimpling and some fern dendrites.

(iii) Specimens Broken On-cooling from 12°C Below the Melting Temperature

Specimens broken on-cooling from this temperature showed similar features to those broken on-cooling from the nil strength temperature, viz., an intergranular failure mode in the zero ductility range and a sharp change in fracture appearance at the temperature where the ductility starts to recover. Again the grains became more angular with decreasing breaking temperature within the zero ductility range, see Figs. 72 to 76. Figs. 72 to 75 are most reminiscent of actual H.A.Z. liquated crack surfaces. Small areas of fern dendrites started to appear on the grain faces at about 1400°C ; however these did not

start to become extensive until ductility was about to recover. Fig. 76 shows such a fern dendrite; this specimen was broken at 1324°C , just on the point where ductility starts to recover. Once ductility starts to recover the failure mode becomes increasingly ductile and is almost completely ductile by 1280°C , see Fig. 77 where the specimen failed with only 30% R.A.

(iv) Impact Specimens Broken at 100°C

Specimens of the high impurity, crack sensitive SAE 4130 steel, SA, experiencing peak temperatures in excess of the nil ductility temperature, but below the bulk melting temperature, exhibited an intergranular failure mode, see Fig. 78. The typical intergranular appearance was not observed in specimens heated above the melting point prior to testing, see Fig. 79. Specimens thermally cycled to peak temperatures below the nil ductility temperature exhibited a transgranular ductile failure mode when impact tested.

The grain faces of specimens exhibiting intergranular failure were covered with both ductile dimples and fern dendrites, although the former were predominant. These areas, of which details are shown in Figs. 80 and 81, were virtually identical to similar areas in the actual H.A.Z. In some cases small areas of grains with free surfaces were observed, indicating that they had parted at high temperatures, Figs. 82 and 83. (The specimens were not subject to a detectable external load). It must be emphasised that these areas were very small in extent, covering less than 2% of fracture surface. These areas were however considered of special interest as fern dendrites were usually associated with the perimeter of the free surfaces.

4.

DISCUSSION

4.1. The Crack Susceptible Zone

Metallographic and fractographic studies of the bead-on-plate tests confirmed that EN 24, SAE 4130 and ASTM A387B are susceptible to high temperature H.A.Z. cracking provided the impurity levels are sufficiently high. The general features of the hot cracks are similar to those observed by other workers. They are of the intergranular liquation type and follow the prior austenite grain boundaries. Cracks ranged in length from 0.01 mm to 0.60 mm normal to the welding direction, but the crack surfaces could extend over 5 mm parallel to the welding direction. The crack surfaces were usually associated with modified MnS type inclusions.

Hot cracking was only observed within a discrete zone, in the high temperature region of the H.A.Z., immediately adjacent to the fusion boundary. Within this zone there were substantial modifications to the Type I MnS inclusions. Hot cracking did not extend beyond this modified inclusion zone. In only one case, namely SG (ultra low S, high P), could this not be positively confirmed, as the inclusion distribution was too sparse and the inclusions too small to permit an assessment of the width of the modified inclusion zone. However, as cracking only extended out to a maximum distance from the fusion boundary of 70% of the measured maximum width of the M.I.Z. in the remaining SAE 4130 steels, it seemed reasonable to conclude that, in this case also, cracking was confined to the modified inclusion zone.

Fractographic examination of the weldment, showed that in the high sulphur steels particularly, the modified inclusion zone was inherently brittle at ambient temperatures owing to extensive intergranular sulphide films. This extensive film network was present regardless of whether hot cracking had occurred.

The examination of weldment fracture faces, using scanning electron microscopy, has highlighted the point that the actual surface area of the liquation crack may be much greater than hitherto realised. This was not readily apparent using conventional two-dimensional surface preparations. What might appear to be a number of unrelated small intergranular cracks, in close proximity, in a polished surface preparation, may in three-dimensional reality be part of an extensive hot crack surface with islands of sulphides acting as solid, albeit brittle, bridges between the grains, see Figs. 16 to 24.

4.2. Correlation between Hot Ductility and Weld Cracking Test Results

4.2.1. Comparison of Metallurgical Features

The main basis for considering weld thermal simulation, in the form of the hot ductility tests, to be a valid representation of the metallurgical processes occurring in the hot crack susceptible zone of the real H.A.Z. must lie in a comparison of the significant features associated with hot cracking. It has been shown that, in the steels investigated, H.A.Z. hot cracking only occurred in a discrete zone in the high temperature region of the H.A.Z., associated with the modification to MnS type inclusions. Cracking did not extend beyond the modified inclusion zone. Examination of polished and etched weld sections shows that these inclusion modifications take the form of arrays of small globular inclusions decorating the prior austenite grain boundaries and clusters of small inclusions within grains, Figs. 12, 13 and 14. Significantly, similar modifications to inclusions in the form of grain boundary arrays and clusters were also observed in hot ductility specimens which had experienced peak temperatures of the nil ductility temperature (N.D.T.) and above (Figs. 57 and 58).

The most convincing evidence of the validity of the weld simulation approach, however, came from a comparative fractographic examination of

the actual crack susceptible zone (intergranular H.A.Z.) and the hot ductility specimens. This examination showed that all major prominent structural features associated with the intergranular region of the actual H.A.Z. were also present in the hot ductility specimens (taken as a composite sequence) which had experienced peak temperatures of the N.D.T. or above. A comparison of the specific significant features is given below:

Specific Feature	Intergranular H.A.Z. Fig. Numbers	Hot Ductility Specimen Fig. Numbers
(a) Clean intergranular surfaces (viz. hot crack surface). Note smooth topography, surface striations and grain boundary grooving	16,17,18,19, 20,21,22,23, 24	60,61,62,64,65, 66,67,72,73,74, 75,83
(b) Holes at grain faces, sometimes associated with surface fern dendrite	17,21,23,24, 25	60,61,62,63,64, 65,66,67,72,73, 74,75
(c) Surface fern dendrites	19,20,24,25, 28	76,80,82,83
(d) Ductile dimpling at grain faces	19,22,23,28	71,78,81,82
(e) Branch cracking	22,23	66,67

The striking similarity between the significant features associated with hot cracking and liquation indicates that weld thermal simulation satisfactorily reproduces the metallurgical processes which occur in the crack susceptible region of the H.A.Z. Thus the data obtained from the hot ductility specimens can, with a considerable degree of confidence, be utilized to gain a deeper insight into the mechanisms and events associated with the hot cracking and liquation processes.

Examination of the intergranular H.A.Z. region reveals a composite picture of the metallurgical features and events which have occurred over a considerable range of temperatures, both in respect of peak temperatures achieved and the cooling cycle. On the other hand, each hot ductility specimen experiences a thermal cycle which represents only one point in the actual H.A.Z. Moreover, it is broken at a specific temperature and so examination of the fracture face will show only those events which have occurred up to the time of breaking. Thus by examining a whole range of hot ductility specimens broken at various stages of the simulated thermal cycle, it is possible to build up a picture of the metallurgical events and the sequence in which they take place in the actual H.A.Z. This is of great advantage in establishing the significant parameters, obtained from the hot ductility test which can be applied to the welding situation, with the particular aim of distinguishing between the relative crack sensitivities of the respective steels.

In many instances the actual hot crack surfaces were very extensive and were usually associated with fern dendrite areas which stand proud of the crack surface. As discussed in section 3.3.4. these dendrite areas were not free surfaces, but solid, albeit brittle, bridges between the grains. This morphology indicates cracking occurred whilst extensive liquation existed around the grain boundaries. As the grains separated, the liquid film collapsed, because of its positive wetting angle, into a more compact area and then solidified to form the distinctive fern dendrite areas. This fern type morphology is consistent with eutectic solidification. In areas of the crack susceptible zone, of high impurity steels where no cracking occurred, the grain faces were covered with both fern dendrites and ductile dimpling. In these areas the films could not collapse but would have

to solidify 'in-situ'.

Comparisons with simulated specimens heated in excess of the nil ductility temperature and later impact tested, indicates that the type of intergranular film formed depends upon film thickness at the time of solidification; the thicker films tending to give rise to fern dendrites and the thinner films to the more uniform ductile dimpling. Examination of impact specimens failing in an intergranular manner show that the ductile dimpled areas predominated over the fern dendrite areas. However, in some specimens there were small areas where the grains had parted under no detectable external load. The perimeter of these free surfaces (hot cracks) were almost always associated with fern dendrites (Figs. 82 and 83). In these cases it is postulated, that as the liquated grain surfaces part, the liquid film, because of its positive wetting angle and in addition because of capillary action, contracts to the apex of the parting grains thereby forming a locally thicker film. This thicker film then solidifies with the characteristic fern dendrite morphology.

Comparison between the actual hot crack surfaces and the fracture faces of hot ductility specimens broken at various stages of the simulated thermal cycle indicates that hot cracking is associated with the zero ductility condition. The particularly striking feature of the actual H.A.Z. hot crack surface was the smooth topography, see Figs. 16 to 24. Significantly similar topographies were observed on the fracture faces of hot ductility specimens broken on-cooling within the zero ductility range from peak temperatures of both the N.S.T. (Figs. 64 to 67) and 12°C below the melting temperature (Figs. 72 to 75). However, once ductility in the simulated specimens started to recover, the similarity with the actual hot crack surface quickly receded. This was readily apparent even in the early stages of

recovery where ductility was low and the failure mode still mainly intergranular; examples are shown in Figs. 68 and 69 (detail) where the specimen was broken on-cooling with 6% R.A. Even though there are areas of free surfaces, which presumably correspond to pockets of liquation, there are large areas of high temperature ductile dimpling. (N.B. The morphology of high temperature ductile dimpling (Fig. 69) is quite distinct from low temperature ductile dimpling (Fig. 81)). Translating this situation back to the actual H.A.Z., then we would expect to find pockets of liquation on part of a grain face, surrounded by large areas of solid/solid interfaces. It has been postulated by Borland (34), that this situation is unfavourable for the occurrence of hot cracking as the welding strains should be accommodated by the large areas of solid/solid interfaces. No areas of high temperature ductile dimpling were observed on the fracture faces of actual H.A.Z.'s which shows that high temperature cracking does not occur after the film has solidified.

The occurrence of ductile dimpling and fern dendrites at the grain faces is associated with film solidification. As the extensive formation of these features does not appear until ductility recovery commences, it seems reasonable to conclude that the width of the on-cooling, zero ductility range can be taken as a measure of film life. Thus steels which exhibit a wide Z.D.R. should be crack susceptible, as extensive liquid films exist around the grain boundaries whilst the tensile strains are increasing.

From this comparison of real and simulated H.A.Z.'s it is evident that not only is hot cracking associated with the zero ductility condition, but also it probably occurs whilst an extensive liquid film exists around the grain boundaries.

Metallographic examination of hot ductility specimens, with high

sulphur contents, showed that substantial modifications to the MnS type inclusions only occurred in specimens experiencing peak temperatures of the N.D.T. or above. These inclusion modifications coincided with the appearance of holes (Fig. 60) in the grain faces, when the fracture face of the same specimen was examined. Holes in the grain faces were a particularly noticeable feature of both the real intergranular H.A.Z. and the hot ductility specimens broken with zero ductility. In many cases these holes were associated with, or at the centre of, surface fern dendrites (Fig. 25). These observations are consistent with the constitutional liquation theory of Pepe and Savage (39), whereby non-metallic inclusions melt in-situ and are impinged upon by migrating grain boundaries, thus 'wetting' them. Boniszewski et al (15,18) have also proposed this process as a mechanism of grain boundary liquation.

In the real H.A.Z., hot cracking was only observed within the modified inclusion zone (as explained in section 4.1 this could not be confirmed in the special case of SG).

These observations indicate that liquation cracking only occurs in those regions of the H.A.Z. which have experienced peak temperatures of the nil-ductility temperature or above. Thus the temperature interval between the nil-ductility temperature and the melting temperature ($\Delta\theta$), obtained from the hot ductility test, should be a parameter of considerable significance as there should be a direct relationship between $\Delta\theta$ and the width of the crack susceptible zone, for given welding conditions.

The results from the present investigation support this postulate. Reference to Table 13, shows that $\Delta\theta$ is relatively constant (ranging from 68°C to 76°C) for all EN 24 and SAE 4130 steels, with the sole exception of SY (ultra low S, ultra low P). The corresponding maximum depths of the actual modified inclusion zones (M.I.Z.) (Table 8) were

also relatively constant, ranging from 0.50 mm to 0.68 mm. However, in the ASTM A387B steels, $\Delta\theta$ fell to 52°C for AA and 57°C for AB. The width of the M.I.Z. could not be determined for AA, but for AB it was considerably less than for the SAE 4130 and EN 24 steels; the maximum values ranging from 0.40 mm to 0.45 mm.

The $\Delta\theta$ values for the special SAE 4130 steels with ultra low S and/or P (SG, SH and SY) were of particular interest. For SY (ultra low S, ultra low P) $\Delta\theta$ fell to 53°C, but when either element was present at the high level, $\Delta\theta$ rose to 74°C, which was the average value for the SAE 4130 steels. This seems to indicate that phosphorus, at the high level, may cause grain boundary liquation independently of sulphur, and that this occurs, in SAE 4130, at a similar temperature to the constitutional liquation of MnS type inclusions. However, as no metallographic examination was made on SG, the role of phosphorus could not be confirmed.

4.2.2. Correlation between Actual Cracking Behaviour and the Hot Ductility Test Parameters

The investigation has provided a unique opportunity for the accumulation of a wealth of hot ductility data covering three types of high strength ferritic steels with a wide range of cracking sensitivities. Specifically it has provided the opportunity for a rigorous examination of the hot ductility test as a means of discriminating between the relative cracking sensitivities of ferritic steels. The interpretation of the various features of the hot ductility curves and their relation to actual cracking behaviour has been considerably aided by the comparative fractographic study of both actual weldment hot cracks and the fracture faces of hot ductility specimens broken at various temperatures during the simulated welding thermal cycle.

Analysis of the several parameters associated with the hot deformation behaviour of the steels tested (section 3.4.4.) demonstrated

that the width of the zero ductility range measured during the cooling portion of the simulated weld thermal cycle, could be related quantitatively to the cracking severity of a steel, providing a peak temperature of the N.S.T. or above was used. In this respect the higher peak temperature of 12°C below melting appeared more discriminatory as it amplified the range of Z.D.R.'s between crack resistant and crack sensitive steels. It was also noted that the width of the zero ductility range appeared to be related to the damage to the recovery rate of on-cooling strength. Thus it was possible to obtain a quantitative relation between cracking propensity, and strength recovery to specific levels up to 30 MN/m^2 . The best correlation was noted at 20 MN/m^2 . In fact, the point at which ductility started to recover, for most steels tested, corresponded to a strength level of just below 30 MN/m^2 .

Analysis of the recovery rate of ductility criterion as proposed by Nippes et al (72) showed that, although there was a certain degree of qualitative correlation between recovery rate and actual cracking behaviour, there were several significant discrepancies between predicted and observed cracking severity. It was thus concluded that this criterion could not distinguish unambiguously between the relative cracking sensitivities of the low alloy steels investigated.

The validity of the zero ductility range criterion is further supported by the conclusions reached previously (section 4.2.1.), that H.A.Z liquation cracking is associated with the zero ductility condition. Once ductility starts to recover, the H.A.Z. is no longer in a crack susceptible condition, hence the rate of ductility recovery is irrelevant. By the same reasoning it can be seen that the recovery rate of ductility criterion of Nippes et al (72) is not a sound basis on which to assess the relative susceptibilities of low alloy steels to H.A.Z. liquation

cracking.

4.3. Effect of Welding Variables

Investigation of the effects of welding variables has shown that the following factors increased the severity of cracking:

- (i) increasing heat input/unit length
- (ii) increasing the depth of finger penetration
- (iii) the application of external restraint
- (iv) increasing distance along the weld bead.

(i) Heat Input:

Metallographic examination has shown that increasing the heat input/unit length, for a given plate thickness, increases the width of the crack susceptible zone, producing a greater volume of material in which cracking can occur. Thus individual cracks tended to be longer and more numerous, and extend further from the fusion boundary in the high heat input/unit length welds.

Moreover, this crack susceptible zone is associated with a zone of inherent brittleness at ambient temperatures, particularly in high impurity materials, which in the context of the weldment as a whole makes a wide crack susceptible zone, doubly undesirable.

The adverse effect of increasing heat input/unit length upon cracking severity would almost appear self-evident were it not for the disagreement which exists in the literature. Thus whilst some investigators (17,18) report an increase in cracking severity with increasing heat input/unit length, others (15,19) report no such effect. Unfortunately these investigators, particularly the latter, have not made quantitative comparisons of crack size distributions, and the distances cracks extend from the fusion boundary, and so the results are of less value than had such comparisons been carried out. On the other hand, the more rigorous approach adopted in the current investigation has

clearly shown that not only is cracking more severe in the high heat input/unit length welds, but that this increase in cracking severity can be accounted for by an increase in volume of the crack susceptible zone surrounding the weld bead.

(ii), (iii) and (iv) Finger Penetration, Restraint and Distance Along Weld Bead:

The adverse effects of finger penetration, external restraint and distance along the weld bead upon the severity and location of cracking, emphasises the stress/strain situation in the H.A.Z. during welding is of considerable importance.

The increase in cracking severity caused by the deep finger penetration profile and the concentration of cracks at the weld bead 'shoulder', together with the preferential direction of cracking, perpendicular to the fusion boundary, is wholly consistent with the results of Meitzner and Stout (14). This concentration and preferential directionality of cracking can be accounted for by tensile stresses being built up in the weld 'shoulder' of the H.A.Z. These localised tensile stresses associated with the weld bead profile could arise in two ways:

(a) Non-uniform solidification, whereby the weld finger, surrounded by cold metal, freezes before the elliptical portion, causing contractional stresses on the 'shoulder' portion of the H.A.Z. whilst it is in a crack susceptible condition.

(b) Plastic deformation of the H.A.Z. whereby the heat from welding initially places the H.A.Z. in compression causing plastic deformation in the crack susceptible zone. As cooling commences, the deformed crack susceptible region must adjust to the restraint offered by the stronger 'shoulder' of metal beneath it. The resistance of this colder metal causes tensile stresses in the crack susceptible region.

Apart from the tensile strain component of the deep finger profile causing an increase in cracking, there is probably also an increase caused by the localised concentration of heat at the weld shoulder. This leads to a spreading out of the temperature isotherms and thus a localised widening of the crack susceptible zone at the weld shoulder where the crack inducing strains are greatest.

From a practical viewpoint the results suggest that welding processes which give rise to a rounded weld bead profile, such as the submerged arc process, would be preferable to those which give a finger profile, such as the M.I.G. process.

The increase in cracking severity caused by the application of external restraint, and the increase in cracking that occurs with distance along the weld bead indicates that joint detail and rigidity can influence cracking severity. This runs counter to an earlier suggestion by Boniszewski and Watkinson ⁽¹⁵⁾, based on the results of Masubuchi and Martin. ⁽¹⁹⁾ They suggested that the long range stress-strain system dependent on joint detail and rigidity has insufficient time to build up so as to influence cracking behaviour. However, re-examination of Masubuchi and Martin's ⁽¹⁹⁾ results show that although three joint details were investigated, the work was carried out on a steel with a low impurity level which resulted in only a small amount of cracking. Furthermore, the results were considered in a most qualitative manner, being described as: 'few, very few and several' respectively. This in effect meant that the results could be open to several interpretations. In contrast the evidence presented in the present work that joint rigidity and detail (in the form of distance along the weld bead) can significantly influence cracking is very strong, being based on a quantitative assessment of the cracking severity of many steels. An obvious next step in this area would be a rigorous

examination of the effect of other specific joint details used in practice upon cracking severity.

The results obtained from these studies should allow further investigations to proceed on a more rational basis. Specifically, it has been shown that both the thermal cycle and the strain situation in the weld H.A.Z. can markedly influence cracking propensity. The heat input/unit length, through its effect on the temperature distribution in the H.A.Z. determines the width of the crack susceptible zone. The strain situation in the crack susceptible zone can be influenced by the weld bead profile, external restraint and distance along the weld bead. It is quite likely that other welding variables also influence cracking behaviour and these should be isolated and the magnitude of their effects investigated so that recommendations for welding procedures can be made on a systematic basis.

4.4. Effect of Composition

The weld cracking tests have highlighted the adverse effects of carbon, sulphur and phosphorus upon H.A.Z. hot cracking. A quantitative estimation of the relative effects of major crack inducing elements for the three steel types investigated, was made using the regression technique. This lead to the following equation:

$$\text{Crack Index} = 4.8 C + 26.8 S + 52.5 P \pm 1.04$$

The equation gives calculated values of crack index (combined crack length per weld section) which show a correlation of 0.92 with observed values. Use of this equation in a practical welding situation should be considered with caution. This point will be considered at a later stage.

Considering the results from a practical viewpoint it can be seen from Fig. 15, that for a given impurity level cracking increases with increasing carbon content. Thus for the low sulphur, low phosphorus

combination (about 0.010 wt % each), no cracking was detected in ASTM A387B (C = 0.12 wt %), but a small amount was detected in SAE 4130 (C = 0.35 wt %) and considerably more in EN 24 (C = 0.37 wt %).

The cracking behaviour of the special SAE 4130 steels with ultra low sulphur and/or phosphorus levels was of particular interest. The weld cracking tests showed that H.A.Z. hot cracking could be completely eliminated in the ultra low sulphur, ultra low phosphorus steel, SY. However, either element at the high level (>0.030 wt %) could induce significant cracking. In this respect phosphorus appeared to be the more deleterious element. Further evidence that phosphorus is the more deleterious element comes from the regression equation which shows that phosphorus has twice the potency of sulphur.

Results from the hot ductility tests further confirm the deleterious nature of phosphorus where it can be seen that the width of the on-cooling zero ductility range, and the damage to the recovery of on-cooling strength, were considerably greater in the high P, low S steels (SD and SG), than in the high S, low P steels (SE and SH).

As few other investigations have specifically considered the effect of composition on hot cracking in the H.A.Z. of ferritic steels, the data obtained from these investigations represents a considerable increase in knowledge in the field. Previous investigations have considered the effects of carbon and sulphur^(14,15,43), which were shown to increase the sensitivity of a steel to H.A.Z. hot cracking with increasing concentration.

An attempt has also been made⁽¹⁴⁾ to relate the Mn:S ratio to H.A.Z. hot cracking severity where it was suggested that cracking increases as the Mn:S ratio decreases. However, closer examination of these results shows that the effect could equally be interpreted as being due to sulphur alone.

Of the two impurity elements, sulphur has received the most attention so far as H.A.Z. hot cracking is concerned. This is probably due to the observed association of sulphide films with hot crack surfaces. On the other hand, the effect of phosphorus upon H.A.Z. hot cracking has received little attention. Indeed, it has been suggested (41) that the effect of phosphorus upon H.A.Z. hot cracking should be secondary to that of sulphur, as it is reasoned there is no driving force to cause phosphorus, which is considerably more soluble in the matrix than sulphur, to segregate to the grain boundaries unless a liquid phase is present. However, the present results show that phosphorus is a highly potent crack inducing element, and can induce significant cracking with only a trace of sulphur. The mechanism of phosphorus segregation to grain boundaries is not clear. As it does not form non-metallic inclusions in steel, a constitutional liquation mechanism cannot be invoked. The answer may well lie in the work of Revière (55) who showed that phosphorus would segregate to low energy sites, like grain boundaries, with increasing temperature and in sufficient concentration to form liquid films at about 1400°C. It must, however, be remembered that this work was done in the context of burning in steel and the measurements were made after long times at temperature, in the order of thirty minutes. In the welding situation only a few seconds are available for the segregation of phosphorus to the grain boundaries.

In view of the deleterious nature of phosphorus, the kinetics of its segregation should prove a fruitful field of study. The reason for the deleterious nature of phosphorus probably lies in its effect upon film life. The longer the film life, in terms of decreasing temperature, the more likely cracking is to occur due to the increasing tensile strains in the crack susceptible zone. Brammar (53) in his

studies of burning in steel has noted that the phosphide is the last constituent of the liquid film to solidify. The results from hot ductility testing in the current investigation lead to the same conclusion. The width of the on-cooling zero ductility range was considerably greater in the high P, low S steels (SD and SG) than for the high S, low P steels (SE and SH). The available evidence strongly suggests that the width of the zero ductility range is indicative of film life.

Phosphorus has been shown to be a more potent hot crack inducing element than sulphur in the present investigation. However, in the context of weldment properties as a whole, sulphur, through its ability to produce extensive intergranular films which are brittle at ambient temperatures, must also be considered most deleterious.

The quantitative estimation of the relative importance of the hot crack promoting elements, in the form of the regression equation, represents the first such estimation for the specific case of the H.A.Z. However, the equation, per se, should be treated with caution and be interpreted in the light of the steels examined and the testing conditions used. This cautionary note applies equally to similar crack susceptibility equations which have been obtained for weld metal solidification cracking and for cold cracking. The equation was based upon the results of laboratory bead-on-plate tests, designed to produce the maximum crack inducing conditions. In addition, the tests were conducted on thirteen steels of similar specifications, namely, the 1½% Ni-Cr-Mo type and the 1% Cr-Mo type.

The experiments were mainly designed to examine the effects of carbon, sulphur and phosphorus and accordingly the steels were selected so that these elements varied over a wide range. In fact the regression analysis found that only carbon, sulphur and phosphorus were significant

at the 5% level. This result should not, of course, automatically be taken to mean that the remaining alloying elements in the steel such as Cr, Mo, Mn, Si etc. do not significantly affect cracking propensity, particularly when it is remembered that there was little variation in the level of these elements in the steels investigated. Indeed it is quite possible that other elements, such as Cr, Mo, Mn, Si, Ni etc. when varied over a sufficiently wide range may also markedly influence cracking propensity.

4.5. Implications of Results in the Context of Weldment Failure

It would be interesting to briefly consider the implication, of the results obtained in this investigation, in the context of weldment failure. Though the work was not specifically concerned with this particular aspect, one of the original reasons behind the study of H.A.Z. hot cracking, was the possibility that it may promote failure in welded structures. In this respect it should be realised that the welded joint is associated with a continuous change in properties from the weld metal through to the unaffected parent plate.

The experimental results showed that H.A.Z. cracking can be quite extensive, and may be more extensive than hitherto realised, especially when associated with, or continuous with, weld metal hot cracking. In many instances, these 'so-called' microcracks could be observed with the naked eye. Moreover this crack susceptible zone, particularly in the high impurity materials, was associated with an extensive brittle intergranular film network. Judging from the extremely low energy necessary to part these films, it seems quite possible that small cracks in this region could jump quickly through this brittle region under the influence of small service loads, thus extending the crack area considerably. Thus it is conceivable that cracking may extend quickly to the edge of the modified inclusion zone and also along the weld direction, under small

service loads, in high impurity materials.

The intergranular films present at ambient temperatures were of the MnS type, with no evidence of phosphorus being present. The absence of phosphorus at ambient temperatures was no doubt due to its redissolution in the matrix under normal cooling conditions.⁽⁵³⁾ Thus in the context of crack extension at ambient temperatures, a high sulphur content would probably be more harmful than a high phosphorus content, except in the specific case where the cooling rate is sufficiently fast to precipitate the phosphide eutectic.

When the crack tip reaches the transgranular region of the H.A.Z., further propagation of the crack will depend on the load, and the toughness of the material at the crack tip. The H.A.Z. of high strength steels, and the high temperature regions of this zone in particular, often have a lower toughness than the parent plate. Thus if the toughness at the crack tip is low enough it may continue to propagate until it runs into material tough enough to halt further growth. On the other hand, the crack area may exceed the critical crack length for the toughest material present, in which case catastrophic brittle failure will ensue. Another mechanism of crack growth from a pre-existing hot crack is fatigue, the rate of fatigue is fastest in materials of low toughness. Thus again the crack may grow until the critical size for fast failure is reached.

5.

CONCLUSIONS

1. Heat Affected Zone hot cracking in the welding of low alloy hardenable steels occurs in a discrete high temperature zone adjacent to the fusion boundary in which liquation of MnS type inclusions has occurred.
2. The severity of H.A.Z. hot cracking is determined by both material composition and the level of the welding parameters.
3. Under fixed welding conditions, the cracking susceptibility increased with increasing carbon, sulphur and phosphorus levels. High levels ($>0.030\%$ wt) of either sulphur or phosphorus could induce cracking; phosphorus being the more deleterious.
4. For a constant steel composition, the cracking increased with:
(i) Increasing Heat Input/unit length; (ii) Increasing depth of finger penetration; (iii) Application of external restraint;
(iv) Increasing distance along the weld bead.
5. The primary effect of increasing Heat Input/unit length was to increase the width of the 'crack susceptible zone'.
6. At high sulphur levels (>0.030 wt %) the 'crack susceptible zone' was also brittle at ambient temperatures due to extensive sulphide films at the grain boundaries.
7. The H.A.Z. hot cracking severity of a steel can be related quantitatively to the zero ductility range, measured during the cooling portion of a simulated weld thermal cycle, providing a peak temperature of the N.S.T. or above is used. The greatest sensitivity was achieved with a peak temperature of 12°C below the bulk melting temperature.
8. Comparison of the metallurgical features of real and simulated heat affected zones confirms that liquation cracking is associated with the zero ductility condition.

6.

RECOMMENDATIONS FOR FURTHER WORK

Arising out of the present investigation are several important areas which still require further work. These are:

1. A long term investigation is needed to relate the H.A.Z. hot cracking problems found in production with the cracking severity observed in the laboratory bead-on-plate tests.
2. The present investigation has shown that the H.A.Z. hot cracking severity, of the 1% Cr-Mo and 1½% Ni-Cr-Mo steels investigated, can be related quantitatively to the zero ductility range, measured during the cooling portion of a simulated weld thermal cycle. Follow-up studies are now needed to see whether the quantitative correlations obtained for these steels can be applied to other ferritic steel types like the C-Mn and Cr-Mo-V steels etc. Such information is still needed before the hot ductility test can be used as a standard laboratory technique capable of confidently predicting the relative cracking sensitivity of any given ferritic steel. To facilitate maximum progress, close collaboration and standardisation of testing techniques is needed between the various groups of investigators in this field.
3. The welding tests have confirmed the powerful crack promoting effects of sulphur and phosphorus. The mechanism of sulphide segregation to grain boundaries can be explained in terms of a constitutional liquation process, but the mechanism and kinetics of phosphorus segregation remain obscure and are in need of further investigation.
4. Fractographic studies on high impurity steels, particularly high sulphur steels, has shown that within the crack susceptible zone there exists an extensive intergranular network of non-metallic sulphides which are extremely brittle at ambient temperatures. The existence of such a brittle zone in the H.A.Z. is very undesirable, especially in the case of single pass, full penetration, butt welds in thin plate. The extent and problems associated with such a brittle zone in thin plate has

considerable practical significance, as for instance in the welding of rocket motor casings, and is in need of investigation.

5. Several parameters associated with welding have been shown to significantly influence cracking propensity. However, there are several more which still require investigation, such as: specific joint detail, plate thickness, welding process, shielding gas, welding speed, etc. Moreover, it is necessary to establish the relative importance of the various parameters so that recommendations for welding procedure can be placed on the most systematic basis possible.

7.

ACKNOWLEDGEMENTS

The author wishes to thank Dr. M.F. Jordan for his supervision and thought provoking discussions throughout this investigation. Thanks are also due to Professor W.O. Alexander, Head of the Department of Metallurgy, and Professor R.H. Thornley, Head of the Department of Production Engineering, for providing laboratory facilities and to the Ministry of Defence for sponsoring the project. The author also appreciates the co-operation of the United Kingdom Atomic Energy Authority in providing the thermal simulation facilities and the assistance of Mr. D. Crichton with this work.

The assistance of the academic and technical staff of the Departments of Metallurgy and Production Engineering with the many practical problems is equally appreciated. The donation of steels by the Redheugh Iron and Steel Company Limited is gratefully acknowledged.

Finally the author wishes to thank his wife for her continuous encouragement, support and patience throughout the project.

8. APPENDIX - PUBLICATIONS

TEMPERATURE MEASUREMENT AND DISTRIBUTION

IN WELD THERMAL SIMULATION

by R. H. Phillips, B.Sc.

M. F. Jordan, B.Sc., Ph.D., A.I.M., M.Weld.I.

To be published in Welding International
Research and Development, October 1973

Synopsis

A study has been made of temperature measurement and distribution in cylindrical steel specimens undergoing weld thermal simulation by resistance heating. It has been shown that large differences can occur between the indicated surface temperature and the internal specimen temperature. This is due to non-reproducibility in thermocouple behaviour and reduced signals mainly attributable to the 'heat-sink' effect. However, it is demonstrated that, by selection of appropriate thermocouple attachment and calibration techniques, measurements can be made that are sufficiently reproducible and accurate for simulation work, i.e. $\pm 7^{\circ}\text{C}$ at 1400°C .

Internal and surface measurements indicate clearly that a temperature plateau exists in a central 5 mm region of specimens of gauge length 12.5 and 25 mm. The longitudinal and transverse temperature differences are not greater than 10°C , thus confirming that the technique can simulate thermal cycles in specimens large enough for normal methods of testing.

Introduction

It is now widely recognised⁽¹⁻⁴⁾ that simulation is a very necessary technique for effective study of weld heat affected zone phenomena. Among other things, this involves the reproduction of the weld thermal cycle uniformly in a specimen large enough for normal methods of testing to be applied. Recent work⁽⁵⁻⁹⁾, however, has indicated that there are difficulties in achieving the necessary degree of accuracy in temperature measurement and control during simulation. Thus the problem needs investigation before simulation techniques can be used with confidence.

The most usual way of achieving the required thermal cycle employs direct current heating of a specimen which is held in water cooled

copper jaws. A thermocouple, attached to the specimen surface, is then used both to measure and control the specimen temperature. The required thermal cycle is generated by offsetting the heating of the current against the cooling of the copper jaws. In such a system it is obviously essential that the temperature measurements should be accurate and reproducible. This is of particular importance in hot ductility testing where the peak temperatures used are close to the solidus of the material and small differences in these peaks can have dramatic effects on subsequent behaviour. It is also necessary to know the temperature distribution in the specimen in order to correlate such features as microstructures, fracture faces, and properties with real weld heat affected zones. A survey of the published literature indicates that while some investigators appear to assume implicitly that the recorded surface temperature was identical to the actual specimen temperature, other investigators report discrepancies. In thermal simulation work on ferritic steels, Vinckier⁽⁵⁾ suggests that 'real temperatures might be higher than recorded temperatures', while Smith et al⁽⁶⁾ measured a 30°C difference between surface and centre of the specimen. Dolby and Widgery⁽⁷⁾ in work with Charpy specimens obtained a similar difference which they attributed to the cross sectional temperature gradient and the technique of thermocouple attachment; attached beads giving lower apparent temperatures than individually attached wires. Indicated surface temperatures over 100°C below the internal values were reported at temperatures of 1200°C by Coleman⁽⁸⁾, who included a third factor, namely that of thermocouple 'heat-sink' effect which had been deduced theoretically by Baker et al.⁽¹⁰⁾ Keane, Bower and Hammond⁽⁹⁾ quote differences of 50°C in the signal from poorly attached thermocouples compared to well attached thermocouples. Furthermore, they report severe transverse and longitudinal temperature gradients in the cycled specimens. At a

centre temperature of 1000°C , their results show an immediate drop of 100°C in the first 10 mm along the specimen, with no evidence of a temperature plateau.

Clearly a great deal of confusion exists and the present work involves an examination of the problem for the particular case of cylindrical specimens in ferritic steels as part of a programme of research into weld heat affected zone phenomena in these materials. This involved the reproducibility of thermocouple signals and their calibration in terms of the internal temperature together with measurement of the temperature distribution in the specimen.

The work was conducted with a 'Gleeble' weld simulator⁽²⁾, using 10 mm diameter cylindrical low alloy steel specimens. All experiments were carried out in a controlled atmosphere box under an argon atmosphere to prevent oxidation.

Thermocouple Reproducibility

It was envisaged that for any specimen material the reproducibility of the signal from a surface thermocouple would be affected by the type of thermocouple and the method of attachment. Accordingly, experiments were conducted with 0.25 mm diameter bare wire couples in Chromel/Alumel and Pt/Pt 13% Rh. The former couple has an emf output four times that of the second for a given temperature, but is restricted in application by its melting temperature of 1400°C . The methods of attachment involved beads and individual wires using percussion (capacitor discharge) and resistance spot welding.

The specimen set-up used to determine the reproducibility is shown in Figure 1. A is the bare wire surface thermocouple and B is a sheathed thermocouple inserted into a close fitting blind hole drilled to the specimen centre. For each temperature determination the surface thermocouple was taken to a constant emf value and the corresponding

internal temperature read directly from a potentiometer. The range of temperatures recorded by the sheathed thermocouples was taken as a direct assessment of the surface thermocouple reproducibility. After each determination the surface thermocouple was removed, the specimen surface cleaned, and a new couple set in place. A total of 10 measurements were made for each system and the results are shown in Table 1.

From the experiments with the percussion welded Chromel/Alumel couples it is clear that the reproducibility is much better with separately attached wires than with the beads. At an indicated surface temperature of 1115°C the internal temperature varied by $\pm 7^{\circ}\text{C}$ for the former to $\pm 33^{\circ}\text{C}$ for the latter. In the case of the Pt/Pt 13% Rh at the higher indicated surface temperature of 1285°C , poor reproducibility ($\pm 38^{\circ}\text{C}$) was obtained with percussion welded separate wires but good reproducibility ($\pm 7^{\circ}\text{C}$) could be recovered by substitution of resistance spot welding as the technique of attachment. These results show that surface attached thermocouples can give reproducible behaviour but that they are very sensitive to the technique of attachment. Furthermore, a technique which is suitable for one thermocouple-material combination may be unsuitable for another combination. Presumably the latter must be explained in terms of the soundness of the metallurgical bond produced by each technique for the materials covered.

Thermocouple Calibration

The experimental work on the reproducibility of thermocouples attached to the specimen surface had shown that the indicated surface temperature was in fact considerably lower than the temperature at the specimen centre. With Chromel/Alumel couples, about 50°C at 1167°C and with Pt/Pt 13% Rh about 110°C at 1285°C , see Table 1. For couples attached as separate wires to the surface these effects could be due to the cross sectional temperature gradient and the thermocouple 'heat-

sink' effect. Examination of the temperature distribution in the specimen which is described later showed that the cross sectional temperature gradient at about 1180°C was $\leq 10^{\circ}\text{C}$. In the light of this fact, it appeared that the major effect was due to the surface thermocouple 'heat-sink' effect and that calibration to take care of this could be carried out by comparison with the temperature at the specimen centre.

Measurement of the internal temperature obviously involves the introduction of thermocouples into the specimen interior. It was recognised that this involved disturbing both the heat flow and heating current flow in the specimen. Furthermore, the internal couple itself would be subject to a 'heat-sink' effect. Both factors could affect the validity of the thermocouple calibration. In order to assess this problem, four different thermocouple assemblies were used which involved both radial and axial insertion:

- A. A 0.50 mm diameter sheathed Chromel/Alumel couple inserted radially into a close fitting blind hole located at the specimen centre.
- B. As for A, but using a 1.56 mm diameter sheathed Pt/Pt 10% Rh thermocouple.
- C. A 0.25 mm diameter bare wire Pt/Pt 13% Rh thermocouple, insulated using twin hole ceramic insulators, inserted axially along a 2.5 mm diameter blind hole drilled to the specimen centre. The thermocouple was percussion welded to the inside surface.
- D. As for C, but the internal couple, though still at centre, was not welded to the inside surface.

In each experiment the temperature of the surface was measured and controlled using a 0.25 mm diameter bare wire Pt/Pt 13% Rh thermocouple spot welded as separate wires. The specimen temperature was

raised in step sequence; being held constant at each step whilst simultaneous potentiometric determinations of surface and internal thermocouple emf were made. Full details of the results are shown in Figure 2 as a graph of surface emf V^S internal temperature and in Figure 3 as Temperature difference (internal-surface) versus Internal temperature. It is apparent from both graphs that there is considerable variation between the four calibrations. Two factors could be responsible for this variation:

- (i) Radial thermocouples cutting across the lines of current flow may give rise to localised heating at the tip of the sheathed thermocouple due to the reduction in cross sectional area. This would give a high reading.
- (ii) All internal couples may be subject to 'heat-sink' effects which would result in a low reading.

To investigate the former effect, the bare wire surface thermocouple and the sheathed 0.5 mm diameter Chromel V^S Alumel thermocouple were differentially connected to measure the temperature difference (ΔT) between the surface and interior. The two resulting emf outputs were fed into the two channels of a multi-channel u.v. recorder. The specimen was then taken up to a temperature plateau and the heating current switched off, and on again, to determine its effect. From the resulting Temperature V^S Time, and $\Delta T V^S$ Time curves shown in Figure 4, it can be seen that there is no localised heating of the sheathed thermocouple due to the passage of heating current. In fact, there actually appears to be a small cooling effect of about 2°C .

Unfortunately, it was not possible to repeat this experiment with the larger diameter (1.56 mm) Pt V^S Pt 10% Rh internal couple because the small ΔT emf output was swamped by background interference. However,

from Figure 3, it can be seen that the recorded temperature difference between the centre and surface is much larger than for the Chromel-Alumel sheathed couple. This probably indicates that considerable localised heating is occurring in this case.

Both axial thermocouples (C and D) give lower temperatures than the Chromel-Alumel radial couple, indicating they may suffer from 'heat-sink' effects. This seems certainly the case in assembly D, where there is considerable resistance to the transfer of heat from the specimen to the thermocouple junction across the air gap.

An approximate assessment of the validity of these calibrations can be made by considering the melting point of SAE 4130. This is given as 1535°C by the Aerospace Structural Metals Handbook.⁽¹¹⁾ In hot ductility tests it was found that all heats of SAE 4130 melted at a surface indicated emf between 16.45 mV and 16.7 mV. The corresponding temperatures obtained by extrapolating the four calibrations to the melting points are listed in Table 2. From this table it can be seen that calibration A gives best correspondence with the published melting temperature. This is in agreement with the tentative conclusions reached previously.

Temperature Distribution

In establishing the temperature distribution of the thermally cycled cylindrical specimen, measurements were made of both the longitudinal and cross sectional temperature gradients at a selected peak temperature, and over the full thermal cycle. Longitudinal temperature distributions were determined for gauge lengths of 12.5 mm and 25 mm.

Temperatures were measured using thermocouples spot welded along the top surface at various distances from the specimen centre. The resulting values were converted to internal temperatures using the calibration curve A in Figure 2 and are plotted in Figure 5. As expected, the shorter gauge length has a much steeper gradient overall. However,

in both cases, there is a central plateau of 5 mm, over which the temperature drops by only 10°C .

The cross sectional gradient was measured at the centre section by inserting a 0.5 mm diameter sheathed Chromel V^S Alumel into a close fitting diametral hole drilled through the specimen. The first measurement was taken at the surface opposite the point of thermocouple entry; in subsequent measurements it was progressively drawn back through the hole by measured distances. The results, shown in Figure 6, indicate an asymmetrical temperature distribution about the centre. This is due to the thermocouple 'heat-sink' effect at the smaller immersion depths. Taking this into account, there is a gradient, from surface to centre, of 10°C at an internal temperature of 1200°C . Temperature measurements over the full thermal cycle were made, where it was found that positions experiencing the same peak temperature, also experienced the same thermal cycle.

Discussion and Conclusions

The results obtained with the different thermocouples and methods of attachment have confirmed that wide differences can occur between the indicated surface temperature and the internal temperature of resistance heated ferritic steel specimens. This is made up of a lack of reproducibility in thermocouple behaviour arising from variations in the bonding to the surface and a reduced signal due mainly to the thermocouple 'heat-sink' effect. However, by appropriate choice of attachment technique and careful calibration against the internal temperature it has proved possible to obtain signals from surface attached thermocouples with a reproducibility of $\pm 7^{\circ}\text{C}$ up to peak temperatures of about 1400°C .

This is considered satisfactory for a wide range thermal simulation work. In fact, this has been confirmed in a programme of research with

1% Cr-Mo steel where specimens have been consistently thermally cycled to peak temperatures about 12°C below the solidus without thermocouple failure.

It is apparent that the reproducibility of signals from surface thermocouples is strongly influenced by the technique of attachment so that in the present work the scatter varied from $\pm 38^{\circ}\text{C}$ to $\pm 7^{\circ}\text{C}$. From the work with the Chromel/Alumel couples it is clear that attachment of separate wires is superior to fused beads. Furthermore, in the case of the Pt/Pt 13% Rh thermocouples it was necessary to use resistance spot welding instead of the more usual practice of percussion welding, in order to obtain comparable reproducibility to that obtained in Chromel/Alumel couples. Clearly the optimum method of attachment can depend upon the thermocouple-material combination being used. It would therefore appear to be essential to confirm experimentally that the optimum thermocouple technique has been established before embarking upon thermal simulation work.

The recorded surface temperatures were consistently lower than the internal temperatures of the cylindrical steel specimens; being about 35°C at 1000°C and about 60°C at 1400°C . Since the cross sectional temperature gradient was $\leq 10^{\circ}\text{C}$, the major part of this difference was due to the thermocouple 'heat-sink' effect. Once reproducible behaviour has been obtained, the surface thermocouple can be calibrated against the internal temperature using small diameter thermocouples inserted radially from the surface.

It is apparent that the temperature distribution in the central region of the 10 mm diameter rods was very uniform for both the 12.5 and 25.0 mm gauge lengths. In particular, the cross sectional temperature gradients were $\leq 10^{\circ}\text{C}$ at an internal temperature of 1200°C , Figure 6, and there was a temperature plateau of 5 mm showing less than a 10°C drop

for an internal temperature of about 1400°C , Figure 5. Thus a region of appreciable size in the centre of the specimen receives a uniform reproduction of the thermal cycle to the selected peak temperature. This meets the requirements for the determination of ductility and strength during the thermal cycle which is required for the study of high temperature liquation cracking. In addition, it yields specimens of suitable size for study of the room temperature microstructure and properties of heat-affected zones.

Acknowledgements

The authors express their thanks to the University for provision of laboratory facilities and to their colleagues for assistance in carrying out the experimental work. The investigation itself was carried out as part of a programme of work supported by the Ministry of Defence (Materials Division).

References

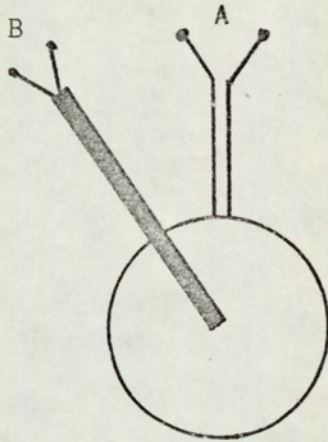
1. E Nippes, W F Savage, B Bastion, H Mason, R Curren,
Weld. J. 1955, 34, 183s-196s
2. W F Savage, J App. Polymer Science, 1962, 6, 303-315
3. R G Baker, F Watkinson, R P Newman. 2nd Commonwealth Welding
Conference, London 1965, Paper M3
4. D J Widgery, Metal Construction, 1970, 2, 333-338
5. A Vinckier, Metal Construction, 1969, 1, 276-277
6. E Smith, M Coward, R Apps, Welding and Metal Fabrication, 1970,
38, 242-251
7. R E Dolby and D J Widgery, Welding Institute Report M/52/70
8. M C Coleman, The Fracture Toughness and Microstructure of the
Heat Affected Zone of a Welded Maraging Steel, Ph.D. Thesis,
University of Aston in Birmingham, 1971
9. D M Kean, E N Bower and J Hammond. Weld Thermal Simulators
for Research and Problem Solving. Welding Institute Seminar,
1972, 44-49
10. H D Baker, E A Ryder, N H Baker, Temperature Measurement in
Engineering, Vol 1, Ch 7, 1953, Chapman and Hall
11. Aerospace Structural Metals Handbook, Vol 1, 1966. Ed. V Weiss,
Syracuse University Press

Table 1. Temperature Reproducibility of Bare Wire Surface Thermocouples

Thermocouple type	0.25 mm Chromel/Alumel		0.25 mm Pt/Pt 13% Rh	
Method of Attachment	Percussion welded as bead	Percussion welded as separate wired	Percussion welded as separate wires	Resistance welded as separate wires
Recorded surface temperature	1115°C	1115°C	1285°C	1285°C
Internal Temperature } mean	1227°C	1167°C	1414°C	1397°C
Internal Temperature } scatter	± 33°C	± 7°C	± 38°C	± 7°C

TABLE 2. Determination of Melting Temperature of SAE 4130

Calibration	Melting Range °C
A	1512 - 1532
B	1596 - 1618
C	1486 - 1504
D	1456 - 1476



Specimen Centre Section

A is bare wire surface thermocouple

B is sheathed internal thermocouple

Fig. 1. Specimen Set-up Used to Determine Temperature
Reproducibility.

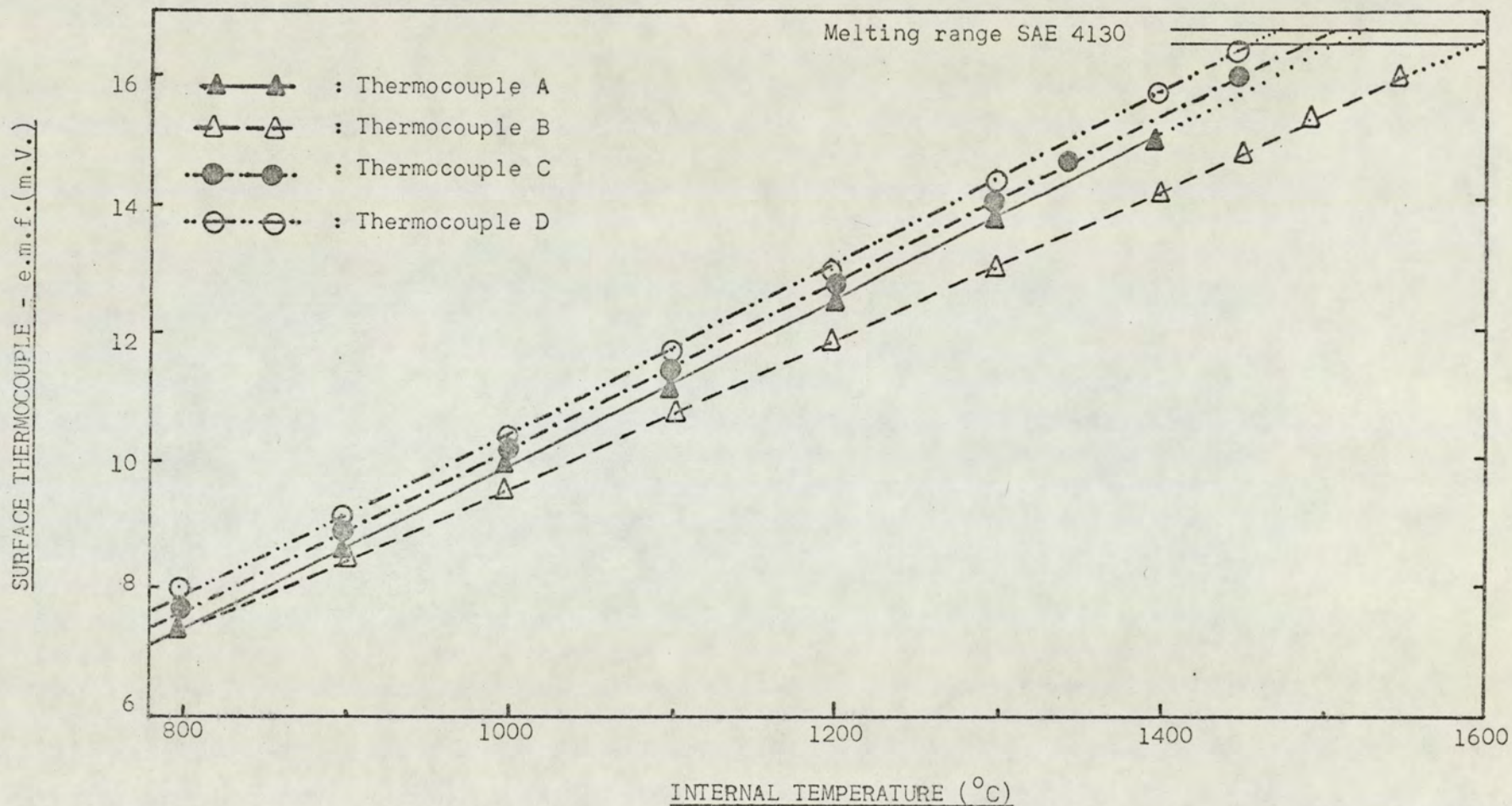


Fig. 2. Temperature Calibration Curves For Hot Ductility Specimen (Surface e.m.f.v. Internal Temperature)

Key to above:

A: 0.50mm diameter sheathed Cr/Al thermocouple

B: 1.56mm diameter sheathed Pt/Rh thermocouple

C: Bare wire Pt/Rh, inserted axially, attached to specimen.

D: Bare wire Pt/Rh, inserted axially, not attached to specimen.

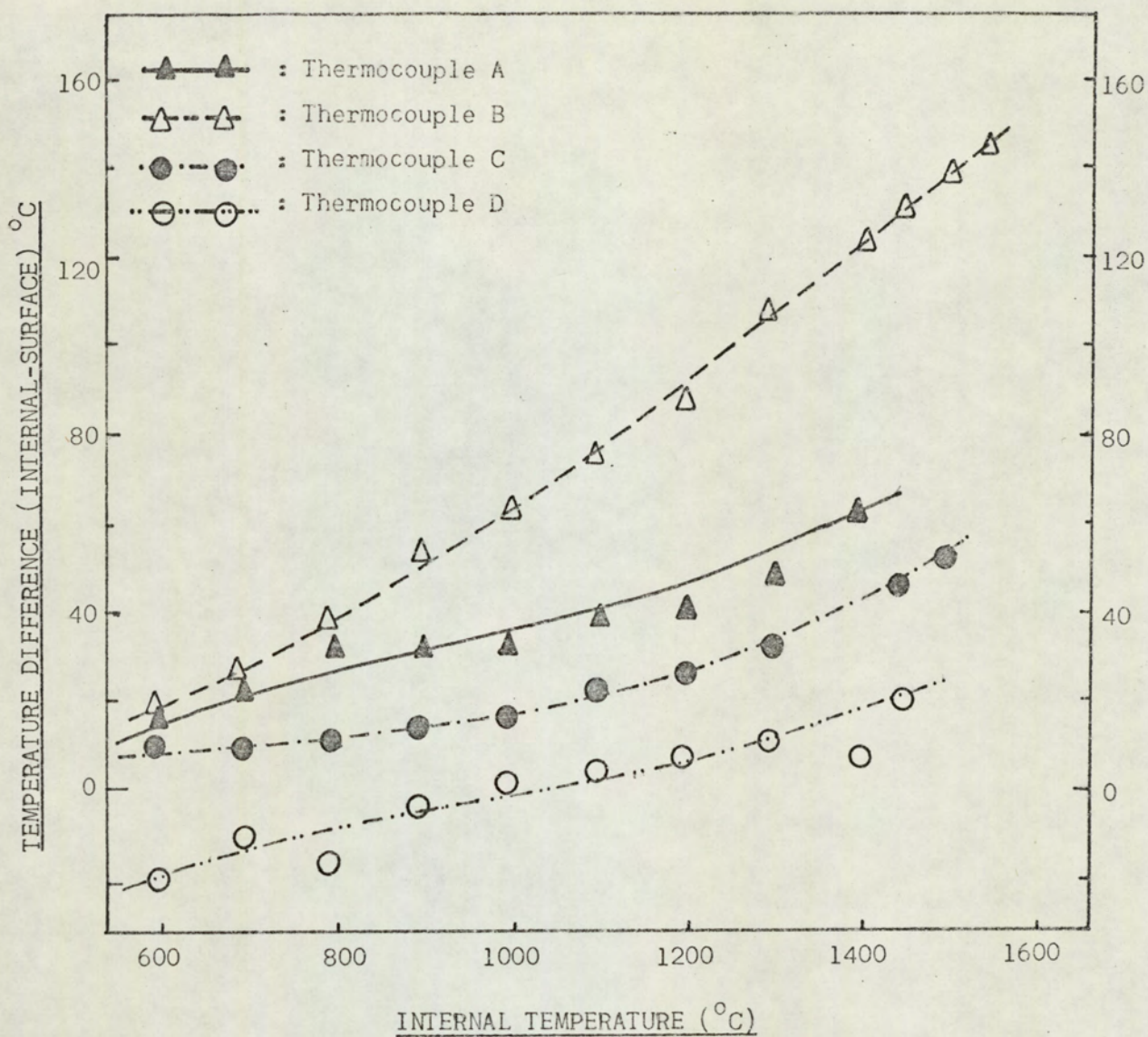


Fig. 3. Temperature Calibration Curves for Hot Ductility Specimen (Temperature Difference v Internal Temperature.)

- A: 0.50mm diameter sheath Cr/Al, inserted radially.
- B: 1.56mm diameter sheath Pt/Rh, inserted radially.
- C: Bare wire Pt/Rh, inserted axially, attached to specimen.
- D: Bare wire Pt/Rh, inserted axially, not attached to specimen.

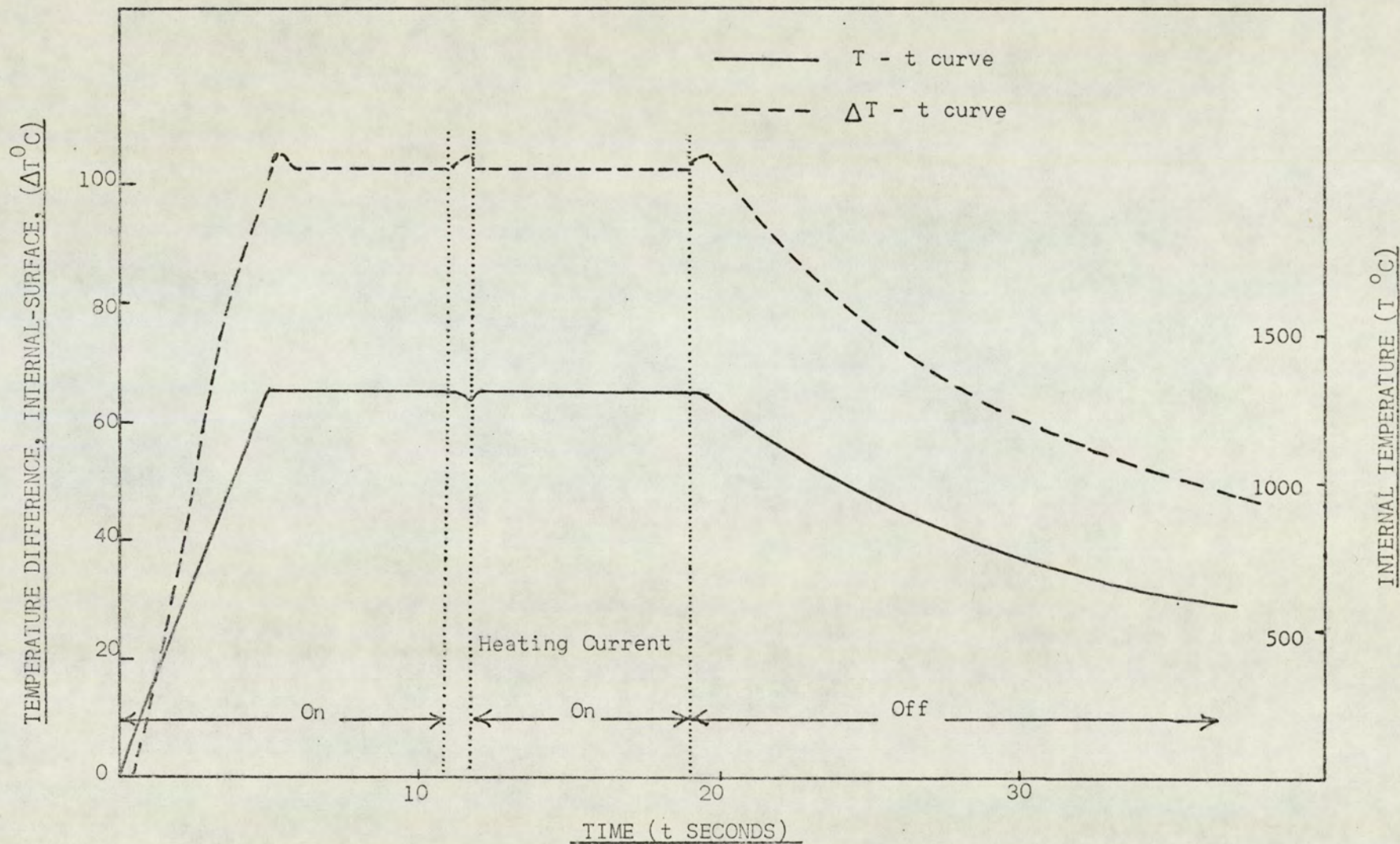


Fig. 4. Effect of Heating Current on the Temperature Difference Between Surface Thermocouple, and Internal 0.050mm Diameter Sheathed Thermocouple.

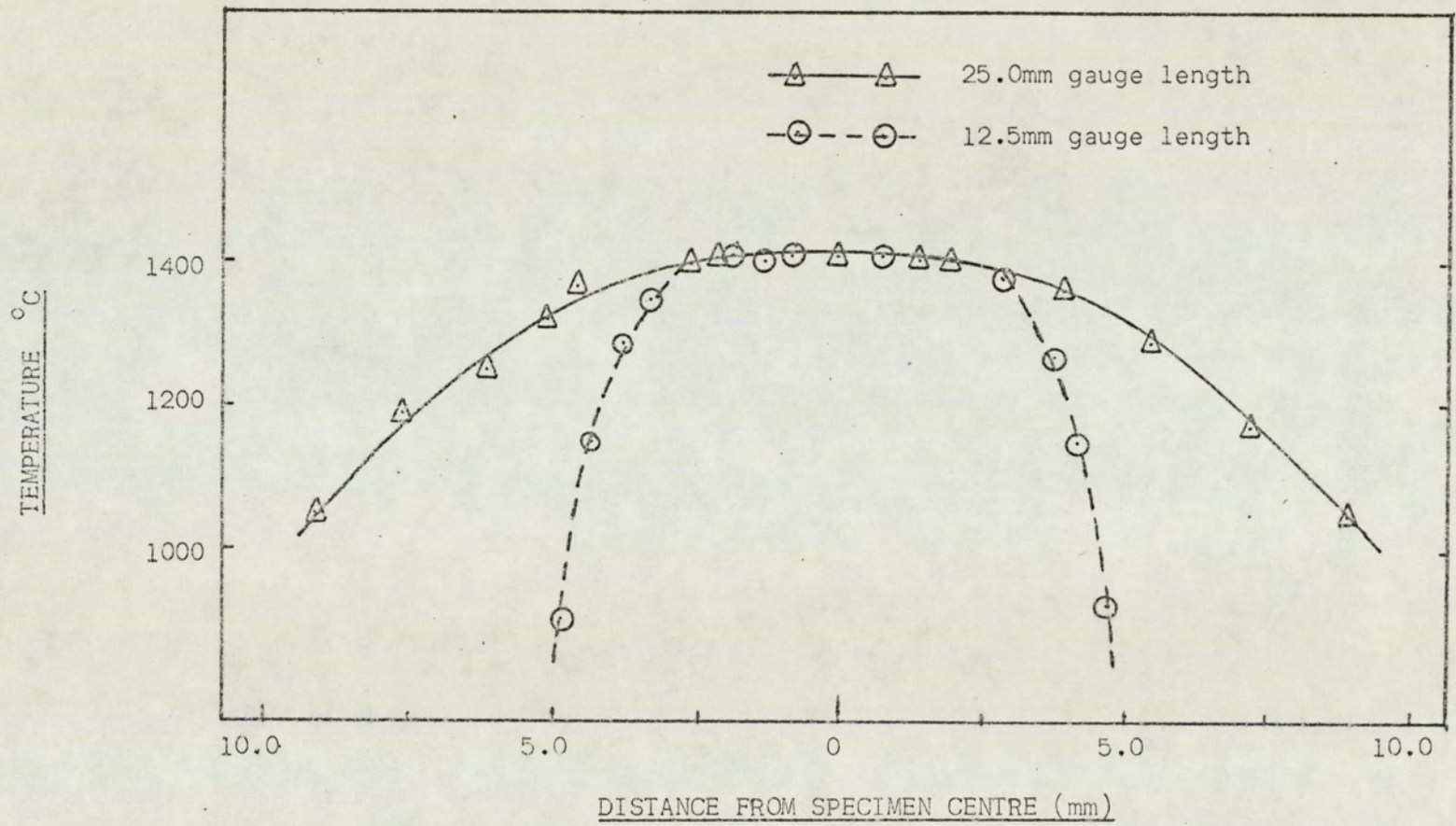


Fig. 5. Temperature Distribution Along 10mm Diameter Steel Specimen for Gauge Lengths of 12.5 and 25.0mm.

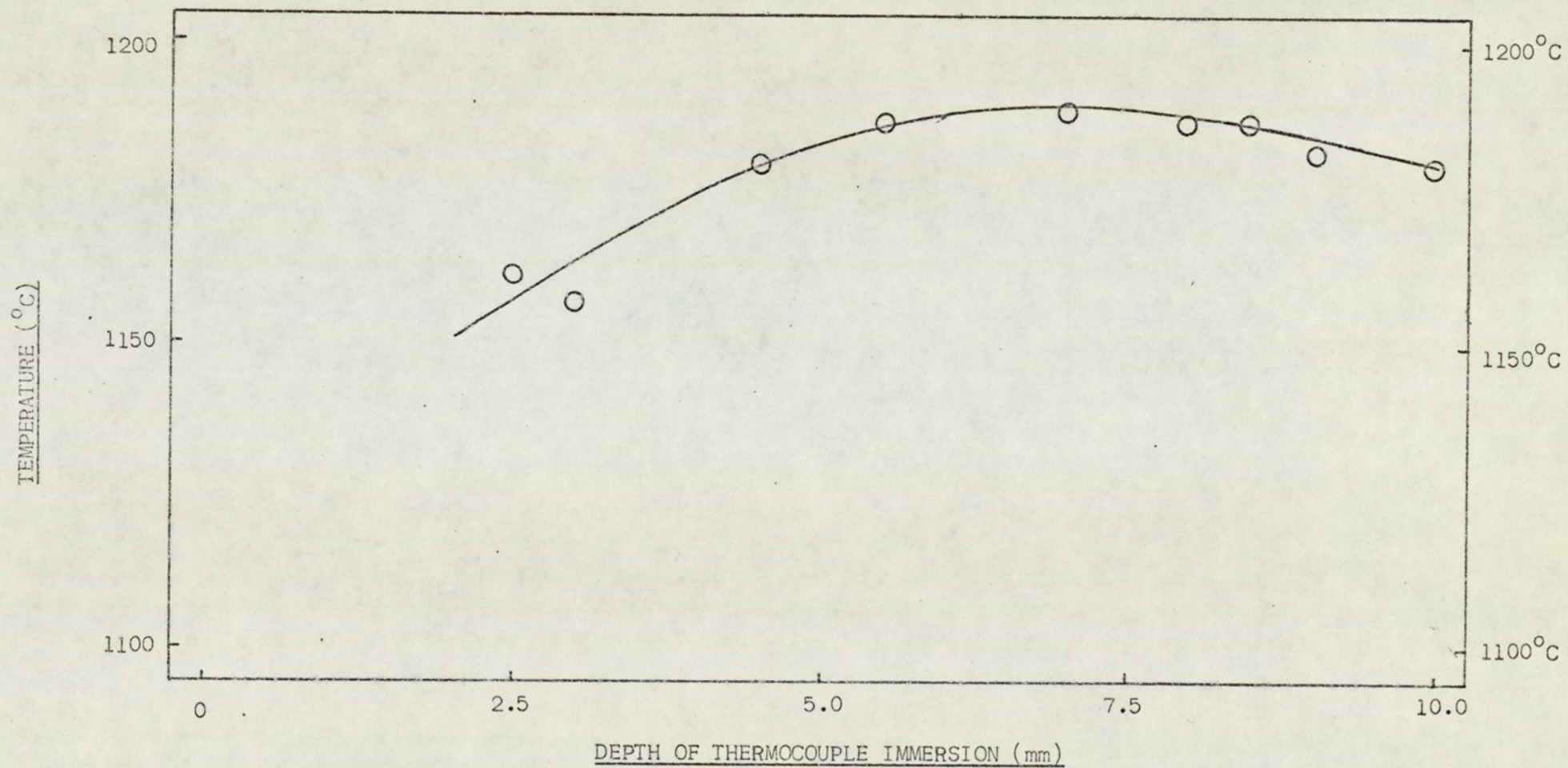


Fig. 6. Diametral Temperature Gradient Across Hot Ductility Specimen.

9.

REFERENCES

9. REFERENCES

1. E. Ineson, The Development and Application of Very Strong Steels. H.M.S.O. 1966
2. R.G. Baker, Brit. Weld. J., 1968, 15, 283-295
3. M.D. Randall, R.E. Monroe and P.J. Rieppel, Weld.J., 1962, 41, 193s-206s
4. B. Hemsworth, T. Boniszewski and N. Eaton, Metal Construction, 1969, 1, 5-14
5. W. Spraragen and G.E. Claussen, Welding Research Supplement, 1938, 17, 1-39
6. W. Spraragen and G.E. Claussen, Welding Research Supplement, 1939, 18, 44-49
7. R.P. Sopher, A.J. Jacobs and P.J. Rieppel, Weld.J., 1955, 34, 544s-552s
8. R.P. Sopher, Weld. J., 1958, 37, 481s-492s
9. F.J. Wilkinson, C.L.M. Cottrell and H.V. Huxley, Brit. Weld. J., 1958, 5, 557-562
10. F.J. Wilkinson and C.L.M. Cottrell, Welding and Metal Fab., 1958, 26, 171-184
11. H.V. Huxley, Welding and Metal Fab., 1963, 31, 29-32
12. F. Bonomo, B.W.R.A. Bulletin, 1968, M/22/68
13. E.J. Morgan-Warren, Ph.D. Thesis, University of Aston in Birmingham, September 1972
14. C.F. Meitzner and R.D. Stout, Weld. J., 1966, 45, 393s-400s
15. T. Boniszewski and F. Watkinson, Brit. Weld. J., 1964, 11, 610-619
16. T. Boniszewski and R.G. Baker, J.I.S.I., 1964, 202, 921-928
17. D. Widgery and T. Boniszewski, J.I.S.I., 1966, 204, 53-54
18. T. Boniszewski, B.W.R.A. Bulletin, 1965, 6, 144-152

19. K. Masubuchi and D. Martin, Weld. J., 1962, 41, 375s-384s
20. A.R.E. Singer and S.A. Cottrell, J. Inst. Metals., 1946, 73, 33-54
21. W.J. Pumphrey and P.H. Jennings, J. Inst. Metals., 1948, 75, 235-256
22. B.A. Movchan, Automatic Welding, 1959, 12, 59-81
23. W.F. Savage and E.S. Szekeres, Weld. J., 1967, 46, 94s-96s
24. W.A. Owczarski, D.S. Duvall, C.P. Sullivan, Weld. J., 1966, 45, 145s-155s
25. M.F. Jordan, University of Aston Report 1970, Weld Heat Affected Zone High Temperature Cracking and Hot Ductility Studies in HY 80
26. A. Vinckier, Metal Construction, 1969, 1, 276-277
27. A. Vinckier, Weld. J., 1971, 50, 19s-24s
28. D.C.G. Lees, J. Inst. Metals., 1946, 72, 343-364
29. A.R.E. Singer and P.H. Jennings, J. Inst. Metals., 1947, 73, 197-212
30. B.I. Medovar, Zhur. Tekh. Fuz., (Soviet Physics Technical Physics), 1957, 27, 1454-1457
31. W.S. Pellini, Foundry, 1952, 80, 124-133
32. W.R. Apblett and W.S. Pellini, Weld. J., 1954, 33, 83s-90s
33. P.P. Puzak, W. Apblett and W.S. Pellini, Weld. J., 1956, 35, 9s-17s
34. J.C. Borland, Brit. Weld. J., 1960, 7, 508-512
35. A. Portevin and M. Dannenmuller, J. Inst. Metals., 1948-49, 75, 949-972
36. B.I. Medovar, Zhur. Tekh. Fuz., (Soviet Physics Technical Physics), 1957, 27, 1454-1457
37. W.F. Savage and B. Krantz, Weld. J., 1966, 45, 13s-25s
38. D. Duvall and W. Owczarski, Weld. J., 1966, 45, 356s-384s
39. J.J. Pepe and W.F. Savage, Weld. J., 1967, 46, 411s-422s
40. L. Reeve, Trans. Inst. Weld., 1945, 8, 80-88

41. D.J. Widgery, B.W.R.A. Report, C139/B4/66
42. P.J. Brockhurst and H. Muir, Welding Fabrication and Design, 1965, 80-85
43. R.G. Baker and H.F. Tremlett, I.S.I. Special Report 76, (1962), 113-116
44. P.W. Jones, Brit. Weld. J., 1959, 6, 282-290
45. J.C. Borland, Brit. Weld. J., 1964, 11, 634-640
46. C.L.M. Cottrell, J.I.S.I., 1965, 203, 597-604
47. C.E. Makepeace, Weld. J., 1972, 51, 1s-8s
48. E.J. Morgan-Warren and M.F. Jordan, J.I.S.I., 1972, 210, 868-869
49. W.K.B. Marshall, Brit. Weld. J., 1960, 7, 451-453
50. B. Weiss, G.E. Grotke and R. Sticker, Weld. J., 1970, 49, 471s-487s
51. A. Preece and J. Nutting, J.I.S.I., 1950, 164, 46-50
52. T. Ko and D. Hanson, J.I.S.I., 1950, 164, 51-62
53. I.S. Brammar, J.I.S.I., 1963, 201, 752-761
54. L.H. Van Vlack, O.K. Reigger, R.J. Warrick and J.M. Dahl, Trans. Met. Soc. of A.I.M.E., 1961, 221, 220-228
55. J.C. Rivière, Atomic Energy Research Establishment Report 7122, May 1972
56. P.H. Salmon Cox and J.A. Charles, J.I.S.I., 1965, 203, 493-499
57. H.C. Chao, L. Thomassen and L.H. Van Vlack, Trans. A.S.M., 1964, 57, 386-398
58. R. Kammer, K. Masubuchi and R. Monroe, D.M.I.C. Report 197, 1964
59. D.S. Duvall and W.A. Owczarski, Weld. J., 1968, 47, 115s-120s
60. R. Younger, J. Borland and R. Baker, Brit. Weld. J., 1961, 8, 575-578
61. J.T. Berry and R.C. Allan, Welding and Metal Fabrication, 1962, 30, 271-276
62. J.M. Cargill, Strain, 1970, 6, 6-13

63. E. Nippes, W.F. Savage, B. Bastian, H. Mason and R. Curran, Weld. J., 1955, 34, 183s-196s
64. D.J. Widgery, Metal Construction & Brit.Weld.J., 1969, 1, 328-332
65. W.F. Savage, J. App. Polymer Science, 1962, 6, 303-315
66. M. Kh. Shorshorov, Brit. Weld. J., 1957, 4, 239-243
67. C.S. Williams, Weld. J., 1963, 42, 1s-8s
68. N.L. Balchin, B.W.R.A. Bulletin, 1968, 9, 3, 66-67
69. W. Yeniscovich, Weld. J., 1966, 45, 344s-356s
70. J. Heuschkel, Weld. J., 1956, 35, 569s-581s
71. H.M. Soldan and C.R. Mayne, Weld. J., 1957, 36, 141s-150s
72. E. Nippes, W. Savage and G. Grotke, W.R.C. Bulletin 33, 1957
73. C.H. Kreischer, Weld. J., 1963, 42, 49s-59s
74. K.C. Wu and R.E. Herbert, Weld. J., 1967, 46, 32s-38s
75. T. Moore, Weld. J., 1959, 38, 457s-474s
76. H.M. Soldan, G. Schnabel and T.J. Moore, Weld. J., 1963, 42, 55s-59s
77. W. Yeniscavich, W.R.C. Symposium 'Methods of High Alloy Weldability Evaluation', 1970, 2-12
78. T.G. Gooch, R.D. Howard, D. McKeon and D.J. Widgery, International Conference on Welding Research Related to Power Plant, Central Electricity Generating Board, September 1972, 1-9
79. D.S. Duvall and W.A. Owczarski, Weld. J., 1967, 46, 423s-432s
80. W.G. Shreitz, Weld. J., 1965, 44, 310s-316s
81. E. Smith, M. Coward and R. Apps, Welding and Metal Fab., 1970, 38, 242-251
82. R.E. Dolby and D.J. Widgery, W.I. Report M/52/70
83. M.C. Coleman, Ph.D. Thesis, University of Aston in Birmingham, 1971
84. H.D. Baker, E.A. Ryder and N.H. Baker, 'Temperature Measurement in Engineering', Vol. 1, 1953, Chapman and Hall, Ch. 7

85. D.M. Keane, E.N. Bower and J. Hammond, Welding Institute Seminar on 'Weld Thermal Simulators for Research and Problem Solving', 1972, 44-49
86. K.A. Brownlee, Industrial Experimentation, H.M.S.O., 1949
87. N. Christenson, V. de L. Davies and K. Gjermundsen, Brit. Weld. J., 1965, 12, 54-75
88. W.E. Duckworth, Statistical Techniques in Technological Research, Methuen and Co. Ltd., 1968
89. J.W. Christian, I.S.I., Special Report 93, 1965, 1-19
90. D. Rosenthal, Trans. A.S.M.E., 1946, 68, 849-866
91. B.L. Shultz and C.E. Jackson, Welding Research Council, 1973, 38, 265-375
92. Aerospace Structural Metals Handbook, Vol. 1., 1966, Ed. V. Weiss, Syracuse University Press

TABLE 1. Planned Compositions of Experimental Materials

Material	Composition % wt		
	Carbon	Sulphur	Phosphorus
SAE 4130	0.30	low < 0.010	low < 0.010
	0.30	high > 0.030	high > 0.030
	0.30	low < 0.010	high > 0.030
	0.30	high > 0.030	low < 0.010
SAE 4130 special casts	(0.30	ultra low < 0.001	ultra low < 0.001
	(0.30	ultra low < 0.001	high > 0.030
	0.30	high > 0.030	ultra low < 0.001
EN 24	0.42	low < 0.010	low < 0.010
	0.42	high > 0.030	high > 0.030
ASTM 387B	0.12	low < 0.010	low < 0.010
	0.12	high > 0.030	high > 0.030

TABLE 2. Actual Compositions of Experimental Materials

Material	Code	Composition % wt								
		C	S	P	O	Si	Mn	Ni	Cr	Mo
SAE 4130	SA ^x	0.28	0.025	0.030	0.0035	0.17	0.67	0.13	0.92	0.19
	SB	0.35	0.009	0.008	0.0032	0.34	0.70	0.02	0.99	0.21
	SC	0.35	0.032	0.032	0.0049	0.37	0.69	0.01	0.99	0.22
	SD	0.35	0.010	0.049	0.0097	0.06	0.85	0.01	0.92	0.27
	SE	0.35	0.033	0.010	0.0089	0.34	0.70	0.01	1.02	0.23
SAE 4130 special casts	(SG _P	0.35	<0.001	0.035	0.0006	0.31	0.70	0.01	0.90	0.22
	(SG _{HD}	0.35	0.0016	0.057	0.0021	0.30	0.79	0.01	1.00	0.22
	(SH _P	0.36	0.031	<0.001	0.0032	0.28	0.66	0.01	0.85	0.22
	(SH _{HD}	0.31	0.040	<0.001	0.0021	0.28	0.75	0.01	1.14	0.24
	(SY _P	0.32	<0.001	<0.001	0.0014	0.29	0.62	0.01	0.93	0.25
	(SY _{HD}	0.37	0.001	<0.001	0.007	0.18	0.64	0.01	0.88	0.22
	EN 24	EA ^x	0.38	0.027	0.013	0.0017	0.35	0.65	1.38	1.17
	EB	0.37	0.010	0.010	0.0052	0.53	0.63	1.37	1.07	0.24
	EC	0.46	0.036	0.008	0.0032	0.58	0.64	1.38	1.08	0.30
ASTM 387B	AA	0.13	0.010	0.008	0.009	0.30	0.50	0.01	0.91	0.37
	AB	0.11	0.036	0.031	0.0062	0.36	0.51	0.01	0.88	0.36

x is Commercial Cast by Redheugh

For SAE 4130 (Special casts only):

P is Plate Composition

HD is Hot Ductility Specimen Composition

TABLE 3. Welding Wire Compositions

Material	Code	Wire Diameter	Composition wt %						
			C	S	P	Si	Mn	Cr	Mo
Mild Steel	MS	1.58 mm	0.082	0.024	0.025	0.93	1.47	-	-
1% Cr-Mo	CM	1.58 mm	0.088	0.011	0.011	0.76	1.55	1.06	0.50

TABLE 4. Effect of Welding Procedural Variables - Welding Conditions and Weld Bead Profile Parameters

Specimen Number	Welding Conditions				Weld Bead Profile Parameters			
	Arc Current (Amps)	Arc Voltage (Volts)	Travel Speed (mm/sec)	Heat Input (KY/mm)	A (mm)	B (mm)	C (mm)	D (mm)
SC 1	500	34	4.2	3.0	27	1.5	8	3.6
SC 2	330	38	2.9	3.0	24	1.2	3.5	2.0
SC 3	500	26	7.6	1.2	12	2.5	7.0	1.4
SC 4	330	38	8.4	1.2	12	0.9	2.2	0.9
SC 5	500	34	4.2	3.0	27	1.2	9.5	3.6
SC 6	330	38	2.9	3.0	27	1.2	3.0	1.7
SC 7	500	26	7.6	1.2	12	1.5	8.5	1.5
SC 8	330	38	8.4	1.2	14	0.7	2.5	1.2
SC 9	500	34	4.2	3.0	29	1.5	11.0	4.8
SC 10	330	38	2.9	3.0	27	1.3	3.0	1.6
SC 11	500	26	7.6	1.2	12	2.0	7.0	1.2
SC 12	330	38	8.4	1.2	11	0.5	1.6	1.0
SC 13	500	34	4.2	3.0	27	1.5	9.0	3.8
SC 14	330	38	2.9	3.0	27	1.0	4.0	2.0
SC 15	500	26	7.6	1.2	13	2.8	7.0	1.6
SC 16	330	38	8.4	1.2	12	0.9	2.1	1.0

Table 5. Effect of Welding Parameters - Results of Metallographic Examination

Specimen Number	Level of Welding Parameter				No. of Cracks	Combined Crack Length (mm)	Crack Length Distribution (mm)				Number >.06 (mm)	Max. Crack Length (mm)	Max. Dist. Fusion Boundary (mm)	Max. Width M.I.Z. (mm)
	Energy Input	Finger Penetration	Restraint	Weld. Metal			<.02	>.02	>.06	>.15				
							≤.06	≤.15						
SC 1	H	H	H	C.M.	21	1.70	9	5	4	3	7	0.26	0.50	0.60
SC 2	H	L	L	C.M.	13	0.32	10	3	0	0	0	0.06	0.08	0.40
SC 3	L	H	L	C.M.	8	0.22	6	1	1	0	1	0.08	0.16	0.24
SC 4	L	L	H	C.M.	2	0.06	1	1	0	0	0	0.04	0.06	0.25
SC 5	H	H	L	M.S.	28	1.10	17	8	3	0	3	0.13	0.45	0.55
SC 6	H	L	H	M.S.	15	0.47	9	6	0	0	0	0.06	0.15	0.42
SC 7	L	H	H	M.S.	15	0.48	7	5	2	0	2	0.11	0.22	0.26
SC 8	L	L	L	M.S.	6	0.22	2	3	1	0	1	0.07	0.26	0.30
SC 9	H	H	H	M.S.	59	2.64	26	19	13	1	14	0.23	0.62	0.65
SC 10	H	L	L	M.S.	16	0.54	10	4	2	0	2	0.10	0.30	0.42
SC 11	L	H	L	M.S.	7	0.26	3	3	1	0	1	0.08	0.10	0.24
SC 12	L	L	H	M.S.	8	0.24	5	2	1	0	1	0.09	0.15	0.24
SC 13	H	H	L	C.M.	39	0.99	26	12	1	0	1	0.09	0.55	0.60
SC 14	H	L	H	C.M.	26	0.93	13	8	4	1	5	0.18	0.40	0.45
SC 15	L	H	H	C.M.	22	0.76	11	8	3	0	3	0.10	0.20	0.30
SC 16	L	L	L	C.M.	7	0.14	5	2	0	0	0	0.05	0.07	0.23

TABLE 6a. Effect of Welding Procedural Variables -
Analysis of Variance

ANALYSIS OF VARIANCE		MAT1	
ANALYSIS OF VARIANCE	MAT1	IP	F TEST
MODEL $Y=A(I)+B(J)+C(K)+D(L)+AB(IJ)+AC(IK)+AD(IL)+BC(JK)+$ $BD(JL)+CD(KL)+ABC(IJK)+ABD(IJL)+ACD(IKL)+BCD(JKL)+$ $ABCD(IJKL)+E$			
NUMBER OF LEVELS OF FACTOR SUBSCRIPTS (4)			
A-I	...	2	
B-J	...	2	
C-K	...	2	
D-L	...	2	
I IS ENERGY INPUT J IS FINGER PENETRATION			
MODEL TERM	SUM OF SQUARES	DEGREES OF FREEDOM	VARIANCE
*****	*****	*****	*****
A(I).	2.44141E	1	2.44141
B(J).	1.67056E	1	1.67056
C(K).	.473063E-	1	0.04731
D(L).	.743906E	1	0.74391
AB(IJ).	.628056E	1	0.62806
AC(IK).	.351563E-	1	0.03516
AD(IL).	.283556E	1	0.28356
BC(JK).	.351563E-	1	0.03516
BD(JL).	.412806E	1	0.41281
CD(KL).	.105625E-	1	0.00106
ABC(IJK).	.209306E	1	0.20931
ABD(IJL).	.451562E-	1	0.04516
ACD(IKL).	.115562E-	1	0.01156
BCD(JKL).	.826562E-	1	0.08266
ABCD(IJKL).	.218556E	1	0.21856
RESIDUAL.	.000000E	0	0.00000
TOTALS.	.686619E	15	0.45775

K is Weld Metal

L is Restraint

TABLE 6b. Effect of Welding Procedural Variables -
Significance Tests

ANALYSIS OF VARIANCE						MAT1	
MODEL TERM	SUM OF SQUARES	D.O.F	RESIDUAL F. VARIANCE	VARIANCE RATIO	SIGNIFICANCE AT % LEVELS		
*****					5	1	
A(I).1963E	1	11	0.178	13.681	YES	YES	
B(J).1963E	1	11	0.178	0.361	YES		
C(K).1963E	1	11	0.178	0.265			
D(L).1963E	1	11	0.178	4.169			
AB(IJ).5672E	0	5	0.113	5.536			
AC(IK).5672E	0	5	0.113	0.310			
AD(IL).5672E	0	5	0.113	2.499			
BC(JK).5672E	0	5	0.113	0.310			
BD(JL).5672E	0	5	0.113	3.630			
CD(KL).5672E	0	5	0.113	0.009			
ABC(IJK).2186E	0	1	0.219	0.958			
ABD(IJL).2186E	0	1	0.219	0.207			
ACD(IKL).2186E	0	1	0.219	0.053			
BCD(JKL).2186E	0	1	0.219	0.378			
ABCD(IJKL).0000E	0	0					

I is Energy Input
K is Weld Metal

J is Finger Penetration
L is Restraint

TABLE 7. Effect of Distance Along Weld Bead on Cracking Propensity in S.C.1.

Distance from Weld Bead Finish (mm)	No. of Cracks	Combined Crack Length (mm)	Crack Length Distribution					No. of Cracks >0.06 (mm)	Max. Crack Length (mm)	Max. distance of cracks from fusion boundary (mm)
			<.02	>.02 <.06	>.06 <.15	>.15 <.30	>.30			
120	30	0.82	22	6	1	1	0	2	0.25	0.35
60	21	1.70	9	5	4	3	0	7	0.26	0.50
50	44	1.88	19	19	7	1	0	8	0.16	0.52
20	85	4.27	36	32	8	7	1	16	0.31	0.54

TABLE 8. Effect of Composition and Restraint on Cracking Propensity

Weld Beads : Deep Finger Penetration at Heat Input of 3KJ/mm

Steel Code	Restraint	Distance from Weld Bead Finish (mm)	Number of Cracks	Combined Crack Length (mm)	Crack Length Distribution (mm)					No. of Cracks >.06 (mm)	Max. Crack Length (mm)	Max. distance of cracks from fusion boundary (mm)	Max. width M.I.Z. (mm)
					≤.02	>.02 ≤.06	>.06 ≤.15	>.15 ≤.30	>.30				
SA 1A	Yes	20	45	1.75	24	15	4	2	0	6	0.24	0.55	0.60
1B	Yes	60	32	1.44	14	11	5	1	0	6	0.17	0.35	0.60
2	No	60	15	0.41	11	3	1	0	0	1	0.15	0.15	0.55
SB 1A	Yes	20	17	0.39	10	6	1	0	0	1	0.10	0.15	0.55
1B	Yes	60	8	0.14	7	1	0	0	0	0	0.03	0.04	0.55
2	No	60	15	0.23	13	2	0	0	0	0	0.04	0.16	0.50
SC 1A	Yes	20	84	4.27	36	32	8	7	1	16	0.31	0.54	0.60
1B	Yes	60	21	1.70	9	5	4	3	0	7	0.26	0.50	0.60
9	Yes	60	59	2.64	26	19	13	1	0	14	0.23	0.62	0.65
5	No	60	28	1.10	17	8	3	0	0	3	0.13	0.45	0.55
13	No	60	39	0.99	26	12	1	0	0	1	0.09	0.55	0.60
SD 1A	Yes	20	73	3.46	32	26	10	3	2	15	0.42	0.60	0.65
1B	Yes	60	61	2.43	30	19	11	1	0	12	0.17	0.50	0.65
2	No	60	24	0.78	10	11	3	0	0	3	0.10	0.25	0.55
SE 1A	Yes	20	58	1.51	38	20	2	0	0	2	0.14	0.35	0.53
1B	Yes	60	20	0.50	14	6	0	0	0	0	0.06	0.20	0.58
2	No	60	12	0.24	9	3	0	0	0	0	0.06	0.18	0.55
SC 1A	Yes	20	69	2.42	40	21	8	0	0	8	0.15	0.40	N.D.
1B	Yes	60	52	1.84	32	14	6	0	0	6	0.12	0.30	N.D.
2A	Yes	20	66	1.96	47	13	5	1	0	6	0.28	0.38	N.D.
2B	Yes	60	41	0.98	31	9	1	0	0	1	0.07	0.40	N.D.
SH 1A	Yes	20	41	1.30	28	8	5	0	0	5	0.14	0.42	0.68
1B	Yes	60	19	0.46	14	5	0	0	0	0	0.04	0.36	0.62
2A	Yes	20	36	1.16	26	7	3	0	0	3	0.14	0.36	0.65
2B	Yes	60	14	0.34	10	4	0	0	0	0	0.04	0.20	0.60
SY 1A	Yes	20	0	0	0	0	0	0	0	0	0	0	N.D.
1B	Yes	60	0	0	0	0	0	0	0	0	0	0	N.D.
2A	Yes	20	0	0	0	0	0	0	0	0	0	0	N.D.
2B	Yes	60	0	0	0	0	0	0	0	0	0	0	N.D.
AA 1A	Yes	20	0	0	0	0	0	0	0	0	0	0	N.D.
1B	Yes	60	0	0	0	0	0	0	0	0	0	0	N.D.
2A	No	60	0	0	0	0	0	0	0	0	0	0	N.D.
AB 1A	Yes	20	44	1.86	25	10	6	3	0	9	0.23	0.40	0.45
1B	Yes	60	34	0.74	28	4	2	0	0	2	0.08	0.27	0.43
2	No	60	15	0.45	10	3	2	0	0	2	0.11	0.30	0.40
EA 1A	Yes	20	43	1.86	20	16	5	2	0	7	0.30	0.48	0.55
1B	Yes	60	47	1.40	36	6	4	1	0	5	0.16	0.48	0.55
2	No	60	21	0.48	15	5	1	0	0	1	0.09	0.25	0.60
EB 1A	Yes	20	54	2.05	27	19	7	1	0	8	0.25	0.50	0.60
1B	Yes	60	26	0.43	24	2	0	0	0	0	0.05	0.09	0.58
2	No	60	25	0.39	22	3	0	0	0	0	0.04	0.18	0.60
EC 1A	Yes	20	102	2.71	65	28	6	2	1	9	0.36	0.60	0.65
1B	Yes	60	66	1.80	43	18	5	0	0	5	0.12	0.34	0.62
2	No	60	28	0.58	21	6	1	0	0	1	0.09	0.25	0.65

N.D. = Not determined

TABLE 9. Paired Comparison Test for Effect of Restraint on Crack Propensity.

Steel Code	Combined crack length at 60 mm		Restrained — Non-Restrained	Deviation from mean	(Deviation from mean) ²
	Non-Restrained	Restrained			
SA	0.41	1.44	1.03	+ .37	.137
SB	0.23	0.14	- .09	- .75	.560
SC	1.05	2.17	1.12	+ .56	.312
SD	0.78	2.43	1.65	+ .99	.985
SE	0.24	0.50	0.26	- .40	.160
SY	0	0	0	- .66	.432
AC	0	0	0	- .66	.432
AD	0.45	0.74	.29	- .37	.137
EA	0.48	1.40	0.92	+ .26	.067
EB	0.39	0.43	0.04	- .62	.385
EC	0.58	1.80	1.22	+ .56	.312
			Mean = 0.66		Total = 3.626

$$\begin{aligned} \text{Standard Deviation} &= \frac{\sqrt{3.626}}{10} \\ &= .601 \end{aligned}$$

The test is whether the mean difference of 0.66 is significantly different from zero, with a standard error of this mean difference of $0.601/\sqrt{11}$

$$\text{Therefore } t = \frac{0.66 - 0}{0.601/\sqrt{11}} = 3.58$$

Inspection of the t tables at $\phi = 10$, we find that the probability is 0.5% i.e. Restraint is highly significant.

TABLE 10. Analysis of Regression of Crack Index on Independent Variables Significant at the 5% Level.

Independent Variable	Regression Co-efficient	Standard Error	T Statistic	Partial Correlation
Carbon	4.804	0.105	4.55	0.70
Sulphur	26.852	0.778	3.45	0.60
Phosphorus	52.585	0.683	7.69	0.86

Intercept term: - 0.3936 Correlation 0.91

Residual Error 0.5031 Degrees of Freedom 21

Table 11. Temperature Reproducibility of Bare Wire Surface Thermocouples

Thermocouple type	0.25 mm Chromel/Alumel		0.25 mm Pt/Pt 13% Rh	
Method of Attachment	Percussion welded as bead	Percussion welded as separate wires	Percussion welded as separate wires	Resistance welded as separate wires
Recorded surface temperature	1115°C	1115°C	1285°C	1285°C
Internal Temperature } mean	1227°C	1167°C	1414°C	1397°C
Internal Temperature } scatter	± 33°C	± 7°C	± 38°C	± 7°C

TABLE 12. Determination of Melting Temperature of SAE 4130

Calibration	Melting Range °C
A	1512 - 1532
B	1596 - 1618
C	1486 - 1504
D	1456 - 1476

TABLE 13. Hot Ductility Results - Basic Parameters

Steel Code	N.D.T. (°C)	N.S.T. (°C)	Melting Temperature (°C)	Temperature Interval (°C) (Melting - N.D.T)
SA	1444	1480	1516	72
SB	1448	1476	1516	68
SC	1440	1476	1516	76
SD	1446	1480	1520	74
SE	1433	1466	1508	75
SG	1446	1480	1520	74
SH	1446	1480	1520	74
SY	1467	1484	1520	53
AA	1488	1510	1540	52
AB	1475	1495	1532	57
EB	1420	1456	1496	76
EC	1416	1452	1492	76

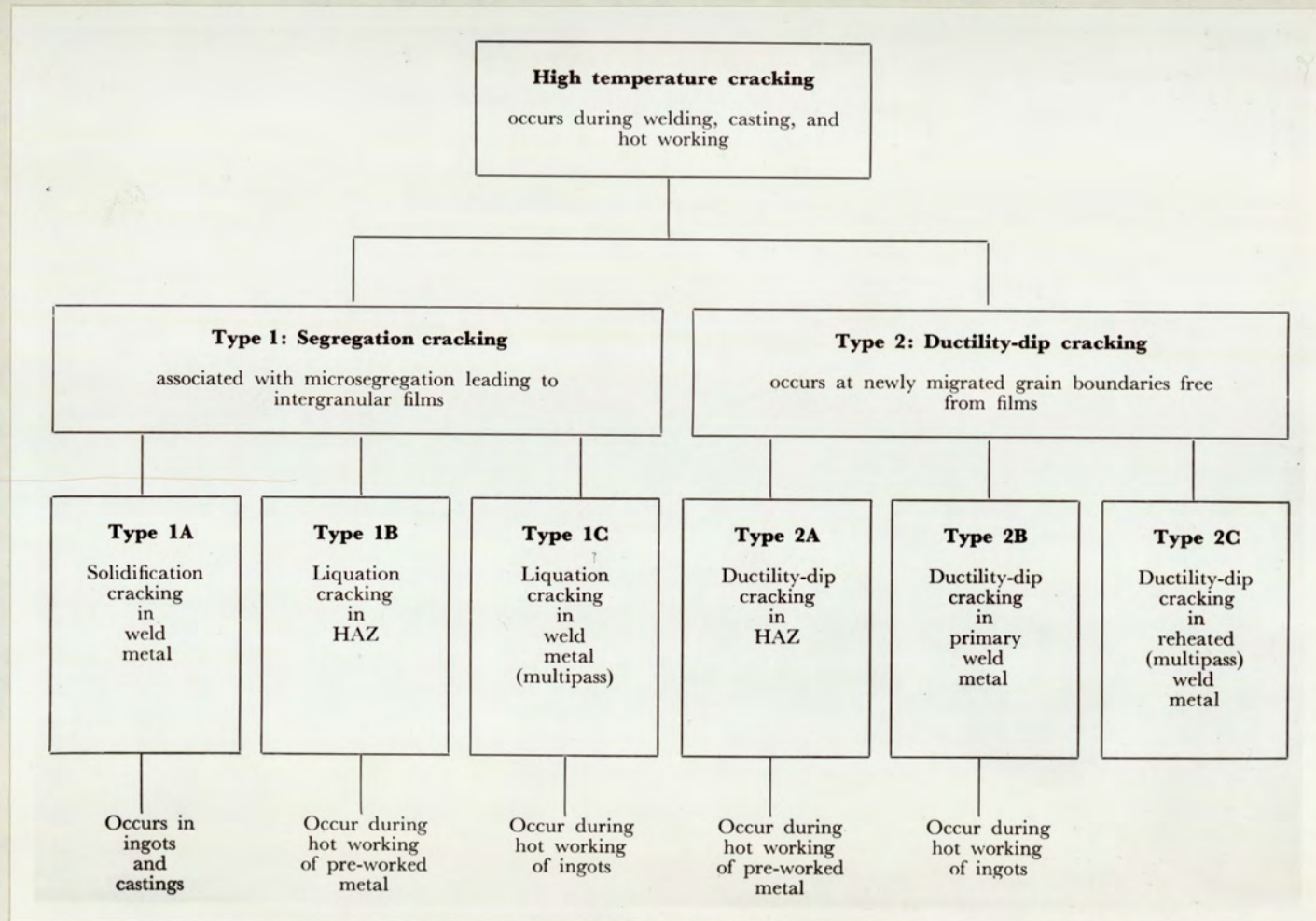


Fig.1. Classification of Intergranular Welding Cracks (after Hemsworth et al⁽⁴⁾)

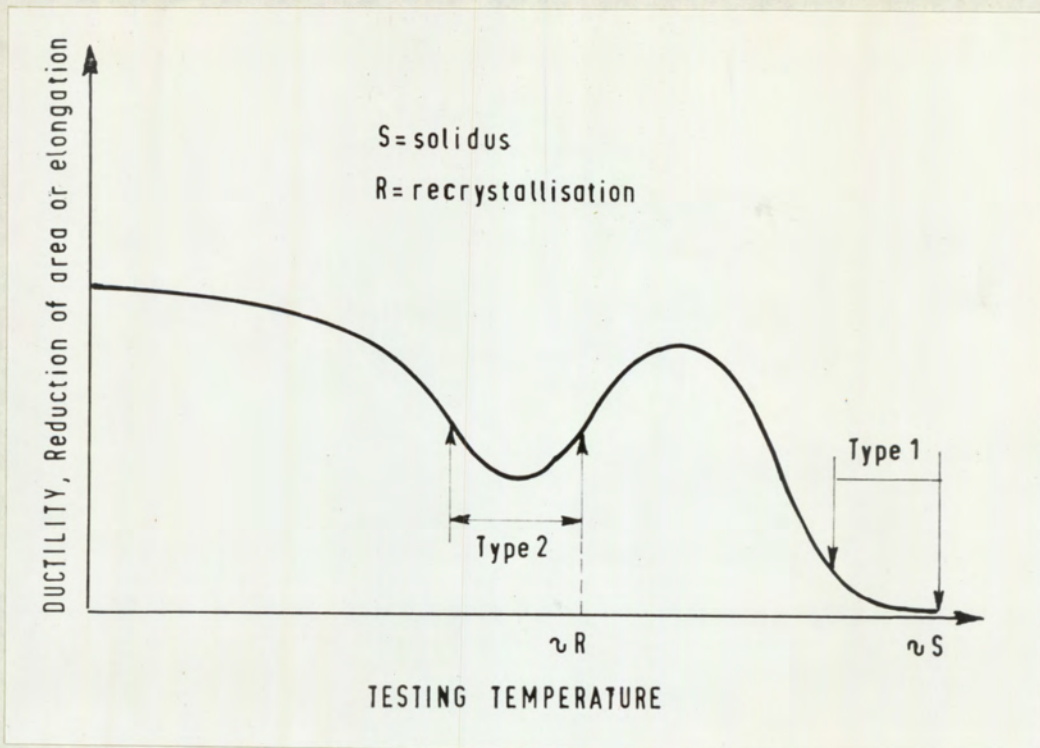
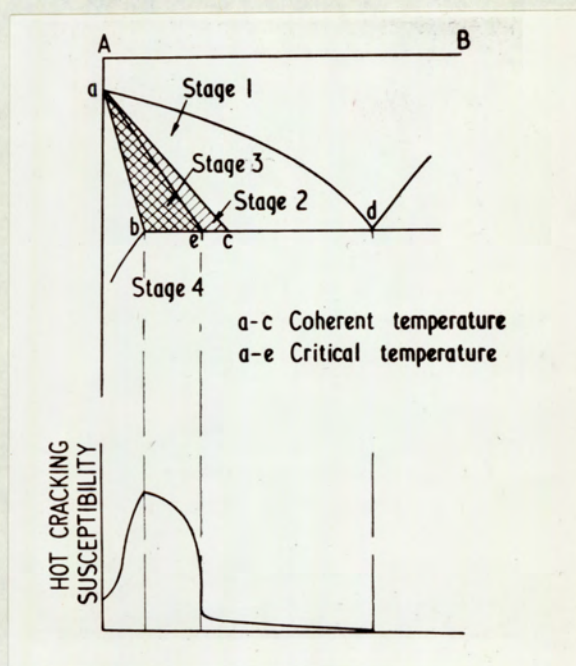


Fig. 2. Schematic Representation of Two Temperature Ranges in which Low Ductility is Conducive to Cracking During Welding. (after Hemsworth et al.⁴)



- Stage 1. Dendrites dispersed freely in liquid - no cracking
- Stage 2. Interlocking of grains. Healing possible. "Accommodation" not important
- Stage 3. Critical solidification range - no healing possible if "accommodation" strain exceeded
- Stage 4. Solid - no cracking

Fig. 3. Effect of Constitutional Features on Solidification Cracking in Binary Systems. (Generalised Theory) (after Borland³⁴)

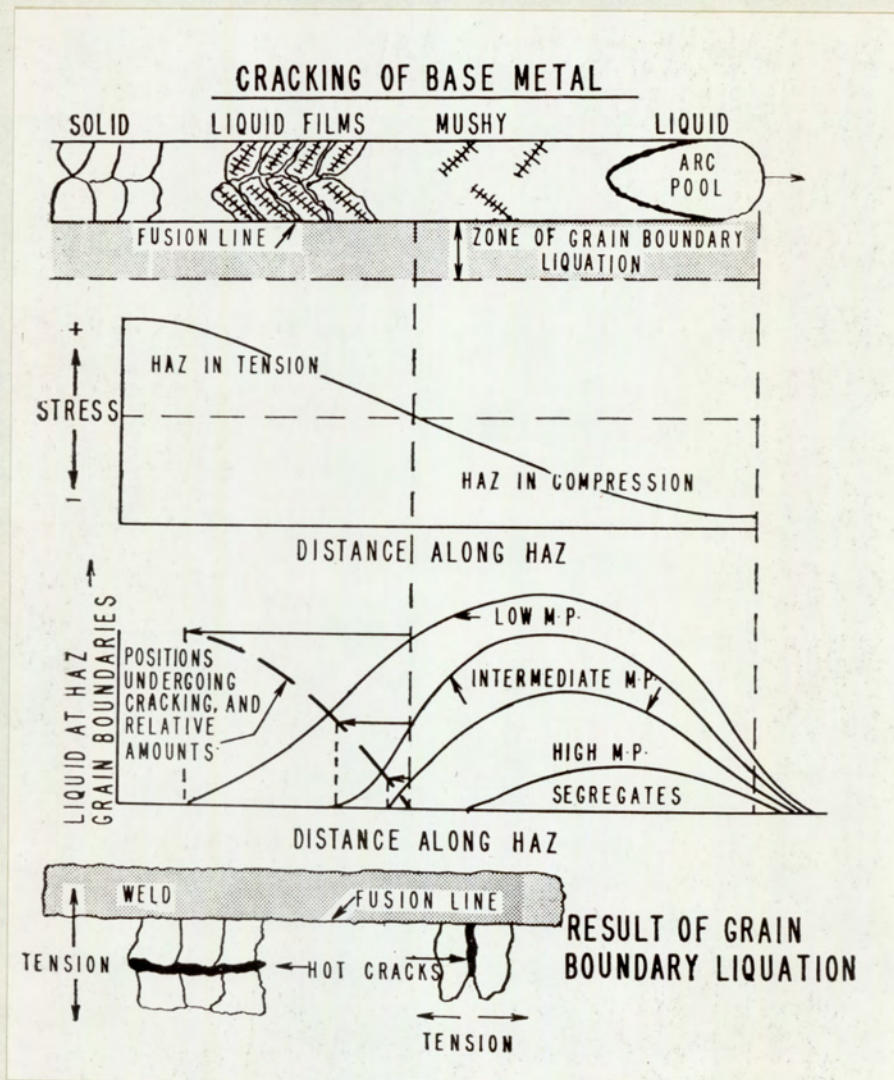
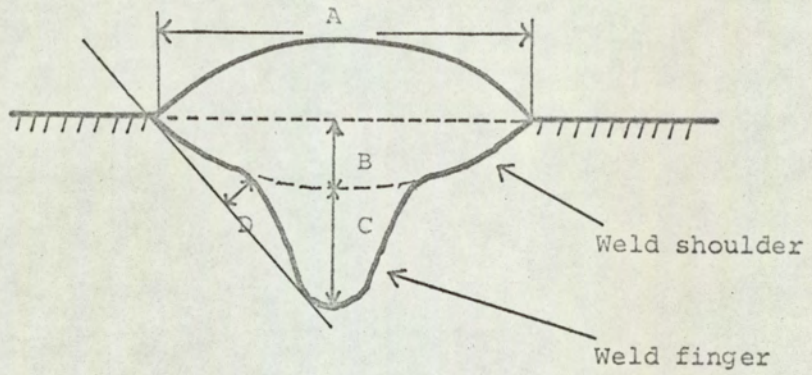


Fig.4. Schematic Representation of the Formation of Heat Affected Zone Liquation Cracks.
 (after Puzak et al³³)



- A = WELD WIDTH
- B = ELLIPTICAL POOL DEPTH
- C = FINGER DEPTH
- D = MAXIMUM DISTANCE FROM TANGENT TO FUSION LINE

Fig.5. Transverse Section of Bead-on-Plate Specimen defining Contour Parameters (14)

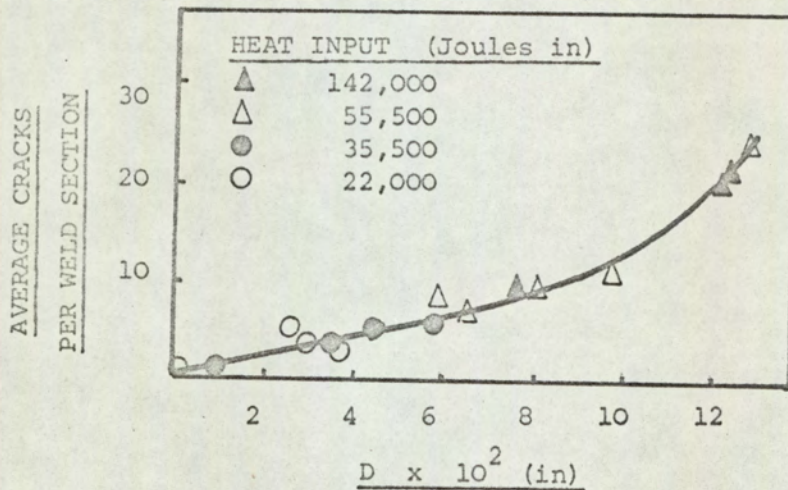


Fig.6. Cracking V^S Weld Bead Parameter D (HY 80 Steel) (14)

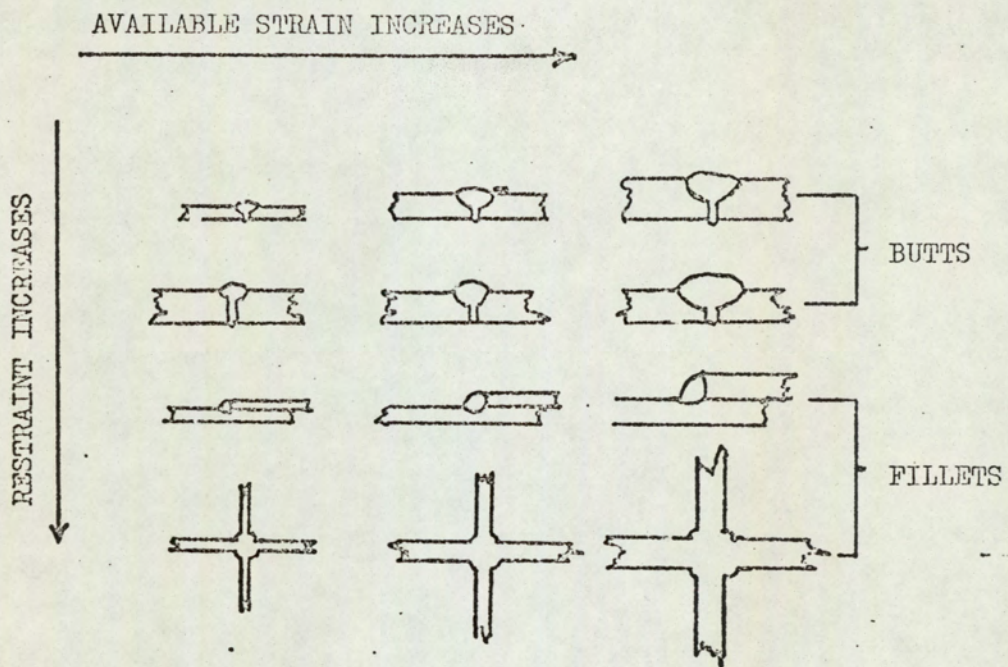
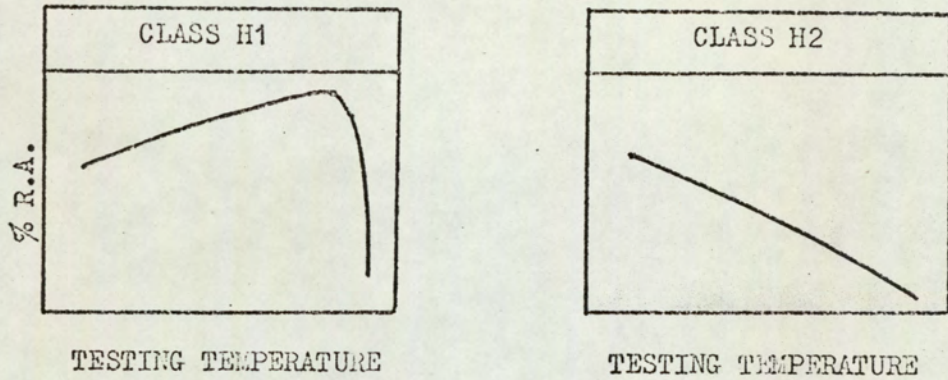


Fig. 7.

Schematic Representation of Effects of Bead Size, Plate Thickness and Joint Geometry on Strain. (61)

TYPICAL 'ON-HEATING' BEHAVIOUR



TYPICAL 'ON-COOLING' BEHAVIOUR

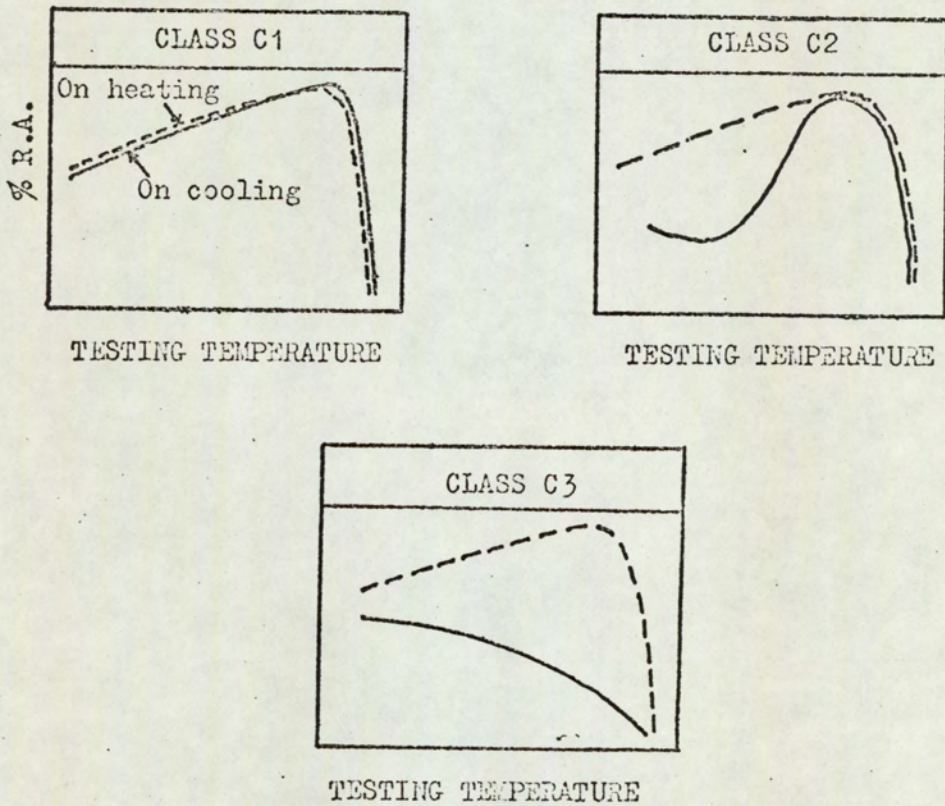


Fig.8. Classification of 'On-Heating' and 'On-Cooling' Ductility Behaviour, According to Nippes et al⁽⁷²⁾.

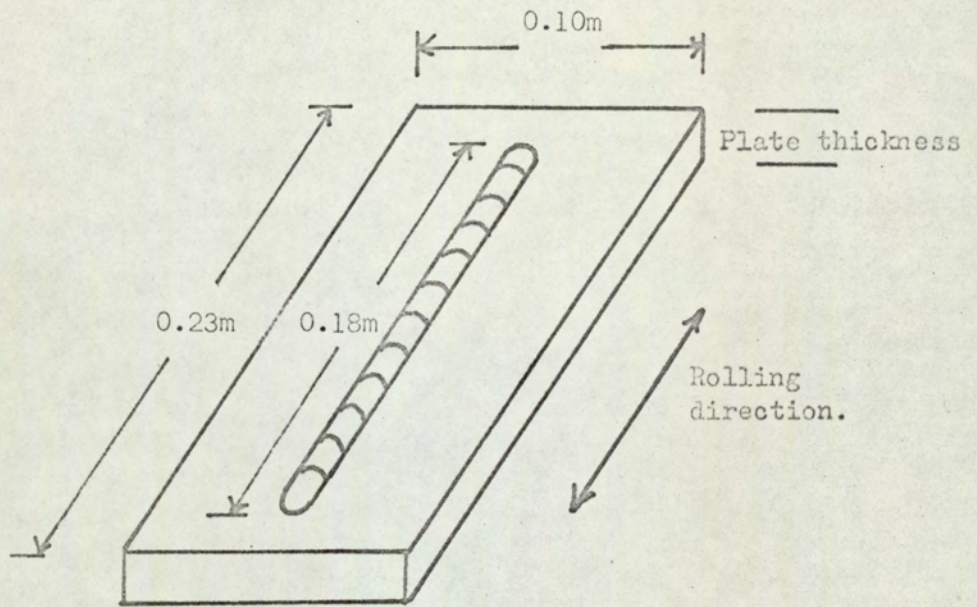


Fig. 9a. Schematic of Bead-on-Plate Test Specimen.

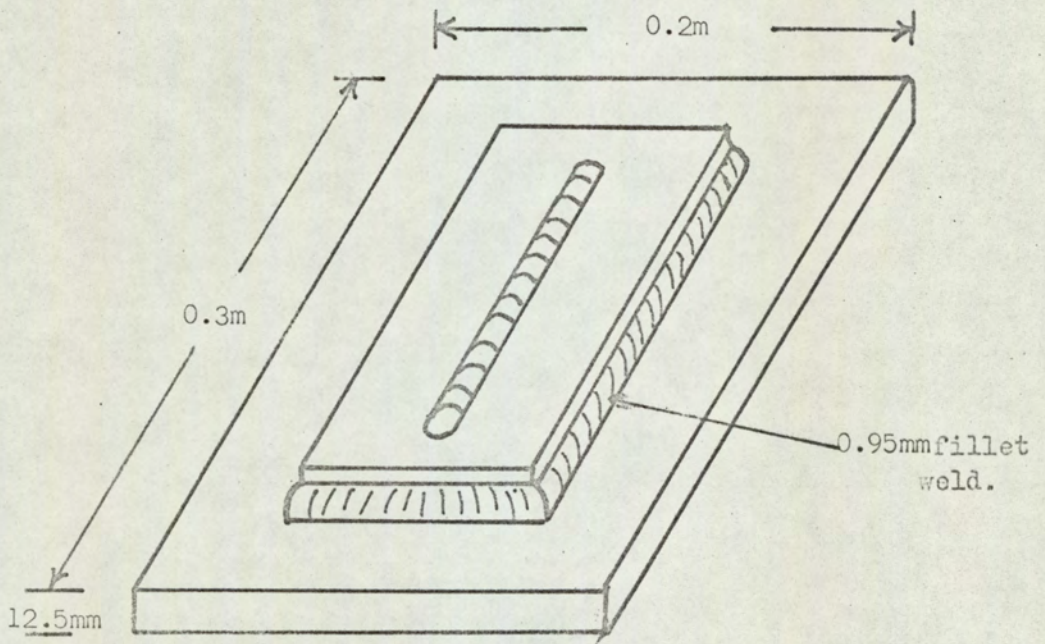


Fig. 9b. Schematic of Restrained Bead-on-Plate Test Specimen.

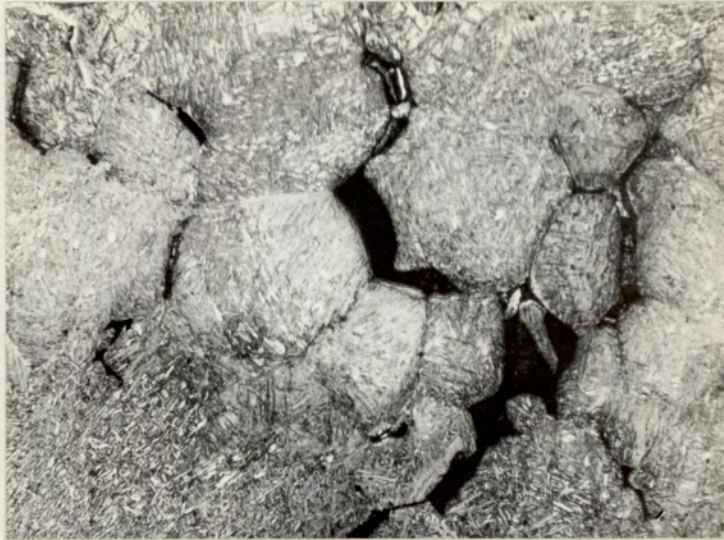
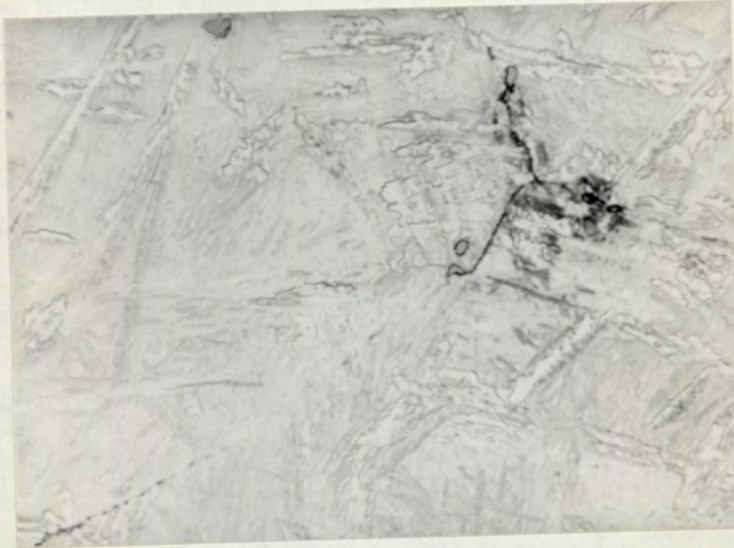
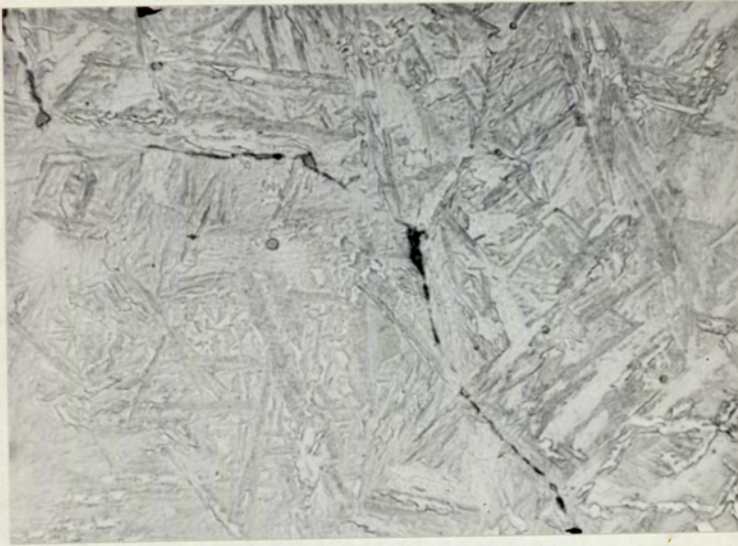


Fig.10. High Temperature Intergranular Cracking in the Weld Heat Affected Zone of SAE 4130.
(Etched 2% Nital x 100)



Fig.11. High Temperature Intergranular Cracking in the Weld Heat Affected Zone of SAE 4130.
(Etched 2% Nital x 500)



Figs. 12 and 13.

Modified Inclusions Decorating Prior Austenite Grain Boundaries in the High Temperature H.A.Z. on SAE 4130. Note association of cracks and inclusions in Fig.13. (etched 2% Nital x 750)



Fig.14. Modified Inclusion Cluster in H.A.Z. of SAE 4130
(Etched 2% Nital x 750)

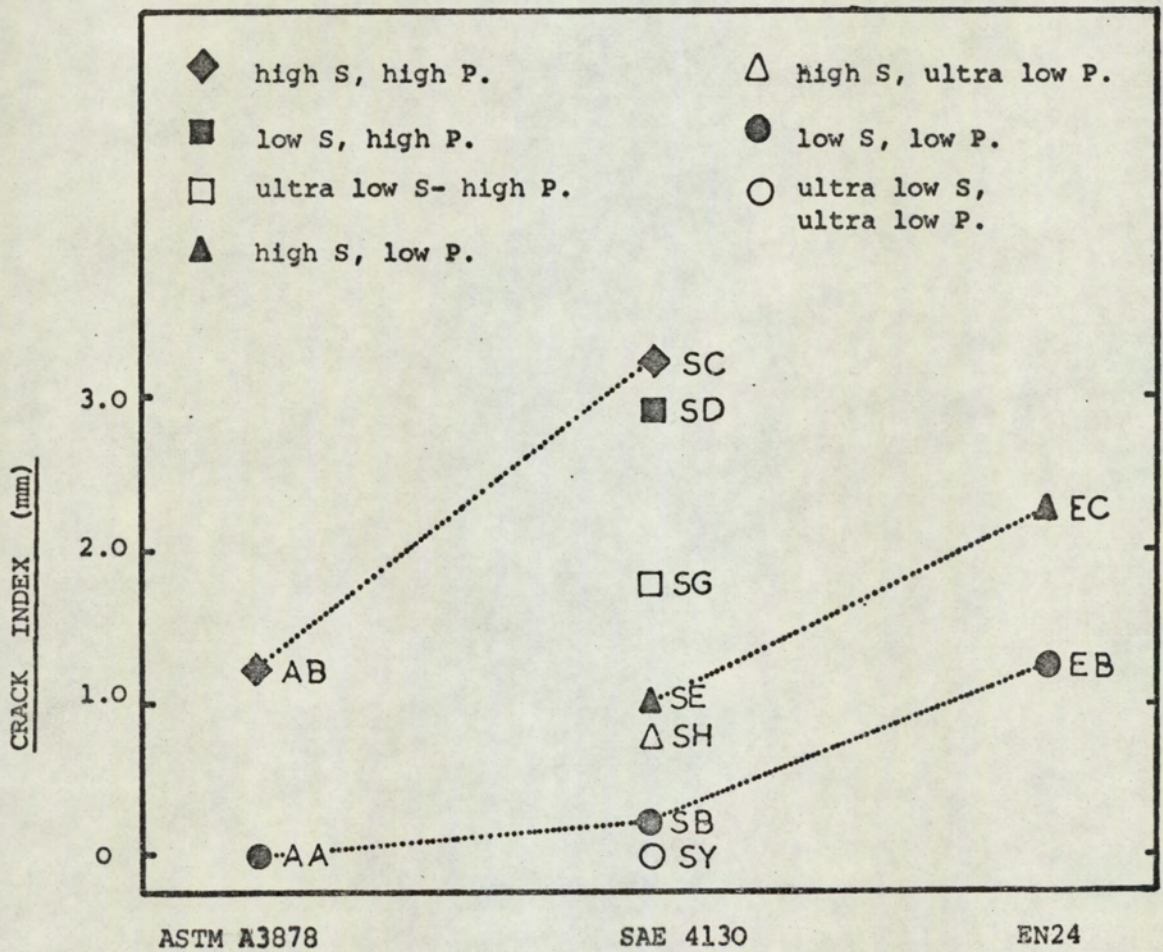


Fig.15. Schematic of Relation between Crack Index and Steel Composition



Fig.16. Crack Sensitive SD Weld Specimen showing 3 zones in Weldment, namely, Weld Metal, Intergranular H.A.Z., and Transgranular H.A.Z.

(x 75)



Fig.17. Crack Sensitive SD Weld Specimen, showing detail of Weld Metal Intergranular H.A.Z. Boundary.

(x 150)



Fig.18. Crack Sensitive SD Weld Specimen showing detail of Intergranular - Transgranular H.A.Z. Boundary.
(x 150)

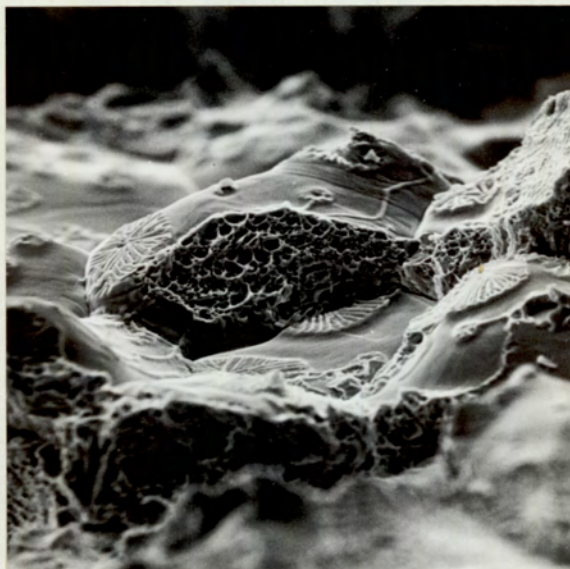


Fig.19. Crack Sensitive SD Weld Specimen showing Intergranular Regions with Free Surfaces, Fern-like Dendrites and Ductile Dimpling.
(x 800)

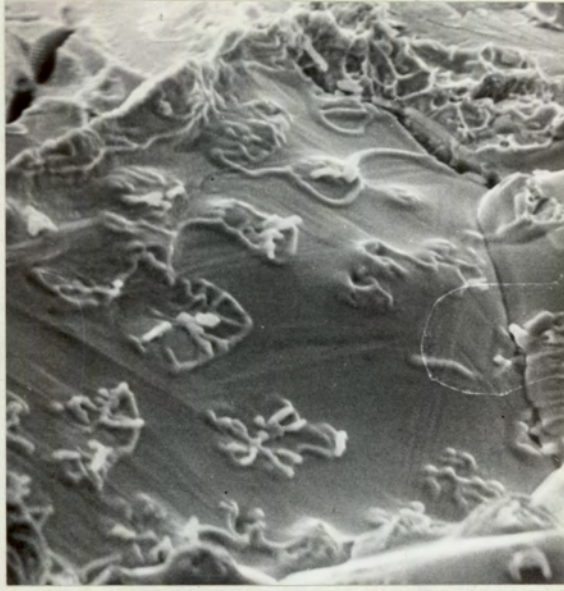


Fig.20. Crack Sensitive SC Weld Specimen showing Detail of Surface Striations.

(x 1400)

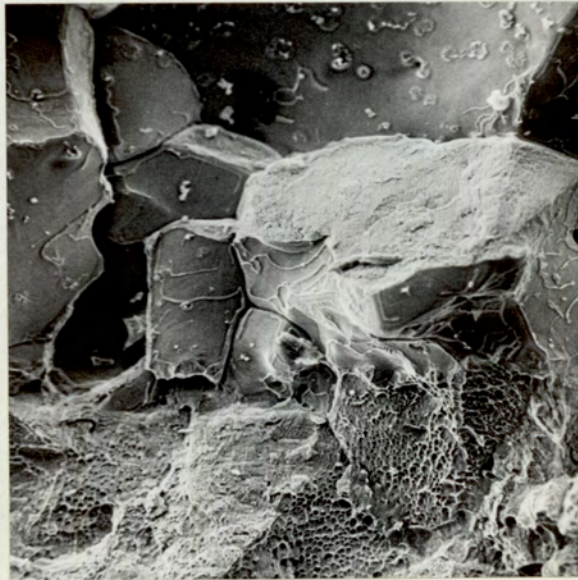


Fig.21. Crack Sensitive AD Weld Specimen showing more Angular Grain Form.

(x 320)



Fig.22. Crack Sensitive SD Weld Specimen showing Branching Cracks
(x 750)



Fig.23. Crack Sensitive SD Weld Specimen, showing Holes
at Grain Faces
(x 300)



Fig.24. Weld Specimen, SD, showing Fern Dendrites standing proud of Crack Surface.

(x 750)

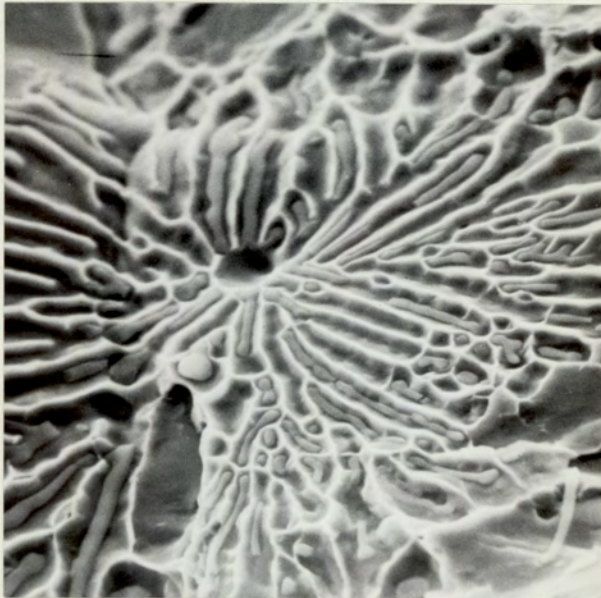


Fig.25. Weld Specimen, SC, showing Detail of Fern Dendrite.

(x 2,800)



Fig.26. Energy Spectrum from Rod Inclusion in Steel, SC.
 Peaks from left to right are: S, Cr, Mn, Fe_{Kα}
 and Fe_{Kβ}



Fig.27. Energy Spectrum from Hot Crack Surface in Steel, SC.
 Peaks from left to right are: Fe_{Kα} and Fe_{Kβ}



Fig.28. Weld Specimen EC showing Intergranular H.A.Z. region with no hot cracks and Grain Faces completely covered with Fern Dendrites and Ductile Dimpling.

(x 220)

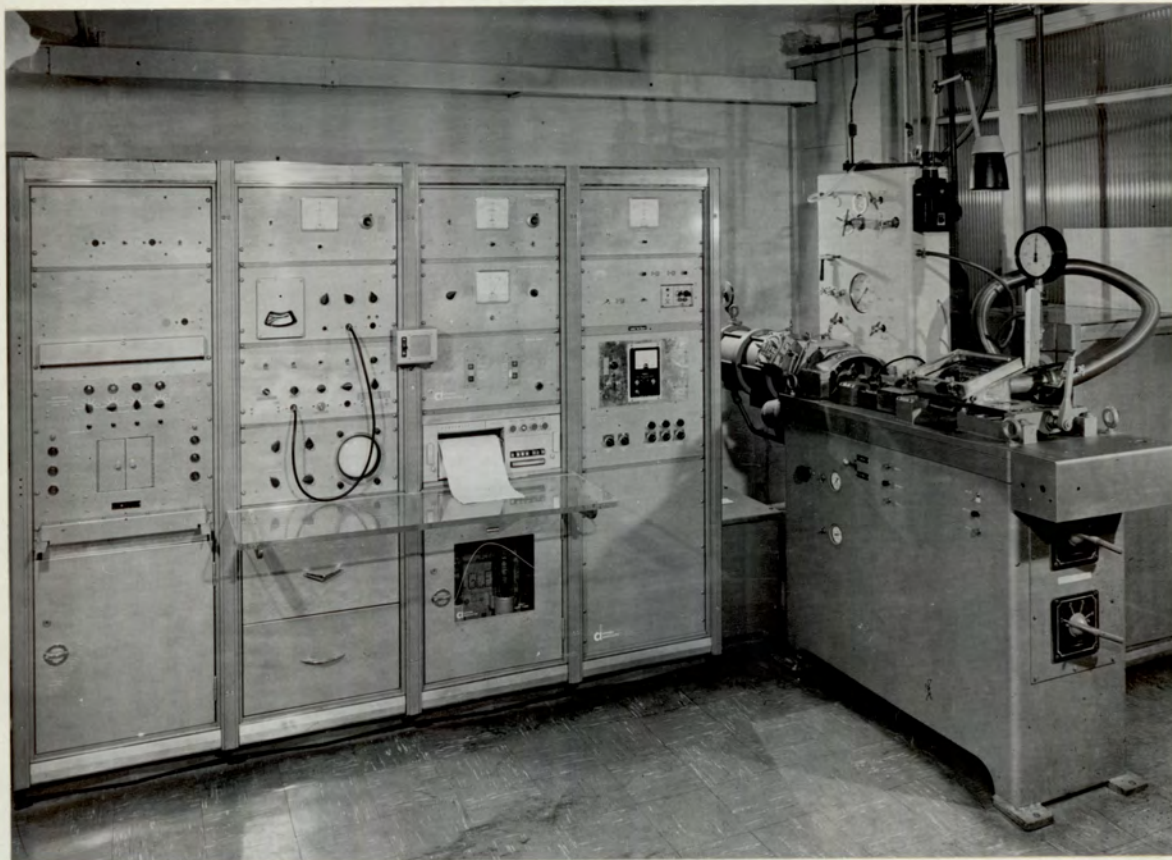


Fig.29. General View of Gleeble Thermo-mechanical Simulator.

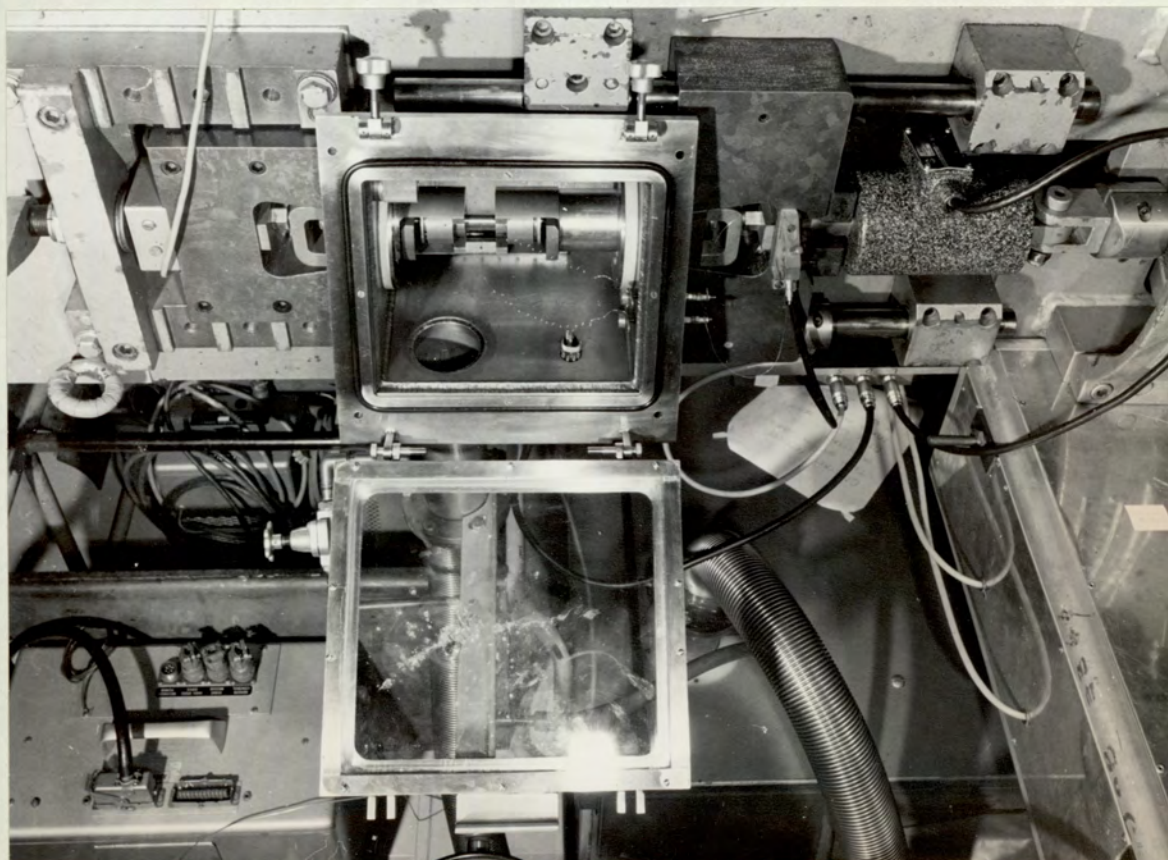


Fig.30. Detail of Tensile Testing System.

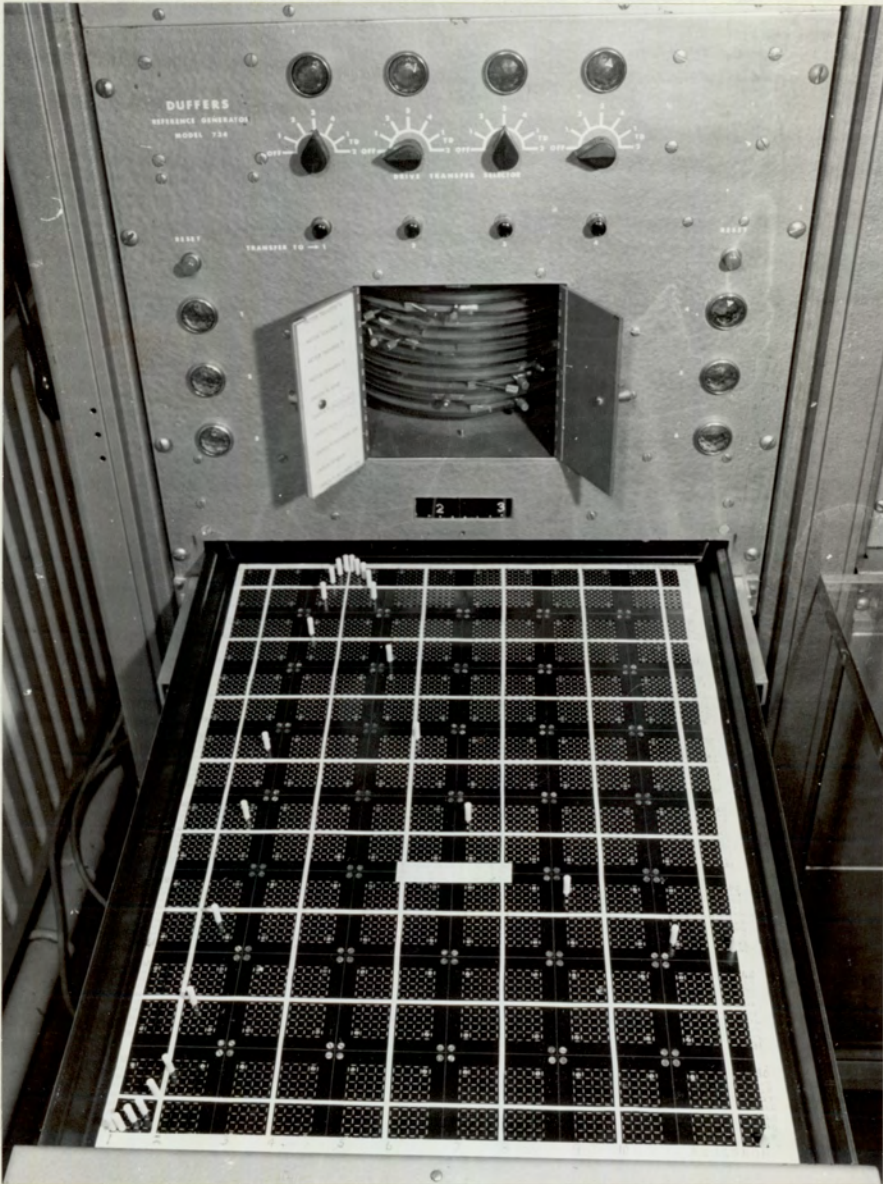


Fig.31. The Gleeble Thermal Cycle Reference Generator.

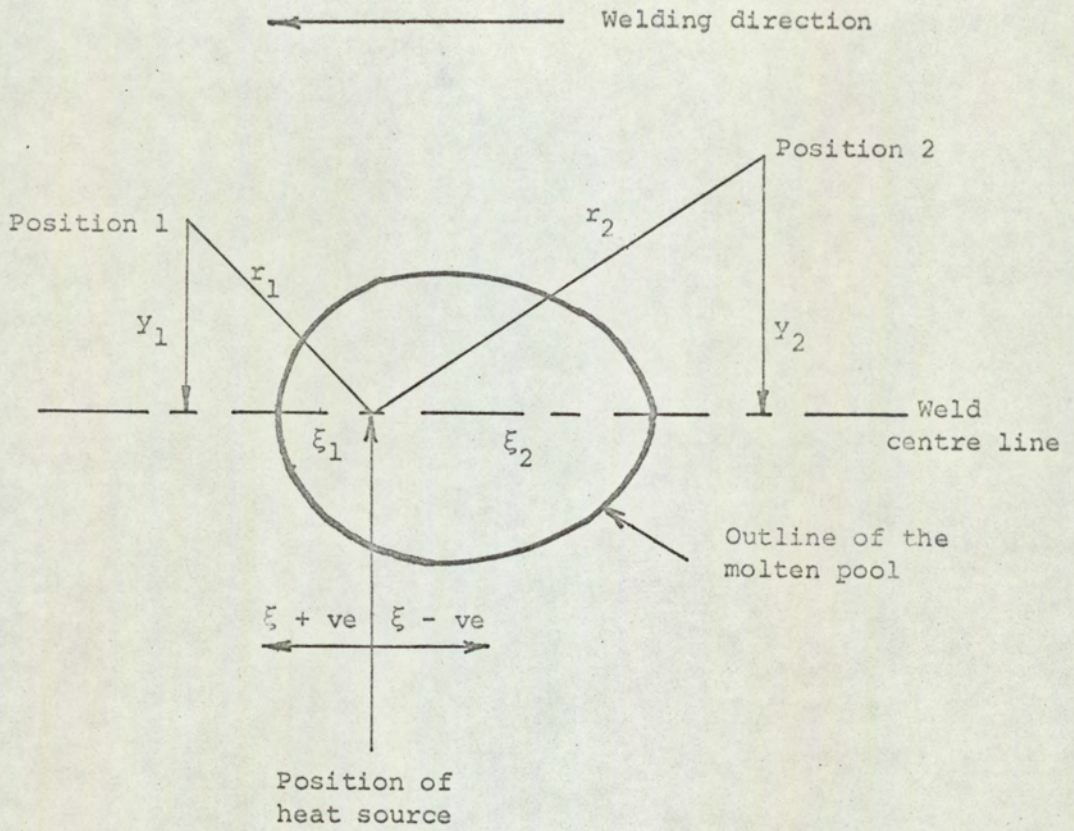


Fig. 32.

The Relationship between the Weld H.A.Z. Position and the co-ordinates ξ , y and r used in Rosenthal's Two Dimensional Heat Flow Equation.

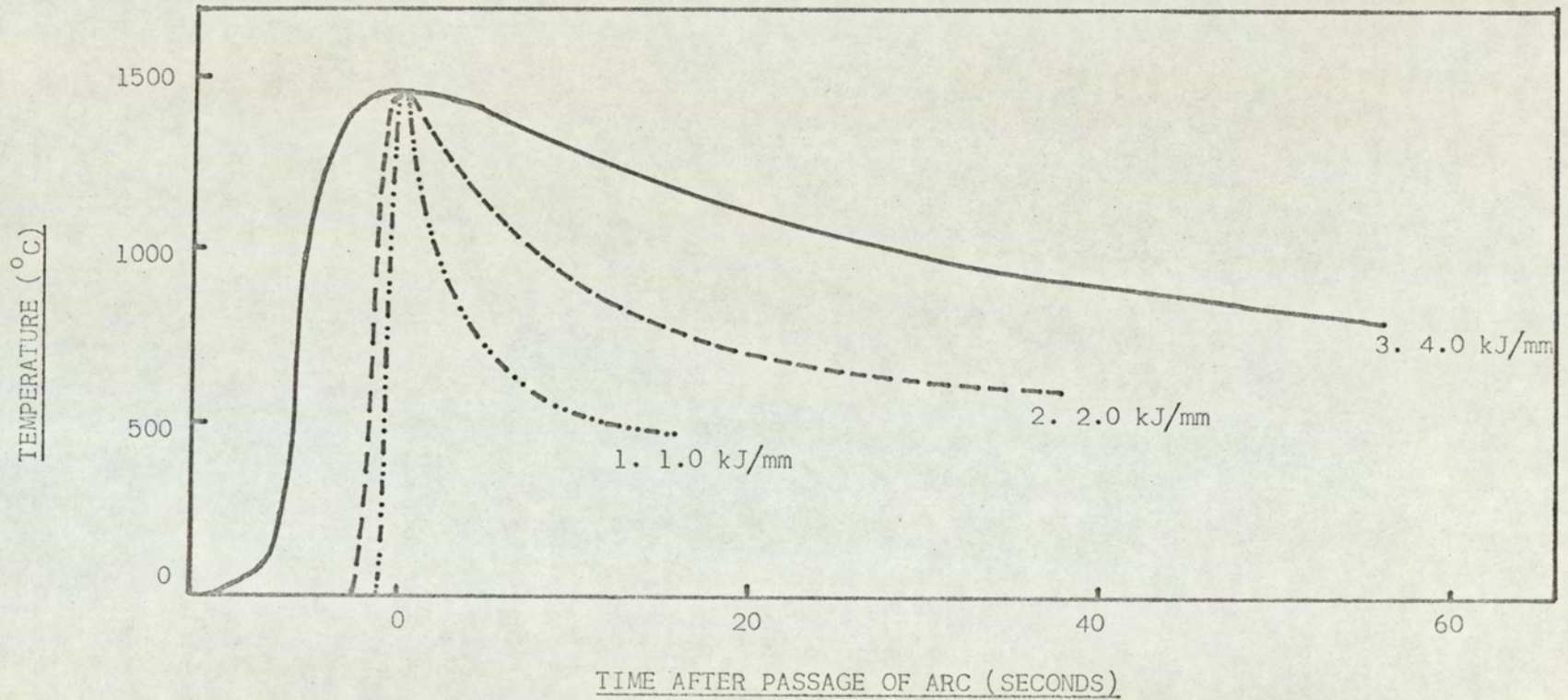


Fig. 33. Computed Weld Thermal Cycles for Heat Inputs of 1.0 kJ/mm, 2.0 kJ/mm and 4.0 kJ/mm Deposited on 12.5mm Thick Plate.

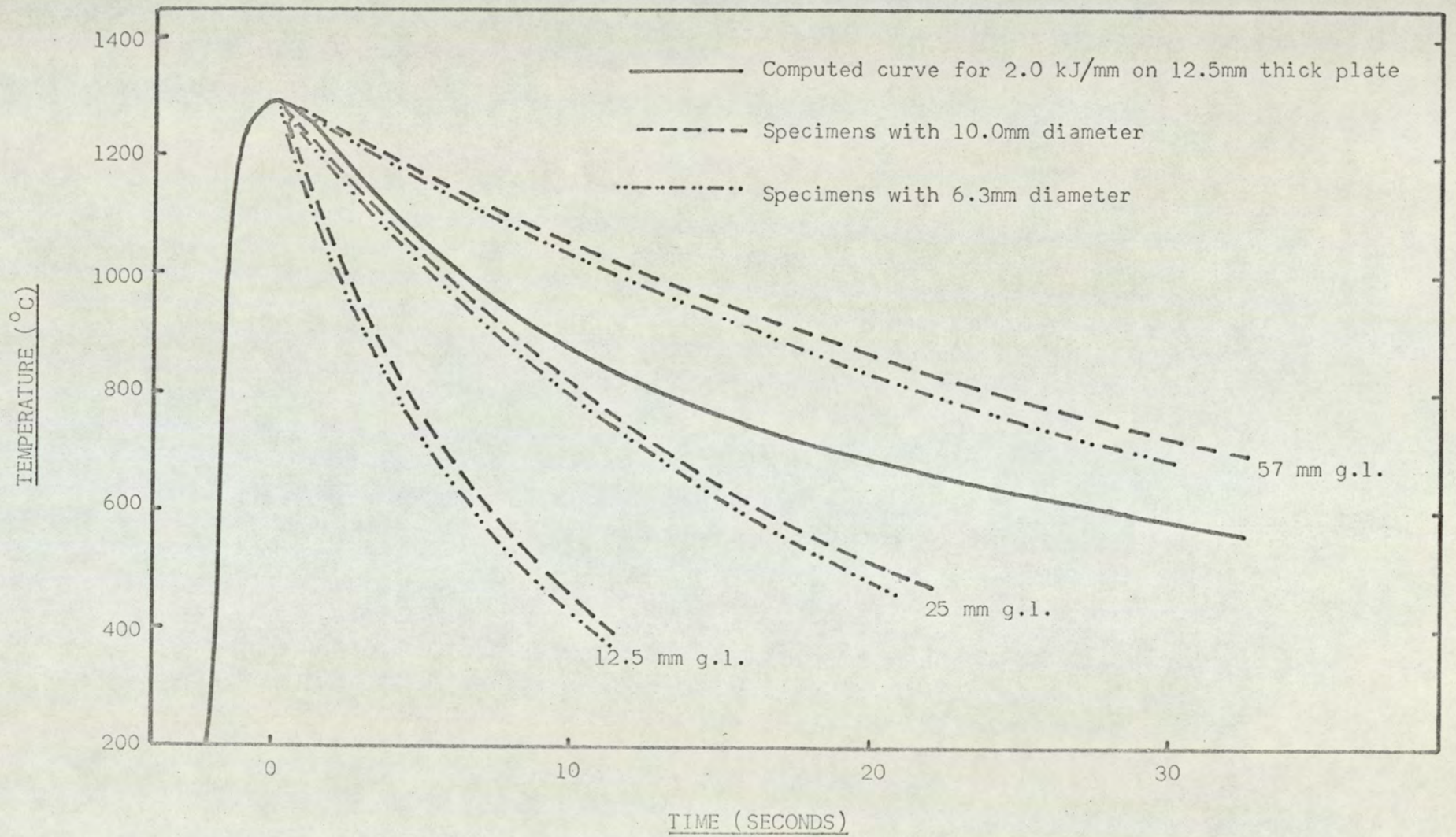
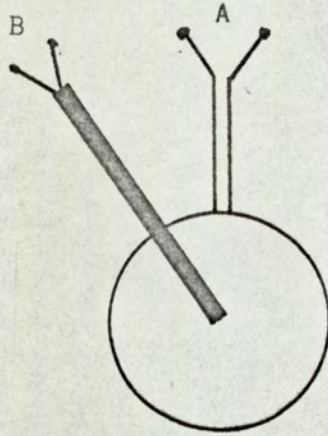


Fig. 34. Effect of Specimen Gauge Length (g.l.) and Diameter on Natural Cooling Rate.



Specimen Centre Section

A is bare wire surface thermocouple

B is sheathed internal thermocouple

Fig.35. Specimen Set-up Used to Determine Temperature
Reproducibility.

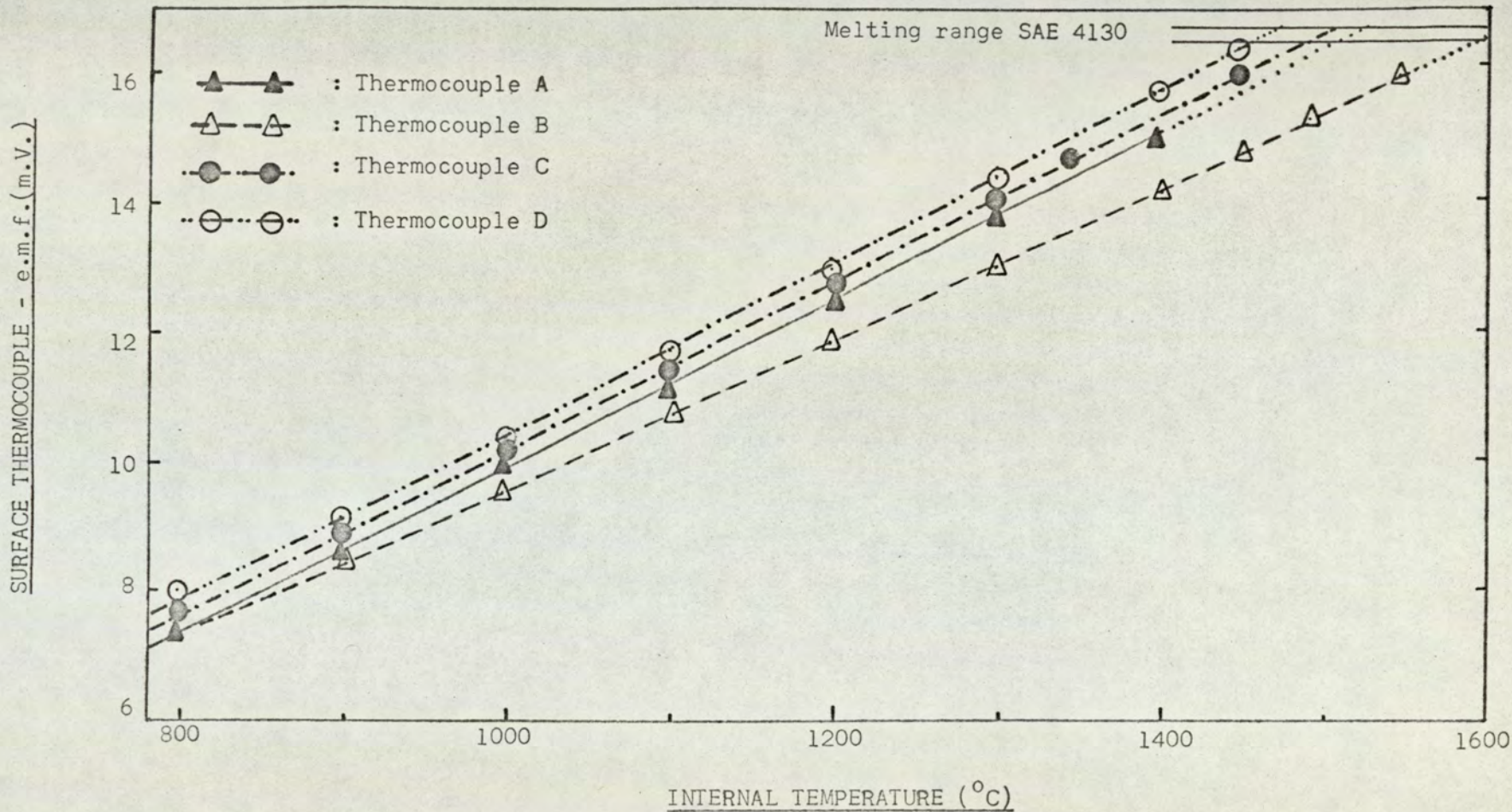


Fig.36. Temperature Calibration Curves For Hot Ductility Specimen (Surface e.m.f.v. Internal Temperature)

Key to above:

A: $\blacktriangle-\blacktriangle$ 0.50mm diameter sheathed Cr/Al thermocouple

B: $\triangle-\triangle$ 1.56mm diameter sheathed Pt/Rh thermocouple

C: $\bullet-\bullet$ Bare wire Pt/Rh, inserted axially, attached to specimen.

D: $\circ-\circ$ Bare wire Pt/Rh, inserted axially, not attached to specimen.

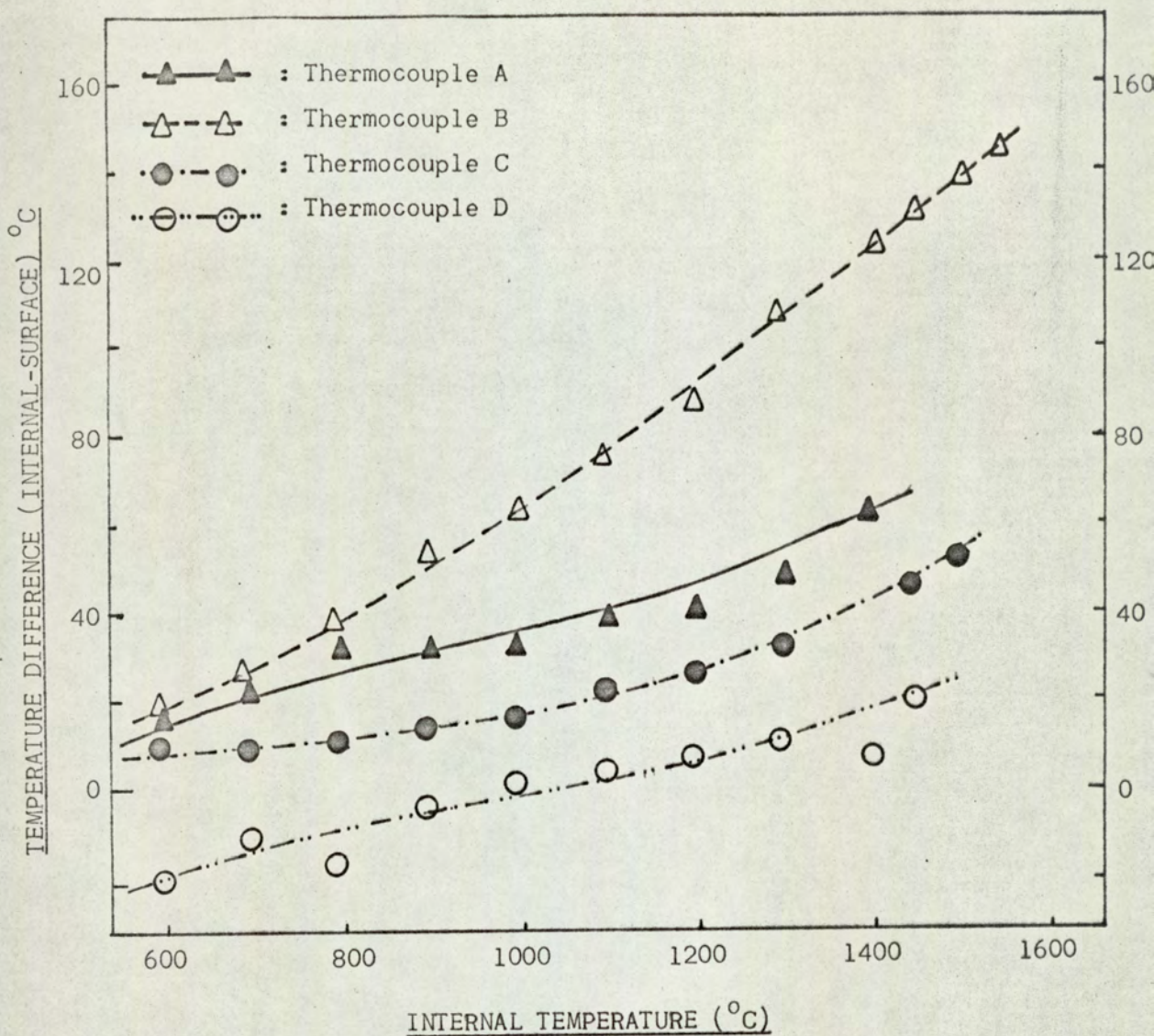


Fig.37. Temperature Calibration Curves for Hot Ductility Specimen (Temperature Difference v Internal Temperature.)

- A: 0.50mm diameter sheath Cr/Al, inserted radially.
- B: 1.56mm diameter sheath Pt/Rh, inserted radially.
- C: Bare wire Pt/Rh, inserted axially, attached to specimen.
- D: Bare wire Pt/Rh, inserted axially, not attached to specimen.

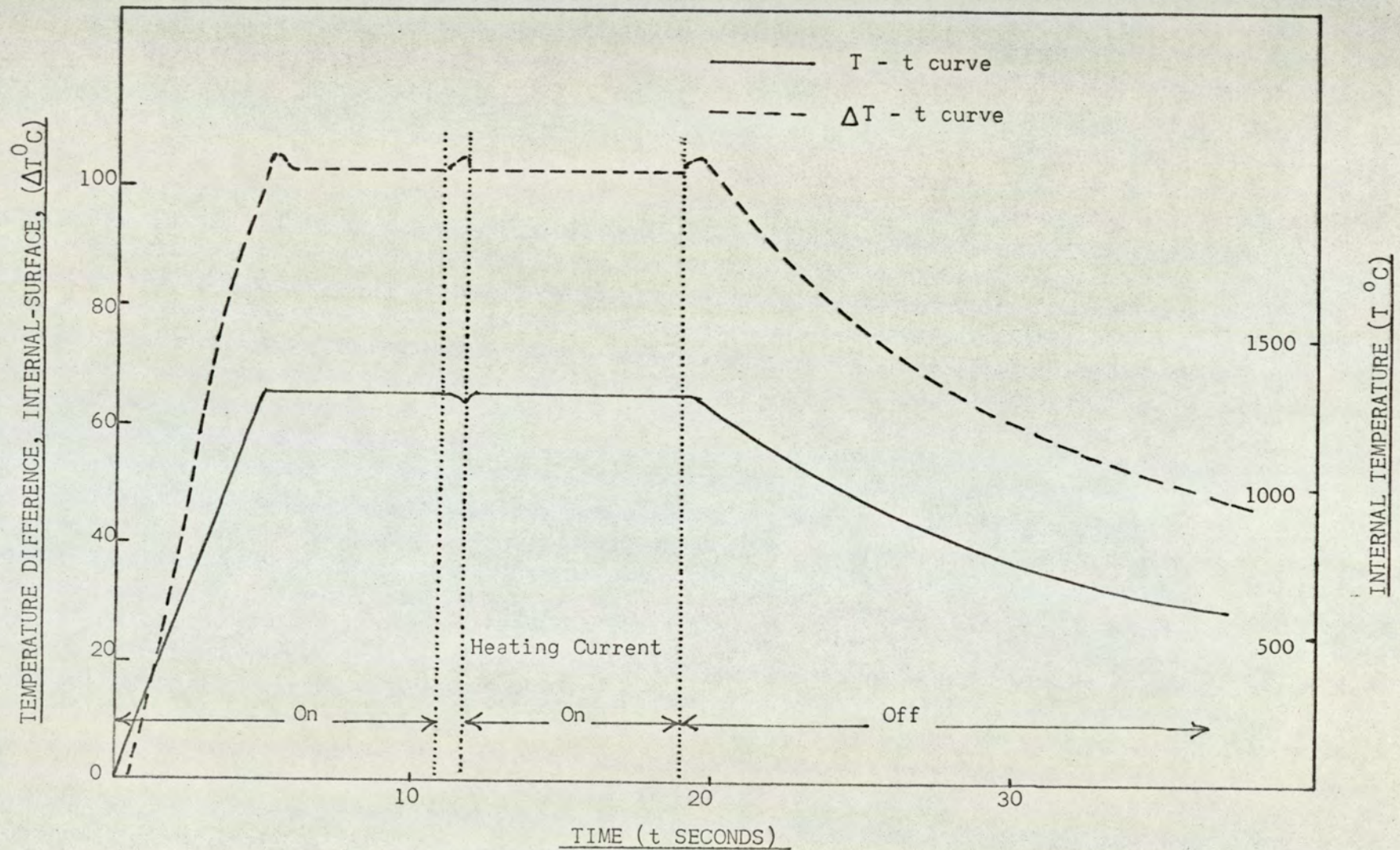


Fig. 38. Effect of Heating Current on the Temperature Difference Between Surface Thermocouple, and Internal 0.050mm Diameter Sheathed Thermocouple.

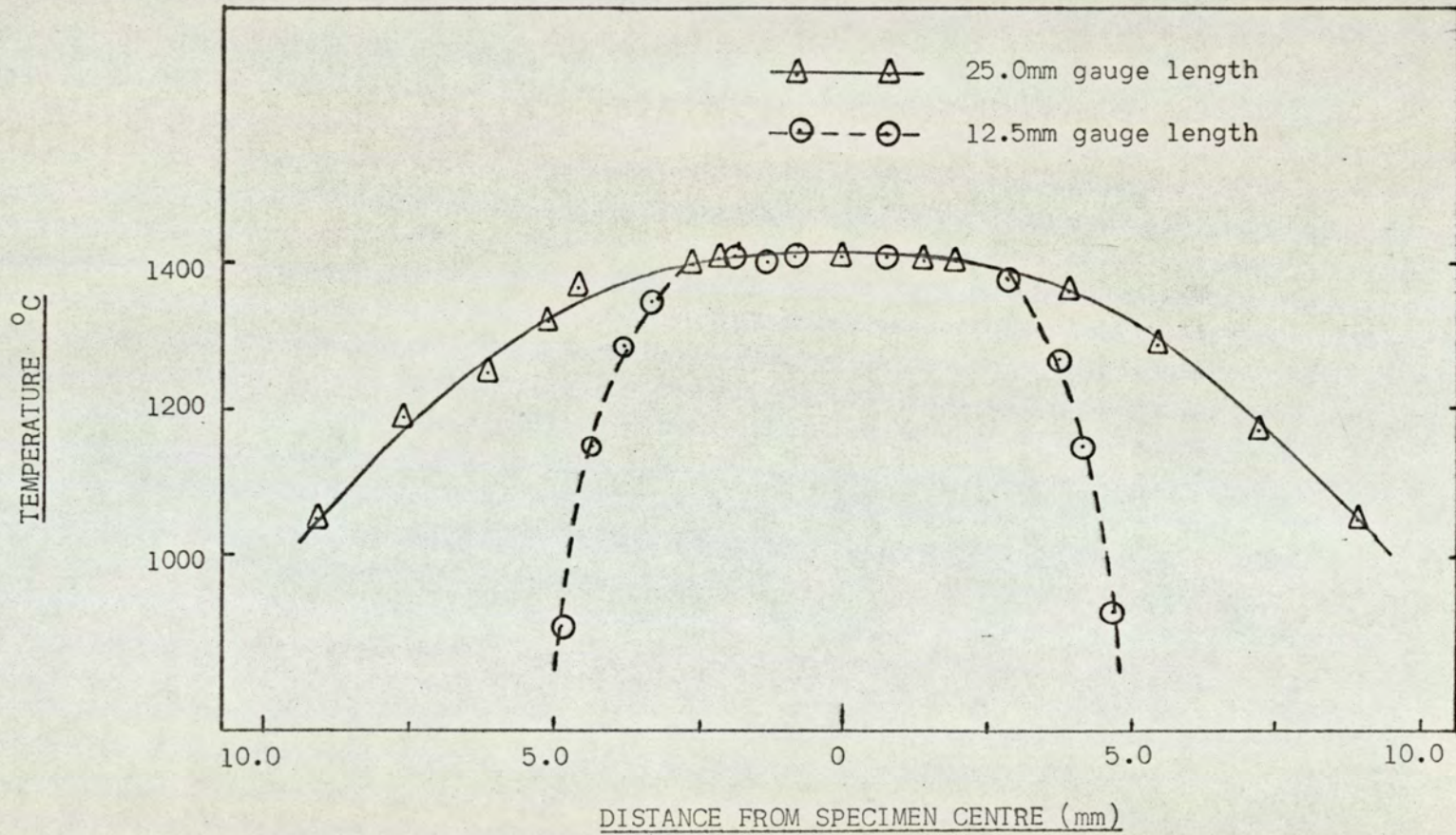


Fig.39. Temperature Distribution Along 10mm Diameter Steel Specimen for Gauge Lengths of 12.5 and 25.0mm.

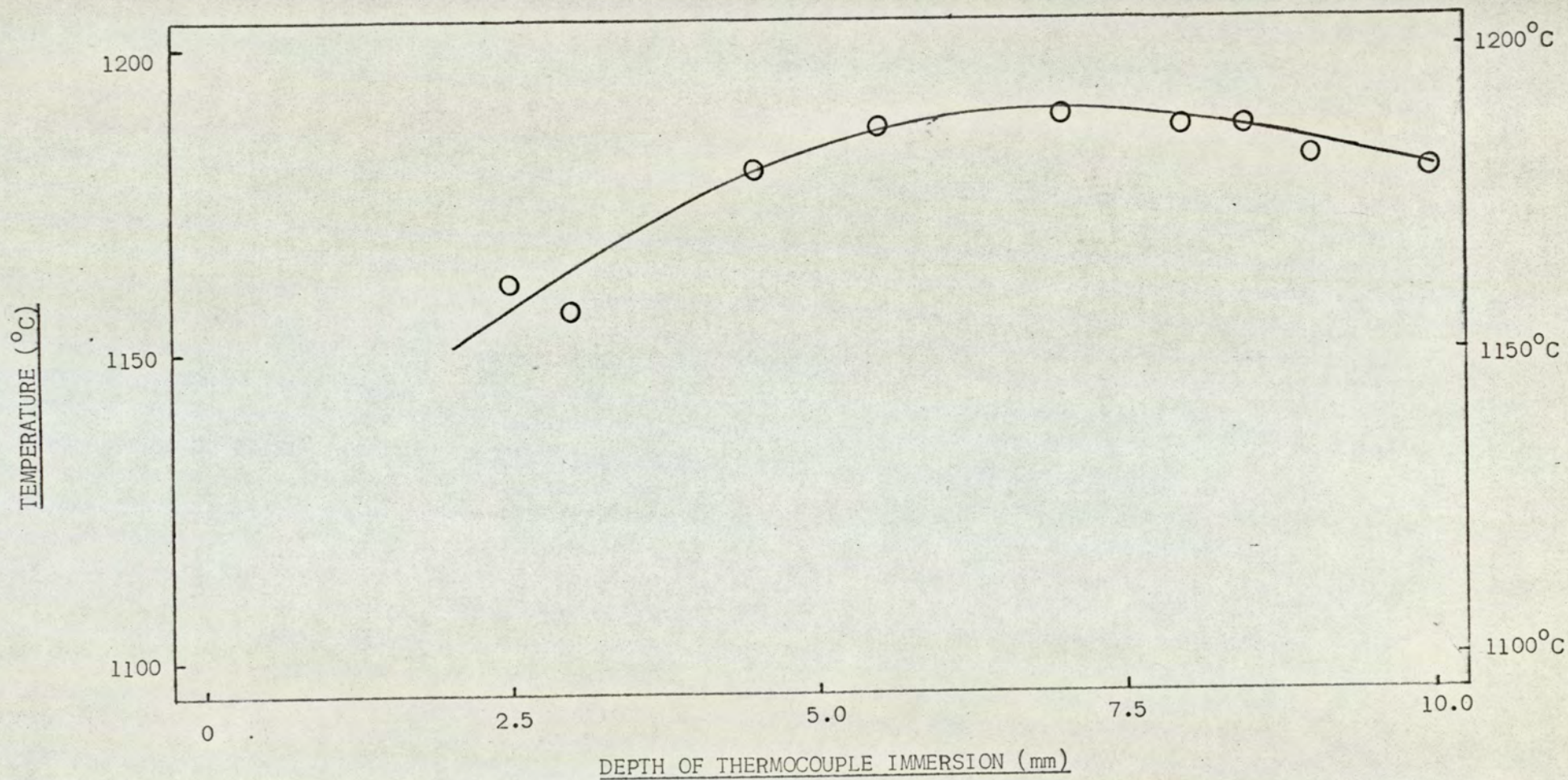


Fig.40. Diametral Temperature Gradient Across Hot Ductility Specimen.

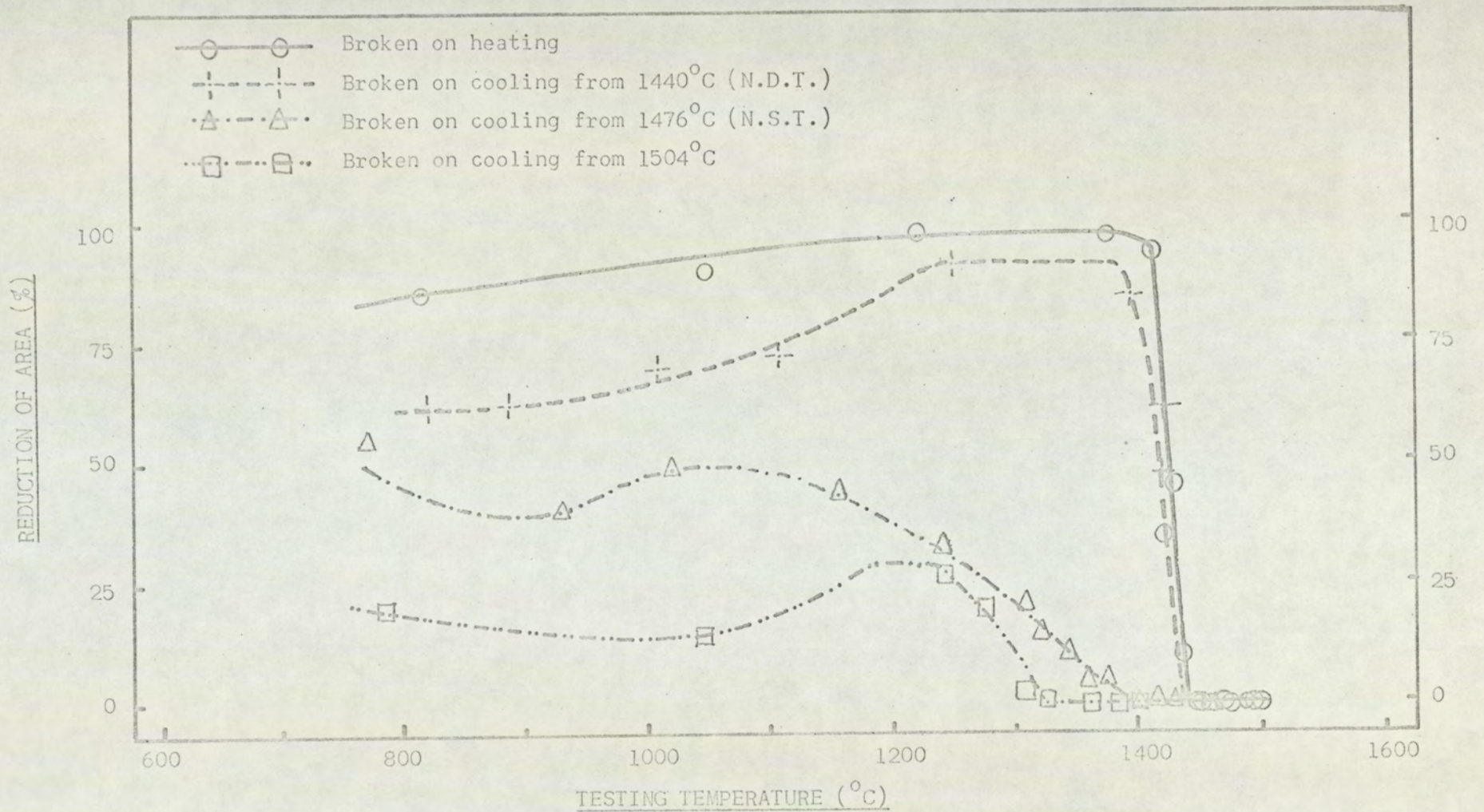


Fig. 41a. Hot Ductility Data for SAE 4130 Steel, SC. (0.35%C; 0.032%S; 0.032%P)

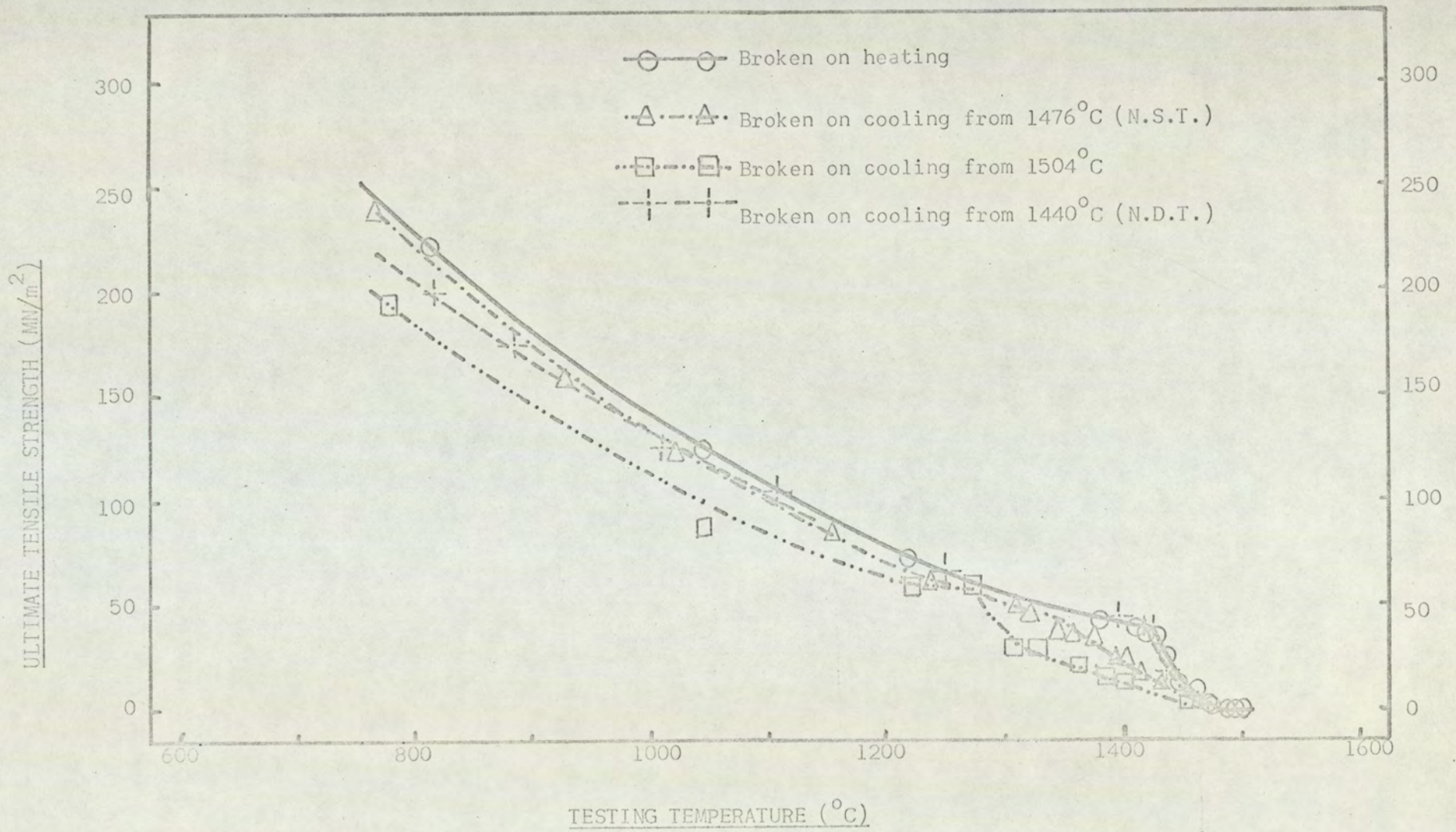


Fig. 41b. Hot Tension Data for SAE 4130 Steel, SC. (0.35%C; 0.032%S; 0.032%P)

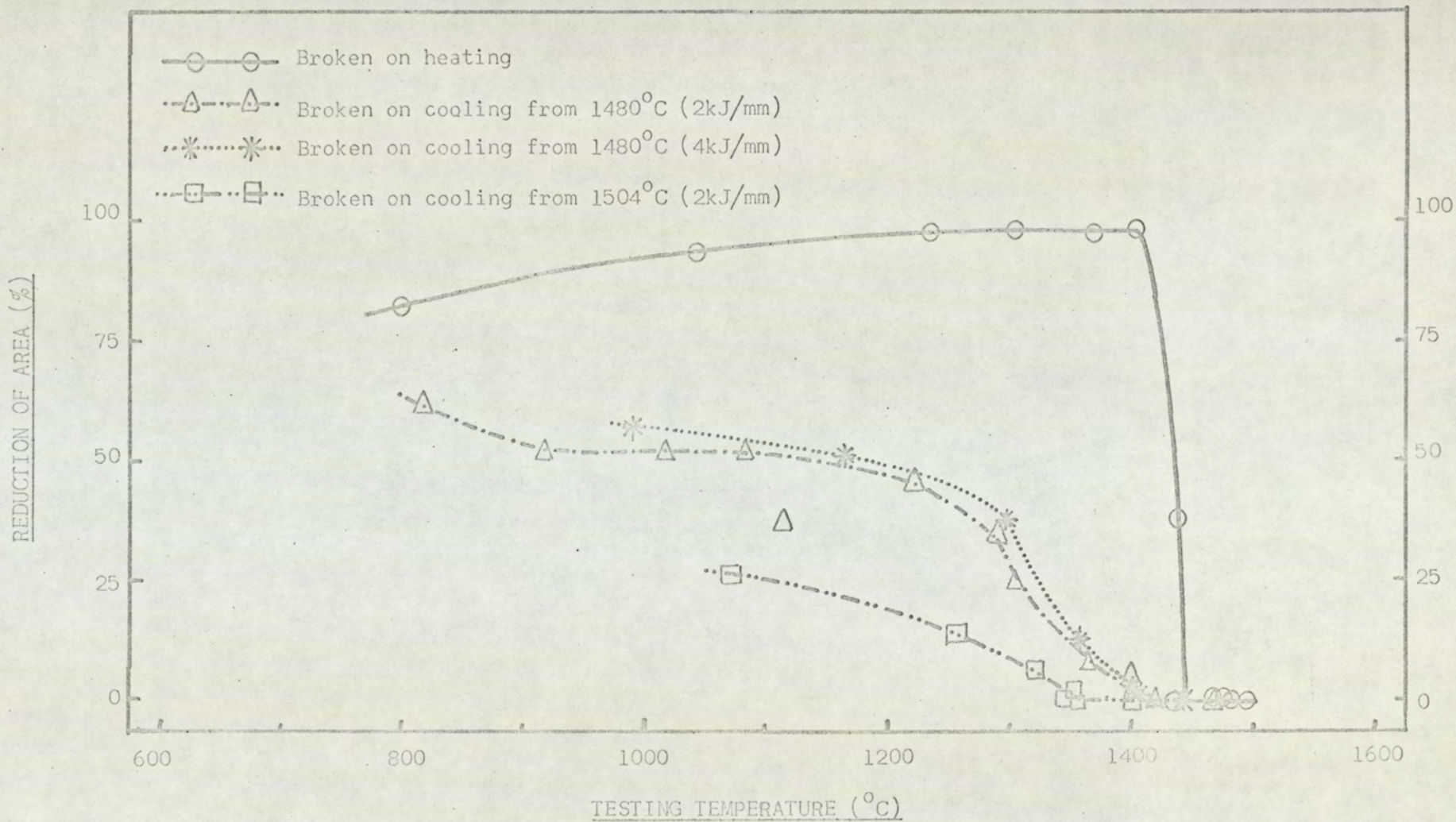


Fig. 42a. Hot Ductility Data for SAE 4130 Steel, SA. (0.28%C; 0.025%S; 0.030%P)

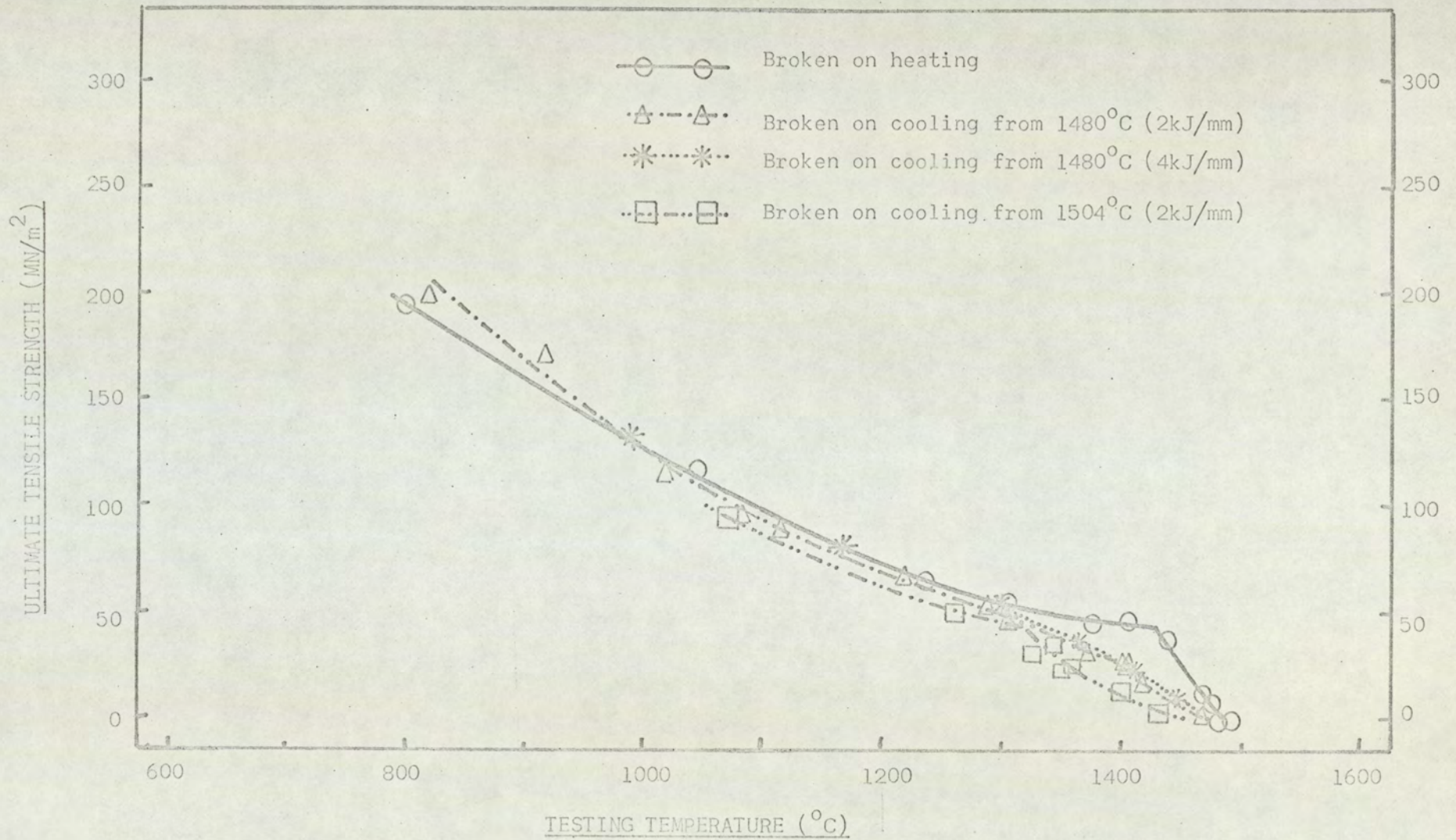


Fig. 42b: Hot Tension Data for SAE 4130 Steel, SA. (0.28%C; 0.025%S; 0.030%P)

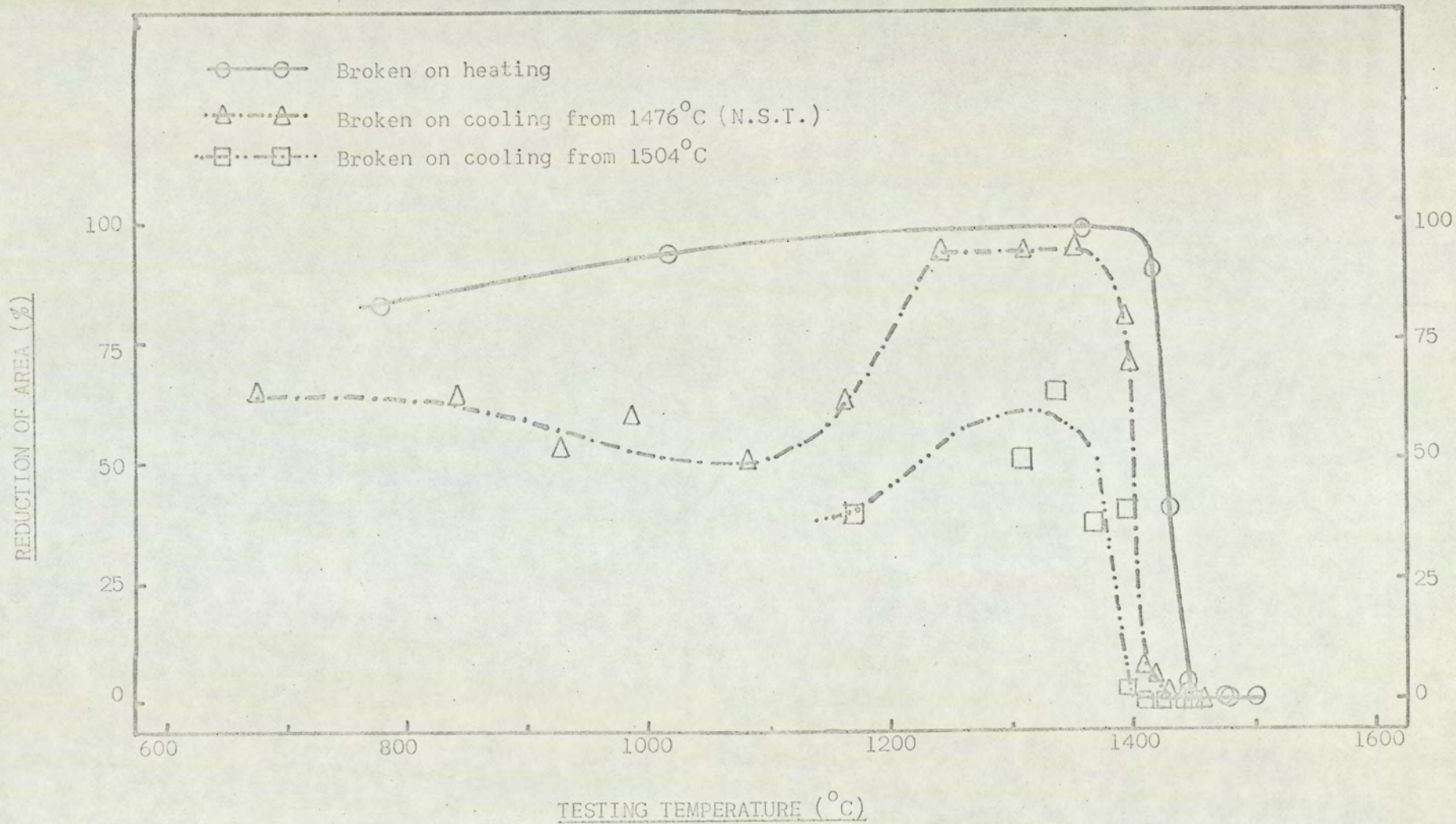


Fig. 43a. Hot Ductility Data for SAE 4130 Steel, SB. (0.35%C; 0.009%S; 0.008%P)

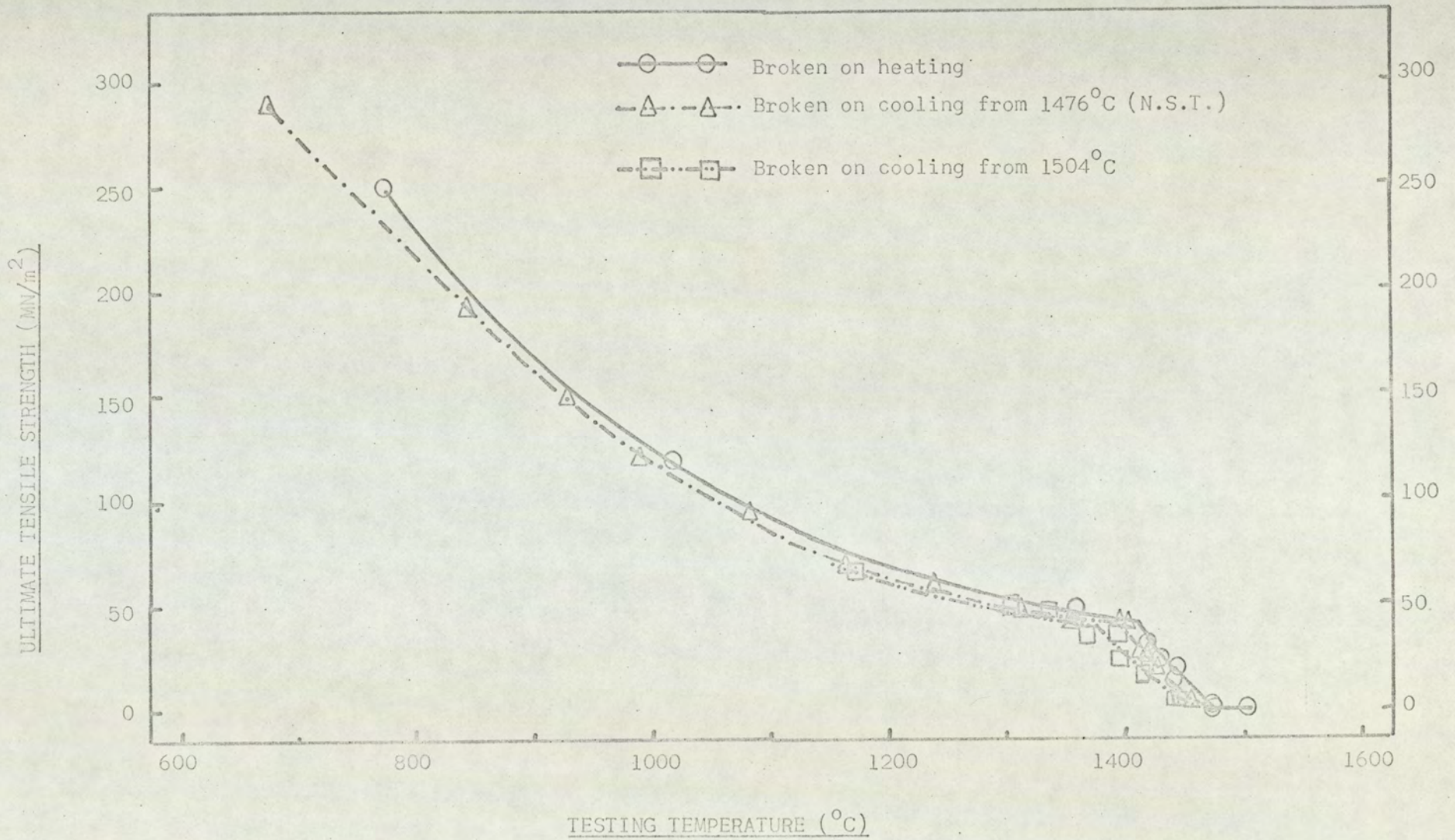


Fig. 43b. Hot Tension Data for SAE 4130 Steel, SB. (0.35%C; 0.009%S; 0.008%P)

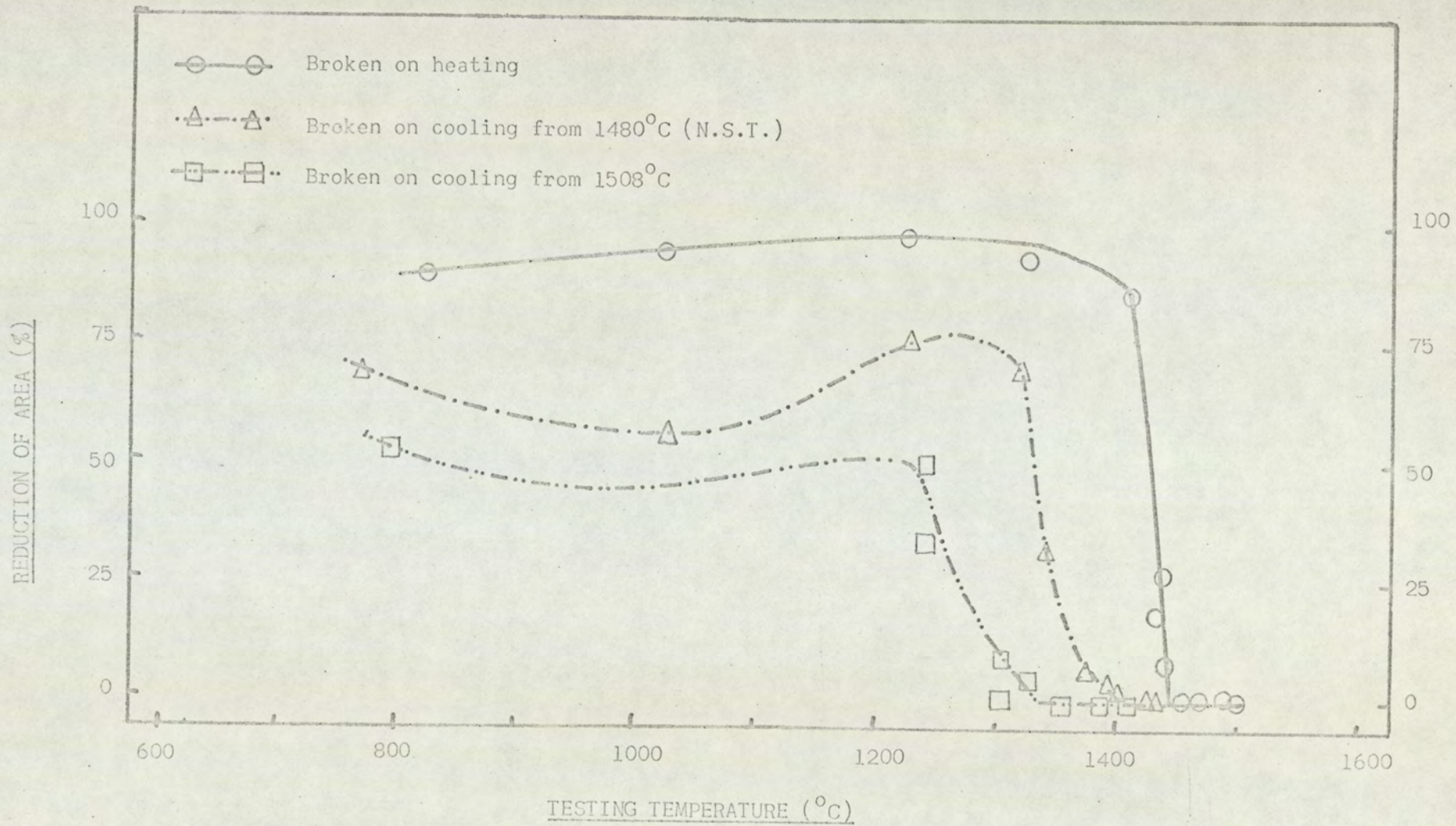


Fig. 44a. Hot Ductility Data for SAE 4130 Steel, SD. (0.35%C; 0.010%S; 0.049%P)

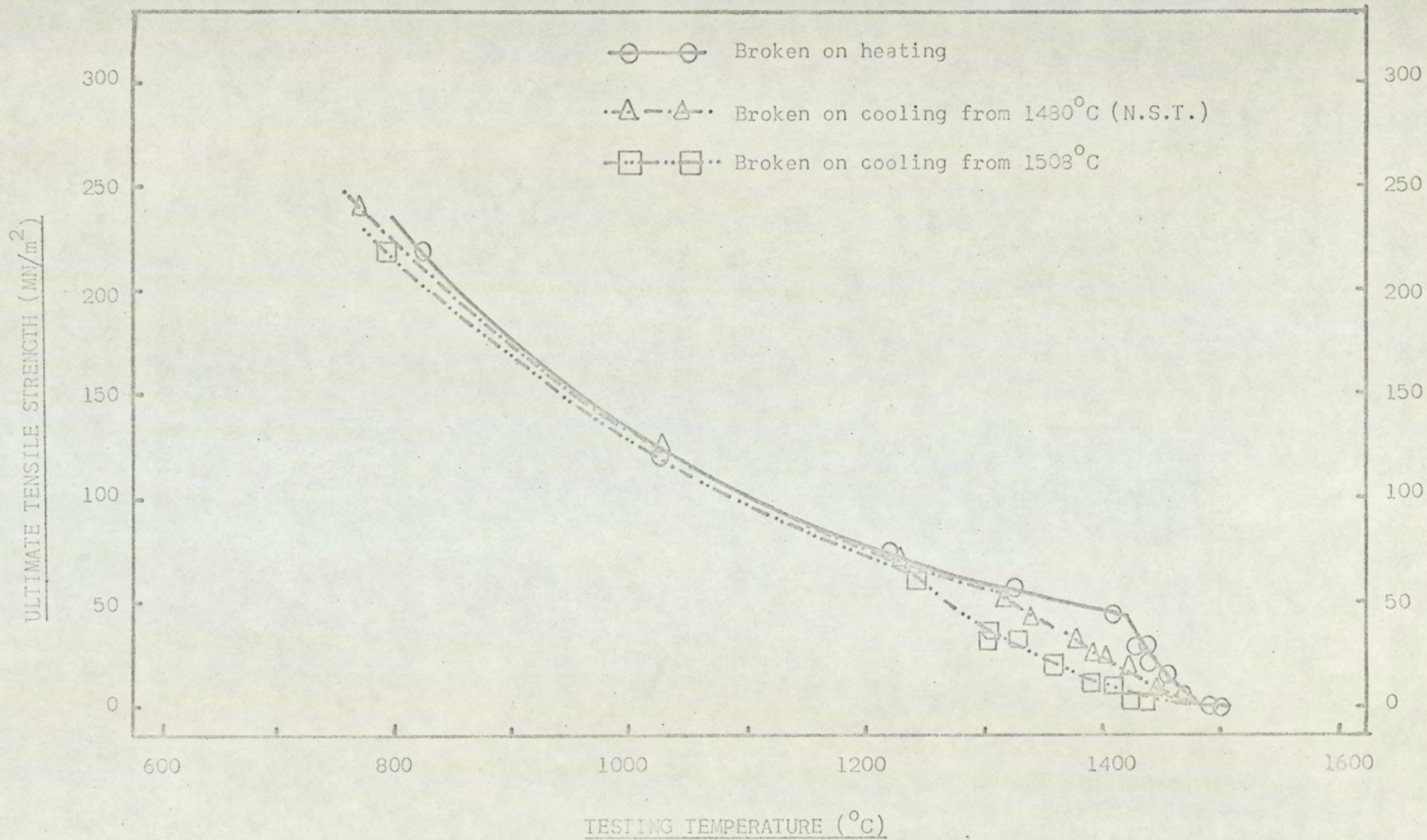


Fig. 44b. Hot Tension Data for SAE 4130 Steel, SD. (0.35%C; 0.010%S; 0.049%P)

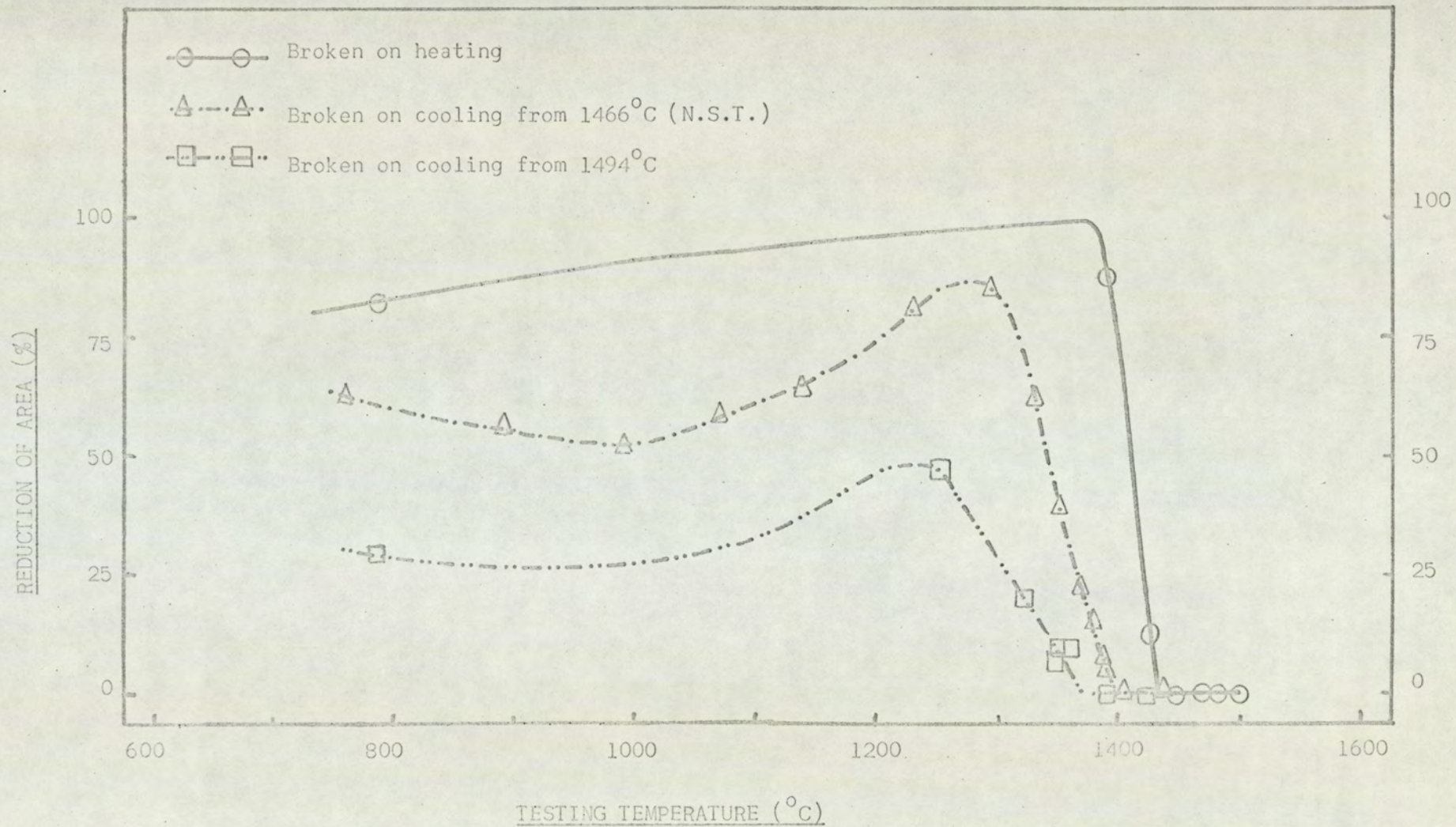


Fig. 45a. Hot Ductility Data for SAE 4130 Steel, SE. (0.39%C; 0.033%S; 0.010%P)

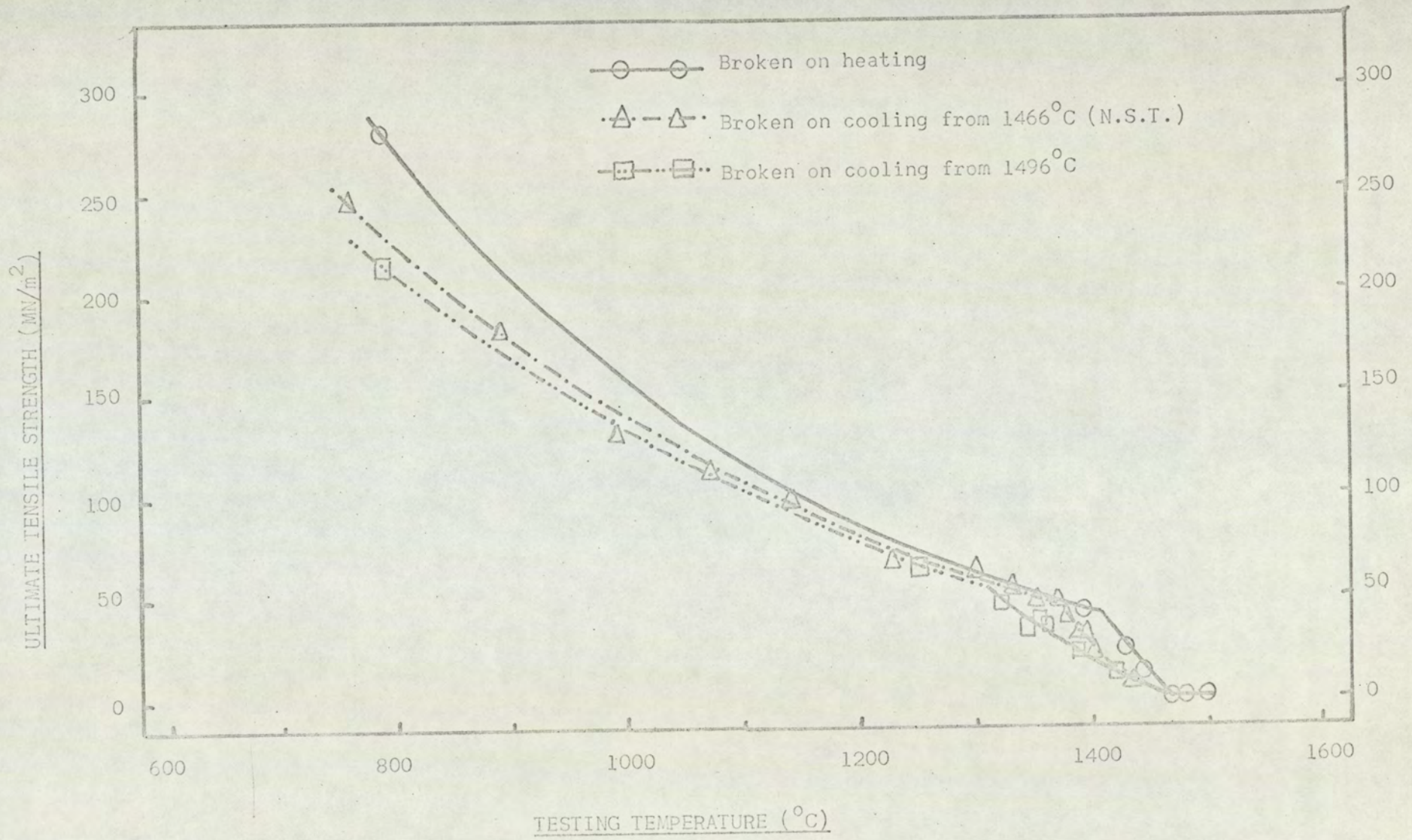


Fig. 45b. Hot Tension Data for SAE 4130 Steel, SE. (0.39%C; 0.033%S; 0.010%P)

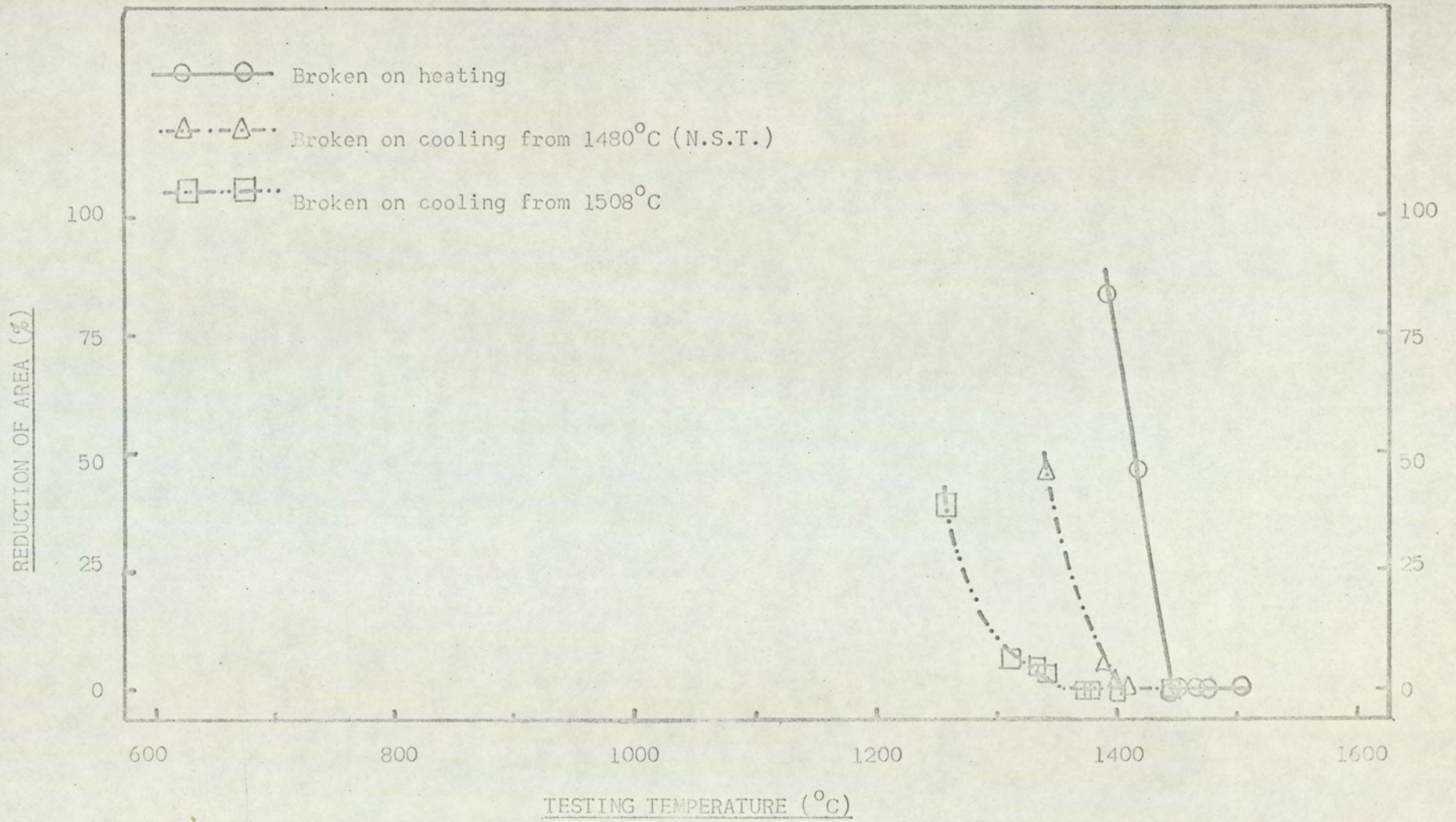


Fig. 46a. Hot Ductility Data for SAE 4130 Steel, SG. (0.35%C; 0.0016%S; 0.057%P)

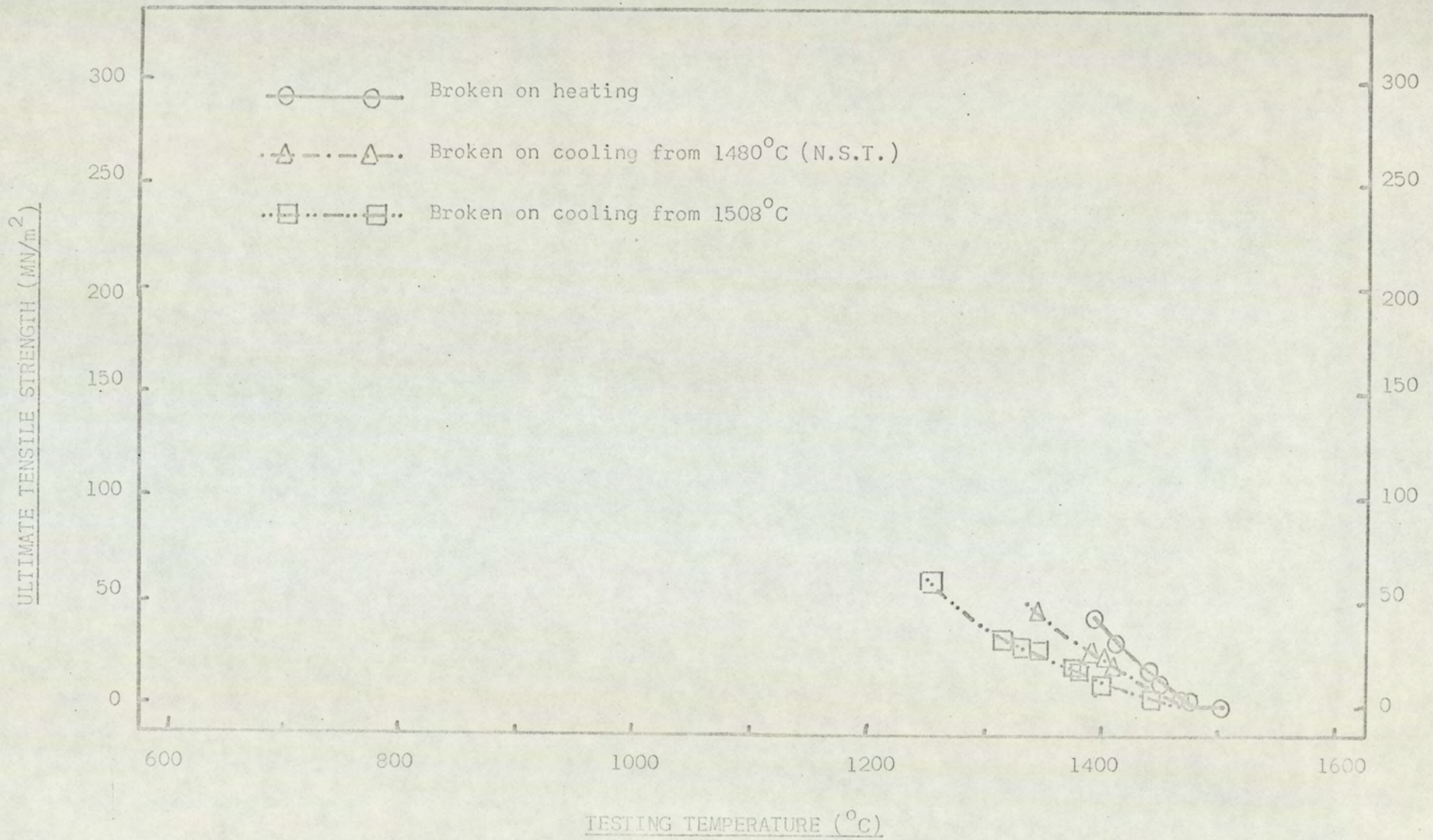


Fig. 46b. Hot Tension Data for SAE 4130 Steel, SG. (0.35%C; 0.0016%S; 0.057%P)

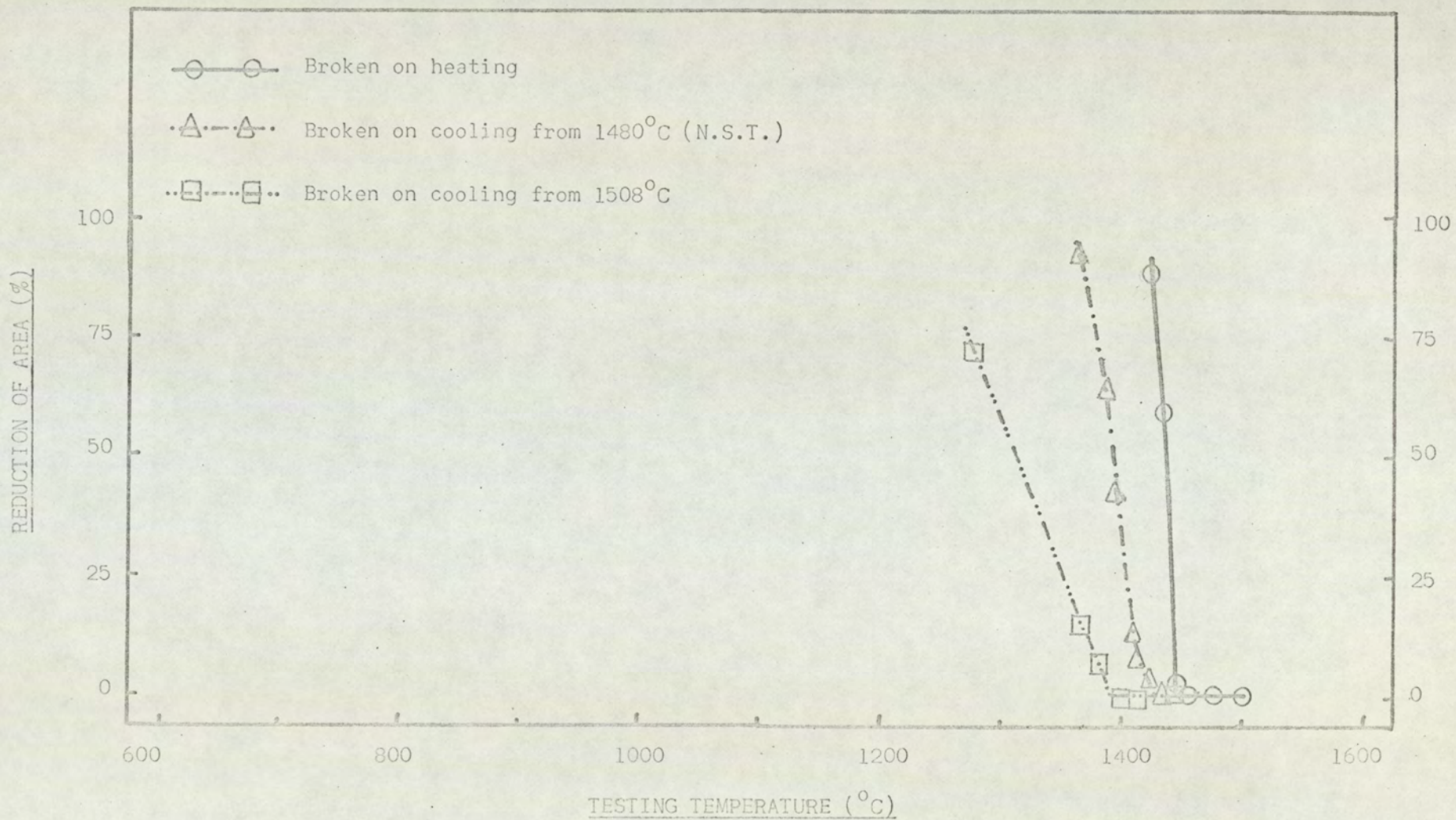


Fig. 47a. Hot Ductility Data for SAE 4130 Steel, SH. (0.31%C; 0.040%S; <0.001%P)

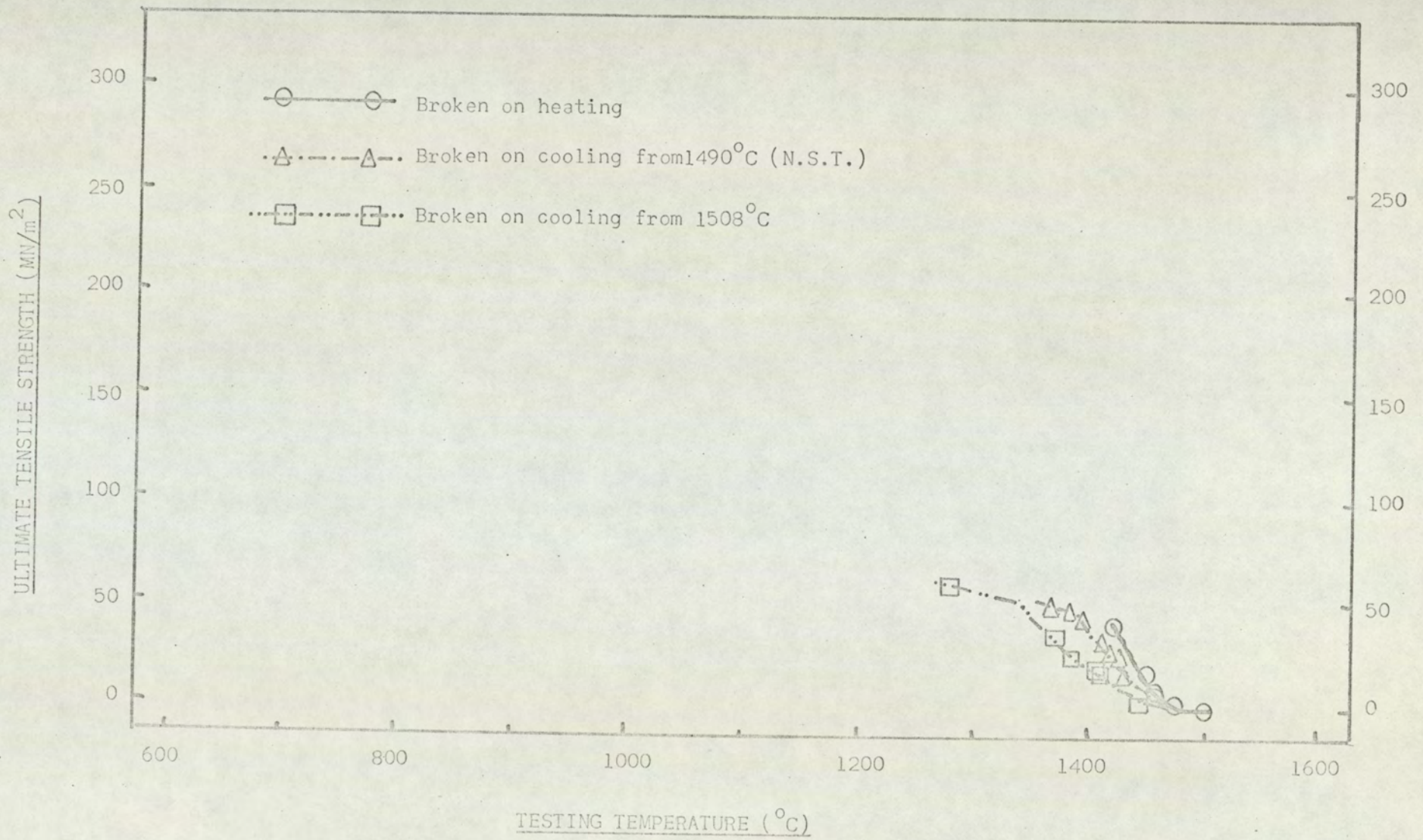


Fig. 47b. Hot Tension Data for SAE 4130 Steel, SH. (0.31%C; 0.040%S; <0.001%P)

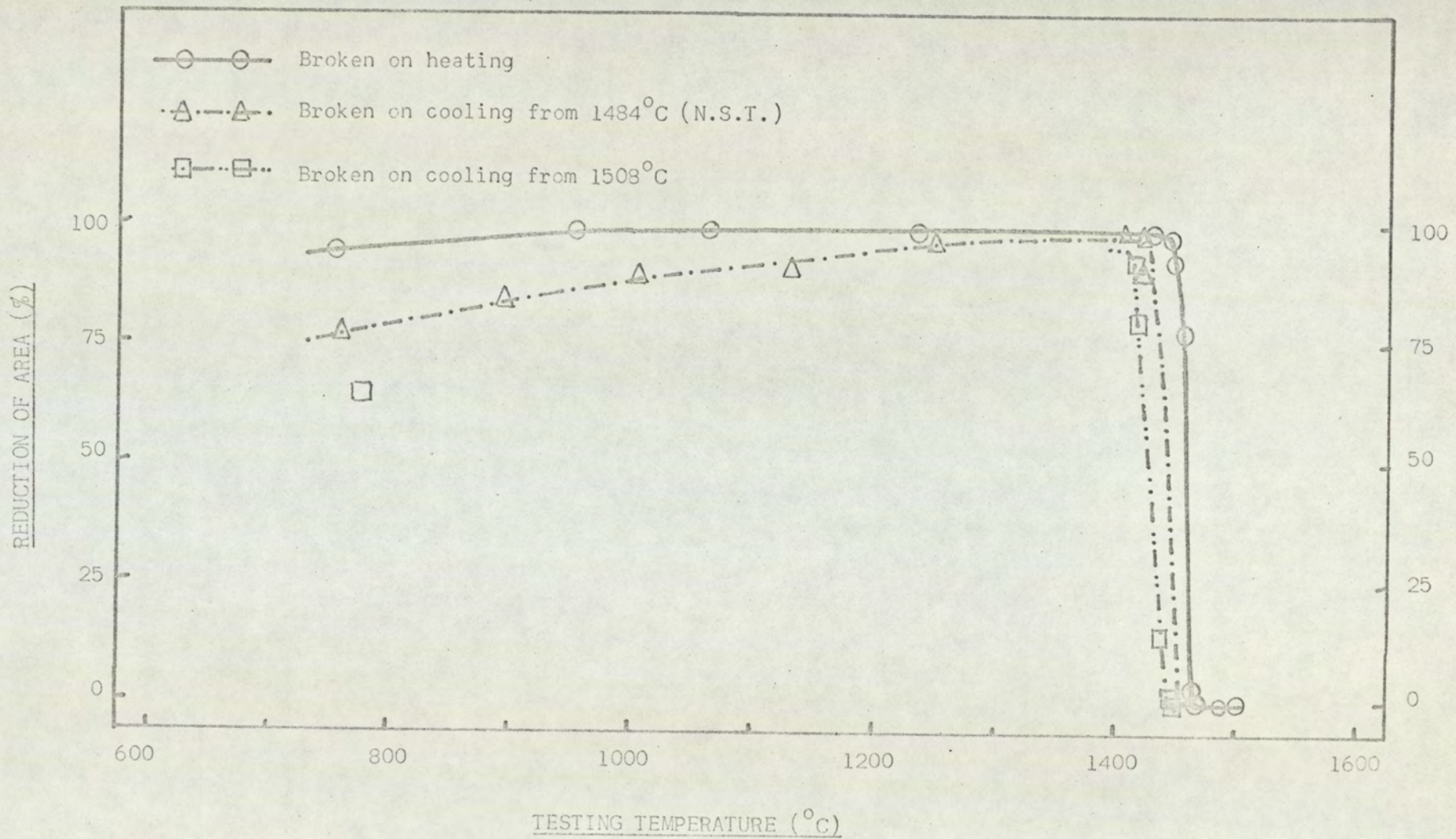


Fig. 48a. Hot Ductility Data for SAE 4130 Steel, SY. (0.37%C; 0.001%S; <0.001%P)

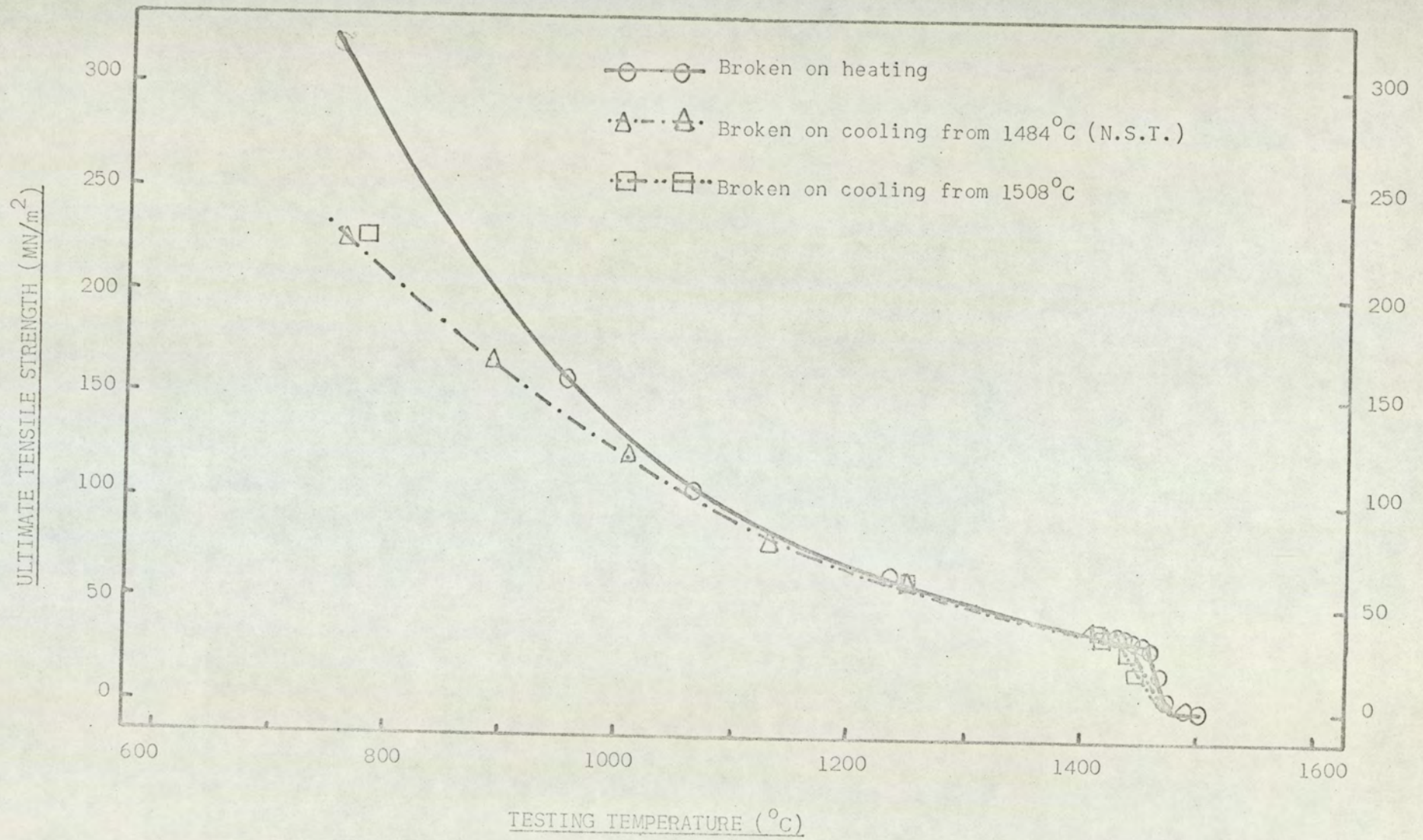


Fig. 48b. Hot Tension Data for SAE 4130 Steel, SY. (0.37%C; 0.001%S; <0.001%P)

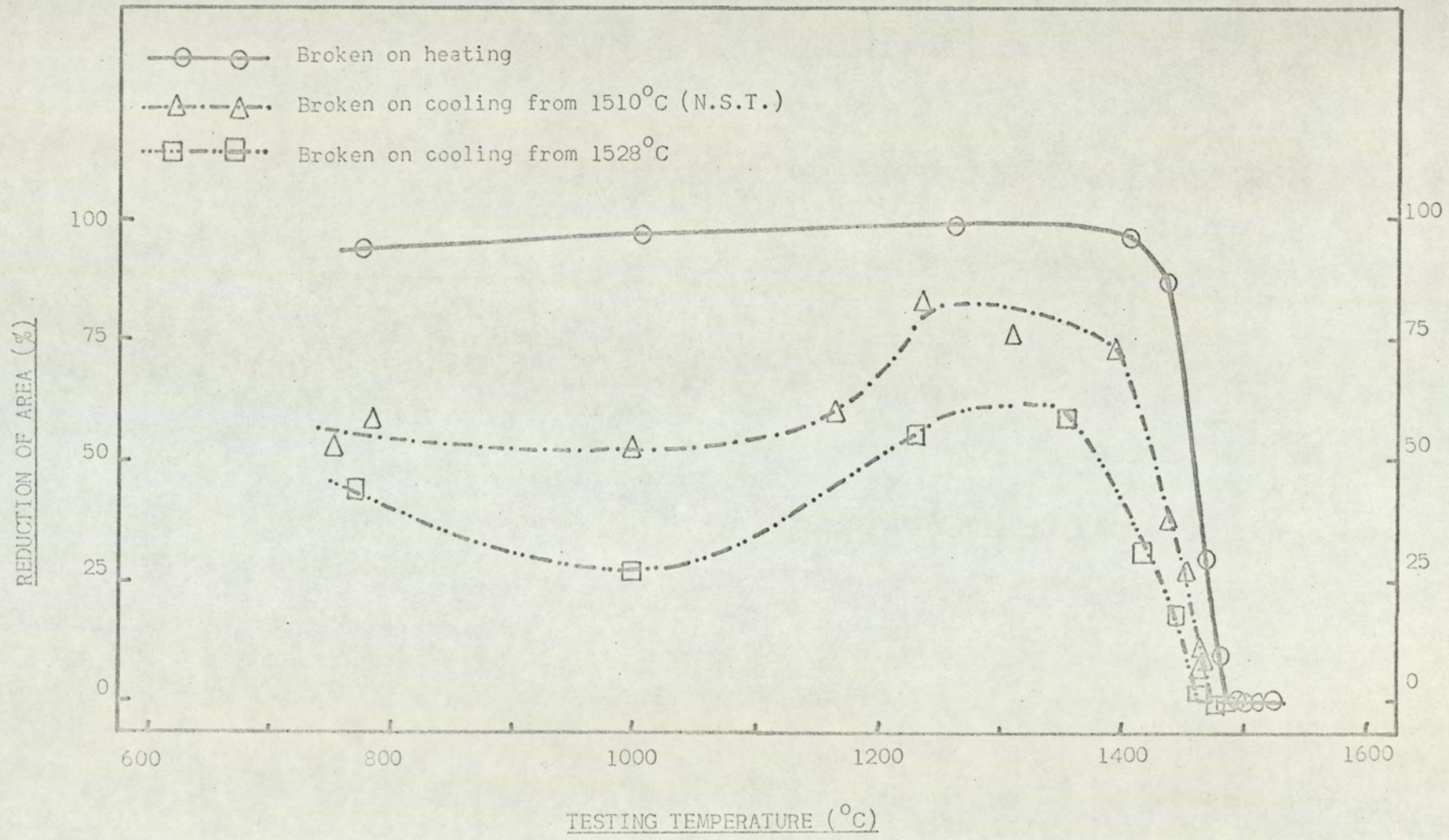


Fig. 49a. Hot Ductility Data for ASTM A387B Steel, AA. (0.13%C; 0.010%S; 0.008%P)

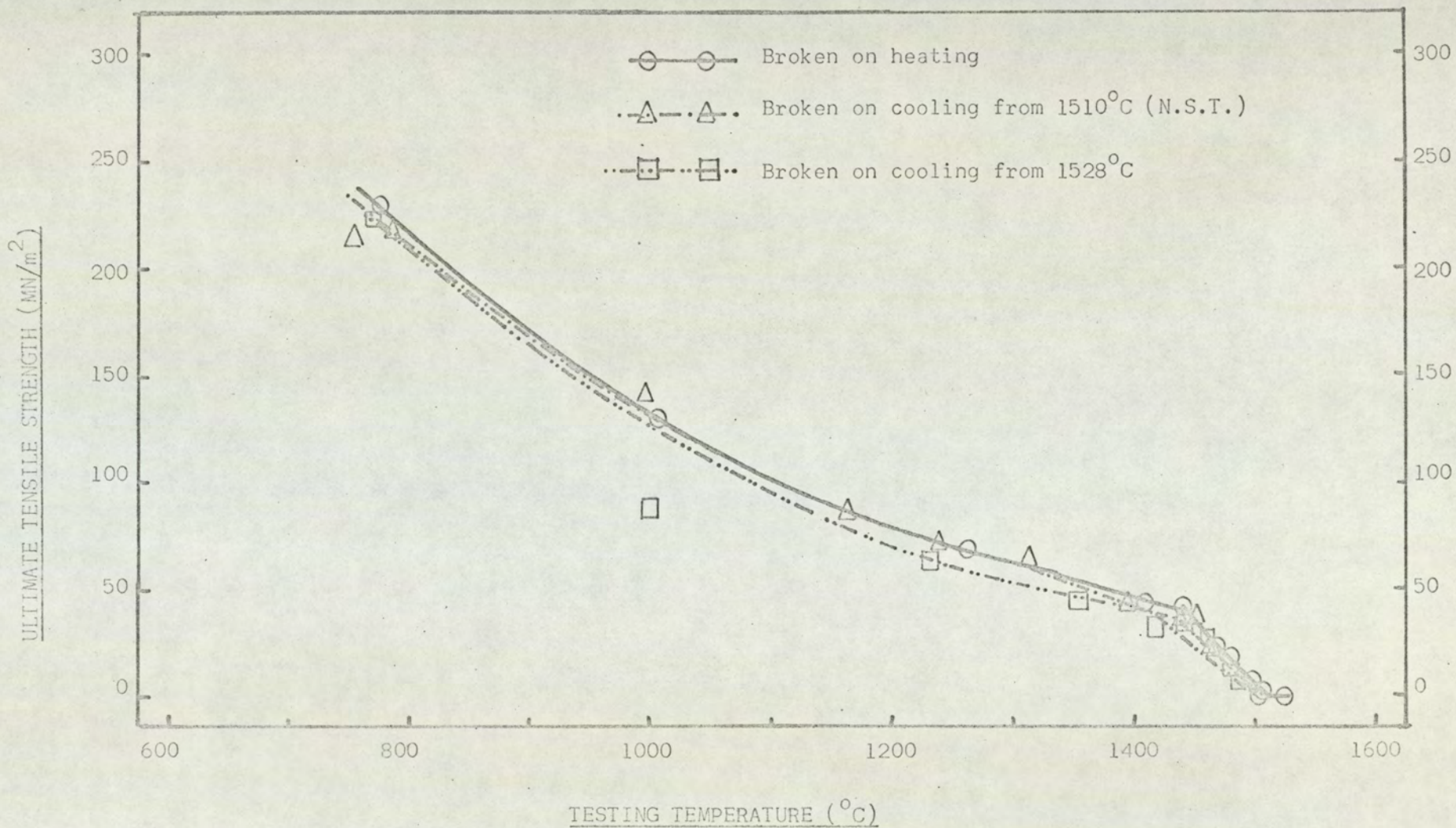


Fig. 49b. Hot Tension Data for ASTM A387B Steel, AA. (0.13%C; 0.010%S; 0.008%P)

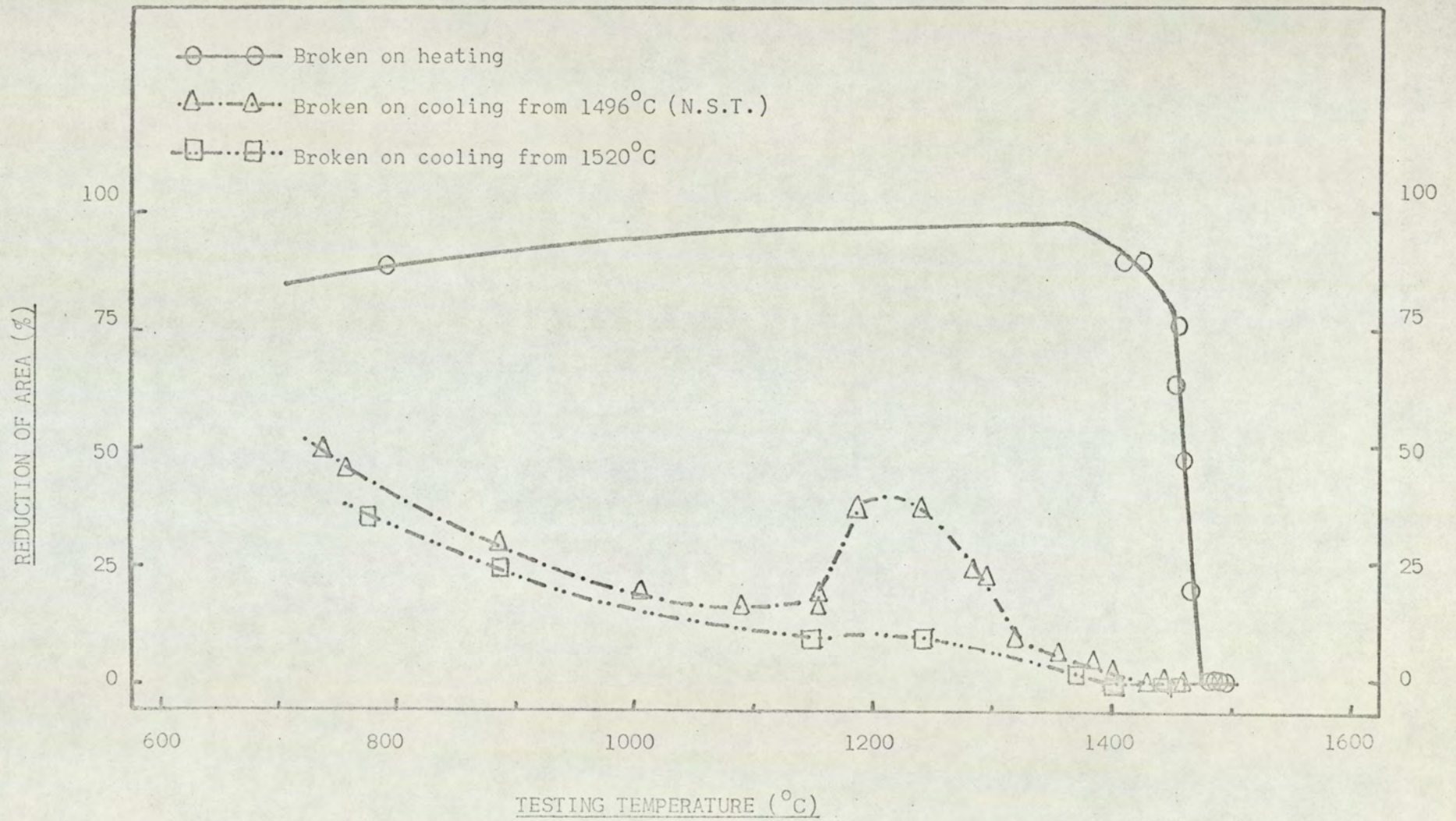


Fig. 50a. Hot Ductility Data for ASTM A387B Steel, AB. (0.11%C; 0.036%S; 0.031%P)

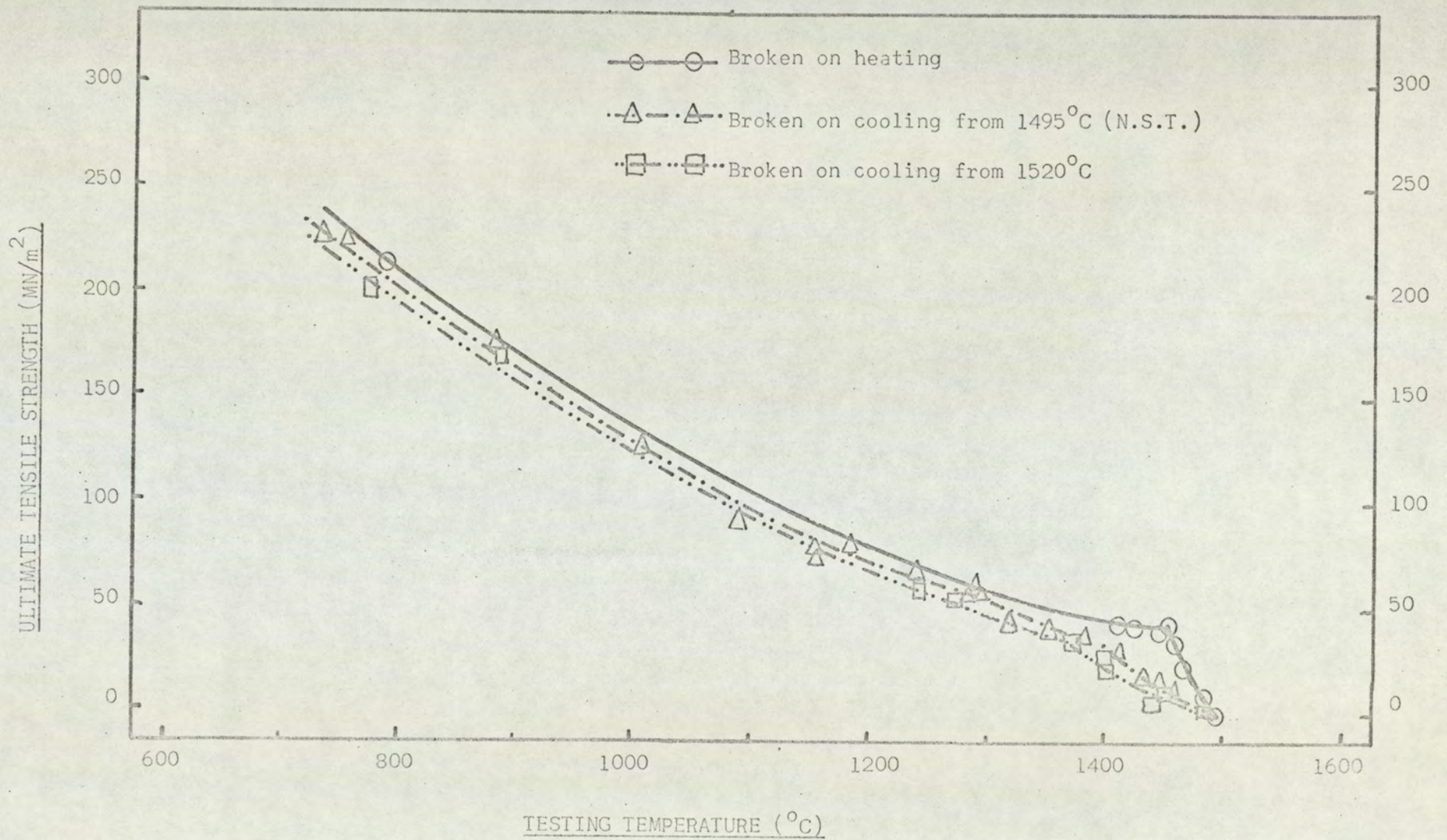


Fig. 50b. Hot Tension Data for ASTM A387B Steel, AB. (0.11%C; 0.036%S; 0.031%P)

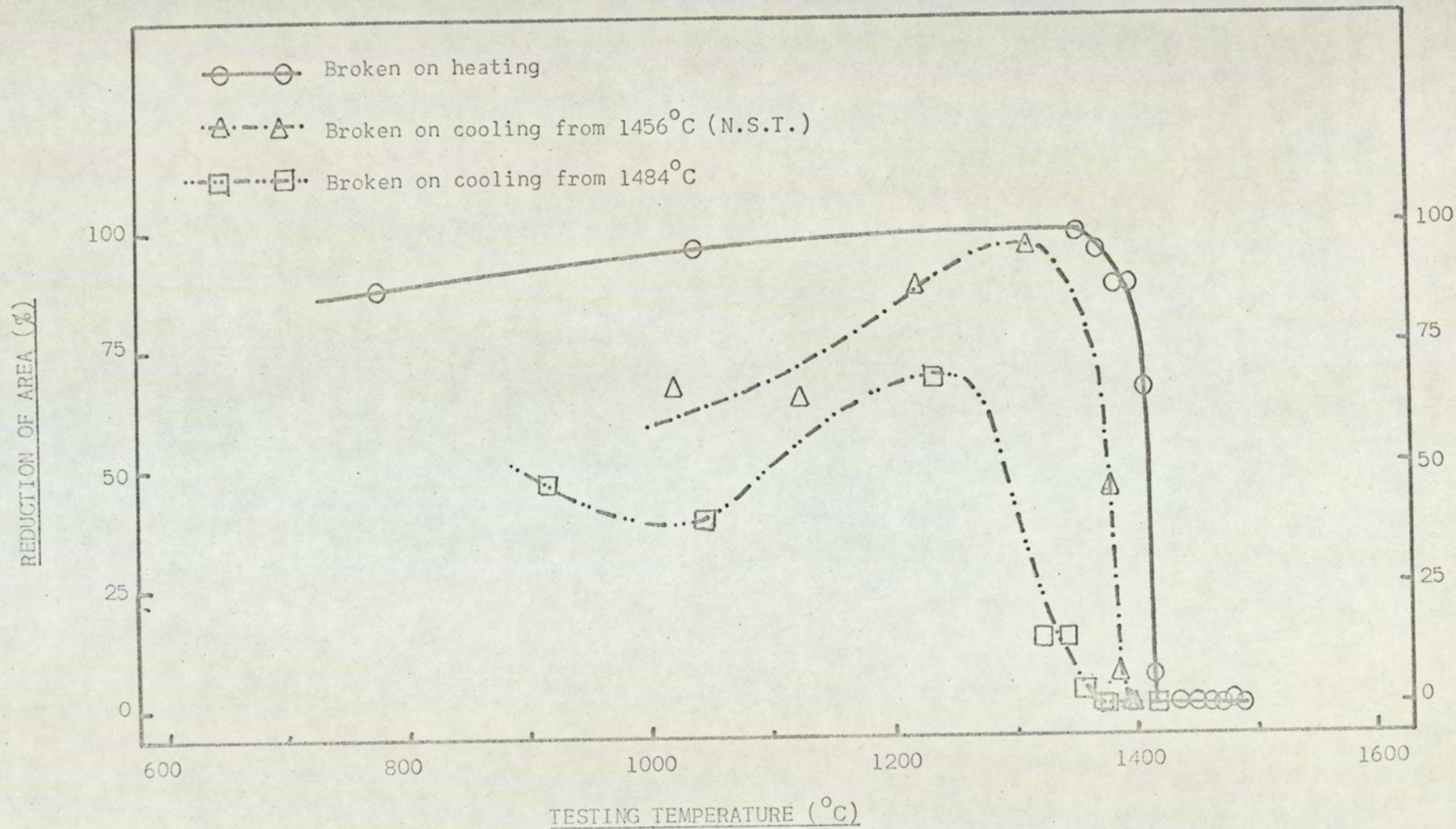


Fig. 51a. Hot Ductility Data for EN24 Steel, EB. (0.37%C; 0.010%S; 0.010%P)

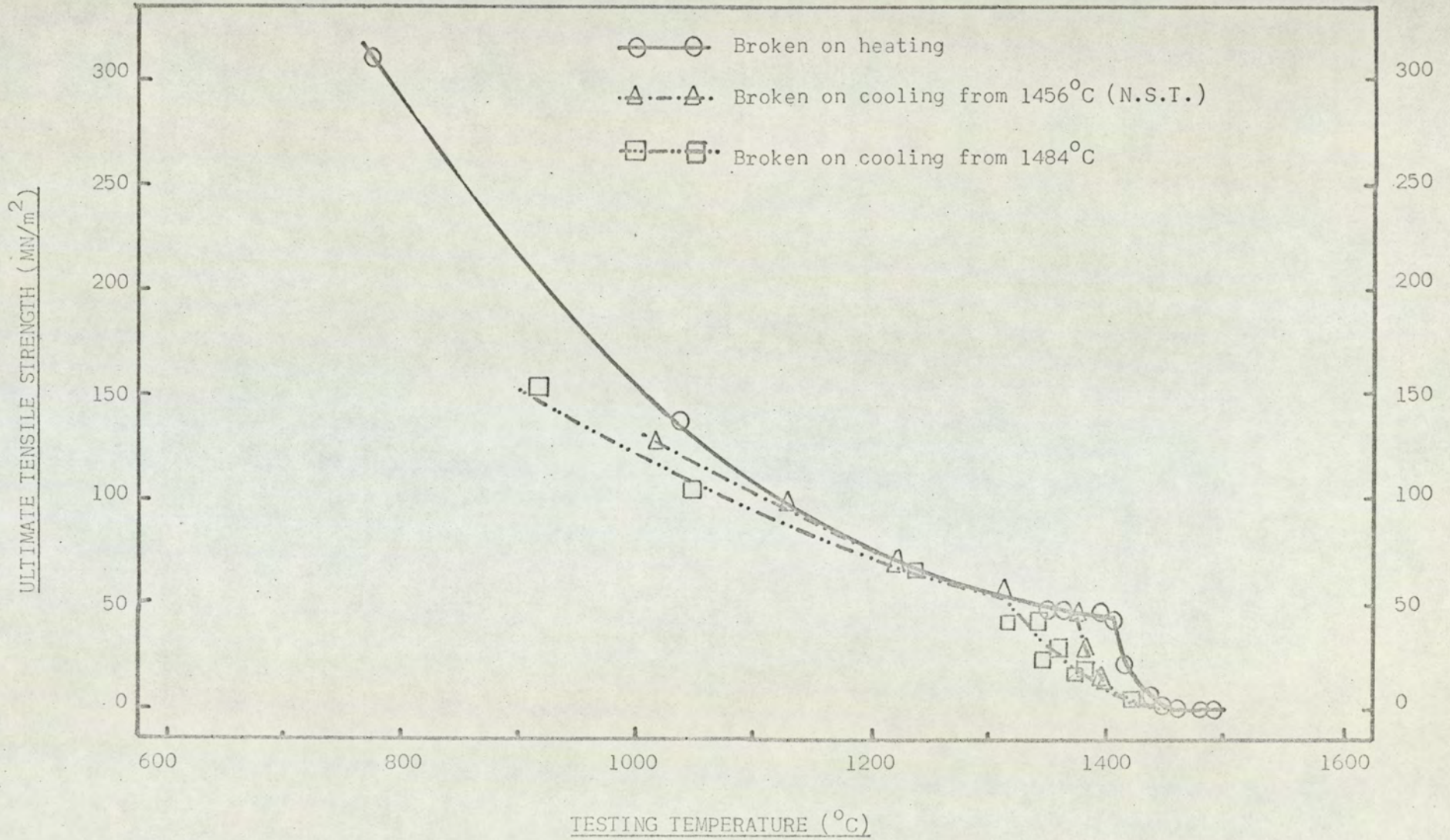


Fig. 51b. Hot Tension Data for EN24 Steel, EB. (0.37%C; 0.010%S; 0.010%P)

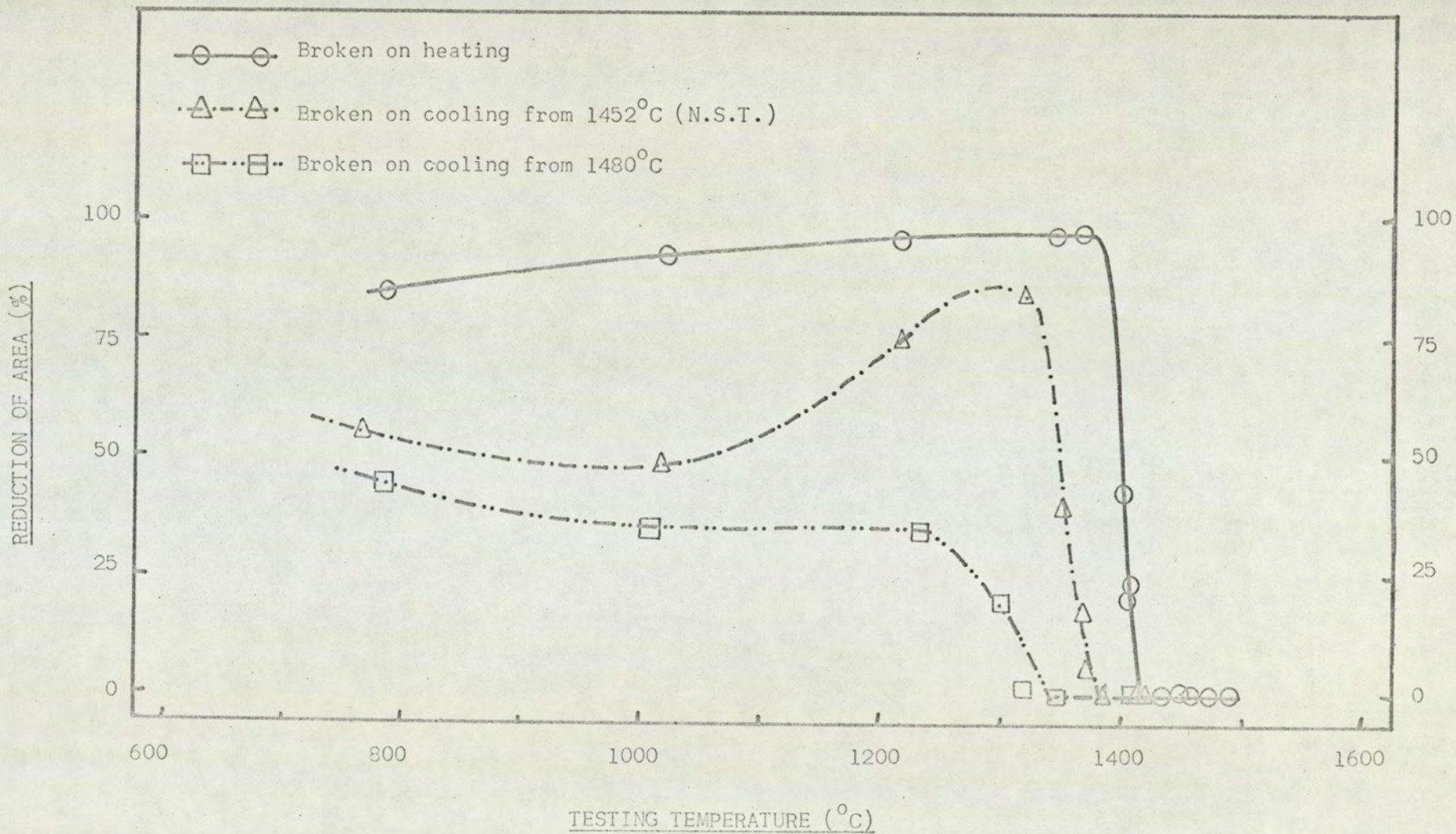


Fig. 52a. Hot Ductility Data for EN24 Steel, EC. (0.46%C; 0.036%S; 0.008%P)

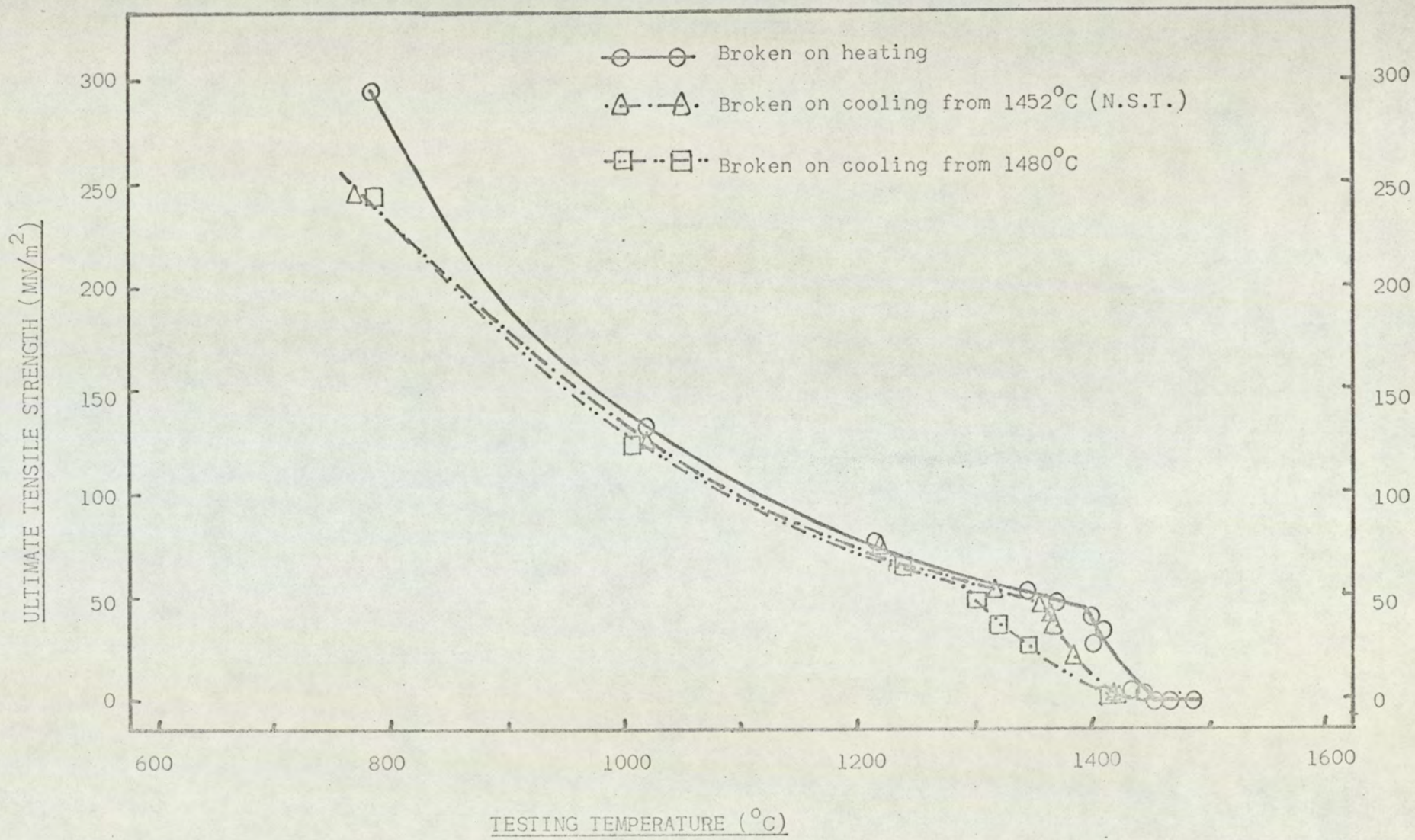


Fig. 52b. Hot Tension Data for EN24 Steel, EC. (0.46%C; 0.036%S; 0.008%P)

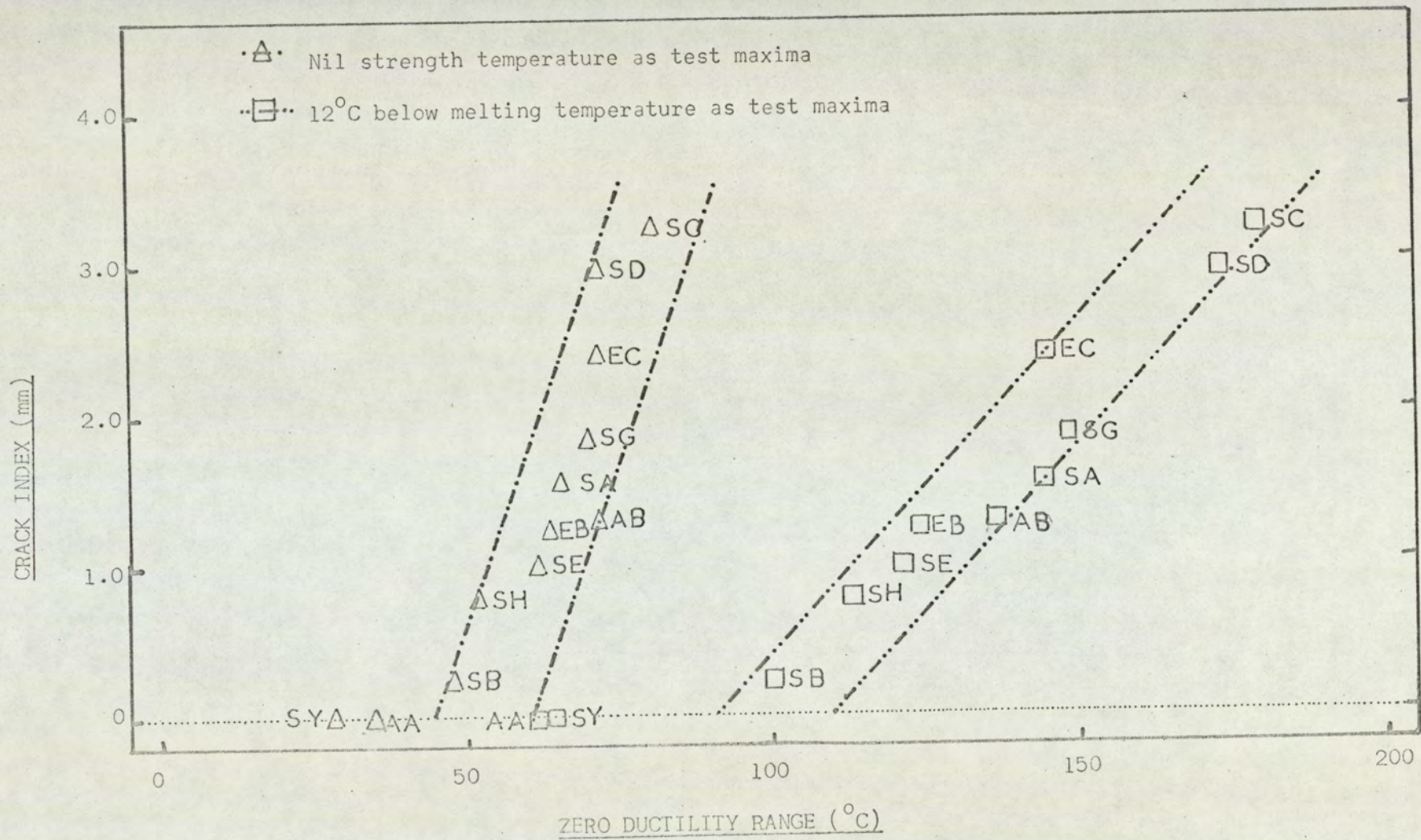


Fig. 53. Crack Index (From Welding Tests) V^S Zero Ductility Range

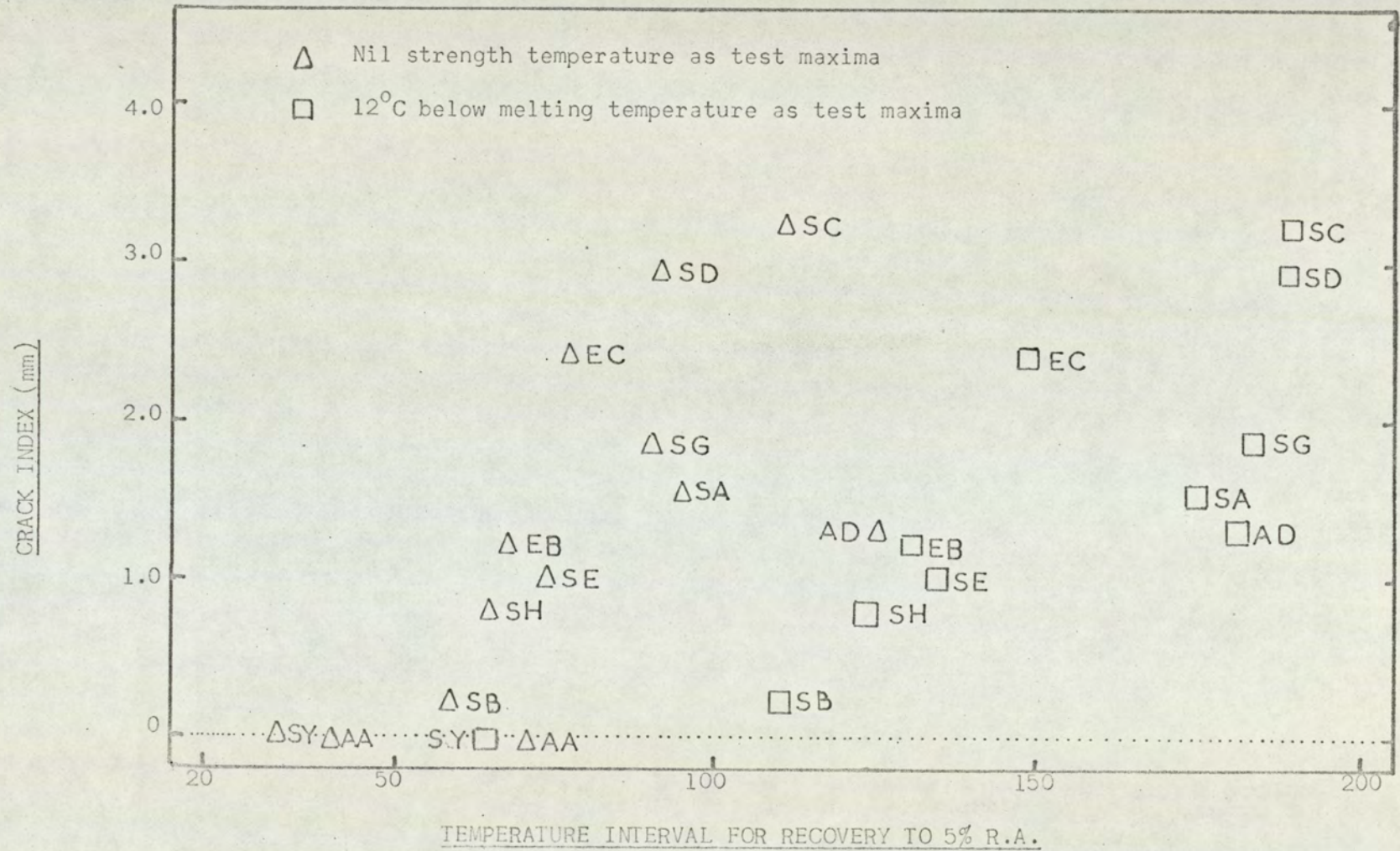


Fig. 54. Crack Index V^S Temperature Interval for Recovery to 5% R.A. ($^{\circ}\text{C}$)

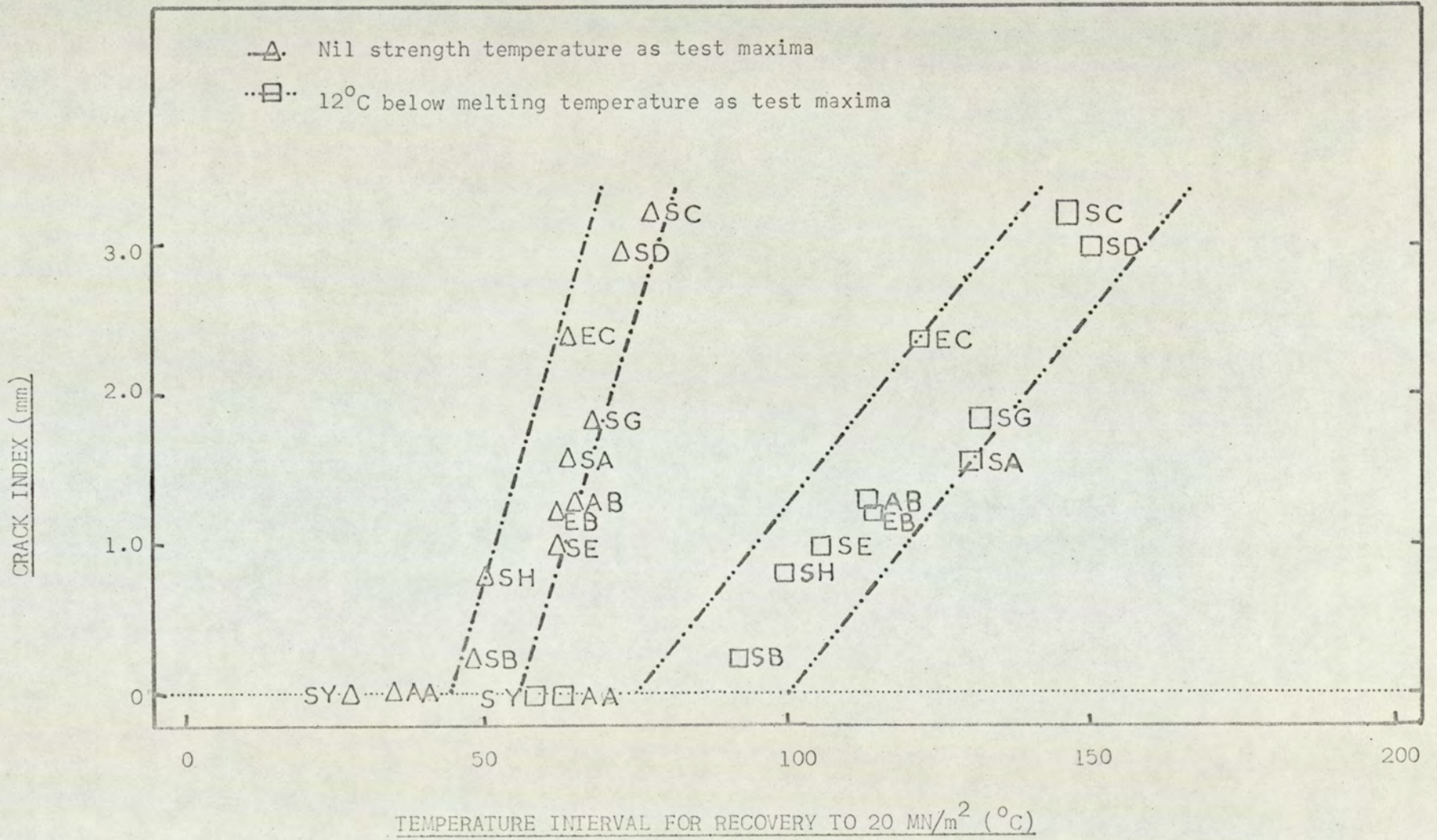


Fig. 55. Crack Index V^S Temperature Interval for Recovery to 20 MN/m^2 .

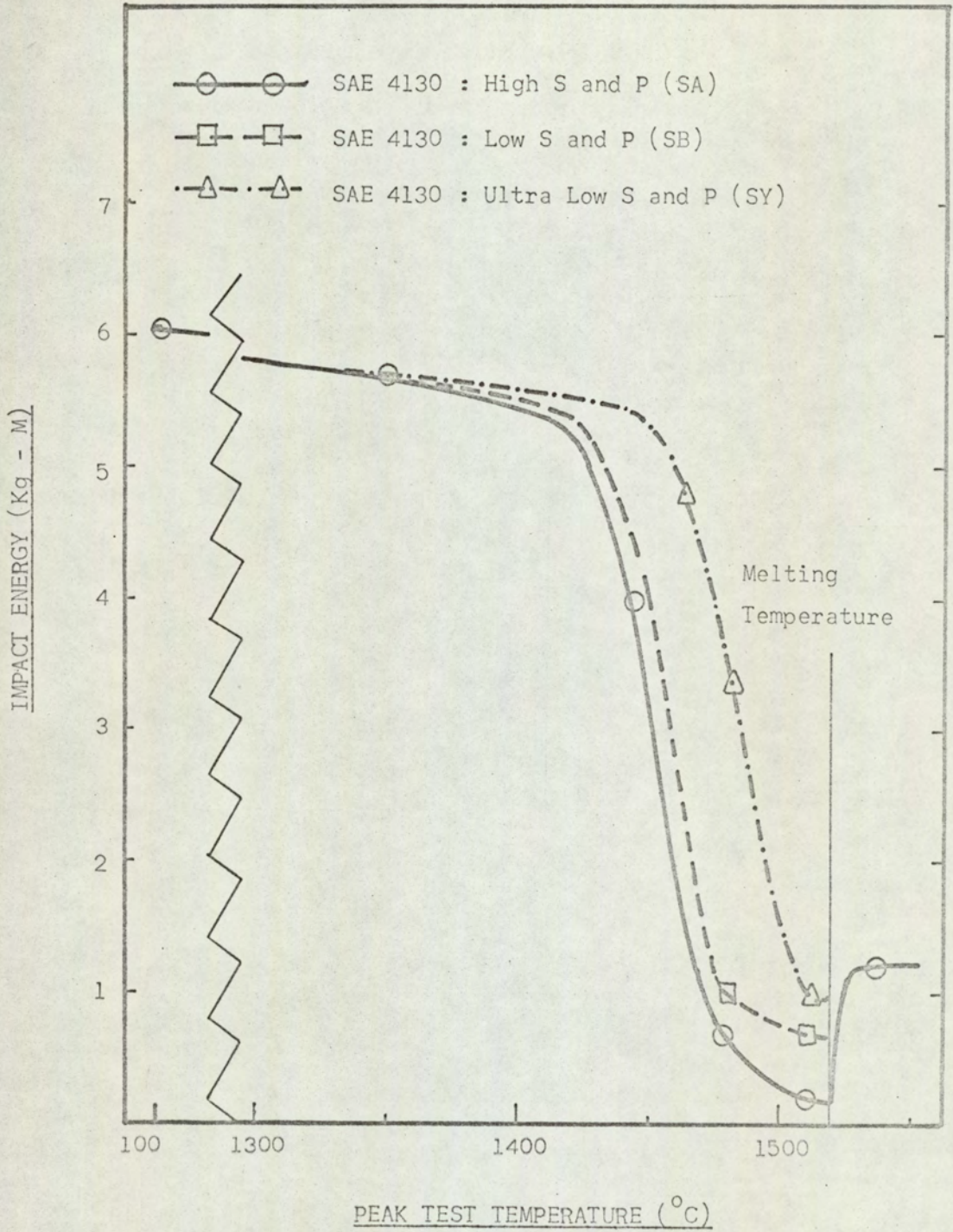


Fig. 56. Effect of Peak Temperature and Impurity Content on Impact Energy in Simulated Weld Specimens.



Figs. 57 & 58

Modified Inclusion Clusters and Modified Inclusions
decorating Prior Austenite Grain Boundaries in SAE 4130⁰
Hot Ductility Specimen after Thermally Cycling to 1500° C.

(Etched Nital x 750)



Fig.59. Fracture Face of SAE 4130₆ SA, Hot Ductility Specimen broken on heating at 1380 C, with 98% R.A., showing Ductile Failure.

(x 500)



Fig.60. Fracture Face of SAE 4130₆ SC, Hot Ductility Specimen, broken on heating at 1446 C, with 0% R.A., showing Intergranular Failure. (Note holes at grain faces).

(x 250)



Fig.61. Fracture Face of SAE 4130, SC, Hot Ductility Specimen, broken on heating at 1474° C, with 0% R.A., showing Intergranular Failure.

(x 230)



Fig.62. Fracture Face of SAE 4130, SC, Hot Ductility Specimen, broken on heating at 1488° C, with 0% R.A., showing Intergranular Failure with a more rounded Profile.

(x 300)



Fig.63. Fracture Face of SAE 4130, SC, Hot Ductility Specimen, broken on heating at 1510° C, (within 6° C of the Bulk Melting Temperature), showing Extensive Rounding of Grains.

(x 250)

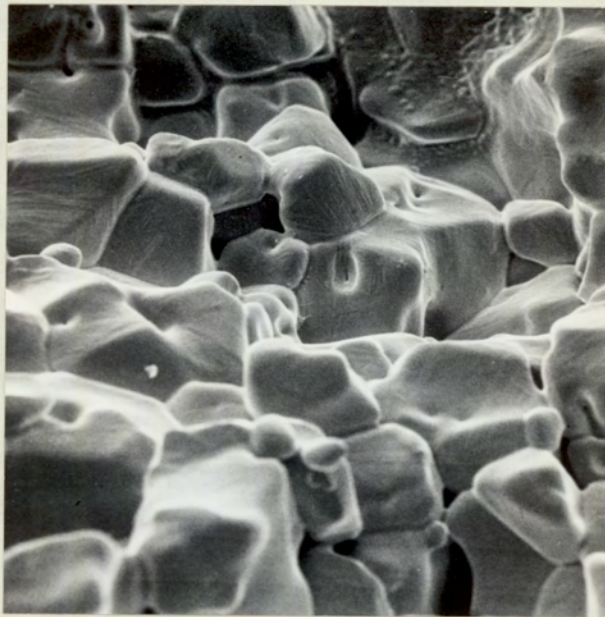


Fig.64. Fracture Face of SAE 4130, SC, Hot Ductility Specimen, broken on Cooling at 1463° C, with 0% R.A., after Peak of 1480° C, showing Rounded Intergranular Failure.

(x 250)



Fig.65. Detail of above Specimen.

(x 1,200)



Fig.66. Fracture Face of SAE 4130, SC, Hot Ductility Specimen, broken on Cooling at 1432° C, with 0% R.A., after Peak of 1480° C, showing Sharper Intergranular Profile.

(x 230)



Fig.67. Detail of above Specimen.
(Note Branching Cracks)

(x 550)



Fig.68. Fracture Face of SAE 4130, SC, Hot Ductility Specimen, broken on Cooling, at 1376°C , with 6% R.A., after peak of 1473°C , showing large Areas of Ductile Dimpling at Grain Faces.

(x 210)

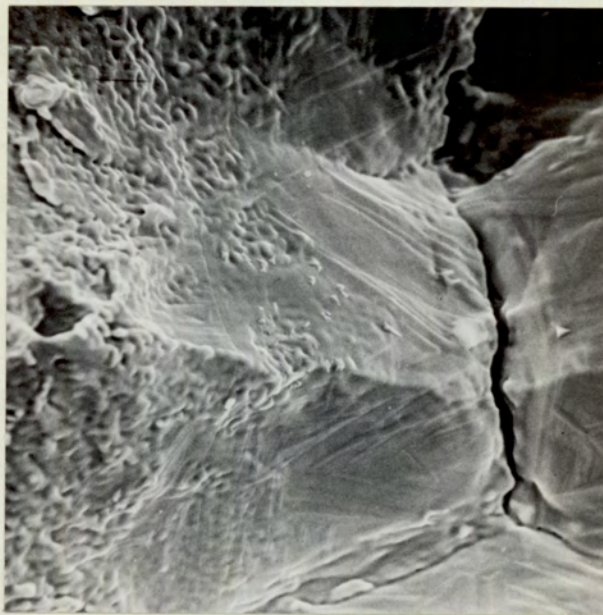


Fig.69. Detail of above Specimen, showing Ductile Dimpling and Free Surface.

(x 1100)



Fig. 70. Fracture Face of SAE 4130, SC, Hot Ductility Specimen, broken on Cooling at 1240° C, with 32% R.A., from a Peak of 1477° C, with 32% R.A., showing a predominantly Ductile Failure Mode.

(x 210)



Fig. 71. Fracture Face of SAE 4130, SC, Hot Ductility Specimen, broken on Cooling at 930° C, with 40% R.A., from a Peak of 1480° C, showing Partial Return to Intergranular Failure.

(x 260)

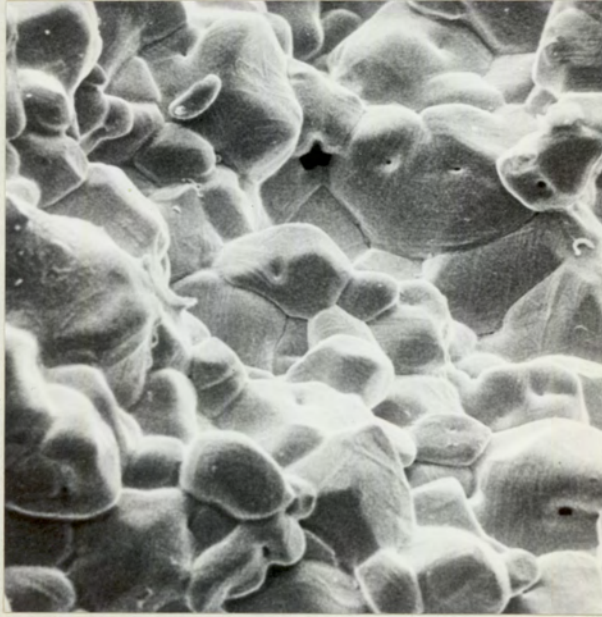


Fig.72. Fracture Face of SAE 4130, SC, Hot Ductility Specimen, broken on Cooling at 1456° C, with 0% R.A., after Peak of 1506° C, showing Rounded Intergranular Failure.

(x 250)

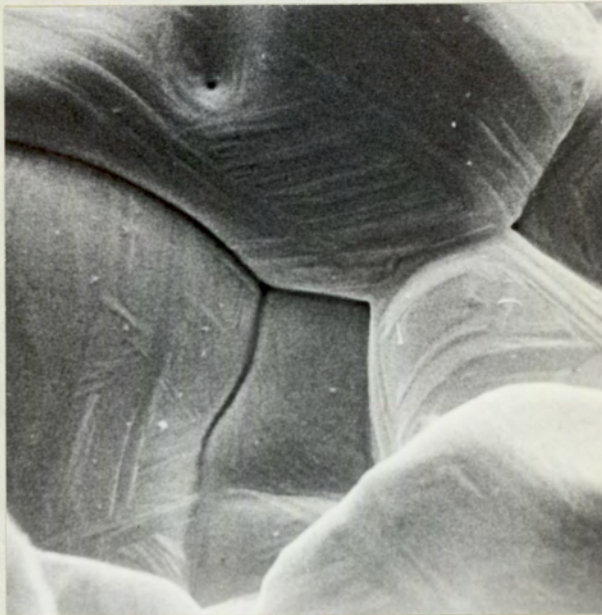


Fig.73. Detail of above Specimen.

(x 1200)



Fig. 74. Fracture Face of SAE 4130, SC, Hot Ductility Specimen, broken on Cooling at 1368° C, with 0% R.A., after Peak of 1504° C, showing more Angular Grain outline.

(x 220)



Fig. 75. Detail of above Specimen.

(x 560)



Fig. 76. Fracture Face of SAE 4130₀ SC, Hot Ductility Specimen, broken on Cooling at 1324° C, with 0% R.A., after Peak of 1506° C. showing Fern Dendrite at Grain Boundary.

(x 1200)

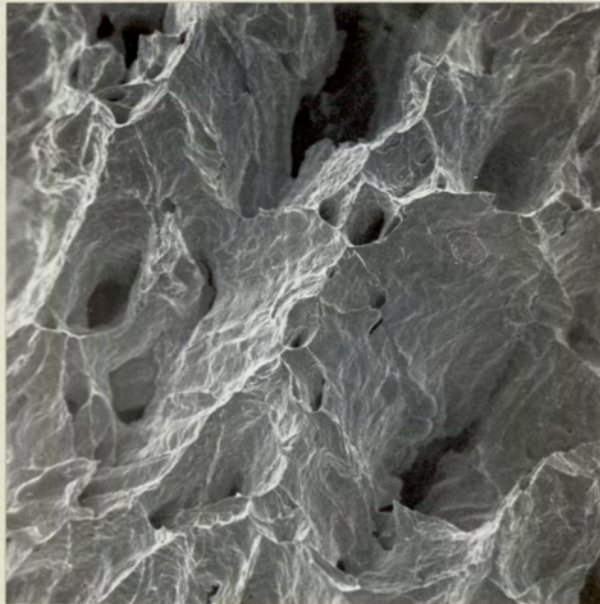


Fig. 77. Fracture Face of SAE 4130₀ SC, Hot Ductility Specimen, broken on Cooling at 1280° C, with 30% R.A., after Peak of 1504° C, showing Ductile Failure Mode.

(x 240)



Fig. 78. Fracture Face of SAE 4130, SA, Hot Ductility Specimen, Thermally Cycled to 1496° C, and Impact Tested at 100° C, showing Intergranular Failure.

(x 210)



Fig. 79. Fracture Face of SAE 4130, SA, Hot Ductility Specimen, Thermally Cycled above the Melting Temperature of 1516° C, and Impact Tested at 100° C, showing no Intergranular Zone.

(x 210)



Fig.80. Fracture Face of SAE 4130, SA, Hot Ductility Specimen, Thermally cycled to 1496° C, and Impact Tested at 100° C, showing detail of Fern Dendrite.

(x 2000)



Fig.81. Fracture Face of SAE 4130, SA, Hot Ductility Specimen, Thermally cycled to 1496° C, and Impact Tested at 100° C, showing detail of Ductile Dimples at the Grain Faces.

(x 600)



Fig.82. Fracture Face of SAE 4130, SA, Hot Ductility Specimen, Thermally Cycled to 1496° C and Impact Tested at 100° C, showing Free Surface Areas and Associated Fern Dendrites.

(x 240)

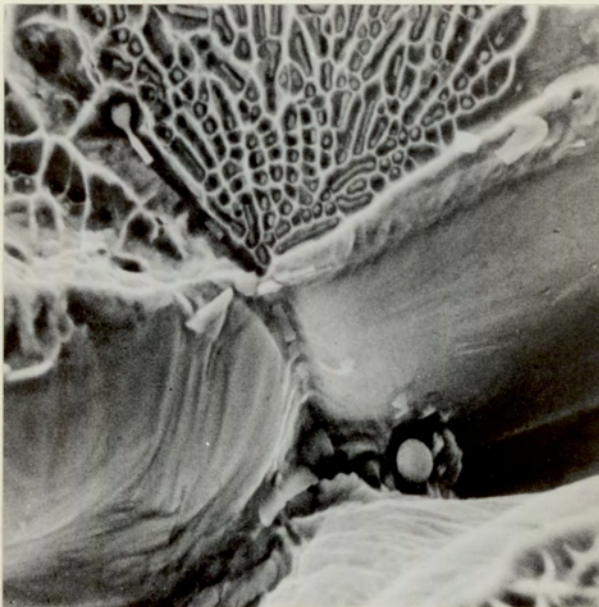


Fig.83. Detail of Fig.82.

(x 2.4K)